

DISSERTATION

REACTION NETWORK MODEL FOR THE PREDICTION OF  
MAMMALIAN METABOLISM OF BENZO[A]PYRENE

Submitted by

Kai-Hsin Liao

Department of Chemical Engineering

In partial fulfillment of the requirements  
For the Degree of Doctor of Philosophy  
Colorado State University  
Fort Collins, Colorado  
Fall 2004

COLORADO STATE UNIVERSITY

July 26, 2004

WE HEREBY RECOMMEND THAT THE DISSERTATION PREPARED UNDER OUR SUPERVISION BY KAI-HSIN LIAO ENTITLED REACTION NETWORK MODEL FOR THE PREDICTION OF MAMMALIAN METABOLISM OF BENZO[A]PYRENE BE ACCEPTED AS FULFILLING IN PART REQUIREMENTS FOR THE DEGREE OF DOCTOR OF PHILOSOPHY.

Committee on Graduate Work

[Redacted]

[Redacted]

[Redacted]

Co-Adviser

[Redacted]

Adviser

[Redacted]

Department Head

## ABSTRACT OF DISSERTATION

### REACTION NETWORK MODEL FOR THE PREDICTION OF MAMMALIAN METABOLISM OF BENZO[A]PYRENE

Humans are exposed to mixtures of environmental pollutants on daily bases. Many of these chemicals undergo biotransformation in our body and often produce toxic metabolites. The biotransformation of mixtures involves complex reaction networks that are difficult to study using conventional experimental techniques. As a first step of developing a predictive tool for the biotransformation of chemical mixtures, a chemical engineering approach, Reaction Network (RN) modeling, was utilized to study the mammalian metabolism of benzo[*a*]pyrene (BaP), a priority environmental carcinogen. A RN pathway model which predicts the theoretically possible reaction network for BaP was first developed based on the existing modeling technology for predicting the reaction networks in petroleum refinery processes, mechanistic organic chemistry, as well as the commonly observed biochemical reactions for mammalian metabolism of BaP. The resulting RN pathway model for BaP predicts that 246 reactions can occur, resulting in unique 150 products in the presence of mammalian cytochrome P450 and epoxide hydrolase. Some of these predicted products might not be experimentally detected due to the slow reactions for their formation or the production of reactive species. A RN kinetics model which reflects the experimentally measurable metabolic pathways was then established to determine the reaction rates of BaP metabolism. To obtain proper

separation of eleven BaP metabolites with high detection sensitivities, high-performance liquid chromatography methods were developed and validated. The RN kinetics model was calibrated and validated using experimental data of BaP metabolism catalyzed by recombinant human enzymes. The biotransformation of BaP and the production of nine BaP metabolites were accurately described by the RN kinetics model. Finally, the RN kinetics model of BaP was linked to a physiologically based pharmacokinetic (PBPK) model to describe the distribution and disposition of BaP and its metabolites in rats. The major advantages of applying RN modeling to study toxicology are: (1) their capabilities of handling complex metabolic systems; (2) their potential for predicting reaction networks of chemicals with limited knowledge on their metabolic pathways; and (3) their abilities to predict the reactive intermediates that are not readily measurable in experiments.

Kai Hsin Liao  
Department of Chemical Engineering  
Colorado State University  
Fort Collins, CO 80523  
Fall 2004

## TABLE OF CONTENTS

<b>Chapter 1. Introduction</b>	<b>1</b>
1.1. Goal and Specific Aims	1
1.2. Background and significance	1
1.2.1. Reaction Network Modeling	1
1.2.2. Application of Reaction Network Modeling to Study Toxicology of Chemical Mixtures	2
1.2.3. Significance of Linking the Reaction Network Model with Physiologically Based Pharmacokinetic Models	3
1.3. Overview	4
1.4. References	5
<b>Chapter 2. Reviews in Mammalian Metabolism of Benzo[a]pyrene</b>	<b>6</b>
<b>Chapter 3. Application of Biologically Based Computer Modeling to Simple or Complex Mixtures</b>	<b>13</b>
3.1. Introduction	13
3.2. Abstract in the Original Publication	14
3.3. Introduction in the Original Publication	15
3.4. Experimental and Computational Approaches	16
3.4.1. Chemical Mixtures and Multiple Stressors	16
3.4.2. Simple Chemical Mixtures: Interaction Thresholds	17
3.4.3. Simple Chemical Mixtures: Mixture Formula	19
3.4.4. A Ray of Hope for Complex Chemical Mixtures: Reaction Network Modeling	20
3.4.4.1. Reaction network modeling and its application to petroleum engineering.	20
3.4.4.2. Reaction network modeling and its application to biomedical research.	25
3.4.4.2.1. Generation of BaP reaction networks	27
3.4.4.2.2. Estimation of BaP metabolic reaction rate constants	28
3.4.5. Future Perspective: Second-Generation PBPK/PD Models	30
3.5. References	32
<b>Chapter 4. Application of Reaction Network Pathway Modeling in Biological Systems: Mammalian Metabolism of Benzo[a]pyrene</b>	<b>41</b>
4.1. Introduction	41

4.2. Methods	42
4.2.1. Representation of Chemical Structures	43
4.2.2. Execution of Chemical Reactions	44
4.2.2.1. Epoxidation reactions	45
4.2.2.2. Hydrolysis reactions of epoxides	48
4.2.2.3. NIH Shift reactions of epoxides	49
4.2.2.4. Oxidation of BaP to BaP-diones	49
4.2.2.4.1. Carbon hydroxylation reactions	50
4.2.2.4.2. Auto-oxidation of BaP-diols to BaP-diones	50
4.2.3. Determination of Species Uniqueness	53
4.2.4. Estimation of Kinetic Parameters	57
4.3. Results and Discussion	58
4.3.1. Reaction Network Pathway Model Predictions	58
4.3.2. Example of Reaction Network Kinetics Model Simulations	60
4.4. Conclusions	61
4.5. References	61

**Chapter 5. High-Performance Liquid Chromatography Method for the Separation and Quantification of Eight Fluorescent Benzo[*a*]pyrene Metabolites including 3-Hydroxy- and 7-Hydroxy-Benzo[*a*]pyrene**

	<b>90</b>
5.1. Introduction	90
5.2. Materials and Methods	92
5.2.1. Chemicals and Reagents	92
5.2.2. Enzymes and Cofactors	92
5.2.3. Instrumentation	93
5.2.4. Chromatographic Conditions	93
5.2.5. Calibration Procedures	94
5.2.6. Limits of Detection, Limits of Quantitation, and Instrument Precision	94
5.2.7. Sample Preparation for Extraction Recovery Study	95
5.2.8. Time-Course Studies of BaP Metabolism Using Recombinant Human Enzymes	95
5.2.9. Other Methods Tested during Method Development	96
5.3. Results	97
5.3.1. Chromatogram	97
5.3.2. Standard Calibration Curve	97
5.3.3. LOD, LOQ, and Instrument Precision	98
5.3.4. Extraction Recovery	98
5.3.5. Application of the Method to a Time-Course Study of BaP Metabolism	98
5.4. Discussion	99
5.5. Conclusions	101
5.6. References	101
5.7. Appendix	103

<b>Chapter 6. A Novel, Sensitive Method for Determining Benzo[a]pyrene-Diones Using High-Performance Liquid Chromatography with Post-Column Zinc Reduction</b>	<b>114</b>
6.1. Introduction	114
6.2. Materials and Methods	116
6.2.1. Chemicals and Reagents	116
6.2.2. Enzymes	116
6.2.3. HPLC Instruments	116
6.2.4. Chromatographic Conditions	117
6.2.5. Post-Column Zinc Reducer	117
6.2.6. Calibration Procedures	118
6.2.7. Limits of Detection, Limits of Quantitation, and Instrument Precision	119
6.2.8. Samples for Extraction Recovery Study	119
6.2.9. Time-Course Studies of BaP Metabolism Using Recombinant Human Enzymes	120
6.2.10. Other Methods Tested during Method Development	120
6.3. Results	121
6.3.1. Chromatogram	121
6.3.2. Standard Calibration Curves and Detection Limits	122
6.3.3. Instrument Precision	123
6.3.4. Impact of the Post-Column Zinc Reducer	123
6.3.5. Extraction Recovery	124
6.3.6. Application of the Method to a Time-Course Study of BaP Metabolism	124
6.4. Discussion	124
6.5. Conclusions	127
6.6. References	127
6.7. Appendix	129
<b>Chapter 7. A Reaction Network Kinetic Model of Benzo[a]pyrene Metabolism Catalyzed by Recombinant Human Enzymes</b>	<b>138</b>
7.1. Introduction	138
7.2. Materials and Methods	139
7.2.1. Chemicals and Reagents	139
7.2.2. Enzymes and Cofactors	140
7.2.3. HPLC Analysis of BaP and its Fluorescent Metabolites	140
7.2.4. HPLC Analysis for BaP-Diones	141
7.2.5. Time-Course Studies of BaP Metabolism Using Recombinant Human Enzymes	142
7.2.6. Extraction Recovery Study	142
7.2.7. Qualitative Prediction of the BaP Metabolic Reactions Using a Reaction Network Pathway Model	143
7.2.8. Rate Equations for BaP Metabolic Pathways	143

7.3. Results and Discussion	145
7.3.1. Chromatogram	145
7.3.2. Metabolic Profiles of BaP Using Recombinant Human Enzymes	145
7.3.3. Extraction Recovery	147
7.3.4. Relationship between Enzyme Concentrations and Metabolite Formation	149
7.3.5. Predictions of BaP Metabolic Reactions by the Reaction Network Pathway Model	151
7.3.6. Reaction Network Kinetics Model Parameters	152
7.3.7. Reaction Network Kinetics Model Simulations	154
7.3.8. Initial Development of the Quantitative Structure/Reactivity Correlations for the Reaction Rates of BaP Metabolism	157
7.4. Conclusions	159
7.5. References	159
7.6. Appendix	162
<b>Chapter 8. Development and Validation of a Hybrid Reaction Network-Physiologically Based Pharmacokinetic Model of Benzo[a]pyrene and Its Metabolites</b>	<b>181</b>
8.1. Introduction	181
8.2. Methods	182
8.2.1. Model Structure	182
8.2.2. Parameters for the PBPK Model	183
8.2.3. Parameters for the Reaction Network Kinetics Model	184
8.3. Results and Discussion	186
8.3.1. BaP Metabolism Catalyzed by Recombinant Rat Enzymes	186
8.3.2. BaP Metabolism Catalyzed by Rat Liver Microsomes	187
8.3.3. PBPK Model parameters and Model Simulations	189
8.3.4. Model Validation	191
8.4. References	194
<b>Chapter 9. Conclusions and Future Perspectives</b>	<b>208</b>
9.1. Conclusions	208
9.2. Future Perspectives	210
9.3. References	213

# Chapter 1.

## Introduction

### **1.1. Goal and Specific Aims**

The primary goal of this research was to apply a chemical engineering approach called Reaction Network (RN) modeling to predict the metabolic pathways and kinetics of benzo[a]pyrene (BaP), a priority carcinogenic environmental pollutant.

The **Specific Aims** for the project were:

**Aim 1:** Establish a RN pathway model for the determination of BaP metabolic reactions.

**Aim 2:** Develop a RN kinetics model for predicting the time course profiles of BaP metabolism.

**Aim 3:** Link the Reaction Network model with physiologically based pharmacokinetic model to describe the distribution and disposition of BaP and its metabolites in whole animals.

### **1.2. Background and Significance**

#### *1.2.1. Reaction Network Modeling*

Reaction Network modeling is a tool for predicting the amounts of intermediates and products as a function of time for a set of coupled chemical reactions. It is usually a mathematical and symbolic formulation, suitable for solution on the computer. The

model building software can be used to not only solve the kinetics equations of interest, but also generate the reaction mechanisms, rate constants, and reaction equations themselves. Originally developed by Broadbelt and coworkers (1-3), RN modeling used concepts of graph theory to represent species connectivity. It also made use of computational quantum chemistry, linear free energy relationships (4, 5), and quantitative structure/reactivity correlations (6) to automate the process of determining reaction rate constants. RN modeling has been used very successfully in the areas of petroleum and chemical engineering for very complex chemical processes involving hundreds and even thousands of chemicals.

### *1.2.2. Application of Reaction Network Modeling to Study Toxicology of Chemical Mixtures*

Many xenobiotics undergo metabolic transformations in biological systems and often produce reactive metabolites, which can be harmful to cells or tissues. Biotransformation may involve complex reaction networks in which multiple enzymes are involved and the species associated with one reaction are participants in many other reactions. Furthermore, humans are likely exposed to chemical mixtures that composed of many different combinations of environmental pollutants. For chemical mixtures, the complexities of the biotransformation pathways further increase with the number of the chemicals composing the mixture. Therefore, predictive tools are desired in order to reduce the number of experiments required for studying the complex reaction networks of biotransformation of numerous analogous chemicals. RN modeling is a logical choice to predict the biotransformation of xenobiotics due to its success in predicting the detailed

reaction kinetics of petroleum refinery processes. Even though we started out with a single chemical, as shall be demonstrated later, the RN pathway model for BaP biotransformation encompasses 150 possible products and 246 possible reactions. Furthermore, RN models are encoded at the level of atomic connectivity using graph theory, and thus this approach can be applied to many kinds of chemical reactions, including the complex reactions encountered by many different types of xenobiotics.

BaP was selected as the substrate to build the first RN model for biochemical reactions. BaP is a ubiquitous environmental pollutant and a probable human carcinogen (7) formed by incomplete combustion of organic matters. The metabolic pathways of BaP are complex (8-10), but extensively studied, making it an ideal candidate for RN modeling. Furthermore, the biochemical reactions BaP undergoes, *e.g.*, epoxidation and hydrolysis, are also common for other xenobiotics, especially polycyclic aromatic hydrocarbons.

### *1.2.3. Significance of Linking the Reaction Network Model with Physiologically Based Pharmacokinetic Models*

A physiologically based pharmacokinetic (PBPK) model describes the processes of absorption, distribution, metabolism, and excretion of chemicals in the body by using basic physiological and biochemical data. A PBPK model coupled with a RN kinetics model, which predicts the detailed metabolic fate of chemicals, can serve as a powerful tool to describe the distribution and disposition of parent compounds and their metabolites from the whole organism down to the molecular interaction levels. The

RN/PBPK modeling approach will be most useful for chemicals that involve complex metabolic pathways and/or exert their toxicities via biotransformation.

### **1.3. Overview**

The topics discussed in the following chapters of this dissertation are outlined in this section. Mammalian metabolism of BaP is reviewed in Chapter 2. The potential of applying the RN modeling approach to study the metabolic fate of chemical mixtures is discussed in Chapter 3. A RN pathway model was developed (Chapter 4) first to qualitatively predict the possible reactions that BaP might encounter in mammals. The RN pathway model was established based on the previously developed modeling technology for the prediction of the reaction networks in petroleum refinery processes (1-3), with the incorporation of the commonly observed biochemical reactions for mammalian metabolism of BaP (8-10). A RN kinetics model for predicting the time course profiles of BaP metabolism was developed using experimental data. To determine BaP and eleven of its metabolites with high detection sensitivities, high-performance liquid chromatography (HPLC) methods were developed and validated (Chapters 5 and 6). The time course profiles of BaP metabolism using recombinant human enzymes were accurately described by the RN kinetics model of BaP (Chapter 7). RN kinetics model of BaP was further linked with a physiologically based pharmacokinetic model (PBPK) to describe the distribution and disposition of BaP in whole animals (Chapter 8).

## **1.4. References**

1. Broadbelt LJ, Stark SM, Klein MT. Computer generated pyrolysis modeling: on-the-fly generation of species, reactions, and rates. *Ind Eng Chem Res* 33:790-799(1994).
2. Broadbelt LJ, Stark SM, Klein MT. Computer-generated reaction networks: on-the-fly calculation of species properties using computational quantum chemistry. *Chem Eng Sci* 49:4991-5010(1994).
3. Broadbelt LJ, Stark SM, Klein MT. Computer generated reaction modelling: decomposition and encoding algorithms for determining species uniqueness. *Comput Chem Eng* 20:113-129(1996).
4. Neurock M, Klein MT. Linear free energy relationships in kinetic analyses: Applications of quantum chemistry. *Polycycl Aromat Comp* 3:231-246(1993).
5. Neurock M, Klein MT. When you can't measure - model. *Chemtech* 23:26-32(1993).
6. Korre SC, Neurock M, Klein MT, Quann RJ. Hydrogenation of polynuclear aromatic hydrocarbons. II. Quantitative structure/reactivity correlations. *Chem Eng Sci* 49:4191-4210(1994).
7. IARC. Polynuclear Aromatic Compounds, Part 1: Chemical, Environmental and Experimental Data, vol 32. Lyon:International Agency for Research on Cancer, 1983.
8. Harvey RG. Polycyclic Aromatic Hydrocarbons: Chemistry and Carcinogenicity. Cambridge:Cambridge University Press, 1991.
9. Levin W, Wood A, Chang R, Ryan D, Thomas P, Yagi H, Thakker D, Vyas K, Boyd C, Chu SY, Conney A, Jerina D. Oxidative metabolism of polycyclic aromatic hydrocarbons to ultimate carcinogens. *Drug Metab Rev* 13:555-580(1982).
10. Miller KP, Ramos KS. Impact of cellular metabolism on the biological effects of benzo[a]pyrene and related hydrocarbons. *Drug Metab Rev* 33:1-35(2001).

## Chapter 2.

### Reviews in Mammalian Metabolism of Benzo[a]pyrene

High incidences of skin cancer were found among workers in coal tar industry in the 19th century (1), which led to the discovery of polycyclic aromatic hydrocarbons (PAHs) being the components in coal tar that caused carcinogenic effects (1).

Benzo[a]pyrene (BaP), isolated from coal tar in 1933 (2), has often been considered as the prototypical PAH (3). BaP is also formed during the combustion of fossil fuels and vegetation, and thus a widespread environmental pollutant (1). The estimated average intake of BaP by the general population in the U.S. is 2.16 µg/day (4). The food chain accounts for 97% of the daily intake of BaP by human, while inhalation and consumption of water account for only 2% and 1%, respectively (4).

BaP is a procarcinogen and metabolically activated to its reactive metabolites to exert toxic effects. Three activation pathways of BaP have been reported (Figure 2.1). The first activation pathway, which is widely accepted, leads to the formation of BaP-7,8-dihydrodiol-9,10-epoxide via a set of reactions catalyzed by cytochrome P450 (CYP) and epoxide hydrolase (EH) (3, 5-7). BaP-7,8-dihydrodiol-9,10-epoxide is reactive and forms N<sup>2</sup> deoxyguanosine adducts within DNA (8, 9). The second pathway involve one-electron oxidation, catalyzed by CYP or peroxidases, at the most electrophilic carbon of BaP (C6) and form radical cations (10). Radical cations are known to form depurinating

adducts with guanine and adenine (10-12). More recently, dihydrodiol dehydrogenases were suggested to catalyze the oxidation reactions converting BaP-7,8-dihydrodiol (7,8-diol) to BaP-7,8-hydroquinone (13). BaP-7,8-hydroquinone is unstable and undergoes autoxidation to form BaP-7,8-dione. The autoxidation of BaP-7,8-hydroquinone also results in the formation of an *o*-semiquinone anion radicals, hydrogen peroxide and superoxide anion, which can all cause DNA damages. BaP-7,8-dione can also form covalent bonds with DNA (13).

In addition to the pathways described above, BaP metabolism constitutes a complex reaction network in mammalian system. The overall BaP metabolism in mammals is summarized in Figure 2.2. BaP is first oxidized at several aromatic bonds to form BaP-oxides via reactions catalyzed by CYP. The major BaP-oxides formed in the presence of mammalian CYP are 2,3-oxide, 4,5-oxide, 7,8-oxide, and 9,10-oxide (14). Once BaP-oxides are formed, they can undergo the following three reactions: (i) abiotic rearrangement to hydroxyl-BaP spontaneously through NIH shift (15); (ii) hydrolysis catalyzed by EH to form trans-dihydrodiols; and (iii) conjugation with glutathione followed by excretion. 2,3-Oxide preferentially undergoes NIH shift and forms 3-hydroxy-BaP (16). 4,5-Oxide is hydrolyzed to form 4,5-diol with no evidence of the formation of 4- or 5- hydroxyl-BaP in vivo (17). 4,5-Oxide is a good substrate for glutathione S-transferase in human (18, 19) and rat (20) livers, while 7,8-oxide and 9,10-oxide are poor substrates in rat liver (20). 7,8-Oxide and 9,10-oxide undergo both NIH shift and hydrolysis reactions to form 7-hydroxy-BaP, 7,8-diol, 9-hydroxy-BaP, and BaP-9,10-dihydrodiol (9,10-diol). Hydroxy-BaP may, in turn, undergo conjugations including

glucuronidation (21) and sulfation (22). 3-hydroxy-BaP might also undergoes non-enzymatic oxidation reactions to form BaP-3,6-dione (23).

As described above, 7,8-diol can undergo epoxidation and dehydrogenation. Bay-region dihydrodiol epoxides, *e.g.* BaP-7,8-dihydrodiol-9,10-epoxide, are unusually reactive to biological macromolecules. The reactivity of these compounds is related to their resistance to enzymatic detoxification (24). It was reported that BaP-9,10-diol-7,8-epoxide and BaP-7,8,9,10-tetrols were the major metabolites of 9,10-diol in hamster embryo cells (25) and in hamster lung (26), but not in rat liver metabolizing systems (27). The non-bay-region dihydrodiol epoxides may hydrolyze spontaneously to tetrahydrotetrols or conjugate with glutathione (5). 7,8-Diol, 9,10-diol, 4,5-diol were converted into glucuronic acid conjugates in cultured rodent trachea (22). 9,10-diol also formed sulphuric acid conjugates in cultured hamster trachea (22). 1,9,10-Trihydroxy-9,10-dihydro-BaP and/or 3,9,10-trihydroxy-9,10-dihydro-BaP were detected when a high concentration of 9,10-diol was incubated with rat microsomes (29).

The radical cation formed via one-electron oxidation can undergo additional reactions catalyzed by CYP and form 6-hydroxy-BaP (6-OH), a labile metabolite of BaP (28-30). 6-OH then undergoes non-enzymatic oxidation and forms BaP-1,6-dione, BaP-3,6-dione, and BaP-6,12-diones (28, 29).

## **References**

1. Phillips DH. Fifty years of benzo(a)pyrene. *Nature* 303:468-72(1983).
2. Cook JW, Hewett CL, Hieger I. The isolation of a cancer-producing hydrocarbon from coal tar. *J Chem Soc*:395-405(1933).
3. Miller KP, Ramos KS. Impact of cellular metabolism on the biological effects of benzo[a]pyrene and related hydrocarbons. *Drug Metab Rev* 33:1-35(2001).

4. Hattemer-Frey HA, Travis CC. Benzo-a-pyrene: environmental partitioning and human exposure. *Toxicol Ind Health* 7:141-157(1991).
5. Harvey RG. Polycyclic Aromatic Hydrocarbons: Chemistry and Carcinogenicity. Cambridge:Cambridge University Press, 1991.
6. Levin W, Wood A, Chang R, Ryan D, Thomas P, Yagi H, Thakker D, Vyas K, Boyd C, Chu SY, Conney A, Jerina D. Oxidative metabolism of polycyclic aromatic hydrocarbons to ultimate carcinogens. *Drug Metab Rev* 13:555-580(1982).
7. Cooper CS, Grover PL, Sims P. The metabolism and activation of benzo[a]pyrene. In: *Progress in Drug Metabolism, Volume 7* (Bridges JW, Chasseaud LF, eds). Chichester:John Wiley & Sons, 1983;295-396.
8. Koreeda M, Moore PD, Wislocki PG, Levin W, Yagi H, Jerina DM. Binding of benzo[a]pyrene 7,8-diol-9,10-epoxides to DNA, RNA, and protein of mouse skin occurs with high stereoselectivity. *Science* 199:778-81(1978).
9. Osborne MR, Thompson MH, Tarmy EM, Beland FA, Harvey RG, Brookes P. The reaction of 7,8-dihydro-7,8-dihydroxybenzo (a) pyrene-9,10-oxide with DNA in relation to the benzo (a) pyrene-DNA products isolated from cells. *Chem Biol Interact* 13:343-8(1976).
10. Cavalieri EL, Rogan EG. Central role of radical cations in metabolic activation of polycyclic aromatic hydrocarbons. *Xenobiotica* 25:677-688(1995).
11. Devanesan PD, RamaKrishna NV, Todorovic R, Rogan EG, Cavalieri EL, Jeong H, Jankowiak R, Small GJ. Identification and quantitation of benzo[a]pyrene-DNA adducts formed by rat liver microsomes in vitro. *Chem Res Toxicol* 5:302-309(1992).
12. Devanesan PD, Higginbotham S, Ariese F, Jankowiak R, Suh M, Small GJ, Cavalieri EL, Rogan EG. Depurinating and stable benzo[a]pyrene-DNA adducts formed in isolated rat liver nuclei. *Chem Res Toxicol* 9:1113-1116(1996).
13. Penning TM, Burczynski ME, Hung CF, McCoull KD, Palackal NT, Tsuruda LS. Dihydrodiol dehydrogenases and polycyclic aromatic hydrocarbon activation: generation of reactive and redox active o-quinones. *Chem Res Toxicol* 12:1-18(1999).
14. Gelboin HV. Benzo[α]pyrene metabolism, activation and carcinogenesis: role and regulation of mixed-function oxidases and related enzymes. *Physiol Rev* 60:1107-1166(1980).
15. Jerina DM, Daly JW. Arene oxides: a new aspect of drug metabolism. *Science* 185:573-582(1974).
16. Yang SK, Roller PP, Fu PP, Harvey RG, Gelboin HV. Evidence for a 2,3-epoxide as an intermediate in the microsomal metabolism of benzo[a]pyrene to 3-hydroxybenzo[a]pyrene. *Biochem Biophys Res Commun* 77:1176-82(1977).
17. Osborne MR, Crosby NT. Benzopyrenes. Cambridge:Cambridge University Press, 1987.
18. Nemoto N, Gelboin HV, Habig WH, Ketley JN, Jakoby WB. K region benzo(a)pyrene-4,5-oxide is conjugated by homogeneous glutathione S-transferases. *Nature* 255:512(1975).

19. Warholm M, Guthenberg C, Mannervik B, von Bahr C. Purification of a new glutathione S-transferase (transferase  $\mu$ ) from human liver having high activity with benzo(a)pyrene-4,5-oxide. *Biochem Biophys Res Commun* 98:512-9(1981).
20. Waterfall JF, Sims P. Epoxy derivatives of aromatic polycyclic hydrocarbons. The preparation and metabolism of epoxides related to benzo(a)pyrene and to 7,8- and 9,10-dihydrobenzo(a)pyrene. *Biochem J* 128:265-77(1972).
21. Nemoto N, Gelboin HV. Enzymatic conjugation of benzo (a) pyrene oxides, phenols and dihydrodiols with UDP-glucuronic acid. *Biochem Pharmacol* 25:1221-6(1976).
22. Moore BP, Cohen GM. Metabolism of benzo(a)pyrene and its major metabolites to ethyl acetate-soluble and water-soluble metabolites by cultured rodent trachea. *Cancer Res* 38:3066-75(1978).
23. Selkirk JK, Croy RG, Roller PP, Gelboin HV. High-pressure liquid chromatographic analysis of benzo( $\alpha$ )pyrene metabolism and covalent binding and the mechanism of action of 7,8-benzoflavone and 1,2-epoxy-3,3,3-trichloropropane. *Cancer Res* 34:3474-3480(1974).
24. Josephy PD. Polycyclic aromatic hydrocarbon carcinogenesis. In: *Molecular Toxicology* (Josephy PD, ed). New York:Oxford University Press, 1997;315-351.
25. MacLeod MC, Kootstra A, Mansfield BK, Slaga TJ, Selkirk JK. Specificity in interaction of benzo[a]pyrene with nuclear macromolecules: implication of derivatives of two dihydrodiols in protein binding. *Proc Natl Acad Sci U S A* 77:6396-400(1980).
26. Cohen GM, Moore BP. The metabolism of benzo(a)pyrene, 7,8-dihydro-7,8-dihydroxybenzo(a)pyrene and 9,10-dihydro-9,10-dihydroxybenzo(a)pyrene leads to (a)pyrene by short-term organ cultures of hamster lung. *Biochem Pharmacol* 26:1481-7(1977).
27. Booth J, Sims P. Different pathways involved in the metabolism of the 7,8- and 9,10-dihydrodiols of benzo(a)pyrene. *Biochem Pharmacol* 25:979-80(1976).
28. Lesko S, Caspary W, Lorentzen R, Ts'o POP. Enzymic formation of 6-oxobenzo[a]pyrene radical in rat liver homogenates from carcinogenic benzo[a]pyrene. *Biochemistry* 14:3978-3984(1975).
29. Lorentzen RJ, Caspary WJ, Lesko SA, Ts'o POP. The autoxidation of 6-hydroxybenzo[a]pyrene and 6-oxobenzo[a]pyrene radical, reactive metabolites of benzo[a]pyrene. *Biochemistry* 14:3970-3977(1975).
30. Cavalieri EL, Rogan EG, Cremonesi P, Devanesan PD. Radical cations as precursors in the metabolic formation of quinones from benzo[a]pyrene and 6-fluorobenzo[a]pyrene. Fluoro substitution as a probe for one-electron oxidation in aromatic substrates. *Biochem Pharmacol* 37:2173-2182(1988).

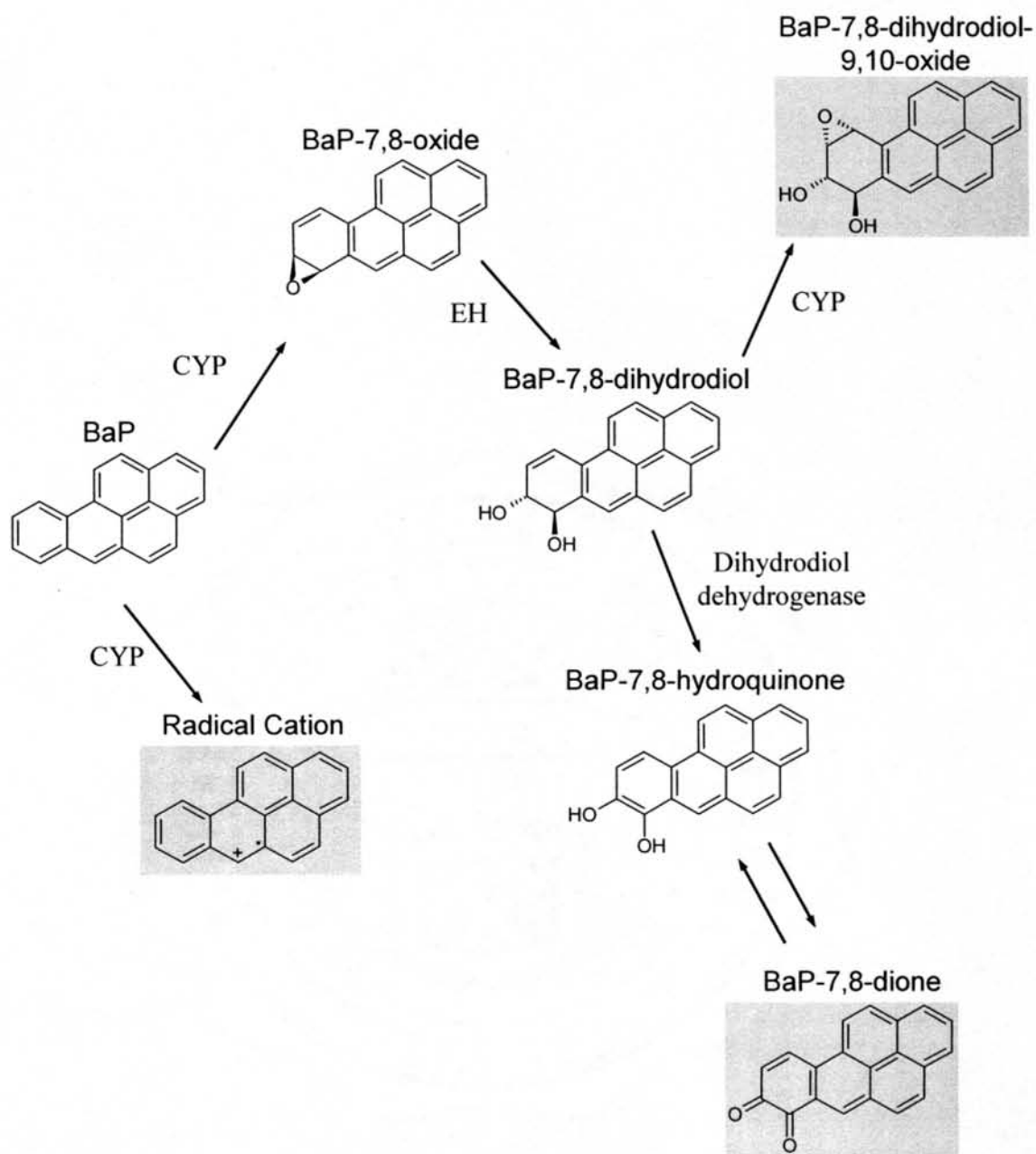


**Figure 2.1.** Metabolic activation pathways of benzo[a]pyrene (BaP). The shaded structures are the reactive metabolites that can damage biological macromolecules. CYP: cytochrome P450; EH: epoxide hydrolase.

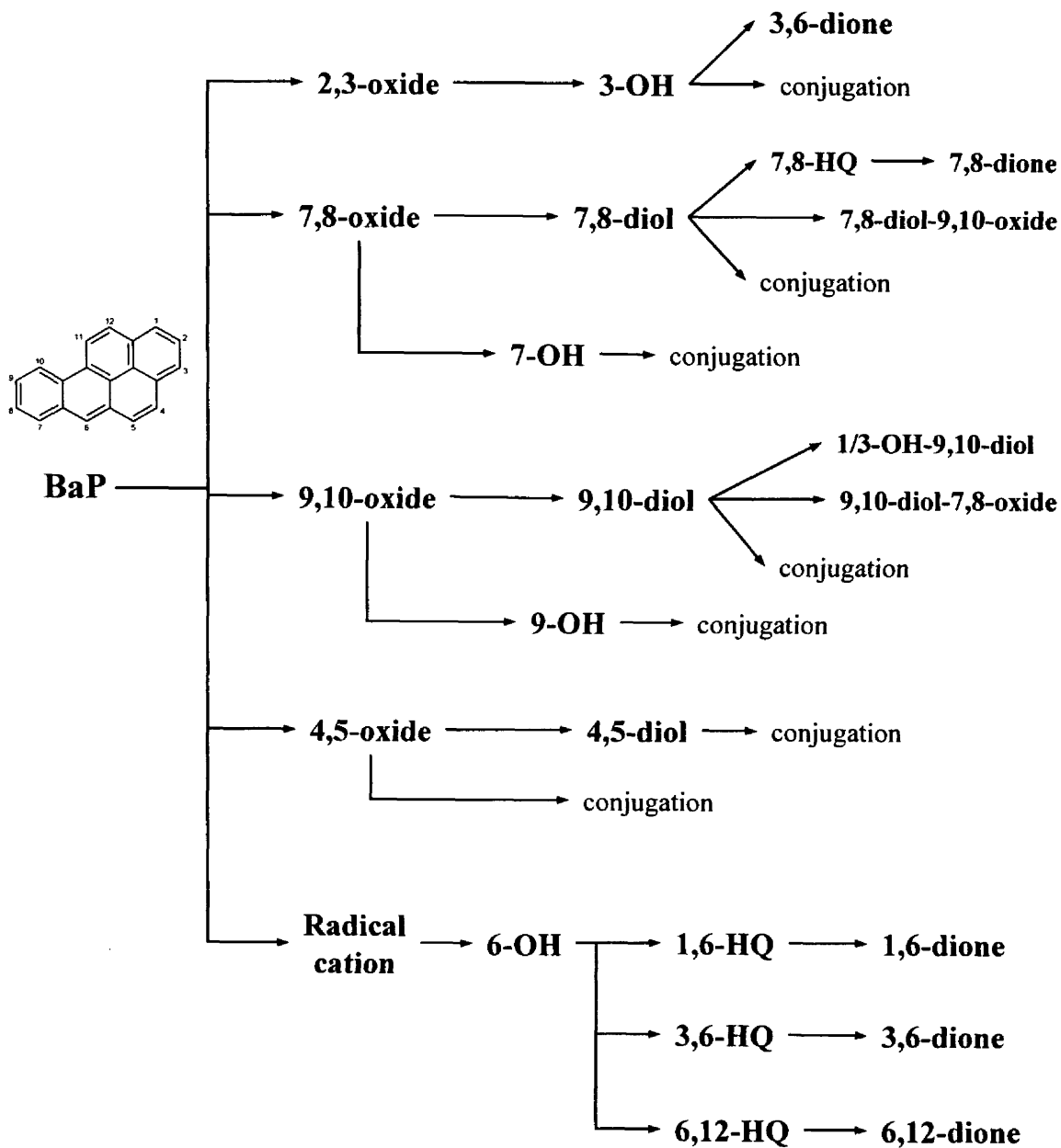


**Figure 2.2.** Mammalian metabolism of benzo[a]pyrene (BaP). Oxide: BaP-dihydroepoxide; OH: hydroxy-BaP; diol: BaP-dihydrodiol; HQ: BaP-hydroquinones.

## **Chapter 3.**

### **Application of Biologically Based Computer Modeling to Simple or Complex Mixtures**

#### **3.1. Introduction**

People are likely to be exposed to chemical mixtures instead of single chemicals from environmental pollution at hazardous waste sites, and thus risk assessments for chemical mixtures are crucial. However, given the current number of existing chemicals and those invented each year, it is not possible to study the toxicological effects for every possible chemical mixture in the environment. In this chapter, we proposed several computational approaches, including Reaction Network (RN) modeling, to serve as powerful tools to predict the toxicological effects of chemical mixtures. The RN modeling approach can be potentially used to predict the complex biotransformation reactions of chemical mixtures. This approach is briefly introduced in this chapter using benzo[*a*]pyrene (BaP) metabolic pathways as an example and is discussed in greater details in Chapters 4 and 7. Furthermore, the concept of linking RN and physiologically base pharmacokinetic (PBPK) models is introduced in this chapter using 5-fluorouracil, a chemotherapeutic agent, as an example, while the development and validation of the RN/PBPK model for BaP is discussed in Chapter 8. The following text has been

published in the journal of *Environmental Health Perspectives*, Volume 110, Supplement 6, pages 957-963 (2002).

### **3.2. Abstract in the Original Publication**

The complexity and the astronomic number of possible chemical mixtures preclude any systematic experimental assessment of toxicology of all potentially troublesome chemical mixtures. Thus, the use of computer modeling and mechanistic toxicology for the development of a predictive tool is a promising approach to deal with chemical mixtures. In the past 15 years or so, physiologically based pharmacokinetic/pharmacodynamic (PBPK/PD) modeling has been applied to the toxicologic interactions of chemical mixtures. This approach is promising for relatively simple chemical mixtures; the most complicated chemical mixtures studied so far using this approach contained five or fewer component chemicals. In this presentation we provide some examples of the utility of PBPK/PD modeling for toxicologic interactions in chemical mixtures. The probability of developing predictive tools for simple mixtures using PBPK/PD modeling is high. Unfortunately, relatively few attempts have been made to develop paradigms to consider the risks posed by very complex chemical mixtures such as gasoline, diesel, tobacco smoke, etc. However, recent collaboration between scientists at Colorado State University and engineers at Rutgers University attempting to use reaction network modeling has created hope for the possible development of a modeling approach with the potential of predicting the outcome of toxicology of complex chemical mixtures. We discuss the applications of reaction network modeling in the

context of petroleum refining and its potential for elucidating toxic interactions with mixtures.

### **3.3. Introduction in the Original Publication**

One question frequently asked in the area of toxicology of chemical mixtures is, “How does one deal with a complex chemical mixture?” Here, when we discuss complex chemical mixtures, we are referring to something such as the smoke from the burning oil fields in Kuwait during the Persian Gulf War. That smoke not only contains hundreds or even thousands of chemicals but also has the characteristics of changing composition with time. When we say “deal with,” we are referring to a systematic way of deducing the composition of the complex chemical mixture as well as the effect(s) from exposure to such a complex chemical mixture. In other words, we are implying some sort of predictive capability. For many years even the eternal optimists have not been able to provide a reasonable answer to this question, though we believe intuitively that there might be a solution to this complex problem.

Soon after the last mixture conference at Colorado State University (1), we felt, for the first time since our involvement with chemical mixture research, that there is hope in dealing with complex chemical mixtures. The approach we are advocating is integrated computer modeling of complex biologic processes. In this article we begin the discussion with some background information, present some recent successes in computer modeling of relatively simple chemical mixtures (i.e., fewer than five chemicals), and then conclude the discussion by introducing reaction network modeling and its integration into physiologically based pharmacokinetic/pharmacodynamic (PBPK/PD) modeling.

### **3.4. Experimental and Computational Approaches**

#### *3.4.1. Chemical Mixtures and Multiple Stressors*

Just as we cannot ignore the scientific issues on chemical mixtures because they are complex, we should not be looking at chemicals alone when we are interested in the global issue of public health. The Gulf War syndrome taught us to look beyond the chemicals into the area of multiple stressors (2,3). Thus, the smoke in the burning oil field is but one piece of the puzzle in the overall assessment of Gulf War syndrome (2,3).

A more detailed discussion on multiple stressors was given elsewhere (3). Briefly, any chemical, physical, or biologic insult on the body is a form of stress; therefore, multiple stressors include chemicals, drugs, and physical and biologic agents. However, in the context of the Gulf War syndrome, multiple stressors may also include environmental hardship (e.g., extreme heat, poor resting conditions, poor food or water intake, heavy and nonbreathable equipment and clothing, insect or other pests), occupational hazard (e.g., dangerous tasks; injuries from work; exposure to fuels, burning oil fields, possible nerve gases, radioactive residues), and psychological stress (e.g., threat of death and injuries, fear of exposure to chemical and biologic warfare agents, being away from home, poor living conditions).

If chemical mixtures are already sufficiently complicated, would not the addition of multiple stressors render the situation impossible? Indeed it might. However, our thinking is that although the number of combinations of chemicals or stressors is infinite, the number of biologic processes is finite. Therefore, in considering an integrated

computer modeling approach, we must work on the finite biologic processes rather than the infinite combinations of chemicals and stressors.

#### *3.4.2. Simple Chemical Mixtures: Interaction Thresholds*

We first demonstrate one utility of PBPK modeling by estimating the threshold point for toxicologic interactions in the low occupational exposure region. Co-exposure to multiple chemicals may significantly affect the pharmacokinetics of one or more mixture components and alter the target tissue dose of the toxic moiety. In 1996 we introduced the idea of interaction thresholds as the minimal level of change in tissue dosimetry associated with a significant health effect (4). When two or more interactive chemicals are studied together, theoretically there could be infinite interaction thresholds. This is because, in the case of a binary or higher-order chemical mixtures, if we vary the concentrations of two or more chemicals, we would get, theoretically, an infinite number of interaction thresholds. However, if we specify certain occupational or environmental exposure concentrations for all the other chemicals in the mixture except one, we may obtain an interaction threshold for that set of exposure conditions. This is important because human risk from exposure to multiple chemicals may not always obey the rule of additivity. In a 2001 publication from our laboratory (5), Dobrev et al. estimated the interaction thresholds of three common volatile organic solvents, trichloroethylene (TCE), tetrachloroethylene (perchloroethylene, PERC), and 1,1,1-trichloroethane (methyl chloroform, MC), under different dosing conditions. Briefly, an interactive PBPK model was built where PERC and MC are competitive inhibitors for TCE. The model was developed and validated by gas uptake pharmacokinetic studies in Fischer 344 (F344)

(Harlan Sprague Dawley, Indianapolis, IN, USA) rats at relatively high doses of single chemicals, binary mixtures, and the ternary mixture. Using computer simulation to extrapolate from high to low concentrations, we investigated the toxicologic interactions at occupational exposure levels, specifically at around threshold limit value/time-weighted average (TLV/TWA). Because long-term toxicity and carcinogenicity of these three solvents are clearly associated with their metabolism, and TCE is the most extensively metabolized among them, we focused our study on changes in internal TCE dose measures related to the mixture coexposure. Using a 10% elevation in parent compound blood level as a criterion for significant interaction, we estimated interaction thresholds with two of the three chemicals remaining at constant concentrations. Thus, we fixed the TCE and PERC exposure concentrations in the gas uptake pharmacokinetic studies to 50 and 25 ppm, respectively, their TLVs/TWAs, and estimated the interaction threshold by varying the exposure concentration of MC to 0, 100, 130, 175, 250, or 350 ppm (350 ppm is the TLV for MC). This latter work is based on computer simulations using the interactive PBPK model; thus, it is experimentation *in silico*. Dobrev et al. (5) reported that under the above exposure conditions (i.e., TCE and PERC at their TLVs), the interaction threshold for the ternary mixture is 50, 130, and 25 ppm for TCE, MC, and PERC, respectively. If one wishes to use a higher criterion than 10% elevation in blood level for interaction threshold, Dobrev et al. (5) provide possible interaction thresholds for 17% (50, 250, 25 ppm for TCE, MC, PERC) and 22% (50, 350, 25 ppm for TCE, MC, PERC) elevations in blood level of TCE. This work has recently been extended, *in silico*, to human exposure to this three-chemical mixture and the estimation of interaction thresholds for humans (6).

### 3.4.3. Simple Chemical Mixtures: Mixture Formula

In the derivation of an occupational exposure limit (OEL) of chemical mixture exposure, the general approach is to first determine if those chemicals in the mixture cause similar toxic responses and then to implement the “mixture formula” (Equation 3.1) to assess if the exposure might be problematic.

$$E_m = \sum \frac{Exposure_i}{OEL_i}, \quad (3.1)$$

The mixture formula, also referred to as the “unity calculation” (denoted  $E_m$ ), calculates the ratio of worker exposure to OEL for each chemical in the mixture. If the sum of these ratios exceeds unity (1.0), an overexposure is suggested. The potential problems with this approach are that it assumes additivity, and pharmacokinetics and pharmacodynamics are not taken into consideration. To illustrate these points, Dennison et al. (7,8) first modified the  $E_m$  by incorporating PBPK modeling and came up with a new pharmacokinetically based  $E_m$ , the  $E_m^{PK}$ , shown in Equation 3.2:

$$PK * E_m = \sum \frac{C_{i,mixture}}{C_{i,OEL}}, \quad (3.2)$$

where  $C_i$  is the concentration of the chemical in the target tissue (obtained through PBPK modeling) either during an exposure to mixtures or to the OEL for the single chemical.

As with the  $E_m$  formula, the  $E_m^{PK}$  is a summation of ratios of the doses for the chemical in a mixture to those of the single chemicals. Using an established PBPK model for alkylsubstituted benzenes published by Tardiff et al. (9), Dennison et al. (7,8) took into consideration both pharmacokinetics and the interactive enzyme inhibition among the component chemicals in the mixture. Dennison et al. (7,8) then gave a few case studies,

one of which is reproduced in Table 3.1, to illustrate the differences between the conventional  $E_m$  approach versus the  $E_m^{PK}$  approach.

As shown in Table 3.1, Dennison et al. (7,8) provided five hypothetical chemical mixtures by varying the concentrations of the three component chemicals, toluene, ethylbenzene, and xylenes. The four columns of data on the left are for the  $E_m$  approach and the four columns of data on the right are derived from the  $E_m^{PK}$  approach. Mixtures 2–5 are all at allowable exposure concentrations under the present  $E_m$  approach because the  $E_m$  values derived are all under unity. However, when we take pharmacokinetics (tissue dosimetry from PBPK modeling) and pharmacodynamics (critical effects) into consideration, we see an immediate problem, which is explained below.

Critical effects for toluene and ethylbenzene, which are used to set the OELs, include depression of the central nervous system. Because it is not clear if xylene also causes such a critical effect, under the  $E_m$  approach, xylene is not considered in the derivation of  $E_m$ . This results in the  $E_m$  values being less than unity in mixtures 2–5. However, as xylene interferes with the metabolism of toluene and benzene thereby increasing their tissue dosimetry, the  $E_m^{PK}$  derived in mixtures 2–5 went over unity by about 1.2- to 3-fold (Table 3.1). Thus, under the  $E_m^{PK}$  approach, these mixtures would have been unallowable. This exercise demonstrates some inadequacies in current risk assessment methodology for chemical mixtures.

#### *3.4.4. A Ray of Hope for Complex Chemical Mixtures: Reaction Network Modeling*

##### **3.4.4.1. Reaction network modeling and its application to petroleum engineering.**

Reaction network modeling has been used very successfully in the area of petroleum and

chemical engineering for very complex chemical processes involving hundreds and even thousands of chemicals. It had never been applied to biology until the interdisciplinary collaborative effort between Colorado State University and Rutgers University. To appreciate the potential of this modeling approach, it is helpful to understand its historical development.

Reaction network modeling in the fields of chemical and petroleum engineering has progressed greatly over the past 25 years, including developments in the areas of group contribution methods (10), graph theory (11,12), Monte Carlo techniques (13–15), and quantum chemistry (16,17).

Intense activity in molecular reaction engineering has generated several approaches to the creation of molecular reaction models by computer (18–23). The essential idea is to input some representation of reactant structure and chemical reaction. Algorithms and grammar for representing and determining species connectivity, uniqueness, and relationships (the reaction network) create an output that is, in some form, the controlling kinetic equation (governing ordinary differential equations) for the reaction model.

Developing a fundamental kinetic scheme requires modeling of the chemistry at the mechanistic level. This, in turn, leads to a large number of species, reactions in the governing network, and associated rate constants. Therefore, although a mechanistic model incorporating detailed molecular representations and fundamental kinetic data is needed, the inherent complexity and size of such a model is a deterrent to its development. This motivates a simplification of the system through the organization of

species into related families of compounds and the automation of not only the solution but also the construction of the model.

In an attempt to describe hydrocarbon mixture properties, early models relied on the techniques of lumping (24), where a relatively small number of lumps were used to describe the mixture. In these coarsely lumped kinetic models, thousands of individual constituents in a complex feedstock were grouped into broad but measurable categories of compound classes or boiling range, with simplified reaction networks between the lumps.

More recently, Quann and Jaffe (23) developed a more fine-grained lumping approach they named structure-oriented lumping (SOL). SOL was developed in response to the need for incorporating molecular detail in petroleum chemistry to predict product compositions and properties. It is a group contribution method describing the structure of molecules, facilitating both molecular property estimation and a description of process chemistry. It was also designed to be consistent with current limitations of analytic capability to determine molecular detail. The concept central to the SOL approach is that any molecule can be described and represented by a set of certain structural features or groups. The SOL method organizes this set as a vector, with the elements of the vector representing the number of specific structural features sufficient to construct any molecule. Different molecules with the same set of structural groups, i.e., certain isomers, are lumped and represented by the same vector. The structure vector provides a framework to enable rule-based generation of reaction networks and rate equations involving thousands of components and many thousands of reactions.

An even finer-grain methodology was developed by Broadbelt and co-workers (16,25,26), who used concepts of graph theory to represent species connectivity. They also made use of computational quantum chemistry (CQC) and linear free-energy relationships (LFERs) (27) to automate the process of determining reaction rate constants. CQC was applied to determine the optimal conformation and molecular properties, such as the electron affinity, electron density, bond order, and heat of formation, associated with each of reactant and product structures (17,28). LFERs were then used to give a correlation of the rate or equilibrium constants with a property of a molecule or intermediate for a family of reactions. Thus, the CQC calculations ultimately provided an estimate of rate or equilibrium coefficients for reactants that had not been studied experimentally.

This general framework, which Klein (29) refers to as the kinetic modeler's toolbox (KMT), allows for the convenient construction and solution of even highly complex chemical reaction networks. Using this approach, various investigators have been able to encode complex hydrocarbon mixtures and create rule sets for a wide variety of reactions within the mixture. Results from model simulations (2,30) have shown good agreement with experimental observations in tracking the evolution of thousands of molecular components, then predicting mixture properties such as normal boiling points, specific gravity, and narrow boiling-cut yields. Joshi and co-workers (22) made use of the KMT for the analysis of gas oil catalytic cracking and were able to derive optimized parameter values (activation energies and frequency factors) and lumped fractions that were in good agreement with experimental results reported in the literature. Along similar lines, Mizan and Klein (31) found good agreement in terms of product yields and yield

profiles between simulation results and experimental data in the reaction network modeling of *n*-hexadecane hydroisomerization.

Reaction network modeling is a tool for predicting the amounts of reactants, intermediates, and products as a function of time for a series of coupled chemical reactions (potentially numbering in the tens of thousands of reactions for some systems). It is usually a mathematic and symbolic formulation suitable for solution on the computer. A reaction network model builder is a tool for the computer generation of a reaction network model. The model builder thus can be used not only to solve the kinetic equations of interest but also to generate the reaction mechanisms, rate constants, and reaction equations themselves.

Essentially, the model builder works as follows:

- The concentrations of the species to be reacted or metabolized are input to the model builder.
- For each species in turn, the model builder performs a test against each of a set of reaction rules to determine whether the species is susceptible to a particular chemical reaction.
- If it is not susceptible to any reactions, no further action is taken on this species.
- If it is susceptible, a transformation of the species into one or more product species is performed based on the particular chemical reaction.
- Each of these product species then undergoes the same susceptibility tests and a similar transformation sequence. This leads to a linking of all reactants with intermediate and ultimately with final products. This linking forms the structure of the chemical reaction network.

- After the reaction network is established, the rate constants for the reactions are retrieved or computed.
- The coupled differential equations governing the reaction kinetics for the network are then formulated by the model builder.

Finally, the kinetic equations, i.e., the model equations, are solved numerically, leading to the concentrations of all species as a function of time. For those interested in a more specific, detailed description of reaction network modeling, the article by Klein et al. in this monograph (32) should be consulted.

**3.4.4.2. Reaction network modeling and its application to biomedical research.** It is important to note that metabolism and toxic mechanisms of chemicals and chemical mixtures often involve complex reactions in which the species associated with one reaction are constituents of many other reactions. Interactions among chemicals are common, and this interplay among reaction pathways is the primary reason for toxicologic interaction. This interdependent, coupled set of biochemical reactions can be regarded as a reaction network and can occur for even relatively simple systems.

In the collaborative research effort between our laboratory (the Quantitative and Computational Toxicology Group) and Klein's group at Rutgers University, we intend to apply reaction network modeling to the metabolic pathways of complex mixtures in biologic systems. The approach and the modeling software being developed is "BioMOL," where "bio" represents biologic and "MOL" is the acronym for molecule-oriented lumping. The framework of KMT has served as the starting point to build BioMOL. Our first application is reaction network modeling of BaP. The metabolic

pathway of BaP in a biologic system is used to build the first model by BioMOL. We use BaP because *a*) BaP is a human carcinogen; *b*) its metabolic pathway is extremely complex but extensively studied; and *c*) the reactions BaP undergoes, e.g., epoxidation and hydrolysis, are also common for other xenobiotics, especially polycyclic aromatic hydrocarbons. BaP is metabolically activated to its ultimate carcinogen, BaP-7,8-dihydrodiol-9,10-epoxide, via a series of reactions catalyzed by cytochrome P450 and epoxide hydrolase (Figure 3.1) (33–35). In addition to the formation of BaP-7,8-dihydrodiol-9,10-epoxide, BaP metabolism constitutes a complex reaction network in biologic systems. Briefly, BaP is first oxidized at several aromatic bonds to form arene oxides via reactions catalyzed by cytochrome P450. Once arene oxides are formed, they can undergo the following three reactions: *a*) rearrangement to phenols spontaneously through an NIH shift (36); *b*) hydrolysis catalyzed by epoxide hydrolase to form *trans*-dihydrodiols; and *c*) conjugation with glutathione, followed by excretion. Dihydrodiols might again form the corresponding epoxides in a reaction catalyzed by cytochrome P450 or undergo sulfation and glucuronidation. Bay-region dihydrodiol epoxides, e.g., BaP-7,8-dihydrodiol-9,10-epoxide, are unusually reactive to biologic macromolecules. The reactivity of these compounds is related to their resistance to enzymatic detoxification (37). The non-bay-region dihydrodiol epoxides may hydrolyze spontaneously to tetraols or conjugate with glutathione (33). The phenols may, in turn, be oxidized to quinones or undergo conjugation (34). On the other hand, a one-electron oxidation pathway may be responsible for the formation of 6-hydroxy-BaP and subsequent metabolites 1,6-, 3,6-, and 6,12-quinones (38).

3.4.4.2.1. Generation of BaP reaction networks. To generate the reaction network at molecule level, we use graph theory to convert chemical structures and reaction rules into computer code. The atomic connectivity of the molecule is represented by the bond–electron matrix. In bond–electron matrices, the off-diagonal elements denote the bond order between two atoms, and the diagonal elements represent the unpaired electron (e.g., free radicals). The structure changes of molecules caused by chemical reactions can also be described by graph theory, i.e., the reaction matrix. Most reactions involve the change of connectivity between only few atoms. Therefore, reaction matrices can be used as a compact representation of bond formation and breakage caused by chemical reactions. The addition of the reaction matrix to the reduced reactant bond–electron matrix, which consists of only the atoms involved in the reaction, forms a new matrix representing the product of the reaction (i.e., product matrix). The epoxidation of an aromatic bond is used as an example to describe the matrix operation of a chemical reaction (Figure 3.2). The product is then checked for its uniqueness to ensure the molecule was not previously created by other reactions. If the product is unique, it is added to the unreacted species list and could become the candidate reactant for other reactions.

The reaction rule, determined by modeler’s understanding the fundamental chemistry and biochemistry of the reaction, plays a central role in the model. Following the reaction rules, BioMOL can search the eligible site of reaction throughout the structure of possible reactants and create the corresponding product by means of the matrix operator. The reaction sites and matrices for major metabolic pathways of BaP are summarized in Table 3.2. Any double bond in BaP is eligible for the epoxidation reaction. However, certain restrictions should be applied in the reaction rule to eliminate

unrealistic products. For instance, arene oxides are unstable and not likely to stay long enough to undergo the second consecutive epoxidation reaction. Instead, arene oxides are more likely to be a substrate for hydrolysis, NIH shift, and glutathione conjugation (Table 3.2). To form the ultimate carcinogenic metabolite BaP-7,8-dihydrodiol-9,10-epoxide, BaP should encounter two distinct epoxidation reactions. In the BioMOL model, these two steps use the same reaction rule and reaction matrix operator. The only difference is that the rule and matrix are applied to distinct reactants, namely, BaP and BaP-dihydrodiol. Therefore, a complex reaction network may start from few reactions with few reaction rules.

3.4.4.2.2. Estimation of BaP metabolic reaction rate constants. By applying the given reaction rule, the BioMOL model generates all the possible reactions and corresponding products. Some of the products may never be observed because the reaction rates are either too low for their formation or too fast for their subsequent metabolism. BioMOL will use quantitative structure/reactivity correlations (QSRCs) to estimate the reaction rate constants ( $k_i$ ). QSRCs are semiempiric methods in which sterically similar reactions are lumped into reaction families. The idea of this correlation is expressed by the following equation:

$$\log k_i = a_j + b_j * RI_i \quad (3.3)$$

where  $i$  is a component in the reaction family  $j$ .  $RI$  represents the reactivity index. The parameters  $a$  and  $b$  are calibrated by experimental data (39). The candidates for the reactivity index of BaP biotransformation are heat of reaction,  $\pi$ -electron density, and bond order. Semiempiric quantum chemistry software like MOPAC 2000 (Schrodinger,

Portland, OR, USA), which is integrated into the BioMOL model, can calculate these reactivity indices.

To calculate the reaction rate based on QSRCs, the rate constants for BaP metabolic activation have been divided into four groups, enzymatic, nonenzymatic, association, and dissociation (Figure 3.3). The QSRCs for enzymatic rate constants rely on the understanding of the chemical mechanism. For instance, the enzymatic epoxidation of double bonds catalyzed by cytochrome P450 is likely to start with the formation of a charge-transfer complex between the ferryl oxygen on P450 and  $\pi$  bond on the substrate (40). Therefore, the rate constants of the enzymatic epoxidation at distinct positions of BaP are expected to correlate with bond order of the reaction site. Loew et al. (41) have shown a qualitative correlation between the observed BaP metabolites and  $\pi$ -bond reactivity calculated by quantum chemistry. The relative abundance of the two possible phenol products resulting from an NIH shift also correlated with the electron densities of the carbon atoms attached to oxygen (41). On the other hand, the nonenzymatic reaction rate constant may correlate with the heat of reaction. The real challenge for QSRCs is the search of reactivity indices for association and dissociation constants. The binding of substrates to enzymes is related to the three-dimensional structure of both the substrate and the enzyme, which is not fully understood. Our laboratory is currently developing the QSRCs from both analytic experiments and literature data. After reaction families are defined, the kinetics of the reaction network become accessible by using QSRC-derived parameters and reactivity indices to represent thousands of rate constants.

In summary, BioMOL is a computer assisted modeling tool and a promising approach to handling extremely complex biologic systems and their related biochemical reactions and reaction networks. The BioMOL model has the potential for predicting a variety of reaction networks in biologic systems, as it is molecule based. The determination of reaction rules and reaction families should be supported by a solid understanding of reaction chemistry. Fundamentals of enzymatic kinetics will help QSRC estimation of reaction rate constants.

#### *3.4.5. Future Perspective: Second-Generation PBPK/PD Models*

One of the areas of interest in our laboratory is combination chemotherapies. We are interested in any type of combination chemo therapy including cancer-, AIDS-, antibioticcombination chemotherapies, and others. Thus, we will use cancer-combination chemotherapy as an example to illustrate our thinking in future directions. As reported in the literature (42), the potential target sites for cancer-combination chemotherapies are in basic biologic processes including purine/pyrimidine metabolic pathways leading to DNA synthesis, RNA production, and protein/enzyme and microtubule production (42). These biochemical pathways are already an immensely complex system without the addition of chemotherapeutic agents. Experimentally, it is almost impossible to study such a complex system simultaneously. Therefore, it is essential to build a simulation platform that can be used to globally examine these biologic pathways in normal and malignant cells with or without chemotherapeutic agents. A variety of terms such as “virtual cells,” “virtual laboratories,” and “*in silico* experimentation” have appeared in the recent literature. Our intent, as an interdisciplinary team of scientists and engineers, is

to conduct experiments on computers, once a validated PBPK/PD model is available for these biologic pathways. With advances in computational technology, the complexity of these biologic pathways and interactions will not be a limiting factor in our understanding of the biologic foundation of combination chemotherapies.

From a modeling perspective, we believe cancer cells represent parameter changes in certain specific biologic processes inherent in normal cells. Similarly, the introduction of chemotherapeutic drugs into the cells also represents perturbations in biologic processes in normal cells. Thus, theoretically, we are proposing one PBPK/PD simulation model for the basal biologic pathways in normal cells; those same pathways in cancer cells or under combination chemotherapies are merely quantitative variations (i.e., parameter changes of certain processes) of the same model.

Our thinking goes beyond the traditional PBPK modeling. We plan to incorporate the concept of reaction network modeling by incorporating the essential biologic pathways involved. For instance, if we are studying breast cancer–combination chemotherapy, we will be adding scores of biochemical reactions into the breast tissue compartment. We will also identify specific genomic and proteomic changes in relation to the biochemical reactions to elucidate mechanistic bases for combination chemotherapies. Thus, pharmacodynamic interaction(s) will be incorporated into the PBPK modeling to transform the model to a PBPK/PD model. In that sense, we are interested in developing second-generation PBPK/PD models.

Figure 3.4 provides an example of such second-generation PBPK/PD modeling. The enzymatic pathway in Figure 3.4 is merely a small portion of the reaction network of purine/pyrimidine metabolic pathways involved in the cancer-combination

chemotherapies. Here, we summarize the mechanism of action of 5-fluorouracil (5-FU) on thymidylate synthase (TS), an important enzyme in DNA synthetic pathway, and provide the enzyme kinetics involved in TS inhibition. The kinetic equations will be incorporated into the breast tissue compartment in the PBPK model for 5-FU. The reaction rate constants for the enzymatic processes may be obtained in three different ways: *a*) by mining the literature for quantitative data (i.e., from step 1); *b*) by calculation via semiempiric quantum chemical methods based on known enzyme–substrate molecular interactions or from QSRCs (32); and *c*) by acquisition through laboratory experimentation with relevant systems. Through such integration of individual reactions into the PBPK/PD modeling process, we will be going through a “de-lumping” process analogous to that which occurred in the field of chemical engineering in the last 30 years or so. In our case we may consider that the transformation of classic compartmental pharmacokinetics into PBPK modeling represents the first stage of de-lumping—that is, going from 2 or 3 compartments to 5–10 or 15 compartments. The second-generation PBPK/PD models will mean that, in the critical compartment, further de-lumping will carry PBPK/PD modeling down to the molecular mechanism level. If we fully utilize the power of computational technology, such second-generation PBPK/PD modeling will have the potential to handle very complex biologic systems, thereby handling exposure to complex chemical, biologic, and physical agents.

### **3.5. References**

1. Yang RSH, Suk WA. Current issues on chemical mixtures. *Environ Health Perspect* 106 (suppl 6):1261-1448 (1998).

2. Jamal GA. Gulf War Syndrome - a model for the complexity of biological and environmental interaction with human health. *Adverse Drug React Toxicol Rev* 17:1-17 (1998).
3. Yang RSH. Health risks and preventive research strategy for deployed U.S. forces from toxicologic interactions among potentially harmful agents. In: *Strategies to Protect the Health of Deployed U.S. Forces: Assessing Health Risks to Deployed U.S. Forces*, Washington, DC:National Academy Press, 2000;150-182.
4. El-Masri HA, Tessari JD, Yang RSH. Exploration of an interaction threshold for the joint toxicity of trichloroethylene and 1,1-dichloroethylene: utilization of a PBPK model. *Arch Toxicol* 70:527-539 (1996).
5. Dobrev I, Andersen ME, Yang RSH. Assessing interaction thresholds for trichloroethylene, tetrachloroethylene, and 1,1,1-trichloroethane using gas uptake studies and PBPK modeling. *Arch Toxicol* 75:134-144 (2001).
6. Dobrev I, Andersen ME, Yang RSH. In silico toxicology: simulating interaction thresholds for human exposure to mixtures of trichloroethylene, tetrachloroethylene, and 1,1,1-trichloroethane. *Environ Health Perspect* 110:1031-1039 (2002).
7. Dennison JE, Andersen ME, Yang RSH. Evaluation of the mixture formula for occupational exposure to solvents. Abstract No. P-7. Conference on Application to Technology to Chemical Mixture Research, 9-11 January 2001, Colorado State University, Fort Collins, Colorado.
8. Dennison J, Andersen M, Yang R. Evaluation of the adequacy of the mixture formula (EM) in preventing overexposure to some neurotoxic gasoline components. Abstract no. 52. American Industrial Hygiene Conference and Exposition, 2-7 June 2001, New Orleans, Louisiana.
9. Tardif R, Charest-Tardif G, Brodeur J, Krishnan K. Physiologically based pharmacokinetic modeling of a ternary mixture of alkyl benzenes in rats and humans. *Toxicol Appl Pharmacol* 144:120-134 (1997).
10. Lowry TH, Richardson KS. *Mechanism and Theory in Organic Chemistry*, 3rd ed. New York:Harper & Row, 1987.
11. Biggs NL, Loyd EK, Wilson RJ. *Graph Theory*. Oxford: Clarendon, 1976;1736-1936.
12. Bonchev D, Rouvray DH. *Chemical Graph Theory Introduction and Fundamentals*. New York:Gordon & Breach Science, 1991.
13. Campbell DM, Klein MT. Construction of a molecular representation of a complex feedstock by Monte Carlo and quadrature methods. *Appl Catal A Gen* 160:41-54 (1997).
14. McDermott JB, Libanati C, LaMarca C, Klein MT. Quantitative use of a model of compound information: Monte Carlo simulations of the reactions of complex macromolecules. *Ind Eng Chem Res* 29:22-29 (1990).
15. Trauth DM, Stark SM, Petti TF, Neurock M, Klein MT. Representation of the molecular structure of petroleum resid through characterization and Monte Carlo modeling. *Energy Fuels* 8:576-580 (1994).
16. Broadbelt LJ, Stark SM, Klein MT. Computer generated reaction networks: on-the-fly calculation of species properties using computational quantum chemistry. *Chem Eng Sci* 49:4991-5010 (1994).

17. Stewart JJP. Semiempirical molecular orbital methods. In: Reviews of Computational Chemistry (Lipkowitz KB, Boyd DD, eds). New York:VCH Publishers, 1990.
18. Chevalier C, Warnatz J, Melenk H. Automatic generation of a reaction mechanism for description of oxidation of higher hydrocarbons. *Ber Bunsen-Ges Phys Chem* 94:1362–1367 (1990).
19. Clymans PJ, Froment GF. Computer-generation of reaction paths and rate equations in the thermal cracking of normal and branches paraffins. *Comp Chem Eng* 8:137–142 (1984).
20. DiMaio FP, Lignola PG. A kinetic network generator. *Chem Eng Sci* 47:2713–2718 (1992).
21. Hillerwaert LP, Dierickx JL, Froment GF. Computer generation of reaction schemes and rate equations for thermal cracking. *AIChE J* 34:17–24 (1988).
22. Joshi PV, Sadasivan DI, Klein MT. Automatic mechanistic kinetic modeling of gas oil catalytic cracking. *Rev Proc Chem Eng* 1:111–140 (1998).
23. Quann RJ, Jaffe SB. Structure-oriented lumping: describing the chemistry of complex hydrocarbon mixtures. *I&EC Res* 31:2483–2497 (1992).
24. Jacob SM, Gross B, Voltz SE, Weekman VW. A lumping and reaction scheme for catalytic cracking. *AIChE J* 22:701–713 (1976).
25. Broadbelt LJ, Stark SM, Klein MT. Computer generated pyrolysis modeling: on-the-fly generation of species, reactions, and rates. *Ind Eng Chem Res* 33:790–799 (1994).
26. Broadbelt LJ, Stark SM, Klein MT. Computer generated reaction modeling: decomposition and encoding algorithms for determining species uniqueness. *Comp Chem Eng* 20:113–129 (1996).
27. Neurock M, Klein MT. When you can't measure - model. *Chemtech* 23:26–32 (1993).
28. Stewart JJP. MOPAC Reference Manual and Release Notes, 6th ed. Colorado Springs, CO:Frank Sella Research Laboratory, U.S. Air Force Academy, 1990.
29. Klein MT. Faculty Activities Publication. Piscataway, NJ:Rutgers University (2000).
30. Quann RJ, Jaffe SB. Building useful models of complex reaction systems in petroleum refining. *Chem Eng Sci* 51:1615–1635 (1996).
31. Mizan TI, Klein MT. Computer-assisted mechanistic modeling of n-hexadecane hydroisomerization over various bifunctional catalysts. *Catal Today* 50:159–172 (1999).
32. Klein MT, Hou G, Quann RJ, Weil W, Liao KH, Yang RSH, Campaign JA, Mazurek M, Broadbelt LJ. BioMOL: a computer-assisted biological modeling tool for complex chemical mixtures and biological processes at the molecular level. *Environ Health Perspect* 110(suppl 6):1025–1029 (2002).
33. Harvey RG. Polycyclic Aromatic Hydrocarbons: Chemistry and Carcinogenicity. Cambridge, England:Cambridge University Press, 1991;50–95.
34. ATSDR. Toxicological Profile for Polycyclic Aromatic Hydrocarbons (PAH) (Update). Atlanta, GA:Agency for Toxic Substances and Disease Registry, 1995.
35. Levin W, Wood A, Chang R, Ryan D, Thomas P, Yagi H, Thakker D, Vyas

- K, Boyd C, Chu SY, et al. Oxidative metabolism of polycyclic aromatic hydrocarbons to ultimate carcinogens. *Drug Metab Rev* 13:555–580 (1982).
36. Jerina DM, Daly JW. Arene oxides: a new aspect of drug metabolism. *Science* 185:573–582 (1974).
  37. Josephy PD. Polycyclic aromatic hydrocarbon carcinogenesis. In: *Molecular Toxicology* (Josephy PD, ed). New York:Oxford University Press, 1997;315–351.
  38. Cavalieri EL, Rogan EG. Central role of radical cations in metabolic activation of polycyclic aromatic hydrocarbons. *Xenobiotica* 25:677–688 (1995).
  39. Neurock M, Klein MT. Linear free energy relationships in kinetic analyses: applications of quantum chemistry. *Polycycl Aromat Comp* 3:231–246 (1993).
  40. Josephy PD. Cytochrome P-450. In: *Molecular Toxicology* (Josephy PD, ed). New York:Oxford University Press, 1997;209–252.
  41. Loew GH, Wong J, Phillips J, Hjelmeland L, Pack G. Quantum chemical studies of the metabolism of benzo(a)pyrene. *Cancer Biochem Biophys* 2:123–130 (1978).
  42. Haskell CM. Principles of cancer chemotherapy. In: *Cancer Treatment*, 5th ed. (Haskell CM, ed). Philadelphia:W.B. Saunders, 2001;62–86.
  43. Hardy LW, Finer-Moore JS, Montfort WR, Jones MO, Santi DV, Stroud RM. Atomic structure of thymidylate synthase: target for rational drug design. *Science* 235:448–455 (1987).
  44. Voet D, Voet JG, ed. Nucleotide metabolism. In: *Biochemistry*, 2nd ed. New York:John Wiley & Sons, 1995;795–828.

**Table 3.1.** Comparison between the *Em* and our new approach of *EmPK*: a case study on OEL of chemical mixture exposure.

	Exposure Dosimetry ( $E_m$ )				Tissue Dosimetry ( $E_m^{PK}$ )			
	Toluene	Ethylbenzene	Xylene	$E_m$	Toluene	Ethylbenzene	Xylene	$E_m^{PK}$
Single Chemical	50	100	100	--	0.62	2.29	1.74	--
Mixture 1	50	100	100	2.0	1.25	3.42	3.29	5.40
Mixture 2	10	79	9	0.99	0.19	1.82	0.18	1.21
Mixture 3	10	79	99	0.99	0.23	2.34	2.84	3.02
Mixture 4	40	19	9	0.99	0.59	0.39	0.15	1.21
Mixture 5	40	19	99	0.99	0.78	0.52	2.55	2.95

**Table 3.2.** Reaction site and matrix for major metabolic pathways of BaP.

Reaction Family	Reaction Site (numbered atoms)	Reaction Matrix																																				
Epoxidation		<table border="1"> <thead> <tr> <th></th> <th>C1</th> <th>C2</th> <th>O1</th> <th>O2</th> </tr> </thead> <tbody> <tr> <th>C1</th> <td>0</td> <td>-1</td> <td>1</td> <td>0</td> </tr> <tr> <th>C2</th> <td>-1</td> <td>0</td> <td>1</td> <td>0</td> </tr> <tr> <th>O1</th> <td>1</td> <td>1</td> <td>0</td> <td>-2</td> </tr> <tr> <th>O2</th> <td>0</td> <td>0</td> <td>-2</td> <td>2</td> </tr> </tbody> </table>		C1	C2	O1	O2	C1	0	-1	1	0	C2	-1	0	1	0	O1	1	1	0	-2	O2	0	0	-2	2											
	C1	C2	O1	O2																																		
C1	0	-1	1	0																																		
C2	-1	0	1	0																																		
O1	1	1	0	-2																																		
O2	0	0	-2	2																																		
Hydrolysis		<table border="1"> <thead> <tr> <th></th> <th>C1</th> <th>O1</th> <th>O2</th> <th>H1</th> </tr> </thead> <tbody> <tr> <th>C1</th> <td>0</td> <td>-1</td> <td>1</td> <td>0</td> </tr> <tr> <th>O1</th> <td>-1</td> <td>0</td> <td>0</td> <td>1</td> </tr> <tr> <th>O2</th> <td>1</td> <td>0</td> <td>0</td> <td>-1</td> </tr> <tr> <th>H1</th> <td>0</td> <td>1</td> <td>-1</td> <td>0</td> </tr> </tbody> </table>		C1	O1	O2	H1	C1	0	-1	1	0	O1	-1	0	0	1	O2	1	0	0	-1	H1	0	1	-1	0											
	C1	O1	O2	H1																																		
C1	0	-1	1	0																																		
O1	-1	0	0	1																																		
O2	1	0	0	-1																																		
H1	0	1	-1	0																																		
NIH Shift		<table border="1"> <thead> <tr> <th></th> <th>C1</th> <th>C2</th> <th>O1</th> <th>H1</th> <th>H2</th> </tr> </thead> <tbody> <tr> <th>C1</th> <td>0</td> <td>1</td> <td>0</td> <td>-1</td> <td>0</td> </tr> <tr> <th>C2</th> <td>1</td> <td>0</td> <td>-1</td> <td>1</td> <td>-1</td> </tr> <tr> <th>O1</th> <td>0</td> <td>-1</td> <td>0</td> <td>0</td> <td>1</td> </tr> <tr> <th>H1</th> <td>-1</td> <td>1</td> <td>0</td> <td>0</td> <td>0</td> </tr> <tr> <th>H2</th> <td>0</td> <td>-1</td> <td>1</td> <td>0</td> <td>0</td> </tr> </tbody> </table>		C1	C2	O1	H1	H2	C1	0	1	0	-1	0	C2	1	0	-1	1	-1	O1	0	-1	0	0	1	H1	-1	1	0	0	0	H2	0	-1	1	0	0
	C1	C2	O1	H1	H2																																	
C1	0	1	0	-1	0																																	
C2	1	0	-1	1	-1																																	
O1	0	-1	0	0	1																																	
H1	-1	1	0	0	0																																	
H2	0	-1	1	0	0																																	
Glutathione Conjugation		<table border="1"> <thead> <tr> <th></th> <th>C1</th> <th>O1</th> <th>S1</th> <th>H1</th> </tr> </thead> <tbody> <tr> <th>C1</th> <td>0</td> <td>-1</td> <td>1</td> <td>0</td> </tr> <tr> <th>O1</th> <td>-1</td> <td>0</td> <td>0</td> <td>1</td> </tr> <tr> <th>S1</th> <td>1</td> <td>0</td> <td>0</td> <td>-1</td> </tr> <tr> <th>H1</th> <td>0</td> <td>1</td> <td>-1</td> <td>0</td> </tr> </tbody> </table>		C1	O1	S1	H1	C1	0	-1	1	0	O1	-1	0	0	1	S1	1	0	0	-1	H1	0	1	-1	0											
	C1	O1	S1	H1																																		
C1	0	-1	1	0																																		
O1	-1	0	0	1																																		
S1	1	0	0	-1																																		
H1	0	1	-1	0																																		

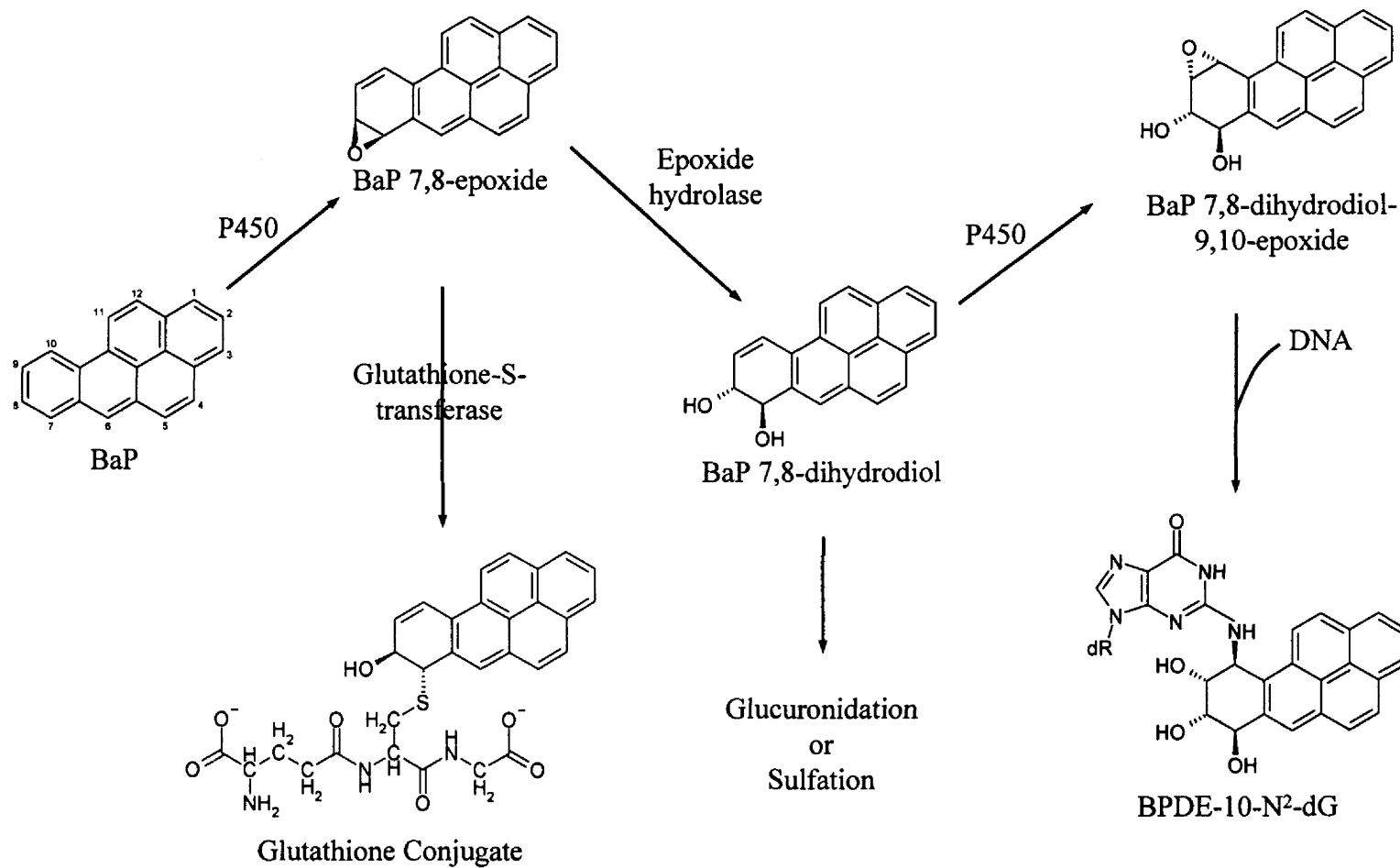


**Figure 3.1.** Major metabolic activation pathways for BaP in biologic systems. BPDE-10-N<sup>2</sup>-dG, 10-(deoxyguanosin-N<sup>2</sup>-yl)-7,8,9-trihydroxy-7,8,9,10-tetrahydrobenzo[a]pyrene.

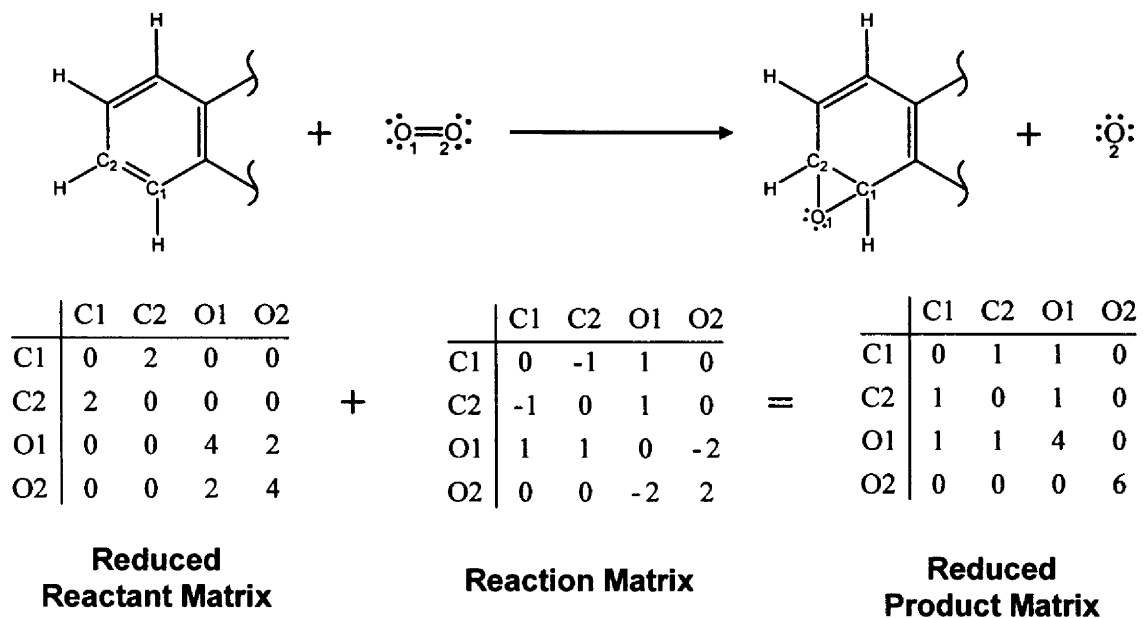


*Figure 3.2.* Matrix representation of epoxidation reaction in aromatic bond.

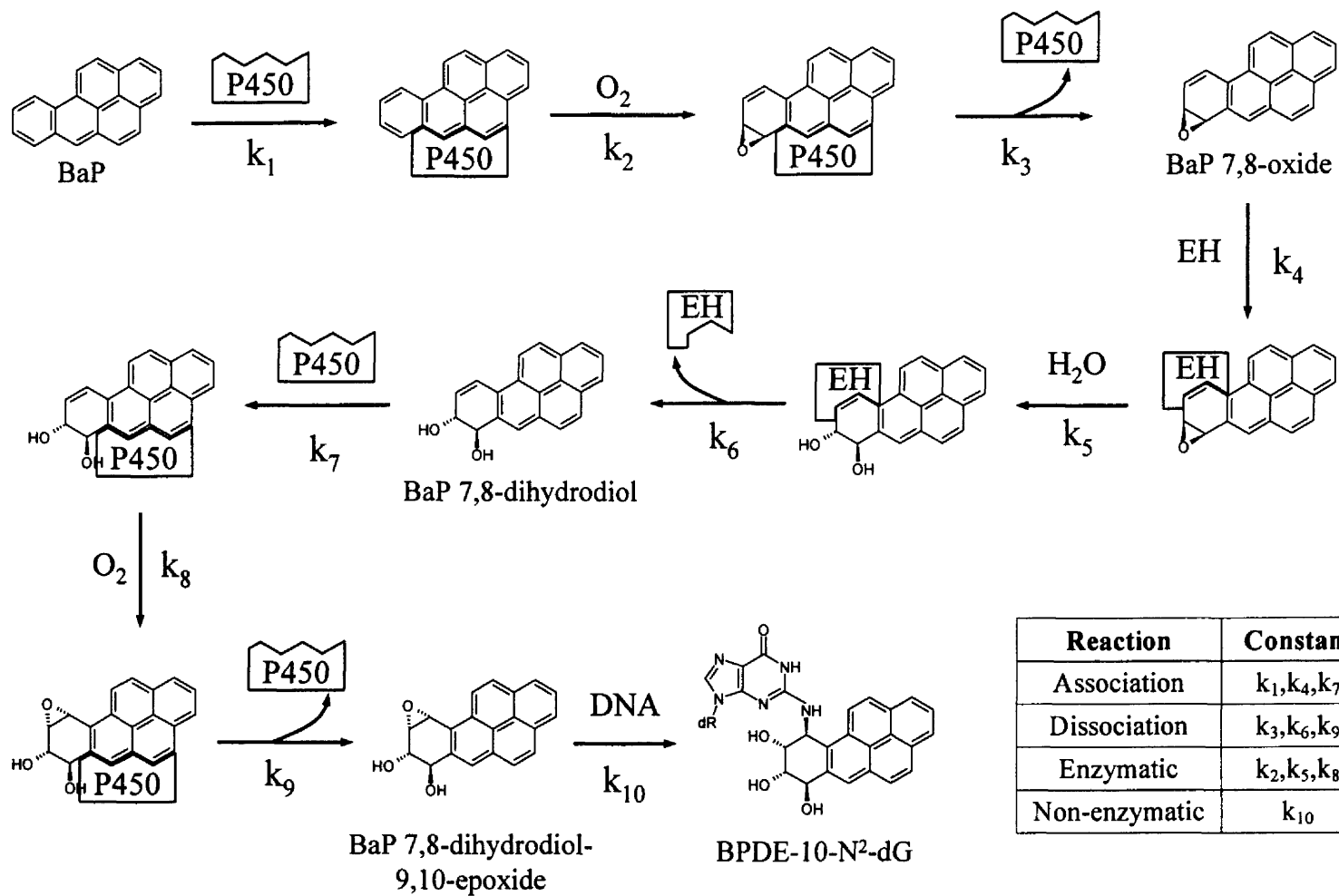
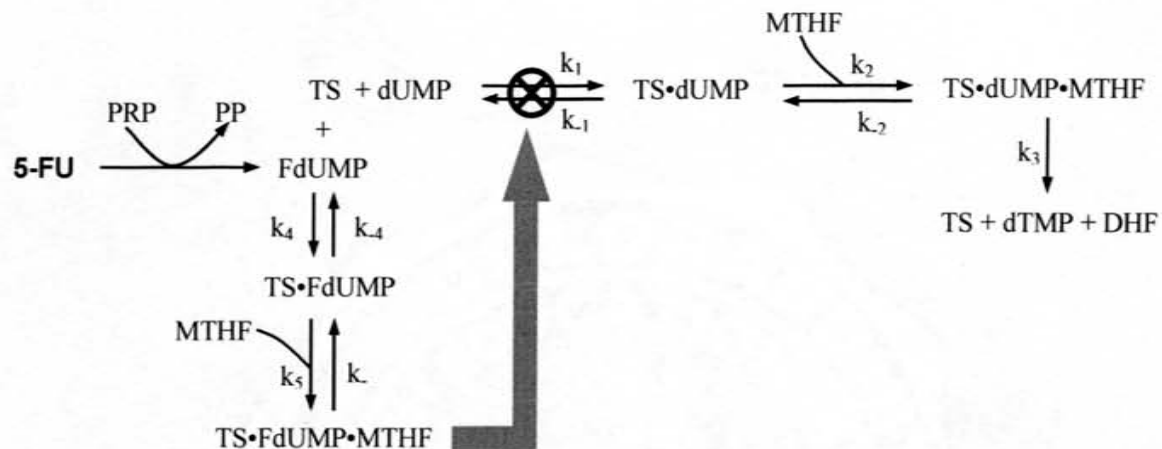


**Figure 3.3.** Classification of rate constants for B[a]P metabolic activation pathways. EH, epoxide hydrolase.



$$v_0 = \left( \frac{d[\text{dTMP}]}{dt} \right)_{t \rightarrow 0} = k_3 [\text{TS} \cdot \text{dUMP} \cdot \text{MTHF}]$$

$$= \frac{k_1 k_2 k_3 [\text{dUMP}] [\text{MTHF}] [\text{TS}_{\text{total}}]}{\left( 1 + \frac{[\text{FdUMP}]}{K_{I_1}} + \frac{[\text{FdUMP}] [\text{MTHF}]}{K_{I_1} K_{I_2}} \right) (k_{-1} k_{-2} + k_{-1} k_3 + k_2 k_3 [\text{MTHF}]) + k_1 k_2 [\text{dUMP}] [\text{MTHF}] + (k_1 k_{-2} + k_1 k_3) [\text{dUMP}]}$$

Where

$$K_{I_1} = \frac{[\text{TS}] [\text{FdUMP}]}{[\text{TS} - \text{FdUMP}]} \quad \text{and} \quad K_{I_2} = \frac{[\text{TS} - \text{FdUMP}] [\text{MTHF}]}{[\text{TS} - \text{FdUMP} - \text{MTHF}]}$$

**Figure 4.** Enzymatic kinetics of the inhibition of FdUMP on dTMP synthesis by 5-FU. Abbreviations: DHF, dihydrofolate; dTMP, deoxythymidine monophosphate; dUMP, deoxyuridine monophosphate; FdUMP, 5-fluorodeoxyuridylate; MTHF,  $N^5, N^{10}$ -methylenetetrahydrofolate; PPi, pyrophosphate; PRPP, 5-phosphoribosyl- $\alpha$ - pyrophosphate. Equations were derived based on the mechanisms proposed by Hardy et al. (43) and Voet and Voet (44).

## Chapter 4

### Application of Reaction Network Pathway Modeling in Biological Systems: Mammalian Metabolism of Benzo[a]pyrene

#### **4.1. Introduction**

Many xenobiotics undergo metabolic transformation in humans and often produce toxic metabolites. Biotransformation may involve complex reaction networks in which multiple enzymes are involved and the reactants and products of one reaction are participants in many other reactions. As the first step of developing a predictive tool for the biotransformation of a variety of xenobiotics, we applied the Reaction Network (RN) pathway modeling approach to predict the complex metabolic reactions encountered by benzo[a]pyrene (BaP) in mammals. RN pathway models, in which the chemical structures and reaction rules are encoded using atomic connectivity (1-3), have been successfully used to predict the reaction pathways of petroleum refinery processes in the field of chemical engineering. In this chapter, the RN pathway model for BaP was established based on the previously developed modeling technology for the petroleum refinery processes (1-3), with the incorporation of the commonly observed biochemical reactions for mammalian metabolism of BaP (4-6). While the details of the metabolic pathways of BaP were discussed in Chapter 2, this chapter is focused on the common reactions (Figure 4.1) observed when BaP is incubated with recombinant human

cytochrome P450 (CYP) and microsomal epoxide hydrolase (EH). CYP and EH are the major enzymes catalyzing the reactions of BaP to form its ultimate carcinogen, BaP-7,8-dihydrodiol-9,10-epoxide (4-6). The reactions considered here in this chapter are, i) epoxidation of BaP and BaP-dihydrodiol catalyzed by CYP; ii) hydrolysis of arene oxides catalyzed by EH; iii) abiotic isomerization of arene oxides to phenols (NIH Shift); iv) one-electron oxidation of BaP catalyzed by CYP; v) auto-oxidation of BaP-diols to BaP-diones.

While this chapter is focused on the RN pathway model predictions of the possible metabolic reactions encountered by BaP in mammals, the quantitative predictions of the time course of BaP metabolism is introduced in Chapter 7 using the RN kinetics modeling approach. Experimental data used to calibrate and validate the RN kinetics model for BaP were obtained using new analytical methods, as described in Chapters 5 and 6.

## **4.2. Methods**

The chemical structures of reactants are first encoded in matrix format to represent atomic connectivity within the molecules. The changes in atomic connectivity as a result of a chemical reaction are also accounted for using a matrix. The uniqueness of all species, including reactants and products, are determined by the comparison of the model-generated unique string codes of the species. The RN pathway model containing all of these elements was written in C language for solution on a standard 900 MHz personal computer. These key components of RN pathway model are discussed stepwise in the following sections.

#### 4.2.1. Representation of Chemical Structures

The atomic connectivity and formal electronic state of a chemical are represented by the bond-electron (BE) matrix (1, 7). The BE matrices of ethane and carbon dioxide are shown in Figure 4.2 as examples. In BE matrices, the off-diagonal elements  $m_{ij}$  denote the bond order between two atoms  $i$  and  $j$ . The diagonal elements in BE matrices represent the number of valence electrons not involved in bonding. The sum of the elements in a given row or column is equal to the number of valence electrons for that atom.

The bond orders for all aromatic bonds were represented as 1.5 bonds in RN pathway model. This was done to simplify the coding process and does not necessarily reflect the actual bond orders for all aromatic bonds. The actual bond orders of all C-C bonds are equal to 1.5 only in the case of benzene, where their corresponding bond lengths are 1.39 angstroms, intermediate between the lengths of single and double bonds (8, 9). For aromatic hydrocarbons containing more than one six-member ring, bond localization results in the nonequivalency of C-C bonds, called partial bond fixation (10-12). Bond orders of 1.5 were used to in the RN pathway to simplify the reaction matrices. If the sum of the elements in a given row or column is equal to 4.5 for a carbon atom in the BE matrix, it is the indication that this carbon is located at a point of fusion between aromatic rings.

The BE matrix consists of many zero entries and is thus inefficient for storage. The adjacency list, which contains the identity of all atoms adjacent to a given atom of interest, were used to efficiently store the molecular bond information. The adjacency

list of a chemical can be converted to the BE matrix within RN pathway model when the BE matrix is required for computation, *e.g.*, matrix operation for chemical reactions. The molecular graph and adjacency list of BaP are shown in Figure 4.3. Each atom in the graph of BaP (Figure 4.3a) was assigned a unique number by the modeler. There are 32 rows in the BaP adjacency list (Figure 4.3b), in which each row represents the atomic connectivity for one of the 32 atoms of BaP. The first three numbers in row  $i$  denote the assigned atom number, number of the valence electrons not involved in bonding, and the type of atom, respectively, for atom  $i$ . The first number enclosed in braces represents the atom number of the atom adjacent to atom  $i$  and, in turn, the second number represents the bond order of the bond connecting these two atoms. For example, the information stored in the first row of BaP adjacency list denotes that carbon 0 is connected to carbon 1, carbon 17, and hydrogen 20 with 1.5, 1.5, and single bonds, respectively. Furthermore, carbon 0 does not contain any valence electron not involved in bonding. The adjacency list of BaP requires much less storage space in the computer than a 32 by 32 BE matrix of BaP does.

#### 4.2.2. Execution of Chemical Reactions

The structural changes of molecules caused by chemical reactions can also be described by a reaction matrix (1, 7). Most reactions involve the change of connectivity between only a few atoms. Therefore, reaction matrices can be used as a compact representation of bond formation and breakage caused by chemical reactions. The addition of the reaction matrix to the reactant BE submatrix, which consists of only the atoms involved in the reaction (converted by the modeling software), forms the product

submatrix. The product submatrix can in turn be incorporated with the submatrix consisting of only the atoms not involved in the reaction, which results in the complete BE matrix of the reaction product. In Figure 4.4, the epoxidation of ethylene is used as an example of the matrix operation of chemical reaction. The program first searches for any carbon-carbon double bonds, *i.e.* the eligible sites of epoxidation reactions, in the entire structure of ethylene. In bimolecular reactions like epoxidation, the BE matrices of the reactants must be merged before the extraction of reactant submatrix. The rest of the matrix operation shown in Figure 4.4 is self-explanatory. The reaction rules and matrices of the reactions included in BaP RN pathway model are described in the following section.

**4.2.2.1. Epoxidation reactions.** All carbon-carbon double bonds are eligible for epoxidation reactions and the reaction matrix is shown in Figure 4.4. This reaction rule is applicable to any compounds containing carbon-carbon double bonds, including aromatic compounds with their BE matrix expressed as alternant single-double bonds. If the RN modeler chooses to use the alternant single-double bonds expression, all the possible combinations of single-double bond structure “canonical” (13) forms, of the aromatic compound of interest would have to be considered. That is, multiple BE matrices in the format of adjacency lists would be included in the input file to represent the same aromatic compound. This would have been too cumbersome. Alternatively, there is no need to use multiple BE matrices if aromatic compounds are represented by 1.5-order bonds. The epoxidation of benzene is used as an example (Figure 4.5) for this latter case. All the six carbons of benzene are involved in the reaction matrix because the aromaticity

of the benzene ring is not maintained following epoxidation at any of its carbon-carbon bonds. As shown in Figure 4.5, C3-C4 and C5-C6 bonds become double bonds in the reaction product, benzene oxide, while other carbon-carbon bonds become single bonds.

For aromatic compounds containing more than one six-membered ring, the ring containing the site of epoxidation will not maintain its aromaticity after the reaction. However, some carbon-carbon bonds of this ring are shared by other rings. These carbons at ring fusions may or may not still be part of the aromatic sextet of another aromatic ring, *i.e.* they could still have bond orders of 1.5. For example, when phenanthrene undergoes epoxidation at the C1-C2 bond (Figure 4.6), C3 and C4 are still part of the aromatic sextet of another ring where its aromaticity is not disrupted. Therefore, the reaction matrix shown in Figure 4.6 is the same as the one for benzene, except that the elements indicating the connectivity change between C3 and C4 are zero. The software for RN pathway model of BaP was written such that the BE submatrix of the carbons belonging to the same ring as the eligible site were first identified. The bonds connecting these carbons were then tested to determine whether they are shared by other aromatic rings. The program, in turn, modifies the reaction matrix by changing the elements connecting these carbons at ring fusions to zero.

When BaP undergoes epoxidation, the number of rings losing their aromaticity varies depending on the reaction site. As shown in Figure 4.7, there are four, three, and two rings retaining their aromaticity in the formation of BaP-7,8-oxide, BaP-2,3-oxide, and BaP-8,9-oxide, respectively. Epoxidation reactions that result in the disruption of aromaticity of more rings are less favorable than those causing fewer rings to lose their aromaticity. This hypothesis is supported by the values of resonance energy, a measure

of the extra stability of the actual molecular entity compared to the contributing structure of lowest potential energy (13). The epoxidation of BaP leading to the formation of BaP-7,8-oxide disrupts the aromaticity of only one ring (Figure 4.7). As a result, BaP-7,8-oxide still maintains the aromaticity of four rings, which is equivalent to a pyrene with resonance energy equal to 108.9 kcal/mol (14, 15). BaP-2,3-oxide and BaP-8,9-oxide maintain the aromaticity equivalent to anthracene (resonance energy = 83.5 kcal/mol) and naphthalene (resonance energy = 61.0 kcal/mol), respectively (13, 15). Therefore, the epoxidation of BaP leading to the formation of BaP-8,9-oxide is less favorable than the formation of BaP-2,3-oxide, and lesser still than the formation of BaP-7,8-oxide. There is no published data suggesting the formation of BaP-8,9-oxide. From the standpoint of modeling, the reaction matrix for epoxidation can become very complicated when more and more rings lose their aromaticity since more atoms must be included in the matrix operation. In the current version of the RN pathway model for BaP, the selection of the sites for epoxidation is limited to those resulting in the disruption of aromaticity for fewer than three rings. The epoxidation of BaP leading to the formation of BaP-2,3-oxide is used as an example to illustrate the execution of epoxidation resulting in the disruption of the aromaticity of two rings (Figure 4.8). Note that the bond orders of C7-C8, C8-C9, and C9-C10 remain unchanged during the course of epoxidation because these bonds are shared by other aromatic rings.

A selection process was devised to determine whether a particular aromatic bond is an eligible site for epoxidation. First, both carbon atoms of this aromatic bond should also each be bonded to a hydrogen atom. This criterion excludes ring fusion sites since the epoxidation reaction is not likely to occur at these sites due to steric hindrance.

Second, the aromatic bond is examined for the “distance” to ring fusions. This “distance” was defined as the number of C-C bonds that are on the path to the ring fusion, starting from one of the carbons of the aromatic bond in question. If the distance involves an even number of bonds, the aromaticity of the neighbor ring will be disrupted if epoxidation occurred. That is, a double bond is connected to the carbon at the ring fusion and as a result, the other two bonds connected to this carbon have to be single bonds. Furthermore, if the “distance” to the ring fusions in both directions (one for each carbon of the potential reaction site) are odd numbers of bonds, the aromaticity of the neighboring ring is retained as in the case of BaP-7,8-oxide (Figure 4.7). For BaP-8,9-oxide, the “distances” to the ring fusions are even numbers for both directions and the aromaticity of the neighboring rings will not be retained. This type of site is not eligible for epoxidation reactions in the current version of the RN pathway model. For BaP-2,3-oxide and BaP-1,2-oxide, the “distances” to the ring fusions are an even number of bonds in one direction and an odd number of bonds in the other direction. An epoxidation reaction at this type of site results in the disruption of aromaticity of two rings when the aromatic compound contains five or fewer rings. This type of site is included in current version of the model.

**4.2.2.2. Hydrolysis reactions of epoxides.** The eligible site for the hydrolysis of an epoxide is the C-O-C ring. The matrix operation for epoxide hydrolysis is shown in Figure 4.9. There are four atoms involved in the reaction. Although C2 of the epoxide molecule and H2 of the water molecule are labeled for the purpose of illustration in

Figure 4.9, the connectivity of these two atoms remains unchanged during the course of hydrolysis reaction.

**4.2.2.3. NIH Shift reactions of epoxides.** NIH Shift is the general term for the phenomenon of hydroxylation-induced intra-molecular migration (16). In the context of the RN pathway model of BaP, the NIH Shift reaction is limited to the isomerization of arene oxides to form phenols (17). The matrix operation for the NIH Shift reaction is shown in Figure 4.10. For each epoxide, two distinct alcohols can potentially be formed via NIH Shift depending on which C-O bond is cleaved. The eligible sites of NIH Shift reactions were defined in the model as any C-O-C-H combinations with the two carbons connected to each other. If the site of C1-O1-C2-H1 is found (Figure 4.10), the NIH Shift reaction results in the formation of the alcohol with hydroxyl group connected to C2. On the other hand, the alcohol with hydroxyl group attached to C1 is formed when the site of C2-O1-C1-H2 is found.

**4.2.2.4. Oxidation of BaP to BaP-diones.** BaP-diones are formed in a three-stage process via 6-hydroxy-BaP (6-OH), a labile metabolite of BaP. 6-OH is believed to be formed via CYP catalyzed one-electron oxidation reactions (18-21) (Figure 4.11). 6-OH then undergoes non-enzymatic oxidation and forms BaP-1,6-dione, BaP-3,6-dione, and BaP-6,12-dione (18, 19). A multi-step mechanism was proposed by Lorentzen et al (19) to describe the oxidation of 6-OH to BaP-diones (Figure 4.12). Since some intermediates shown in Figures 4.11 and 4.12 are very labile and difficult to measure, a simplified pathway (Figure 4.13) was used to describe the oxidation of BaP to BaP-diones for RN

pathway modeling. BaP first undergoes CYP-catalyzed carbon hydroxylation, initiated with one-electron oxidation, to form hydroxyl-BaPs. The hydroxyl-BaPs then undergo another round of carbon hydroxylation reactions and form BaP-diols. Finally, BaP-diols are auto-oxidized to form BaP-diones. The matrix operations for carbon hydroxylation and auto-oxidation are discussed in the following two sections.

4.2.2.4.1. Carbon hydroxylation reactions. Although the carbon hydroxylation of BaP and hydroxy-BaPs shown in Figures 4.11 and 4.12 are multi-step reactions, the net change in the structure can be represented as the insertion of an oxygen atom between a carbon atom and a hydrogen atom. The matrix operation of the carbon hydroxylation is shown in Figure 4.14 and the eligible site for this type of reaction is any carbon-hydrogen bonds. The hydroxylation of BaP results in the formation of hydroxy-BaPs, which could also be formed via the combination of the epoxidation of BaP and a subsequent NIH Shift reaction of arene oxides.

4.2.2.4.2. Auto-oxidation of BaP-diols to BaP-diones. All BaP-diols are potentially eligible for auto-oxidation. Several reaction matrices were used for the auto-oxidation of BaP-diols to BaP-diones depending on the location of the two hydroxyl groups in BaP-diols. For BaP-diols with two hydroxyl groups located on the same ring, their reaction matrices of auto-oxidation are very similar to the ones for benzene-1,2-diol (Figure 4.15) and benzene-1,4-diol (Figure 4.16). The auto-oxidation of benzene-1,3-diol to benzene-1,3-dione is excluded from the model because meta-quinone is not stable. The same principle is applied to the auto-oxidation of all hydroquinones in that only hydroquinones

with two C-O-H sites separated by an odd number of C-C bonds are eligible for auto-oxidation reactions. The aromaticity of both benzene-diols was disrupted after auto-oxidized to form quinones.

The reaction matrices shown in Figures 4.15 and 4.16 must be modified when applied to aromatic compounds containing multiple rings. As discussed in the section on epoxidation, some carbon-carbon bonds of the ring containing the reaction sites are shared by other rings. These carbons at ring fusions may or may not still be part of the aromatic sextet of another aromatic ring, *i.e.* they could still have bond orders of 1.5. Using the auto-oxidation of BaP-7,8-diol as an example (Figure 4.17), C2 and C3 are still part of the aromatic sextet of another ring where its aromaticity is not disrupted. Therefore, the reaction matrix shown in Figure 4.17 is the same as the one for benzene-1,2-diol, except that the elements indicating the connectivity change between C2 and C3 are zero. The model for this reaction was encoded to first identify that the BE submatrix of the carbons belong to the same ring as the eligible sites. The bonds connecting these carbons were then tested to determine whether they are shared by other aromatic rings. The program, in turn, modifies the reaction matrix by changing the elements connecting these carbons at ring fusions to zero. For the auto-oxidation of BaP-4,5-diol and BaP-11,12-diol to their corresponding diones, three C-C bonds within the same ring as the eligible sites retain their 1.5-bond-order status. The current model does not consider the auto-oxidation reactions of BaP-8,9-diol and other BaP-diols with both OH moieties on the same ring that result in the disruption of the aromaticity of more than one ring.

For BaP-diols with their hydroxyl groups connected to different rings, the reaction matrix of auto-oxidation is composed of two identical conceptual submatrices, each

containing one hydroxyl group and the carbons belonging to the same ring as the hydroxyl group (Figure 4.18). Note that the two free electrons shown in Figure 4.18 are reassigned to the carbonium ion and proton after the conceptual reaction submatrices are combined to form the complete reaction matrices. The rings to which the hydroxyl groups connected might be separated from (*e.g.* BaP-1,6-diol shown in Figure 4.19) or adjacent to (*e.g.* BaP-1,11-diol shown in Figure 4.20) each other. For the former case (Figure 4.19), we simply combine two conceptual submatrices, one containing H1, O1, and C1 to C6 and the other containing H2, O2, and C7 to C12, to form a 16 by 16 reaction matrix. The C-C bonds shared by other aromatic rings are then identified and the corresponding elements in the reaction matrix are set to zero because these carbons are still part of the aromatic sextet for other rings. For the latter case (Figure 4.20), further modification of the reaction matrix is required in addition to the two-step process described above. The modification is made due to the sharing of two carbon atoms by the two rings with hydroxyl groups attached to them. C4 and C5 of Ring 1 represent the same atoms as C11 and C12 of Ring 2. To avoid duplication, the connectivity associated with C11 and C12 are transferred to C4 and C5, respectively, and the columns and rows representing C11 and C12 are eliminated from the reaction matrix. To be exact, the elements indicating the connectivity changes for C7-C11 are used to overwrite the elements for C7-C5. Furthermore, the elements for C10-C11 overwrite the ones for C10-C4. The final reaction matrix contains 14×14 elements and is shown in Figure 4.20.

In the current model, the auto-oxidation reactions of BaP-diols are limited to those causing the disruption of aromaticity for fewer than three rings if the hydroxyl groups are attached to different rings. That is, the aromaticity for the rings without

hydroxyl groups should be retained after the auto-oxidation reaction. The reactions resulting in the loss of aromaticity for more rings are less favorable than those causing the loss of aromaticity for fewer rings, as discussed in the section of the epoxidation reactions. Each C-O-H site should be separated from the nearest two ring fusions by odd numbers of C-C bonds in order to maintain the aromaticity for the adjacent rings. Using BaP-1,6-diol as an example (Figure 4.19), the C7-O2-H2 site is separated by three C-C bonds (C7-C8, C8-C9, and C9-C10) from C10 at a ring fusion, and by one C-C bond (C7-C12) from C12 at a ring fusion. The C1-O1-H1 site is also separated from C2 and C6 by single C-C bonds (C1-C2 and C1-C6, respectively). Therefore, BaP-1,6-diol is eligible for auto-oxidation. In the case of BaP-1,11-diol (Figure 4.20), the C1-O1-H1 site is separated from C5 at ring fusion by even number of C-C bonds (C1-C6 and C6-C5) and the auto-oxidation can cause the disruption of the aromaticity for the adjacent rings. However, this adjacent ring is the one to which the other hydroxyl group is attached and its aromaticity will be disrupted regardless. As a result, BaP-1,11-diol is still eligible for auto-oxidation.

#### 4.2.3. *Determination of Species Uniqueness*

Every product formed through matrix operation of chemical reactions is checked for its uniqueness (1, 3) to ensure that the molecule was not previously created by other reactions. If the product is unique, it is added to the unreacted species list. Every compound in the unreacted species list, which is updated in real time, could become a candidate reactant for other reactions.

The determination of species uniqueness was achieved by comparing the unique string codes of the molecules. The unique string codes were generated in RN pathway model by decomposing the molecular graph into “components” and reassembling these components in a tree structure (decomposition tree) with proper connectivity (3). The special components used to build the decomposition tree are called “biconnected components” (bicomps) (3). Each bicomps is either a bond or a cycle (benzene or polycyclic rings), which is the subgraph of the molecular graph. The bicomps in a molecular graph are separated by “articulation points” (3). An articulation point is defined as the point  $a$  in a distinct triple  $(v, w, a)$  such that  $a$  is on every path  $p$  from  $v$  to  $w$  (3). Using benzene-1,2-diol in Figure 4.21a as an example, an articulation point  $a$  is on every path from points  $v$  to  $w$ . Once  $a$  is removed, there is no path connecting  $v$  and  $w$ , and two distinct subgraphs are formed. A bicomps is formed if and only if there is no articulation point in the component. Therefore, C-O-H is not a bicomps due to the existence of articulation point  $a$  in Figure 4.21a. Instead, C-O and O-H are defined as two distinct bicomps. In Figure 4.21b, each subgraph of benzene-1,2-diol enclosed in a circle represents a bicomps. The benzene ring in the molecule benzene-1,2-diol is a bicomps (Figure 4.21b), because if any one vertex (a point such as a carbon atom in the ring) is removed from the ring, any pair of the remaining vertices can still be connected by traversing the ring in an alternate direction. The details of the algorithm used to identify bicomps were previously reported by Broadbelt et al. (3).

After the bicomps were identified, the decomposition tree of a molecule was constructed by successively removing the bicomps with the same degree. The degree of a bicomps is equal to the number of its member atoms that are also members of other

bicomps. For example, the benzene ring bicomps has a degree of six, *i.e.* all of its six carbon atoms are also members of other bicomps (two C-O and four C-H bicomps). The construction of the decomposition tree of benzene-1,2-diol is shown in Figure 4.22a. The first iteration results in the removal of all degree 1 bicomps (two O-H and four C-H bicomps). In the remaining three bicomps, C-O bicomps have degrees of 1 and are removed in the next iteration. As a result, the single remaining bicomps, the benzene ring, becomes the root of the decomposition tree. The decomposition tree is then constructed by reassembling the bicomps starting with the root bicomps and appending the bicomps sharing atoms with the root bicomps, *i.e.* the descendants of the root bicomps. The decomposition tree of benzene-1,2-diol is shown in Figure 4.22b.

The unique string code is constructed based on the decomposition tree. The atom code of each member atoms in the root bicomps is written first, followed by the subtree code enclosed in parentheses. The subtree code is composed of the atom members in the descendent bicomps of the root bicomps. If the unvisited atom member in the descendent bicomps belonging to no other bicomps, the subtree code is simply equal to the atom code. Using benzene-1,2-diol as an example, the root of the decomposition tree is a benzene ring composed of six carbons which are all members of other bicomps (two C-O and four C-H bicomps). For the four descendent C-H bicomps, the only unvisited members are hydrogens, which belong to no other bicomps. As a result, the four C-H bicomps are simply encoded as C(H). For each of the C-O bicomps, the unvisited oxygen atom is also a member of an O-H bicomps, whereas the hydrogen in the O-H bicomps belongs to no other bicomps. Therefore, the code of C(O(H)) is formed for the carbon member of the

C-O bicomps. To this point, all bicomps to which the six carbons in the root bicomps belong have been visited and encoded.

For non-cyclic bicomps, the final assembly of the unique string code simply requires the lexicographical sorting of the atom subtree codes (3). On the other hand, the final step of constructing the unique string code of a cyclic bicomps is to sort the atom subtree codes according to a specific direction of traversal around the exterior of the bicomps (3). The direction and starting point of traversal for a cyclic bicomps is selected to obtain the lexicographically minimal string code. The starting points could be any of the member atoms with highest degree of connectivity to other atom members within the bicomps. The algorithm begins with each starting point, and traverses one atom away in each direction, clockwise and counterclockwise. The subtree codes of the adjacent atom are concatenated with the string code for the starting atom. The process of traversal is illustrated in Figure 4.23 using benzene-1,2-diol. The starting points can be any of the six carbons in the root bicomps because they have the same degrees of connectivity, degrees of 2, to other member in the bicomps. Carbons 2 and 4 were randomly selected as the starting points for demonstration purpose. These two starting points result in four possible paths, *w*, *x*, *y*, and *z*. The following codes form when the algorithm moves one atom away from the starting points

*w* C(H)C(O(H))  
*x* C(H)C(H)  
*y* C(H)C(H)  
*z* C(H)C(H).

Path *w* is eliminated after one iteration due to the lexicographical comparison. After two additional atoms beyond the starting points are visited, path *x* is determined to

be lexicographically minimal (Figure 4.23). Therefore, the unique string code of benzene-1,2-diol, C(H)C(H)C(H)C(H)C(O(H))C(O(H)), is formed by encoding through path  $x$ . Using the algorithm described above, the resultant unique string code for benzene-1,3-diol is C(H)C(H)C(H)C(O(H))C(H)C(O(H)), which is clearly different from the unique string of the structural isomer benzene-1,2-diol.

The direction of traversal for constructing the unique string code of BaP is shown in Figure 4.24. In the presence of the interior atoms for cyclic bicomps, the algorithm traverses the entire perimeter of the bicomps before any interior atoms are visited. A colon is appended to the atom codes of the interior atoms. The interior codes are sorted lexicographically and concatenated to the perimeter code.

#### 4.2.4. *Estimation of Kinetic Parameters*

By applying the given reaction rule, the RN pathway model software generates the possible reactions and corresponding products. Some of the products may never be observed because either the reaction rates are too low for their formation or the subsequent products have very high reaction rates. Accurately estimated kinetic parameters provide quantitative predictions of reaction rates in RN kinetics model and reflect the relative concentrations of the products. In the case of BaP metabolism and many other biochemical reactions, the reaction rates can be expressed as Michaelis-Menten kinetics with competitive inhibition. The reason for including competitive inhibition is that several arene oxides in the BaP metabolic network all bind to epoxide hydrolase and undergo hydrolysis. Furthermore, BaP-dihydrodiols can also compete with BaP for the active site of CYP1A1.

In the petroleum refinery application of RN kinetics model, Quantitative Structure/Reactivity Correlations (QSRCs) were used to estimate kinetic parameters associated with the reactions predicted by the model (22, 23). QSRCs are semi-empirical methods in which sterically similar reactions are lumped into reaction families. The form of this correlation is expressed as:

$$\log k_i = a_j + b_j * RI_i \quad (1)$$

where  $i$  is a component in the reaction family  $j$ .  $RI$  represents the reactivity index, which is a measurable structural property pertinent to the reaction family. The parameters  $a$  and  $b$  are calibrated by experimental data (22). The construction and validation of QSRCs requires the support from a large kinetics database (23-26), which is not readily available for the BaP metabolic pathways or many other biochemical reactions. To initiate the construction of a database for kinetic parameters, time course profiles of BaP metabolites were studied using recombinant human enzymes and reported in the following chapters.

## **4.3. Results and Discussion**

### *4.3.1. Reaction Network Pathway Model Predictions*

The RN pathway model of the BaP metabolic network predicts that 246 reactions can occur, resulting in 150 unique products when BaP is incubated with recombinant human CYP and EH (Figure 4.25). Several different reactions can lead to the formation of the same products, and thus the number of possible products is smaller the amount of possible reactions. For example, 12 hydroxy-BaPs can be formed through the hydroxylation of BaP initiated with one-electron oxidation. The epoxidation of BaP followed by NIH Shift can lead to the formation of 11 hydroxy-BaPs. When the unique

string codes of these 23 hydroxyl-BaPs were compared, only 12 unique species were found. This is because 11 of these hydroxyl-BaPs can be formed via both pathways while 6-OH is only formed through one-electron oxidation pathway.

The products of one reaction can become the reactants for other reactions. Thus the number of possible reactions predicted by the RN pathway model might increase exponentially with the number of products. In order to prevent the generation of undesirable reactions, certain constraints can be applied to the reaction rules. For example, each BaP-oxide contains several aromatic bonds eligible for further epoxidation. However, this type of reaction was not considered in the model because epoxides are very labile and will preferentially undergo reactions targeting the epoxide rings, *e.g.* hydrolysis and NIH Shift, instead of forming diepoxides.

The incorporation of additional reaction rules can be easily achieved, if experimental data for the presence of additional metabolites are available for the validation of the model. For example, the NIH Shift reactions of dihydrodiol-epoxides were not included in the current reaction rules, because the possible products, dihydrodiol-phenols, have not been well studied. Although 1,9,10-trihydroxy-9,10-dihydro-BaP and/or 3,9,10-trihydroxy-9,10-dihydro-BaP were detected when a high concentration (80  $\mu\text{M}$ ) of BaP-9,10-dihydrodiol was incubated with rat microsomes (27), dihydrodiol phenols were not considered to be major metabolites of BaP. Once the kinetics data for the NIH Shift of dihydrodiol-epoxides are available, this reaction rule can be easily incorporated by instructing the program to search for epoxide rings on dihydrodiol-epoxides and follow the matrix operation for NIH Shift reactions (Figure 4.10).

Fewer than 15% of the 150 products predicted by the RN pathway model of BaP have been observed in published reports of BaP metabolism (6, 28). As described in Chapter 7, only 21 metabolites of BaP were included in the current version of the RN kinetics model for BaP (Figure 7.7). The number of BaP metabolites that can be analyzed from the experiments is often limited by the availability of the authentic standards and by the analytical methods. For instance, 3- and 7-hydroxy-BaPs have often been found to co-elute and were thus reported as a lumped component (29).

#### 4.3.2. Example of Reaction Network Kinetics Model Simulations

Although it is desirable to use QSRCs to predict the kinetic parameters in a RN kinetics model, the data required to develop these correlations is rarely available for xenobiotics such as BaP. In these cases, the kinetics model parameters can be estimated by fitting the model to experimental data. An example of this approach is provided here (Figure 4.26) using the results of an *in vitro* study by Gautier et al. (30). In this study, 5  $\mu$ M BaP was incubated with recombinant human cytochrome P450 1A1 (5.8 nM) and human epoxide hydrolase (100 nM) at 37°C and pH 7.4. The time course profiles of BaP metabolites were successfully fit by the RN kinetics model of BaP (Figure 4.26) when Michaelis-Menten kinetics with competitive inhibition were used as the rate equation to describe the enzymatic reactions. While five BaP metabolites were measured by Gautier et al. (30), several other major metabolites, *e.g.* 7-hydroxy-BaP, BaP-1,6-dione, BaP-,3,6-dione, and BaP-6,12-dione, were not included.

#### **4.4. Conclusions**

RN pathway model of BaP metabolism predicts the possible pathways and their corresponding products, including some reactive intermediates that might be harmful to tissues and cells. This RN pathway model can be readily applied to predict the possible pathways of the mammalian metabolism of other polycyclic aromatic hydrocarbons.

With the incorporation of additional reaction rules, RN pathway model can be applied to predict the metabolic pathways of many different types of xenobiotics.

#### **4.5. References**

1. Broadbelt LJ, Stark SM, Klein MT. Computer generated pyrolysis modeling: on-the-fly generation of species, reactions, and rates. *Ind Eng Chem Res* 33:790-799(1994).
2. Broadbelt LJ, Stark SM, Klein MT. Computer-generated reaction networks: on-the-fly calculation of species properties using computational quantum chemistry. *Chem Eng Sci* 49:4991-5010(1994).
3. Broadbelt LJ, Stark SM, Klein MT. Computer generated reaction modelling: decomposition and encoding algorithms for determining species uniqueness. *Comput Chem Eng* 20:113-129(1996).
4. Levin W, Wood A, Chang R, Ryan D, Thomas P, Yagi H, Thakker D, Vyas K, Boyd C, Chu SY, Conney A, Jerina D. Oxidative metabolism of polycyclic aromatic hydrocarbons to ultimate carcinogens. *Drug Metab Rev* 13:555-580(1982).
5. Harvey RG. *Polycyclic Aromatic Hydrocarbons: Chemistry and Carcinogenicity*. Cambridge:Cambridge University Press, 1991.
6. Miller KP, Ramos KS. Impact of cellular metabolism on the biological effects of benzo[a]pyrene and related hydrocarbons. *Drug Metab Rev* 33:1-35(2001).
7. Ugi I, Bauer J, Brandt J, Friedrich J, Gasteiger J, Jochum C, Schubert W. *New Applications of Computers in Chemistry*. *Angew Chem Int Ed Engl* 18:111-123(1979).
8. Morrison RT, Boyd RN. *Organic Chemistry*. Boston:Allyn and Bacon, 1987.
9. Doerksen RJ, Thakkar AJ. Bond orders in heteroaromatic rings. *Int J Quantum Chem* 90:534-540(2002).
10. Efros LS. The Aromatic Bond and Some Problems of the Structure of Aromatic Compounds. *Russ Chem Rev* 29:66-78(1960).
11. Cremer D, Gunther H. Proton-resonance spectroscopy of unsaturated ring-systems. 17. Benzene nucleus as a probe for pi-electronic structure of annulenes. *Annalen Der Chemie-Justus Liebig* 763:87-108(1972).

12. Mitchell RH. Measuring aromaticity by NMR. *Chem Rev* 101:1301-1315(2001).
13. Wheland GW. *Resonance in Organic Chemistry*. New York:Wiley, 1955.
14. Klages F. Über Eine Verbesserung Der Additiven Berechnung Von Verbrennungswarmen Und Der Berechnung Der Mesomerie-Energie Aus Verbrennungswarmen. *Chemische Berichte-Recueil* 82:358-375(1949).
15. Streitwieser A. *Molecular Orbital Theory for Organic Chemists*. New York:Wiley, 1961.
16. Guroff G, Daly JW, Jerina DM, Renson J, Witkop B, Udenfrie.S. Hydroxylation-induced migration: the NIH shift. *Science* 157:1524-1530(1967).
17. Jerina DM, Daly JW. Arene oxides: a new aspect of drug metabolism. *Science* 185:573-582(1974).
18. Lesko S, Caspary W, Lorentzen R, Ts'o POP. Enzymic formation of 6-oxobenzo[a]pyrene radical in rat liver homogenates from carcinogenic benzo[a]pyrene. *Biochemistry* 14:3978-3984(1975).
19. Lorentzen RJ, Caspary WJ, Lesko SA, Ts'o POP. The autoxidation of 6-hydroxybenzo[a]pyrene and 6-oxobenzo[a]pyrene radical, reactive metabolites of benzo[a]pyrene. *Biochemistry* 14:3970-3977(1975).
20. Cavalieri EL, Rogan EG, Cremonesi P, Devanesan PD. Radical cations as precursors in the metabolic formation of quinones from benzo[a]pyrene and 6-fluorobenzo[a]pyrene. Fluoro substitution as a probe for one-electron oxidation in aromatic substrates. *Biochem Pharmacol* 37:2173-2182(1988).
21. Cavalieri EL, Rogan EG. Central role of radical cations in metabolic activation of polycyclic aromatic hydrocarbons. *Xenobiotica* 25:677-688(1995).
22. Neurock M, Klein MT. Linear free energy relationships in kinetic analyses: Applications of quantum chemistry. *Polycycl Aromat Comp* 3:231-246(1993).
23. Korre SC, Neurock M, Klein MT, Quann RJ. Hydrogenation of polynuclear aromatic hydrocarbons. II. Quantitative structure/reactivity correlations. *Chem Eng Sci* 49:4191-4210(1994).
24. Korre SC, Klein MT. Polynuclear aromatic hydrocarbons hydrogenation. 1. Experimental reaction pathways and kinetics. *Ind Eng Chem Res* 34:101-117(1995).
25. Korre SC, Klein MT. Development of temperature-independent quantitative structure/reactivity relationships for metal- and acid-catalyzed reactions. *Catalysis Today* 31:79-91(1996).
26. Korre SC, Klein MT, Quann RJ. Hydrocracking of polynuclear aromatic hydrocarbons. Development of rate Laws through inhibition studies. *Ind Eng Chem Res* 36:2041-2050(1997).
27. Thakker DR, Yagi H, Lehr RE, Levin W, Buening M, Lu AY, Chang RL, Wood AW, Conney AH, Jerina DM. Metabolism of trans-9,10-dihydroxy-9,10-dihydrobenzo[a]pyrene occurs primarily by arylhydroxylation rather than formation of a diol epoxide. *Mol Pharmacol* 14:502-513(1978).
28. Cooper CS, Grover PL, Sims P. The metabolism and activation of benzo[a]pyrene. In: *Progress in Drug Metabolism, Volume 7* (Bridges JW, Chasseaud LF, eds). Chichester:John Wiley & Sons, 1983;295-396.
29. Kim JH, Stansbury KH, Walker NJ, Trush MA, Strickland PT, Sutter TR. Metabolism of benzo[a]pyrene and benzo[a]pyrene-7,8-diol by human

- cytochrome P450 1B1. [erratum appears in *Carcinogenesis* 1999 Mar;20(3):515]. *Carcinogenesis* 19:1847-1853(1998).
30. Gautier JC, Urban P, Beaune P, Pompon D. Simulation of human benzo[a]pyrene metabolism deduced from the analysis of individual kinetic steps in recombinant yeast. *Chem Res Toxicol* 9:418-425(1996).

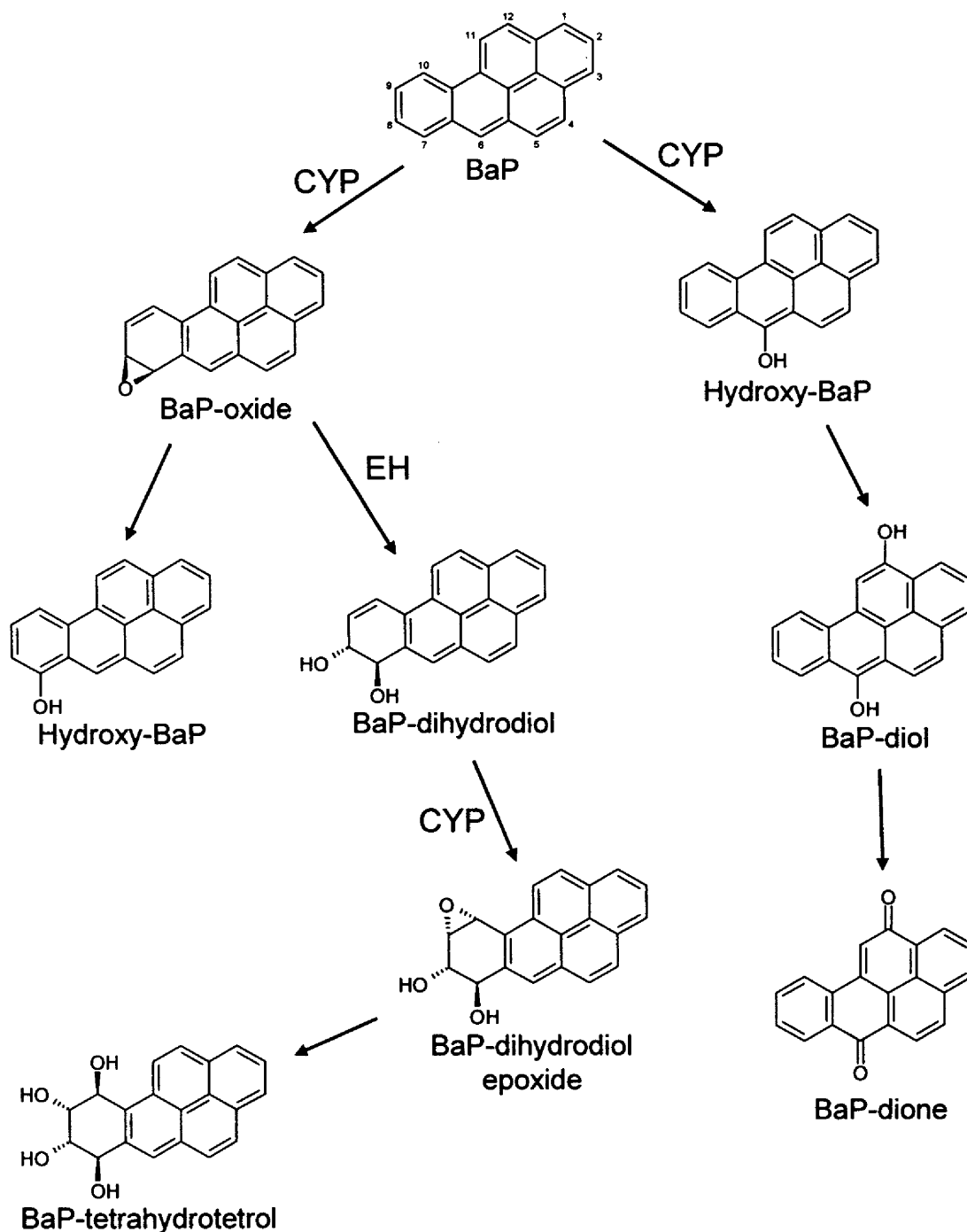
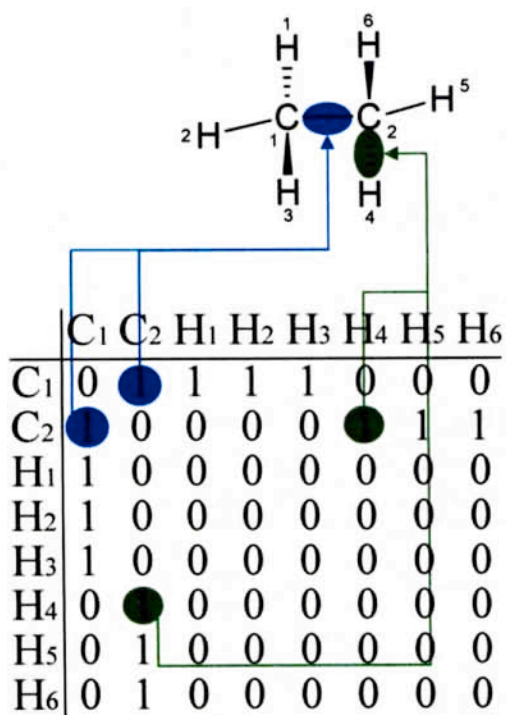


**Figure 4.1.** Common metabolic pathways of BaP when incubated with recombinant human cytochrome P450 (CYP) and epoxide hydrolase (EH) (only one structural isomer is shown).

### Ethane:



### Carbon dioxide:

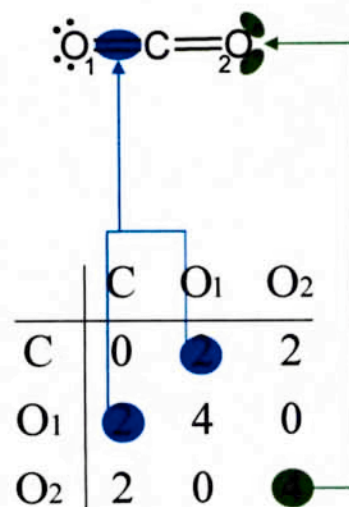
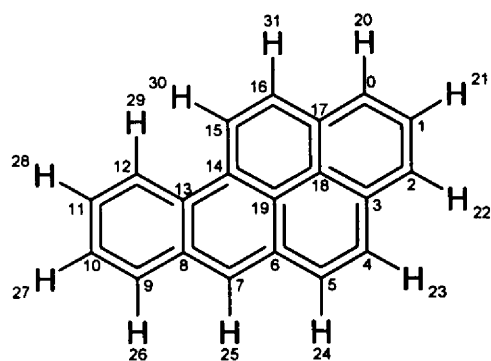


**Figure 4.2.** Bond-electron matrix representations of atomic connectivity and electronic environment for ethane and carbon dioxide. Off-diagonal elements represent the bond order between two atoms. Diagonal elements represent valence electrons not involved in bonding

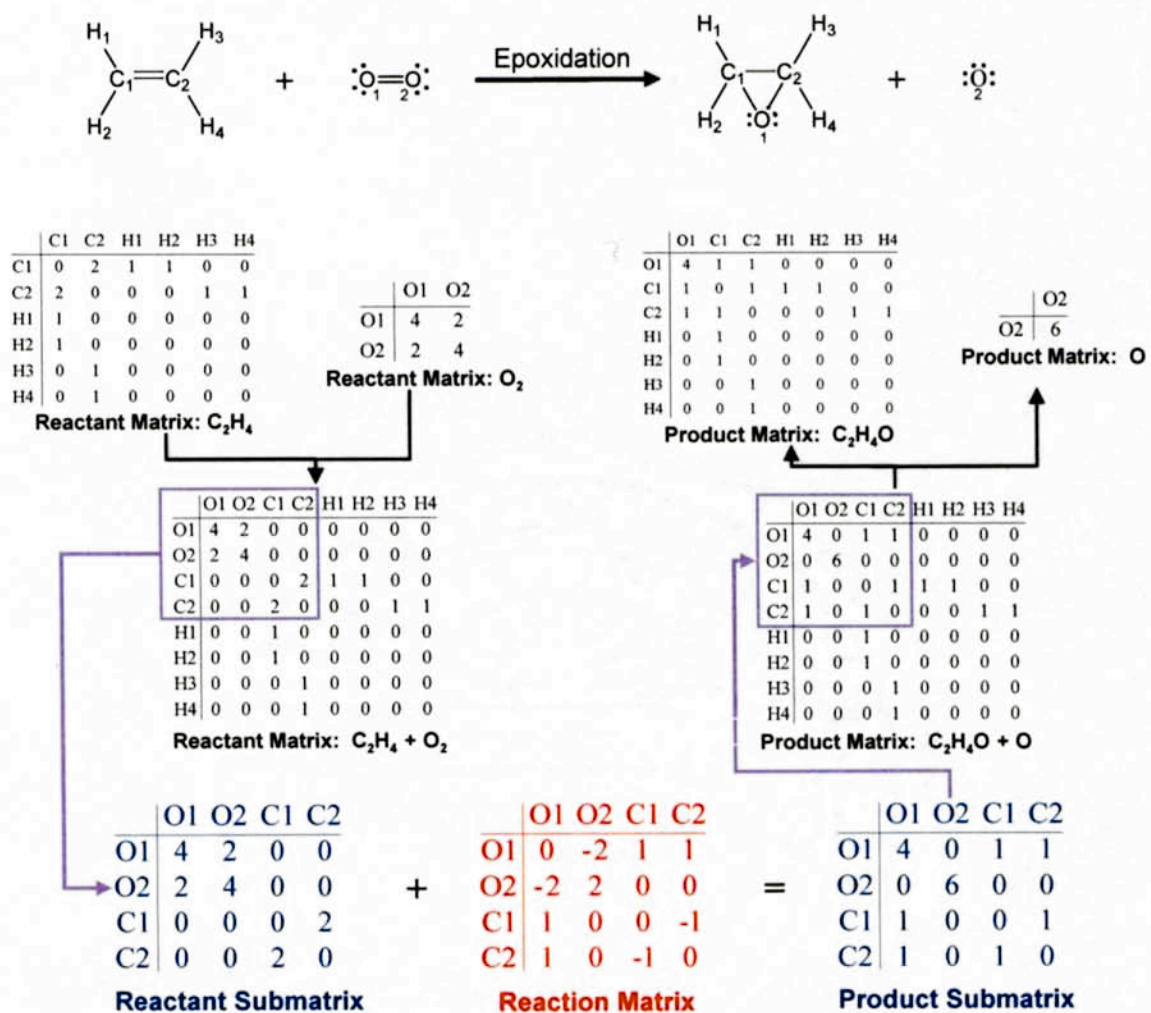


(a)

0 0 C : {1, 1.5}, {17, 1.5}, {20, 1};  
 1 0 C : {0, 1.5}, {2, 1.5}, {21, 1};  
 2 0 C : {1, 1.5}, {3, 1.5}, {22, 1};  
 3 0 C : {2, 1.5}, {4, 1.5}, {18, 1.5};  
 4 0 C : {3, 1.5}, {5, 1.5}, {23, 1};  
 5 0 C : {4, 1.5}, {6, 1.5}, {24, 1};  
 6 0 C : {5, 1.5}, {7, 1.5}, {19, 1.5};  
 7 0 C : {6, 1.5}, {8, 1.5}, {25, 1};  
 8 0 C : {7, 1.5}, {9, 1.5}, {13, 1.5};  
 9 0 C : {8, 1.5}, {10, 1.5}, {26, 1};  
 10 0 C : {9, 1.5}, {11, 1.5}, {27, 1};  
 11 0 C : {10, 1.5}, {12, 1.5}, {28, 1};  
 12 0 C : {11, 1.5}, {13, 1.5}, {29, 1};  
 13 0 C : {12, 1.5}, {14, 1.5}, {8, 1.5};  
 14 0 C : {13, 1.5}, {15, 1.5}, {19, 1.5};  
 15 0 C : {14, 1.5}, {16, 1.5}, {30, 1};  
 16 0 C : {15, 1.5}, {17, 1.5}, {31, 1};  
 17 0 C : {16, 1.5}, {0, 1.5}, {18, 1.5};  
 18 0 C : {17, 1.5}, {3, 1.5}, {19, 1.5};  
 19 0 C : {6, 1.5}, {14, 1.5}, {18, 1.5};  
 20 0 H : {0, 1};  
 21 0 H : {1, 1};  
 22 0 H : {2, 1};  
 23 0 H : {4, 1};  
 24 0 H : {5, 1};  
 25 0 H : {7, 1};  
 26 0 H : {9, 1};  
 27 0 H : {10, 1};  
 28 0 H : {11, 1};  
 29 0 H : {12, 1};  
 30 0 H : {15, 1};  
 31 0 H : {16, 1};

(b)

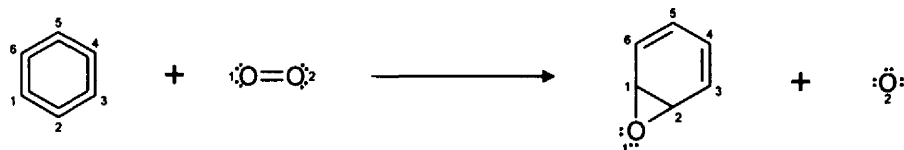
**Figure 4.3.** The molecular graph (a) and adjacency list (b) of BaP



	O1	O2					
O1	4	1	1	0	0	0	0
C1	1	0	1	1	1	0	0
C2	1	1	0	0	0	1	1
H1	0	1	0	0	0	0	0
H2	0	1	0	0	0	0	0
H3	0	0	1	0	0	0	0
H4	0	0	1	0	0	0	0

Product Matrix: O

**Figure 4.4.** Matrix operation of the epoxidation reaction of ethylene



<table style="width: 100%; border-collapse: collapse;"> <tr><th style="border-bottom: 1px solid black;">C1</th><th style="border-bottom: 1px solid black;">C2</th><th style="border-bottom: 1px solid black;">C3</th><th style="border-bottom: 1px solid black;">C4</th><th style="border-bottom: 1px solid black;">C5</th><th style="border-bottom: 1px solid black;">C6</th><th style="border-bottom: 1px solid black;">O1</th><th style="border-bottom: 1px solid black;">O2</th></tr> <tr><td>C1</td><td>0</td><td>1.5</td><td>0</td><td>0</td><td>0</td><td>1.5</td><td>0</td><td>0</td></tr> <tr><td>C2</td><td>1.5</td><td>0</td><td>1.5</td><td>0</td><td>0</td><td>0</td><td>0</td><td>0</td></tr> <tr><td>C3</td><td>0</td><td>1.5</td><td>0</td><td>1.5</td><td>0</td><td>0</td><td>0</td><td>0</td></tr> <tr><td>C4</td><td>0</td><td>0</td><td>1.5</td><td>0</td><td>1.5</td><td>0</td><td>0</td><td>0</td></tr> <tr><td>C5</td><td>0</td><td>0</td><td>0</td><td>1.5</td><td>0</td><td>1.5</td><td>0</td><td>0</td></tr> <tr><td>C6</td><td>1.5</td><td>0</td><td>0</td><td>0</td><td>1.5</td><td>0</td><td>0</td><td>0</td></tr> <tr><td>O1</td><td>0</td><td>0</td><td>0</td><td>0</td><td>0</td><td>0</td><td>4</td><td>2</td></tr> <tr><td>O2</td><td>0</td><td>0</td><td>0</td><td>0</td><td>0</td><td>0</td><td>2</td><td>4</td></tr> </table>	C1	C2	C3	C4	C5	C6	O1	O2	C1	0	1.5	0	0	0	1.5	0	0	C2	1.5	0	1.5	0	0	0	0	0	C3	0	1.5	0	1.5	0	0	0	0	C4	0	0	1.5	0	1.5	0	0	0	C5	0	0	0	1.5	0	1.5	0	0	C6	1.5	0	0	0	1.5	0	0	0	O1	0	0	0	0	0	0	4	2	O2	0	0	0	0	0	0	2	4	+	<table style="width: 100%; border-collapse: collapse;"> <tr><th style="border-bottom: 1px solid black;">C1</th><th style="border-bottom: 1px solid black;">C2</th><th style="border-bottom: 1px solid black;">C3</th><th style="border-bottom: 1px solid black;">C4</th><th style="border-bottom: 1px solid black;">C5</th><th style="border-bottom: 1px solid black;">C6</th><th style="border-bottom: 1px solid black;">O1</th><th style="border-bottom: 1px solid black;">O2</th></tr> <tr><td>C1</td><td>0</td><td>-0.5</td><td>0</td><td>0</td><td>0</td><td>-0.5</td><td>1</td><td>0</td></tr> <tr><td>C2</td><td>-0.5</td><td>0</td><td>-0.5</td><td>0</td><td>0</td><td>0</td><td>1</td><td>0</td></tr> <tr><td>C3</td><td>0</td><td>-0.5</td><td>0</td><td>0.5</td><td>0</td><td>0</td><td>0</td><td>0</td></tr> <tr><td>C4</td><td>0</td><td>0</td><td>0.5</td><td>0</td><td>-0.5</td><td>0</td><td>0</td><td>0</td></tr> <tr><td>C5</td><td>0</td><td>0</td><td>0</td><td>-0.5</td><td>0</td><td>0.5</td><td>0</td><td>0</td></tr> <tr><td>C6</td><td>-0.5</td><td>0</td><td>0</td><td>0</td><td>0.5</td><td>0</td><td>0</td><td>0</td></tr> <tr><td>O1</td><td>1</td><td>1</td><td>0</td><td>0</td><td>0</td><td>0</td><td>0</td><td>-2</td></tr> <tr><td>O2</td><td>0</td><td>0</td><td>0</td><td>0</td><td>0</td><td>0</td><td>-2</td><td>2</td></tr> </table>	C1	C2	C3	C4	C5	C6	O1	O2	C1	0	-0.5	0	0	0	-0.5	1	0	C2	-0.5	0	-0.5	0	0	0	1	0	C3	0	-0.5	0	0.5	0	0	0	0	C4	0	0	0.5	0	-0.5	0	0	0	C5	0	0	0	-0.5	0	0.5	0	0	C6	-0.5	0	0	0	0.5	0	0	0	O1	1	1	0	0	0	0	0	-2	O2	0	0	0	0	0	0	-2	2	=	<table style="width: 100%; border-collapse: collapse;"> <tr><th style="border-bottom: 1px solid black;">C1</th><th style="border-bottom: 1px solid black;">C2</th><th style="border-bottom: 1px solid black;">C3</th><th style="border-bottom: 1px solid black;">C4</th><th style="border-bottom: 1px solid black;">C5</th><th style="border-bottom: 1px solid black;">C6</th><th style="border-bottom: 1px solid black;">O1</th><th style="border-bottom: 1px solid black;">O2</th></tr> <tr><td>C1</td><td>0</td><td>1</td><td>0</td><td>0</td><td>0</td><td>1</td><td>1</td><td>0</td></tr> <tr><td>C2</td><td>1</td><td>0</td><td>1</td><td>0</td><td>0</td><td>0</td><td>1</td><td>0</td></tr> <tr><td>C3</td><td>0</td><td>1</td><td>0</td><td>2</td><td>0</td><td>0</td><td>0</td><td>0</td></tr> <tr><td>C4</td><td>0</td><td>0</td><td>2</td><td>0</td><td>1</td><td>0</td><td>0</td><td>0</td></tr> <tr><td>C5</td><td>0</td><td>0</td><td>0</td><td>1</td><td>0</td><td>2</td><td>0</td><td>0</td></tr> <tr><td>C6</td><td>1</td><td>0</td><td>0</td><td>0</td><td>2</td><td>0</td><td>0</td><td>0</td></tr> <tr><td>O1</td><td>1</td><td>1</td><td>0</td><td>0</td><td>0</td><td>0</td><td>4</td><td>0</td></tr> <tr><td>O2</td><td>0</td><td>0</td><td>0</td><td>0</td><td>0</td><td>0</td><td>0</td><td>6</td></tr> </table>	C1	C2	C3	C4	C5	C6	O1	O2	C1	0	1	0	0	0	1	1	0	C2	1	0	1	0	0	0	1	0	C3	0	1	0	2	0	0	0	0	C4	0	0	2	0	1	0	0	0	C5	0	0	0	1	0	2	0	0	C6	1	0	0	0	2	0	0	0	O1	1	1	0	0	0	0	4	0	O2	0	0	0	0	0	0	0	6
C1	C2	C3	C4	C5	C6	O1	O2																																																																																																																																																																																																																																													
C1	0	1.5	0	0	0	1.5	0	0																																																																																																																																																																																																																																												
C2	1.5	0	1.5	0	0	0	0	0																																																																																																																																																																																																																																												
C3	0	1.5	0	1.5	0	0	0	0																																																																																																																																																																																																																																												
C4	0	0	1.5	0	1.5	0	0	0																																																																																																																																																																																																																																												
C5	0	0	0	1.5	0	1.5	0	0																																																																																																																																																																																																																																												
C6	1.5	0	0	0	1.5	0	0	0																																																																																																																																																																																																																																												
O1	0	0	0	0	0	0	4	2																																																																																																																																																																																																																																												
O2	0	0	0	0	0	0	2	4																																																																																																																																																																																																																																												
C1	C2	C3	C4	C5	C6	O1	O2																																																																																																																																																																																																																																													
C1	0	-0.5	0	0	0	-0.5	1	0																																																																																																																																																																																																																																												
C2	-0.5	0	-0.5	0	0	0	1	0																																																																																																																																																																																																																																												
C3	0	-0.5	0	0.5	0	0	0	0																																																																																																																																																																																																																																												
C4	0	0	0.5	0	-0.5	0	0	0																																																																																																																																																																																																																																												
C5	0	0	0	-0.5	0	0.5	0	0																																																																																																																																																																																																																																												
C6	-0.5	0	0	0	0.5	0	0	0																																																																																																																																																																																																																																												
O1	1	1	0	0	0	0	0	-2																																																																																																																																																																																																																																												
O2	0	0	0	0	0	0	-2	2																																																																																																																																																																																																																																												
C1	C2	C3	C4	C5	C6	O1	O2																																																																																																																																																																																																																																													
C1	0	1	0	0	0	1	1	0																																																																																																																																																																																																																																												
C2	1	0	1	0	0	0	1	0																																																																																																																																																																																																																																												
C3	0	1	0	2	0	0	0	0																																																																																																																																																																																																																																												
C4	0	0	2	0	1	0	0	0																																																																																																																																																																																																																																												
C5	0	0	0	1	0	2	0	0																																																																																																																																																																																																																																												
C6	1	0	0	0	2	0	0	0																																																																																																																																																																																																																																												
O1	1	1	0	0	0	0	4	0																																																																																																																																																																																																																																												
O2	0	0	0	0	0	0	0	6																																																																																																																																																																																																																																												
Reactant Submatrix		Reaction Matrix		Product Submatrix																																																																																																																																																																																																																																																

**Figure 4.5.** Matrix operation for the epoxidation of benzene with the BE matrix expressed using 1.5-order bonds.

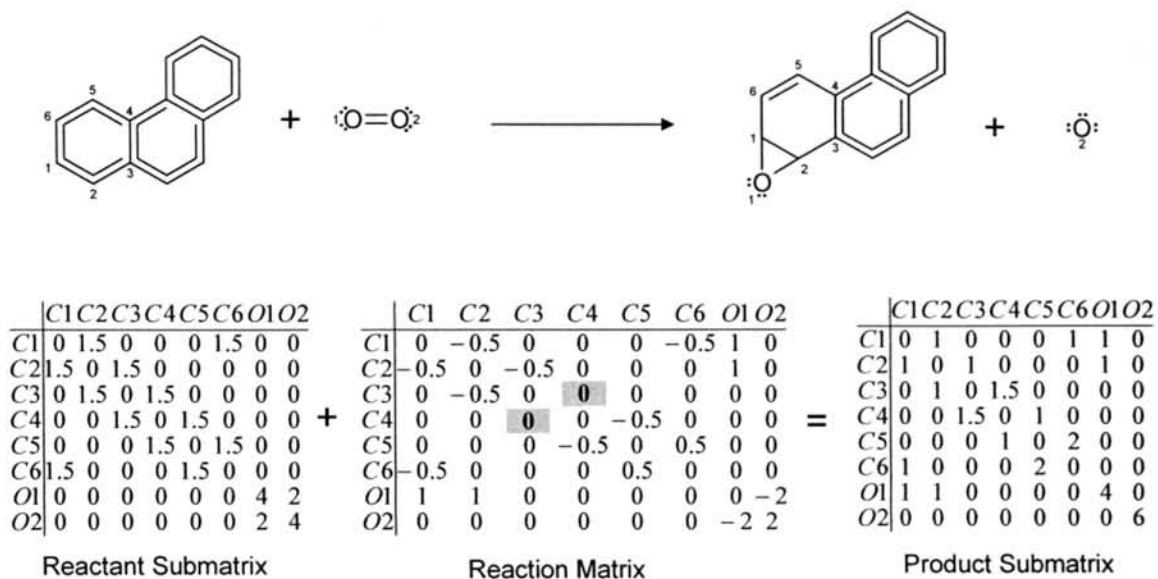
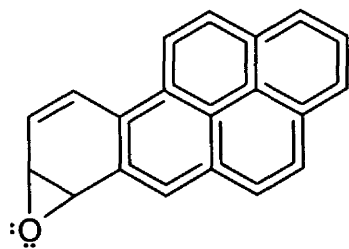
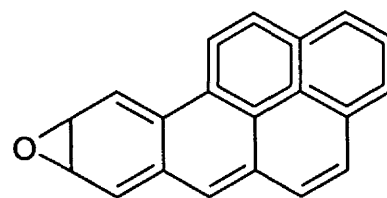


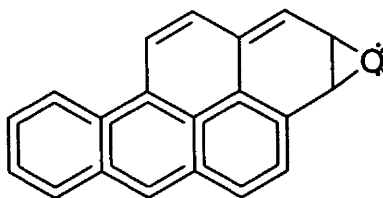
**Figure 4.6.** Matrix operation of the epoxidation of an aromatic bond within a multi-ring aromatic compound. Shaded elements represent the bonds that are part of the aromatic sextet of another ring and thus their aromaticities are not disrupted.



BaP-7,8-oxide



BaP-8,9-oxide



BaP-2,3-oxide

**Figure 4.7.** Chemical structures of some BaP-oxides



	C1	C2	C3	C4	C5	C6	C7	C8	C9	C10	O1	O2
C1	0	1.5	0	0	0	0	0	0	0	1.5	0	0
C2	1.5	0	1.5	0	0	0	0	0	0	0	0	0
C3	0	1.5	0	1.5	0	0	0	0	0	0	0	0
C4	0	0	1.5	0	1.5	0	0	1.5	0	0	0	0
C5	0	0	0	1.5	0	1.5	0	0	0	0	0	0
C6	0	0	0	0	1.5	0	1.5	0	0	0	0	0
C7	0	0	0	0	0	1.5	0	1.5	0	0	0	0
C8	0	0	0	0	0	0	1.5	0	1.5	0	0	0
C9	0	0	0	1.5	0	0	0	1.5	0	1.5	0	0
C10	1.5	0	0	0	0	0	0	0	1.5	0	0	0
O1	0	0	0	0	0	0	0	0	0	0	4	2
O2	0	0	0	0	0	0	0	0	0	0	2	4

Reactant Submatrix

	C1	C2	C3	C4	C5	C6	C7	C8	C9	C10	O1	O2
C1	0	-0.5	0	0	0	0	0	0	0	-0.5	1	0
C2	-0.5	0	-0.5	0	0	0	0	0	0	0	1	0
C3	0	-0.5	0	0.5	0	0	0	0	0	0	0	0
C4	0	0	0.5	0	-0.5	0	0	0	-0.5	0	0	0
C5	0	0	0	-0.5	0	0.5	0	0	0	0	0	0
C6	0	0	0	0	0	0.5	0	-0.5	0	0	0	0
C7	0	0	0	0	0	0	-0.5	0	0	0	0	0
C8	0	0	0	0	0	0	0	0	0	0	0	0
C9	0	0	0	-0.5	0	0	0	0	0	0	0	0
C10	-0.5	0	0	0	0	0	0	0	0	0	0	0
O1	1	1	0	0	0	0	0	0	0	0	0	-2
O2	0	0	0	0	0	0	0	0	0	0	0	-2

Reaction Matrix

	C1	C2	C3	C4	C5	C6	C7	C8	C9	C10	O1	O2
C1	0	1	0	0	0	0	0	0	0	1	1	0
C2	1	0	1	0	0	0	0	0	0	0	1	0
C3	0	1	0	2	0	0	0	0	0	0	0	0
C4	0	0	2	0	1	0	0	0	1	0	0	0
C5	0	0	0	1	0	2	0	0	0	0	0	0
C6	0	0	0	0	2	0	1	0	0	0	0	0
C7	0	0	0	0	0	1	0	1.5	0	0	0	0
C8	0	0	0	0	0	0	1.5	0	1.5	0	0	0
C9	0	0	0	1	0	0	0	1.5	0	1.5	0	0
C10	1	0	0	0	0	0	0	0	1.5	0	0	0
O1	1	1	0	0	0	0	0	0	0	0	4	0
O2	0	0	0	0	0	0	0	0	0	0	0	6

Product Submatrix

**Figure 4.8.** Matrix operation for the epoxidation of BaP resulting in the disruption of the aromaticity of two rings.



	C1	O1	C2	H1
C1	0	1	1	0
O1	1	4	1	0
C2	1	1	0	1
H1	0	0	1	0

+

	C1	O1	C2	H1
C1	0	-1	1	0
O1	-1	0	0	1
C2	1	0	0	-1
H1	0	1	-1	0

=

	C1	O1	C2	H1
C1	0	0	2	0
O1	0	4	1	1
C2	2	1	0	0
H1	0	1	0	0

Reactant Submatrix
Reaction Matrix
Product Submatrix

**Figure 4.10.** Matrix operation of the NIH Shift reaction of epoxides.

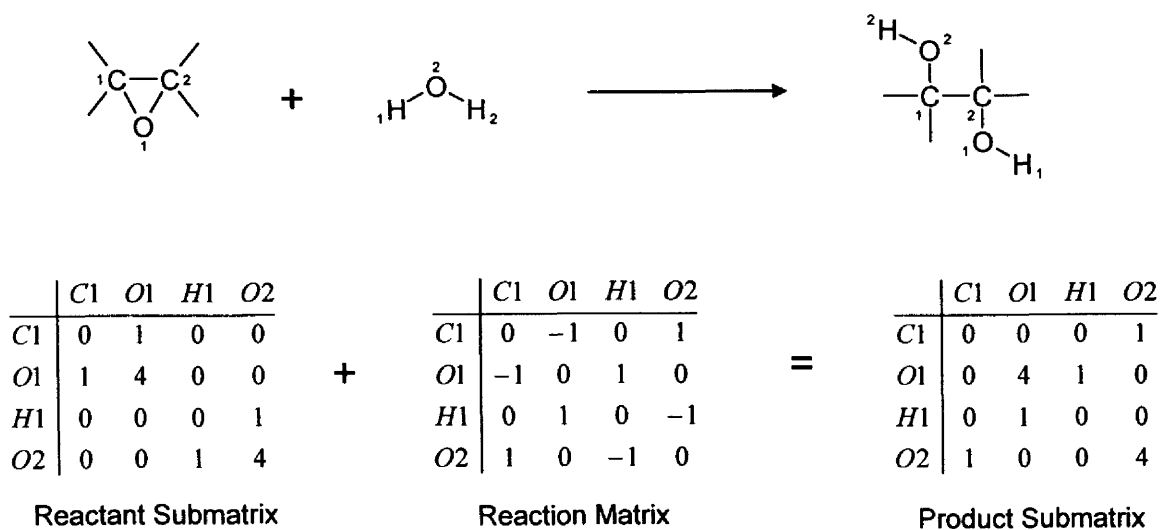


**Figure 4.9.** Matrix operation of the hydrolysis reaction of epoxides.

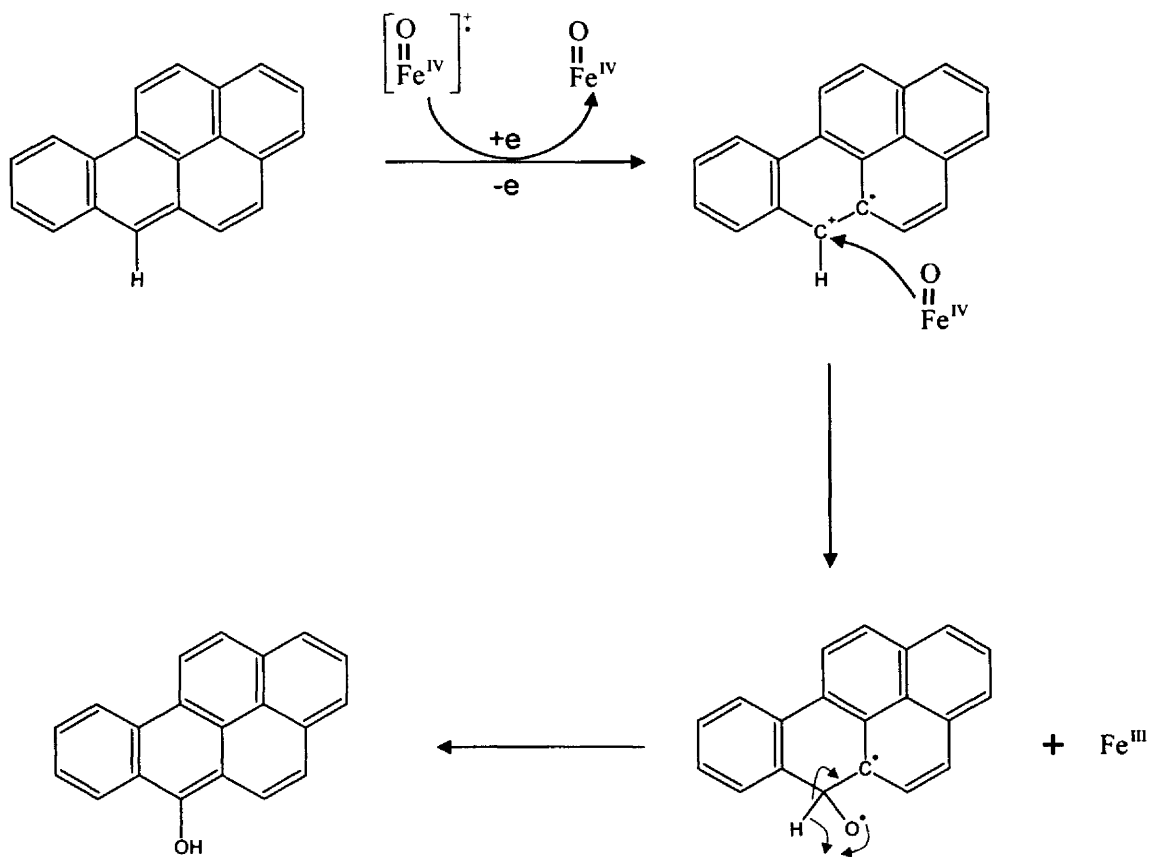


**Figure 4.11.** Mechanism of cytochrome P-450 catalyzed one-electron oxidation of BaP to form 6-hydroxy-BaP (adapted from Cavalieri et al (20, 21)).

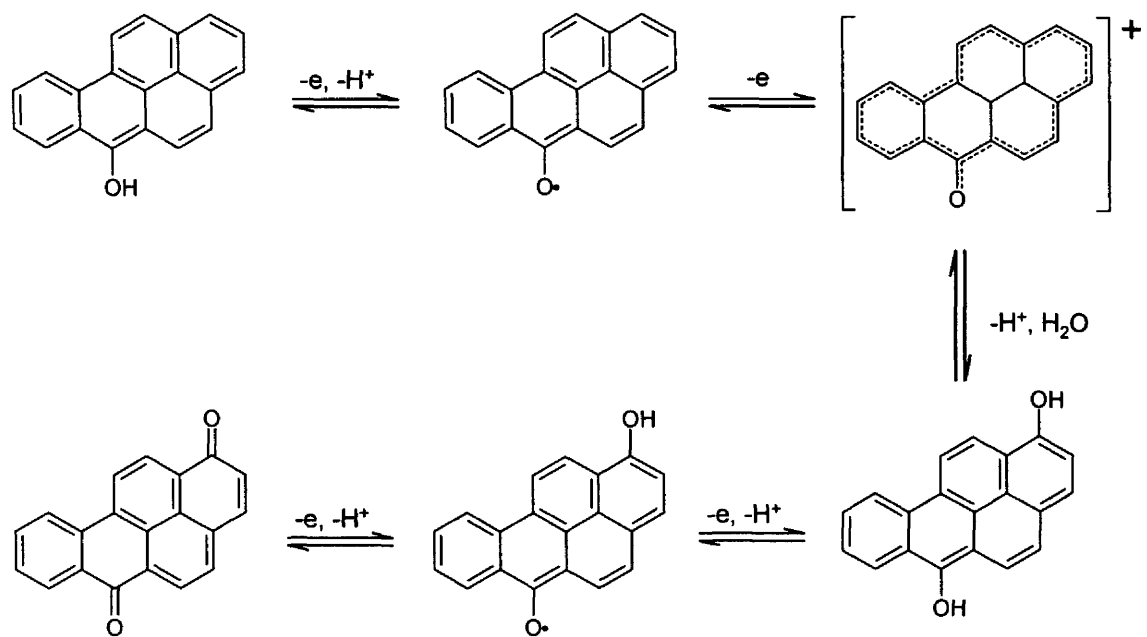


**Figure 4.12.** Mechanism of the oxidation of 6-hydroxy-BaP to BaP-diones, adapted from Lorentzen et al (19). Only the formation of BaP-1,6-dione is shown.

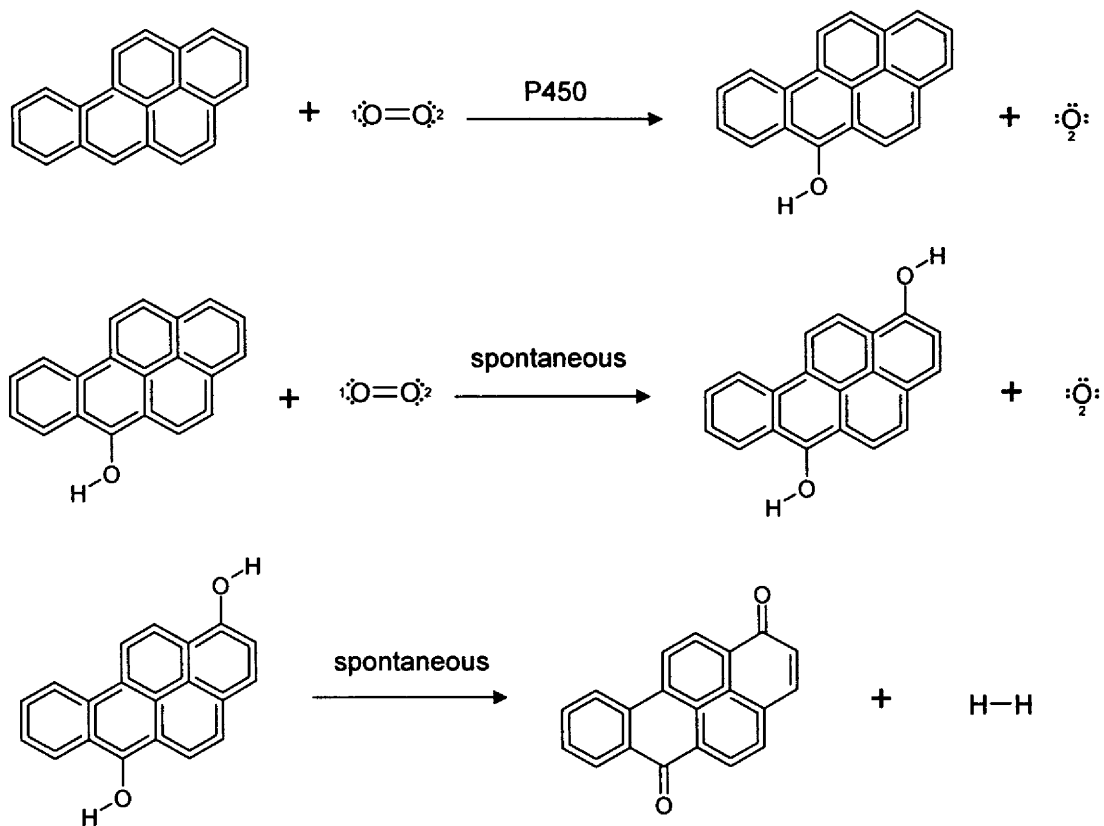


**Figure 4.13.** Simplified mechanism for multi-step oxidation of BaP to BaP-diones (only the formation of BaP-1,6-dione is shown).

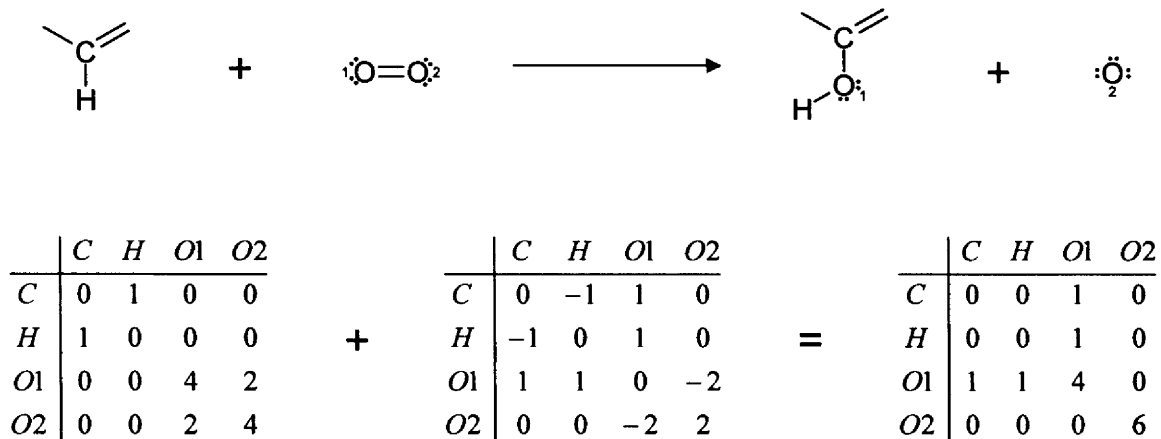
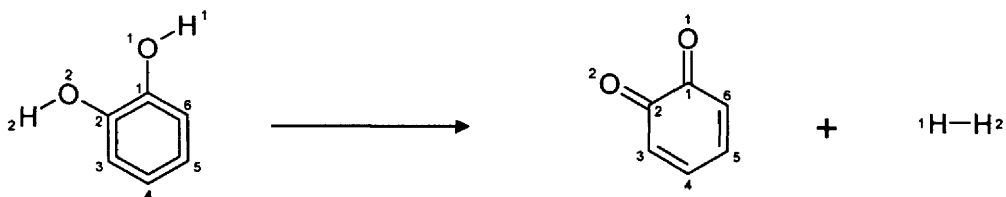


**Figure 4.14.** Matrix operation for carbon hydroxylation reactions



	H1	O1	C1	C2	C3	C4	C5	C6	O2	H2
H1	0	1	0	0	0	0	0	0	0	0
O1	1	4	1	0	0	0	0	0	0	0
C1	0	1	0	1.5	0	0	0	1.5	0	0
C2	0	0	1.5	0	1.5	0	0	0	1	0
C3	0	0	0	1.5	0	1.5	0	0	0	0
C4	0	0	0	0	1.5	0	1.5	0	0	0
C5	0	0	0	0	0	1.5	0	1.5	0	0
C6	0	0	1.5	0	0	0	1.5	0	0	0
O2	0	0	0	1	0	0	0	0	4	1
H2	0	0	0	0	0	0	0	0	0	1

Reactant Submatrix

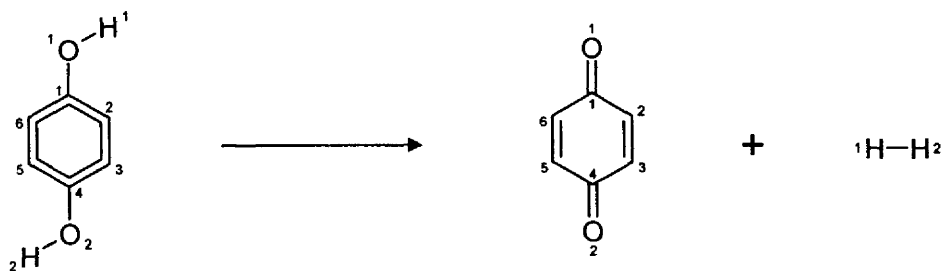
	H1	O1	C1	C2	C3	C4	C5	C6	O2	H2
H1	0	-1	0	0	0	0	0	0	0	1
O1	-1	0	1	0	0	0	0	0	0	0
C1	0	1	0	-0.5	0	0	0	-0.5	0	0
C2	0	0	-0.5	0	-0.5	0	0	0	1	0
C3	0	0	0	-0.5	0	0.5	0	0	0	0
C4	0	0	0	0	0.5	0	-0.5	0	0	0
C5	0	0	0	0	0	-0.5	0	0.5	0	0
C6	0	0	-0.5	0	0	0	0.5	0	0	0
O2	0	0	0	1	0	0	0	0	0	-1
H2	1	0	0	0	0	0	0	0	0	-1

Reaction Matrix

	H1	O1	C1	C2	C3	C4	C5	C6	O2	H2
H1	0	0	0	0	0	0	0	0	0	1
O1	0	4	2	0	0	0	0	0	0	0
C1	0	2	0	1	0	0	0	1	0	0
C2	0	0	1	0	1	0	0	0	2	0
C3	0	0	0	1	0	2	0	0	0	0
C4	0	0	0	0	2	0	1	0	0	0
C5	0	0	0	0	0	1	0	2	0	0
C6	0	0	1	0	0	0	2	0	0	0
O2	0	0	0	2	0	0	0	0	4	0
H2	1	0	0	0	0	0	0	0	0	0

Product Submatrix

**Figure 4.15.** Matrix operation of the auto-oxidation of benzene-1,2-diol to benzene-1,2-dione.



	H1	O1	C1	C2	C3	C4	C5	C6	O2	H2
H1	0	1	0	0	0	0	0	0	0	0
O1	1	4	1	0	0	0	0	0	0	0
C1	0	1	0	1.5	0	0	0	1.5	0	0
C2	0	0	1.5	0	1.5	0	0	0	0	0
C3	0	0	0	1.5	0	1.5	0	0	0	0
C4	0	0	0	0	1.5	0	1.5	0	1	0
C5	0	0	0	0	0	1.5	0	1.5	0	0
C6	0	0	1.5	0	0	0	1.5	0	0	0
O2	0	0	0	0	0	1	0	0	4	1
H2	0	0	0	0	0	0	0	0	1	0

Reactant Submatrix

+

	H1	O1	C1	C2	C3	C4	C5	C6	O2	H2
H1	0	-1	0	0	0	0	0	0	0	1
O1	-1	0	1	0	0	0	0	0	0	0
C1	0	1	0	-0.5	0	0	0	-0.5	0	0
C2	0	0	-0.5	0	0.5	0	0	0	0	0
C3	0	0	0	0.5	0	-0.5	0	0	0	0
C4	0	0	0	0	-0.5	0	-0.5	0	1	0
C5	0	0	0	0	0	-0.5	0	0.5	0	0
C6	0	0	-0.5	0	0	0	0.5	0	0	0
O2	0	0	0	0	0	1	0	0	0	-1
H2	1	0	0	0	0	0	0	0	0	-1

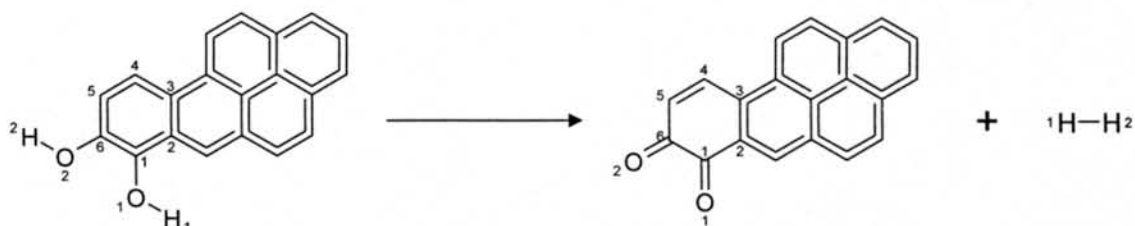
Reaction Matrix

=

	H1	O1	C1	C2	C3	C4	C5	C6	O2	H2
H1	0	0	0	0	0	0	0	0	0	1
O1	0	4	2	0	0	0	0	0	0	0
C1	0	2	0	1	0	0	0	1	0	0
C2	0	0	1	0	2	0	0	0	0	0
C3	0	0	0	2	0	1	0	0	0	0
C4	0	0	0	0	1	0	1	0	2	0
C5	0	0	0	0	0	1	0	2	0	0
C6	0	0	1	0	0	0	2	0	0	0
O2	0	0	0	0	0	2	0	0	4	0
H2	1	0	0	0	0	0	0	0	0	0

Product Submatrix

**Figure 4.16.** Matrix operation of the auto-oxidation of benzene-1,4-diol to benzene-1,4-dione.



	H1	O1	C1	C2	C3	C4	C5	C6	O2	H2
H1	0	1	0	0	0	0	0	0	0	0
O1	1	4	1	0	0	0	0	0	0	0
C1	0	1	0	1.5	0	0	0	1.5	0	0
C2	0	0	1.5	0	1.5	0	0	0	0	0
C3	0	0	0	1.5	0	1.5	0	0	0	0
C4	0	0	0	0	1.5	0	1.5	0	0	0
C5	0	0	0	0	0	1.5	0	1.5	0	0
C6	0	0	1.5	0	0	0	1.5	0	1	0
O2	0	0	0	0	0	0	0	1	4	1
H2	0	0	0	0	0	0	0	0	0	1

Reactant Submatrix

+

	H1	O1	C1	C2	C3	C4	C5	C6	O2	H2
H1	0	-1	0	0	0	0	0	0	0	1
O1	-1	0	1	0	0	0	0	0	0	0
C1	0	1	0	-0.5	0	0	0	-0.5	0	0
C2	0	0	-0.5	0	0	0	0	0	0	0
C3	0	0	0	0	0	-0.5	0	0	0	0
C4	0	0	0	0	-0.5	0	0.5	0	0	0
C5	0	0	0	0	0	0.5	0	-0.5	0	0
C6	0	0	-0.5	0	0	0	-0.5	0	1	0
O2	0	0	0	0	0	0	0	1	0	-1
H2	1	0	0	0	0	0	0	0	0	-1

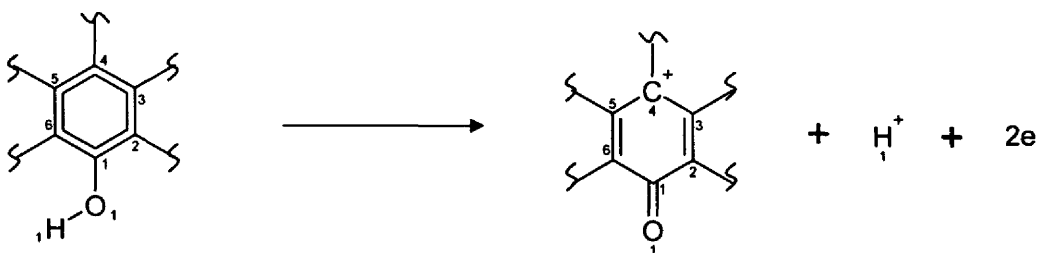
Reaction Matrix

=

	H1	O1	C1	C2	C3	C4	C5	C6	O2	H2
H1	0	0	0	0	0	0	0	0	0	1
O1	0	4	2	0	0	0	0	0	0	0
C1	0	2	0	1	0	0	0	1	0	0
C2	0	0	1	0	2	0	0	0	0	0
C3	0	0	0	2	0	1	0	0	0	0
C4	0	0	0	0	1	0	1.5	0	0	0
C5	0	0	0	0	0	1.5	0	1	0	0
C6	0	0	1	0	0	0	1	0	2	0
O2	0	0	0	0	0	0	0	2	4	0
H2	1	0	0	0	0	0	0	0	0	0

Product Submatrix

Figure 4.17. Matrix operation of the auto-oxidation of BaP-7,8-diol to BaP-7,8-dione.



(representative of two identical submatrices)

	H1	O1	C1	C2	C3	C4	C5	C6
H1	0	1	0	0	0	0	0	0
O1	1	4	1	0	0	0	0	0
C1	0	1	0	1.5	0	0	0	1.5
C2	0	0	1.5	0	1.5	0	0	0
C3	0	0	0	1.5	0	1.5	0	0
C4	0	0	0	0	1.5	0	1.5	0
C5	0	0	0	0	0	1.5	0	1.5
C6	0	0	1.5	0	0	0	1.5	0

Conceptual Reactant Submatrix

+

	H1	O1	C1	C2	C3	C4	C5	C6
H1	0	-1	0	0	0	0	0	0
O1	-1	0	1	0	0	0	0	0
C1	0	1	0	-0.5	0	0	0	-0.5
C2	0	0	-0.5	0	0.5	0	0	0
C3	0	0	0	0.5	0	-0.5	0	0
C4	0	0	0	0	-0.5	0	-0.5	0
C5	0	0	0	0	0	-0.5	0	0.5
C6	0	0	-0.5	0	0	0	0.5	0

Conceptual Reaction Submatrix

=

	H1	O1	C1	C2	C3	C4	C5	C6
H1	0	0	0	0	0	0	0	0
O1	0	4	2	0	0	0	0	0
C1	0	2	0	1	0	0	0	1
C2	0	0	1	0	2	0	0	0
C3	0	0	0	2	0	1	0	0
C4	0	0	0	0	1	0	1	0
C5	0	0	0	0	0	1	0	2
C6	0	0	1	0	0	0	2	0

Conceptual Product Submatrix

**Figure 4.18.** Conceptual submatrices for the auto-oxidation of BaP-diols with hydroxyl groups connected to different rings.

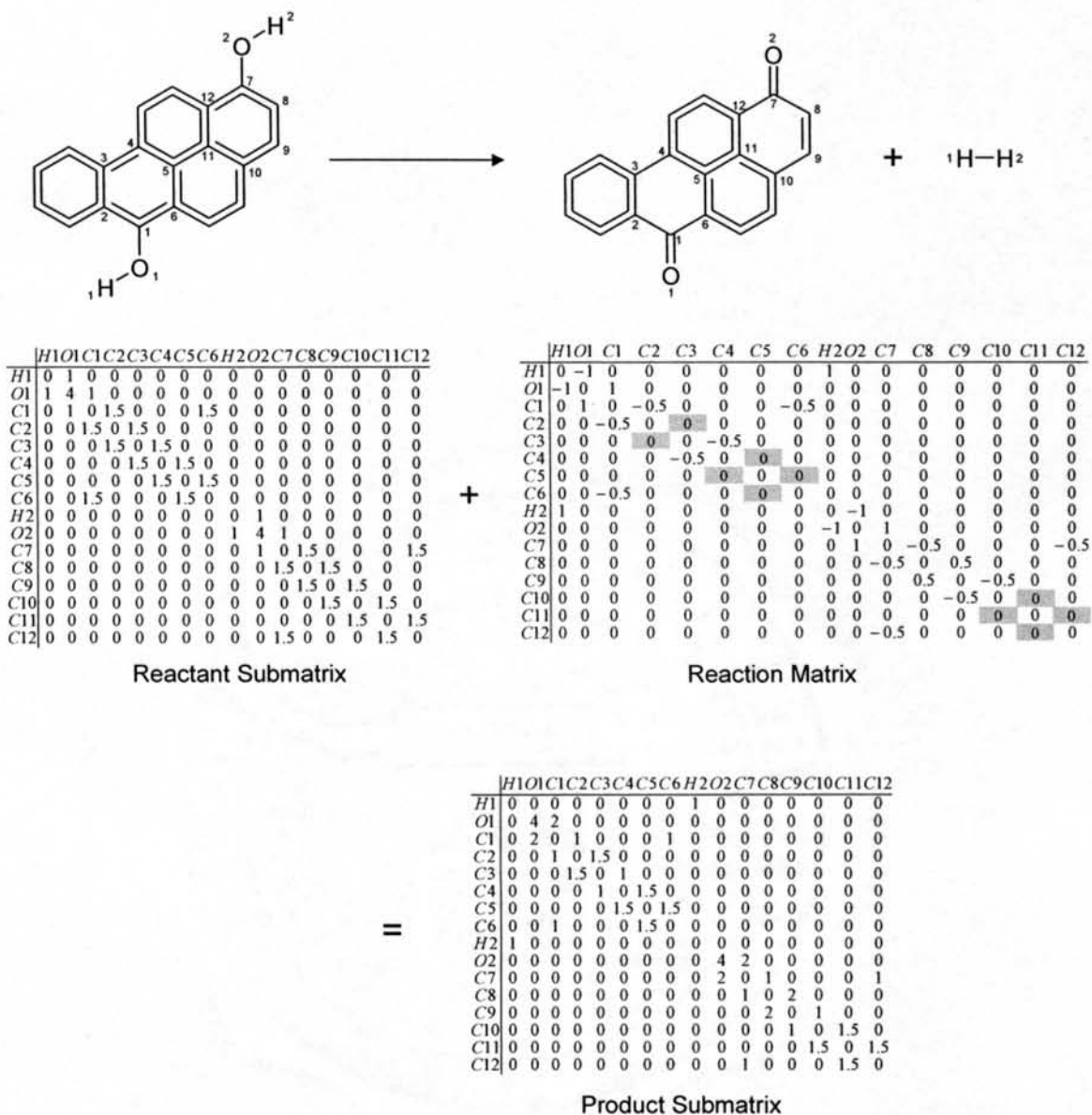
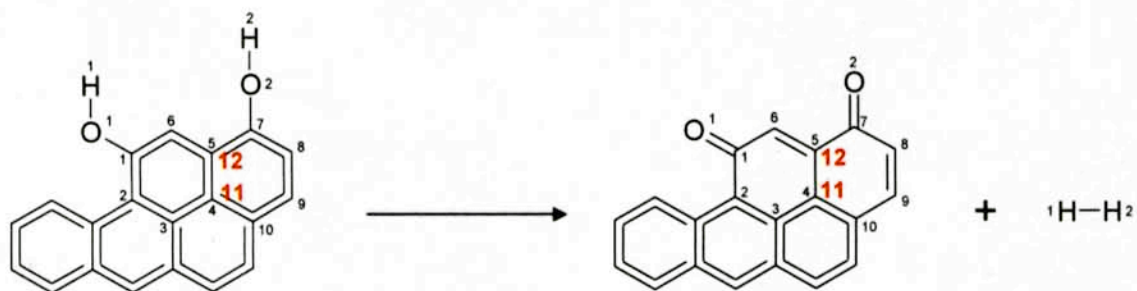


Figure 4.19. Matrix operation of the auto-oxidation of BaP-1,6-diol to BaP-1,6-dione.



	H1	O1	C1	C2	C3	C4	C5	C6	H2	O2	C7	C8	C9	C10	C11	C12
H1	0	-1	0	0	0	0	0	0	1	0	0	0	0	0	0	0
O1	-1	0	1	0	0	0	0	0	0	0	0	0	0	0	0	0
C1	0	1	0	-0.5	0	0	0	-0.5	0	0	0	0	0	0	0	0
C2	0	0	-0.5	0	0	0	0	0	0	0	0	0	0	0	0	0
C3	0	0	0	0	0	0	0	0	0	0	0	0	0	0	0	0
C4	0	0	0	0	0	0	-0.5	0	0	0	0	0	0	0	0	0
C5	0	0	0	0	0	-0.5	0	0.5	0	0	0	0	0	0	0	0
C6	0	0	-0.5	0	0	0	0.5	0	0	0	0	0	0	0	0	0
H2	1	0	0	0	0	0	0	0	-1	0	0	0	0	0	0	0
O2	0	0	0	0	0	0	0	0	-1	0	1	0	0	0	0	0
C7	0	0	0	0	0	0	0	0	0	1	0	-0.5	0	0	0	-0.5
C8	0	0	0	0	0	0	0	0	0	0	-0.5	0	0.5	0	0	0
C9	0	0	0	0	0	0	0	0	0	0	0	0.5	0	-0.5	0	0
C10	0	0	0	0	0	0	0	0	0	0	0	0	-0.5	0	0	0
C11	0	0	0	0	0	0	0	0	0	0	0	0	0	0	0	0.5
C12	0	0	0	0	0	0	0	0	0	0	-0.5	0	0	0	0.5	0

Combined Conceptual Submatrix



	H1	O1	C1	C2	C3	C4	C5	C6	H2	O2	C7	C8	C9	C10
H1	0	-1	0	0	0	0	0	0	1	0	0	0	0	0
O1	-1	0	1	0	0	0	0	0	0	0	0	0	0	0
C1	0	1	0	-0.5	0	0	0	-0.5	0	0	0	0	0	0
C2	0	0	-0.5	0	0	0	0	0	0	0	0	0	0	0
C3	0	0	0	0	0	0	0	0	0	0	0	0	0	0
C4	0	0	0	0	0	0	-0.5	0	0	0	0	0	0	0
C5	0	0	0	0	0	-0.5	0	0.5	0	0	-0.5	0	0	0
C6	0	0	-0.5	0	0	0	0.5	0	0	0	0	0	0	0
H2	1	0	0	0	0	0	0	0	0	-1	0	0	0	0
O2	0	0	0	0	0	0	0	0	-1	0	1	0	0	0
C7	0	0	0	0	0	0	-0.5	0	0	1	0	-0.5	0	0
C8	0	0	0	0	0	0	0	0	0	0	-0.5	0	0.5	0
C9	0	0	0	0	0	0	0	0	0	0	0	0.5	0	-0.5
C10	0	0	0	0	0	0	0	0	0	0	0	0	-0.5	0

Final Reaction Matrix

**Figure 4.20.** Reaction Matrices for the auto-oxidation of BaP-1,11-diol to BaP-1,11-dione.

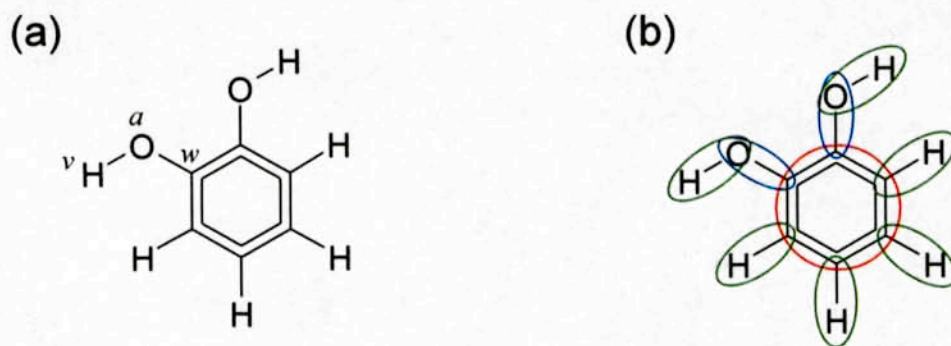
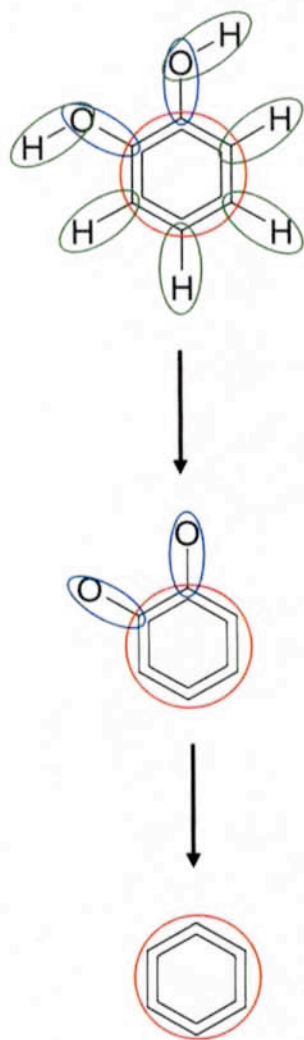


**Figure 4.21.** Molecular graph (a) and biconnected components representation (b) of benzene-1,2-diol. In part (b), each subgraph of benzene-1,2-diol enclosed in a circle represents a biconnected component (bicomponent).

(a)



(b)

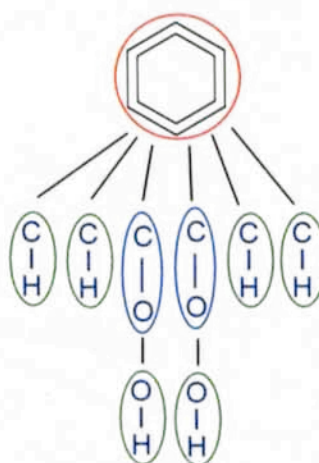


**Figure 4.22.** Successive removal of bicomps with lowest degrees (a) to construct the decomposition tree of benzene-1,2-diol (b).

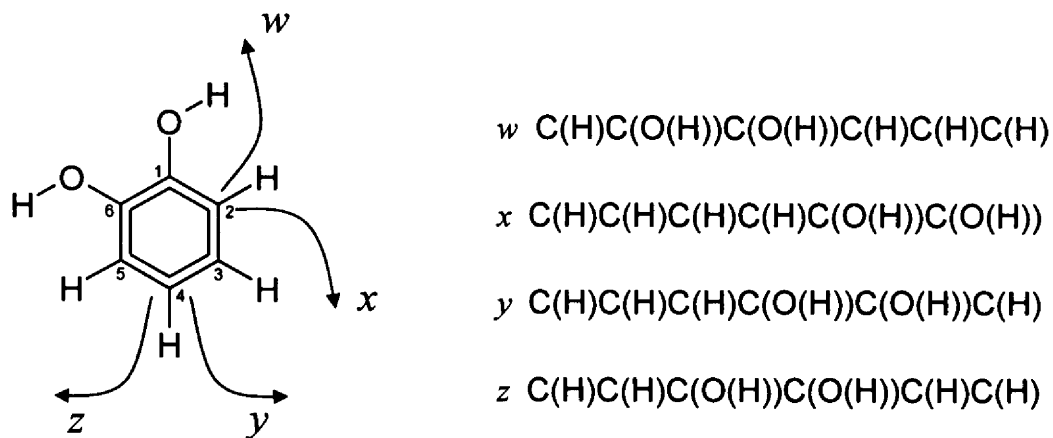
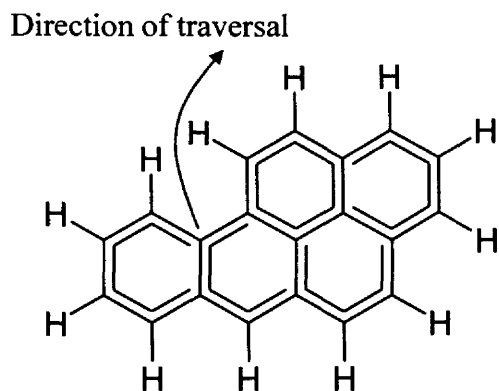


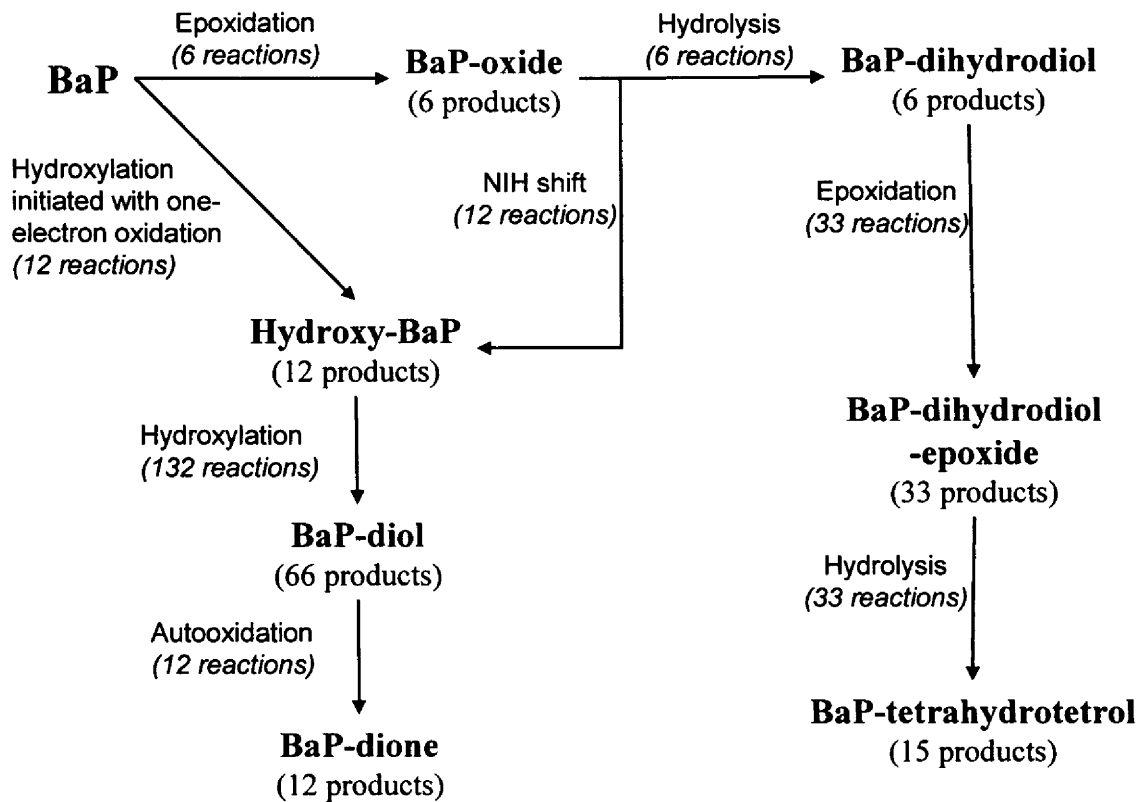
**Figure 4.23.** The traversal process for determining the unique string code of benzene-1,2-diol. Paths  $w$ ,  $x$ ,  $y$ , and  $z$  were randomly selected for demonstration and resulted in four possible string codes. Encoding via path  $x$  results in the lexicographically minimal string code.



Unique string code for BaP:

CCC(H)C(H)CC(H)C(H)C(H)CC(H)C(H)CC(H)CC(H)C(H)C(H)C(H)C:C:

**Figure 4.24.** The direction of traversal for constructing the unique string code of BaP



Total:  
 246 reactions  
 150 products

**Figure 4.25.** The RN pathway model prediction of BaP metabolic pathways.

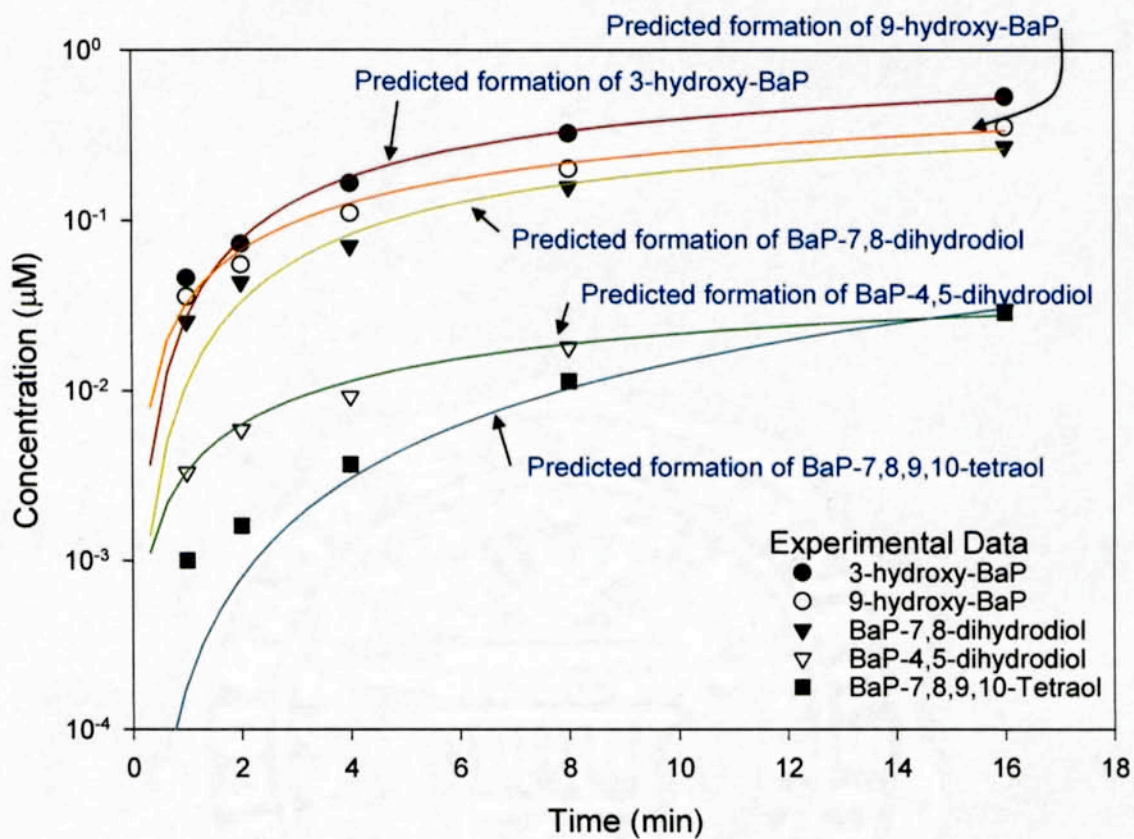


**Figure 4.26.** The RN kinetics model simulation of the time course of BaP metabolism using experimental data reported by Gautier et al. (30). Symbols represent experimental data and solid lines represent model simulations.

## Chapter 5

### **High-Performance Liquid Chromatography Method for the Separation and Quantification of Eight Fluorescent Benzo[*a*]pyrene Metabolites including 3-Hydroxy- and 7-Hydroxy-Benzo[*a*]pyrene**

#### **5.1. Introduction**

As part of our overall plan of building a Reaction Network (RN) model for the complex biotransformation pathways of benzo[*a*]pyrene (BaP) (1, 2), enzyme kinetics data are essential for determining the rate constants for key metabolic reactions. However, despite the fact that there were over 8600 publications on BaP (PubMed search on July 26, 2004), detailed enzyme kinetics studies on BaP and its metabolites, particularly using human enzymes, were scarce. Thus, BaP biotransformations were studied in our laboratory using recombinant human cytochrome P450 1A1 (CYP1A1) and microsomal epoxide hydrolase (EH). Due to the high cost of the enzymes, these experiments were carried out in small volumes (1000  $\mu$ L), yielding limited amounts of metabolites at relatively low concentrations. Therefore, analytical methods with high detection sensitivities were required to determine the level of BaP metabolites. However, analytical methods resolving all the relevant BaP metabolites at the sensitivity that we required were not available. Thus, we developed analytical methodologies for the quantitation of various BaP metabolites in our enzyme kinetic studies.

3-Hydroxy-benzo[*a*]pyrene (3-OH) and 7-hydroxy-benzo[*a*]pyrene (7-OH) are both major metabolites of BaP, especially in the presence of CYP1A1 without EH (3-5). High-performance liquid chromatography (HPLC) is frequently used to analyze polycyclic aromatic hydrocarbons and their metabolites. However, no published HPLC methods were able to provide high detection sensitivities while still maintaining good separation of these two compounds (3, 4, 6, 7). Here, we report the development and validation of a sensitive HPLC method with fluorescence detection that separates 3-OH and 7-OH, as well as six other fluorescent BaP metabolites, namely 9-hydroxy-BaP (9-OH), BaP-*trans*-4,5-dihydrodiol(±) (4,5-diol), BaP-*trans*-7,8-dihydrodiol(±) (7,8-diol), BaP-*trans*-9,10-dihydrodiol(±) (9,10-diol), BaP-7,8,9,10-tetrol-7,8,9,10-tetrahydro-(7 $\alpha$ ,8 $\beta$ ,9 $\beta$ ,10 $\alpha$ )-(±) (7,10/8,9-tetrol), and BaP-7,8,9,10-tetrol-7,8,9,10-tetrahydro-(7 $\alpha$ ,8 $\beta$ ,9 $\alpha$ ,10 $\beta$ )-(±) (7,9/8,10-tetrol). The chemical structures of these metabolites are shown in Figure 5.1. The use of a fluorescence detector provided limits of quantification (LOQ) below 1 nM for all compounds other than 7-OH (for which the LOQ was < 2 nM). The method also separates three non-fluorescent BaP metabolites, BaP-1,6-dione (1,6-dione), BaP-3,6-dione (3,6-dione), and BaP-6,12-dione (6,12-dione). These BaP-diones were monitored by UV absorbance, but the LOQs were much higher than those of the fluorescent metabolites. A novel HPLC method using post-column zinc reducer was developed and validated to improve the detection sensitivities for BaP-diones, and is described in Chapter 6.

The analytical methods described in this chapter and Chapter 6 were used to determine the concentrations of BaP and 11 of its metabolites in time-course experiments using human (Chapter 7) and rat (Chapter 8) enzymes. Based on the experimental data

obtained from these time-course studies, the RN kinetics model for BaP metabolism (Chapter 7) and the RN/physiologically based pharmacokinetic model for BaP and its metabolites (Chapter 8) were calibrated and validated.

## **5.2. Materials and Methods**

### *5.2.1. Chemicals and Reagents*

BaP, benzo[ghi]perylene (BghiP), acetic acid (99.7%, A.C.S. reagent), and Trizma Pre-set crystal (pH 7.4 at 37°C) were purchased from Sigma-Aldrich (St. Louis, MO). 3-OH, 7-OH, 9-OH, 4,5-diol, 7,8-diol, 9,10-diol, 1,6-dione, 3,6-dione, 6,12-dione, 7,10/8,9-tetrol (listed as BaP-r-7,t-8,t-9,c-10-tetrahydrotetrol in the catalog), and 7,9/8,10-tetrol (listed as BaP-r-7,t-8,c-9,t-10-tetrahydrotetrol in the catalog) were purchased from National Cancer Institute Chemical Carcinogen Reference Standard Repository (Kansas City, MO) and stored at -20°C. HPLC grade methanol, acetonitrile, acetone, ethyl acetate, and dimethyl sulfoxide (DMSO) were purchased from Fisher Scientific (Hampton, NH).

### *5.2.2. Enzymes and Cofactors*

Microsomal preparations of recombinant human cytochrome P450 1A1 expressed in *Escherichia coli* (Bactosomes CYP1A1; 106 pmol/mg protein) were purchased from XenoTech, LLC (Lenexa, KS). Human lymphoblast microsomes containing human microsomal epoxide hydrolase (styrene oxide hydrolase activity of 25 nmol/min/mg protein) were purchased from BD Gentest (Bedford, MA). NADPH regenerating system,

containing glucose-6-phosphate dehydrogenase, NADP<sup>+</sup>, glucose-6-phosphate, and MgCl<sub>2</sub>, was also purchased from BD Gentest.

### 5.2.3. Instrumentation

The HPLC system consisted of a Beckman Coulter System Gold (Fullerton, CA), composed of Model 126 pumps, Model 507 autosampler, and Model 166 UV detector, coupled, in line, to a Jasco (Easton, MD) FP-920 fluorescence detector. BaP and its metabolites were separated on a Discovery RP-AmideC16 column (250 × 4.6 mm I.D., 5 μm; Supelco, Bellefonte, PA). A 0.5 μm precolumn filter (Upchurch Scientific, Oak Harbor, WA) and a Discovery RP-AmideC16 Superguard cartridge (5 μm; Supelco) were used to protect the analytical column. An eight-channel Degasys Populaire vacuum degasser (Chrom Tech, Inc., Apple Valley, MN) was used to de-gas the mobile phases.

### 5.2.4. Chromatographic Conditions

Twenty μL of sample dissolved in methanol was injected for HPLC analysis. The flow rate was 0.7 mL/min during separation (0-59 min) and increased to 1.0 mL/min to re-equilibrate the column (60-69 min). Mobile phase A consisted of 0.3% (v/v) acetic acid in water (pH 4.1), and mobile phase B, acetonitrile:methanol (50/50). The time program for the multi-step gradient is described in Table 5.1. BaP in the column effluent was monitored by UV absorbance at 280 nm. Metabolites were monitored by the fluorescence detector, in which a time program (Table 5.2) was created to adjust excitation and emission wavelengths to maximize detection of the individual compounds (8).

### 5.2.5. Calibration Procedures

Six calibration standards each containing a mixture of 3-OH, 7-OH, 9-OH, 7,8-diol, 4,5-diol, 9,10-diol, 7,10/8,9-tetrol, 7,9/8,10-tetrol, BaP, and BghiP were prepared in methanol. The concentrations for metabolites ranged from 1 to 220 nM, and the concentrations of BaP and BghiP were fixed at 10  $\mu$ M and 1.6  $\mu$ M, respectively. Two extra standards containing all the chemicals listed above except the tetrols were prepared at the concentrations of 356 and 570 nM for metabolites. Standard calibration curves were obtained by plotting the peak area ratio of individual metabolites to internal standard ( $A_M/A_{IS}$ ) as a function of the concentrations of individual metabolites ( $C_M$ ). Standard curves were then used to determine the recovery of BaP metabolites from solutions containing recombinant human enzymes. The equations used to calculate the response factors are listed in the appendix.

### 5.2.6. Limits of Detection, Limits of Quantitation, and Instrument Precision

The limit of detection (LOD) was determined as the concentration of the metabolite corresponding to a peak height that is three times the baseline noise of the fluorescence detector. A 10:1 ratio of peak height to baseline noise was used to determine the limit of quantitation (LOQ). Instrument precision was measured as the relative standard deviation (RSD) of the peak area ratio of the metabolite to internal standard ( $A_M/A_{IS}$ ) from six consecutive injection of a mixture of authentic standards each at 170 nM.

### *5.2.7. Sample Preparation for Extraction Recovery Study*

One mL of a solution containing 0.34 mg CYP1A1 protein and 0.34 mg EH protein in 50 mM Tris-HCl buffer (pH 7.4 at 37°C) was spiked with a mixture of BaP, 3-OH, 7-OH, 9-OH, 7,8-diol, 4,5-diol, 9,10-diol, 7,10/8,9-tetrol, and 7,9/8,10-tetrol in 10 µL of DMSO to achieve final concentrations of 1 to 570 nM of metabolites and 10 µM of BaP (see Table 5.4). After incubation at 37 °C for 50 min, one mL of acetone containing 1.6 nmol of BghiP as an internal standard was added to simulate the termination of reactions. The extraction procedures were adapted from a previously published method (3). BaP and its metabolites were extracted with ethyl acetate (4.0 mL). The solution containing the reaction mixture, acetone, and ethyl acetate was centrifuged at 3000 rpm for 10 min to separate the organic and aqueous layers. The organic solvent extracts were evaporated to dryness using a SPD121P SpeedVac concentrator (Thermo Electron, Woburn, MA) at 35°C. The residues were dissolved in 1 mL methanol and analyzed by HPLC. Samples were diluted for HPLC analysis if any off-scale peaks were detected. The equations used to calculate the percentage recovery of BaP metabolites are listed in the appendix.

### *5.2.8. Time-Course Studies of BaP Metabolism Using Recombinant Human Enzymes*

Incubation mixtures contained 9.0 pmol CYP1A1, 0.05 mg EH protein, 1.3 mM NADP<sup>+</sup>, 3.3 mM glucose-6-phosphate, 0.4 U/mL glucose-6-phosphate dehydrogenase, 3.3 mM magnesium chloride in 50 mM Tris-HCl buffer (pH 7.4 at 37°C), in a final volume of 1.0 mL. After pre-incubation at 37°C for 2 min, reactions were initiated by adding BaP in DMSO to achieve final concentration of 10 µM of BaP and 1.0% (v/v)

DMSO. Reactions were stopped at various time points by adding 1.0 mL acetone containing 1.6 nmol of internal standard (BghiP). The same extraction procedures described in previous section were used to recover BaP and its metabolites from the reaction mixture. The final concentrations of BaP metabolites were calculated using equations listed in the appendix.

#### *5.2.9. Other Methods Tested during Method Development*

Methods described in this section were tested but did not provide results as good as the one described in the previous section. A published method (9) using methanol/water as the mobile phase and multi-step gradient from 55% to 100% methanol was tested with a Discovery C18 Column (250 × 4.6 mm I.D., 5 μm; Supelco). The method provided reasonable separation of 7-OH and 3-OH when their concentrations were equivalent. However, baseline separation could not be achieved when the concentration of 3-OH was more than twice that of 7-OH. The mobile phases were modified by using 10% acetonitrile, 10% isopropanol, 10% tetrahydrofuran, and 50% acetonitrile in methanol as the organic phases. The multi-step gradients were adjusted as required within ±10% of the value reported by James et al. (9) to best separate 7-OH and 3-OH while maintaining good separations of other BaP metabolites. A SYNERGI 4μ Max-RP column (150 × 4.60 mm; Phenomenex, Torrance, CA) was also tested using these same combinations of multi-step gradients and mobile phases. The organic mobile phases tested for RP-AmideC16 column, other than 50% acetonitrile in methanol used as the optimal condition, include 100% methanol and 100% acetonitrile. None of these combinations of mobile phases, gradients, and columns yielded adequate results.

## **5.3. Results**

### *5.3.1. Chromatogram*

A representative HPLC profile composed of the authentic standards of BaP and its fluorescent metabolites is shown in Figure 5.2. Each peak in the chromatogram was well separated. The separation shown in Figure 5.2 was achieved with a new RP-AmideC16 column, and the retention times of all chemicals may varied a function of the column age. The chromatogram shown in Figure 5.3 represents the reaction product mixture after incubation of BaP with CYP1A1 and EH for 31 min. Clearly, this method provides good separation of 7-OH and 3-OH, even when the concentration of 3-OH is greater than that of 7-OH (4.2:1 in Figure 5.3), thus overcoming important limitations of other HPLC methods.

### *5.3.2. Standard Calibration Curve*

Standard calibration curves of the peak area ratio ( $A_M/A_{IS}$ ) as a function of concentrations are shown in Figures 5.4 and 5.5. Linear calibration curves were achieved at concentration ranges varying among the eight BaP metabolites with coefficients of determination ( $R^2$ ) of or greater than 0.999. The low limit of the linear range for all metabolites was 1.0 nM (the lowest concentration of standards prepared). However, the high limits were constrained by the dynamic range of fluorescence detector for each specific chemical, *i.e.* the highest “on-scale” concentrations detected by the detector at the assigned wavelengths.

### 5.3.3. LOD, LOQ, and Instrument Precision

The LOD and LOQ for each analyte are shown in Table 5.3. The compound with the lowest LOD was 9,10-diol (0.031 nM), while 7-OH was detected with the least sensitivity (LOD = 0.55 nM) of the eight BaP metabolites tested. Instrument precision was measured as RSD of the peak area ratio ( $A_M/A_{IS}$ ) from six consecutive injections of a mixture of authentic standards at 170 nM. The RSD for 7,10/8,9-tetrol, 7,9/8,10-tetrol, 9,10-diol, 4,5-diol, 7,8-diol, 9-OH, 7-OH, and 3-OH were 1.0%, 1.0%, 0.93%, 0.98%, 0.97%, 0.84%, 1.0%, and 0.62%, respectively.

### 5.3.4. Extraction Recovery

The results of extraction recoveries are shown in Table 5.4. The mean of the percentage recovery of the internal standard BghiP ( $RCV_{IS}$ ) was 98.7%. Generally, larger fractions of the spiked concentrations were recovered from metabolites with greater hydrophilicities (*e.g.* BaP-tetrols) compared with those with lower hydrophilicities (*e.g.* hydroxyl-BaPs). The percentage recoveries for hydroxy-BaPs increase with increasing spiked concentrations.

### 5.3.5. Application of the Method to a Time-Course Study of BaP Metabolism

To demonstrate an application of the method, the dynamics of BaP metabolism were studied using recombinant human CYP1A1 and EH. The time course of the formation of BaP metabolites are shown in Figures 5.6 and 5.7. The concentrations of all metabolites measured, except for 7,9/8,10-tetrol (not shown in the figures), increased during the incubation period. The peak areas of 7,9/8,10-tetrol were below the detection

limit under the current experimental conditions. The data shown in Figure 5.7 indicate that 7-OH is a major metabolite of BaP using recombinant human enzymes.

#### **5.4. Discussion**

In an attempt to apply a proven chemical engineering technology, Reaction Network modeling, for complex interwoven reaction pathways to biomedical research (1), we chose BaP and its metabolic pathways for our initial effort. Despite thousands of published papers in the scientific literature, we found very little useful time-course quantitative data for building a Reaction Network kinetics model for BaP. Particularly apparent is the lack of human enzyme kinetics data for estimating reaction rate constants for our Reaction Network kinetics model for BaP. Thus, we underwent a series of enzyme kinetics studies using human CYP1A1 and EH. However, we soon discovered that the published analytical methodologies were not adequate for our studies. Therefore, the development of sensitive analytical methods for our BaP enzyme kinetics studies became an essential part of our overall plan for Reaction Network modeling of BaP.

This study reports the development and validation of an HPLC method for qualitative and quantitative analysis of BaP and its eight fluorescent metabolites. A major advantage of this method is its ability to separate 7-OH and 3-OH using a simple HPLC system, which has not been previously reported. Toriba and colleagues (7) recently described the development of a method that separates 7-OH, 3-OH, and other hydroxyl-BaPs. However, this method is complex and thus potentially problematic because it is performed on an HPLC system containing a column switch, RP-AmideC16 column, C18 column,  $\beta$ -CD-bonded silica gel column, and column oven. Selkirk and

colleagues (6) also reported an HPLC method that separated these two important hydroxyl-BaPs using a recycling system with three analytical columns.

Time course studies of BaP metabolism using recombinant human CYP1A1 and EH suggest that 7-OH is one of the major metabolites of BaP whose concentration increases with reaction time (Figure 5.7). In previous studies using recombinant human CYP1A1, 7-OH was identified as a BaP metabolite in some studies (3, 4) but not others (8, 10, 11). The lack of a simple HPLC method that can separate 7-OH from 3-OH (4, 12), which is also a major metabolite of BaP, might be the cause of this discrepancy. Although Shou and colleagues (3) observed that 7-OH accounts for up to 18% of the total metabolites, the chromatogram shown in the report did not completely resolve 3-OH from 7-OH, and thus the concentrations of 3-OH and 7-OH might not be accurately measured. Kim and colleagues (4) acknowledged the importance of 7-OH as a BaP metabolite, but did not separate 7-OH from 3-OH and lumped together as a co-eluted peak.

The recoveries of hydroxy-BaPs from the enzymatic reaction mixture increased with spiked concentration, with lower concentrations showing poor recoveries. These results suggest saturable binding of hydroxyl-BaPs to proteins. This interpretation is supported by the finding in a recent study (13) that 3-OH bound covalently to bovine hemoglobin and albumin. Furthermore, the formation of DNA adducts were observed after mouse aortic smooth muscle cells were exposed to 3-OH (14). The low recovery of 3-OH may be also the result of the conversion of 3-OH to 3,6-dione via non-enzymatic oxidation reactions (15). Bouchard and Viau (16) reported 50% and 43% recovery of the

spiked 3-OH and 9-OH, respectively, from rat urine samples. These values fall into the ranges we observed in the present study (Table 5.4).

The LODs and linearity ranges of the standard curves for the eight BaP metabolites detected here are consistent with previous reports. Toriba *et al.* (7) reported the LODs of 0.22 to 6.0 nM for hydroxyl-BaPs based on 5- $\mu$ L injections in acetonitrile using HPLC and fluorescence detection. Lee *et al.* (17) reported linear ranges of approximately 0.7 to 150 nM for 3-OH, 4,5-diol, and 7,8-diol based on 5- $\mu$ L injections of plasma samples.

## **5.5. Conclusions**

A simple HPLC method for determining eight fluorescent BaP metabolites was developed and validated. The method separates 7-OH from 3-OH without the need of multiple columns and column switches. Both 7-OH and 3-OH are major metabolites of BaP using recombinant human CYP1A1 and EH. 9-OH, 7,8-diol, and 9,10-diol were also identified as the major metabolites, while 4,5-diol and 7,10/8,9-tetrol were the minor metabolites. The method is very sensitive with LODs below 1 nM for all BaP metabolites tested based on 20- $\mu$ L injections. Wide linear ranges were also observed with this method.

## **5.6. References**

1. Liao KH, Dobrev ID, Dennison JE, Jr., Andersen ME, Reisfeld B, Reardon KF, Campaign JA, Wei W, Klein MT, Quann RJ, Yang RS. Application of biologically based computer modeling to simple or complex mixtures. *Environ Health Perspect* 110 Suppl 6:957-63(2002).

2. Klein MT, Hou G, Quann RJ, Wei W, Liao KH, Yang RS, Campaign JA, Mazurek MA, Broadbelt LJ. BioMOL: a computer-assisted biological modeling tool for complex chemical mixtures and biological processes at the molecular level. *Environ Health Perspect* 110 Suppl 6:1025-9(2002).
3. Shou M, Korzekwa KR, Crespi CL, Gonzalez FJ, Gelboin HV. The role of 12 cDNA-expressed human, rodent, and rabbit cytochromes P450 in the metabolism of benzo[a]pyrene and benzo[a]pyrene trans-7,8-dihydrodiol. *Mol Carcinog* 10:159-168(1994).
4. Kim JH, Stansbury KH, Walker NJ, Trush MA, Strickland PT, Sutter TR. Metabolism of benzo[a]pyrene and benzo[a]pyrene-7,8-diol by human cytochrome P450 1B1. [erratum appears in *Carcinogenesis* 1999 Mar;20(3):515]. *Carcinogenesis* 19:1847-1853(1998).
5. James MO, Altman AH, Morris K, Kleinow KM, Tong Z. Dietary modulation of phase 1 and phase 2 activities with benzo(a)pyrene and related compounds in the intestine but not the liver of the channel catfish, *Ictalurus punctatus*. *Drug Metab Dispos* 25:346-354(1997).
6. Selkirk JK, Croy RG, Gelboin HV. High-pressure liquid chromatographic separation of 10 benzo(a)pyrene phenols and the identification of 1-phenol and 7-phenol as new metabolites. *Cancer Res* 36:922-926(1976).
7. Toriba A, Nakamura H, Chetiyankornkul T, Kizu R, Makino T, Nakazawa H, Yokoi T, Hayakawa K. Method for determining monohydroxybenzo[a]pyrene isomers using column-switching high-performance liquid chromatography. *Anal Biochem* 312:14-22(2003).
8. Gautier JC, Urban P, Beaune P, Pompon D. Simulation of human benzo[a]pyrene metabolism deduced from the analysis of individual kinetic steps in recombinant yeast. *Chem Res Toxicol* 9:418-425(1996).
9. James MO, Altman AH, Li CL, Schell JD, Jr. Biotransformation, hepatopancreas DNA binding and pharmacokinetics of benzo[a]pyrene after oral and parenteral administration to the American lobster, *Homarus americanus*. *Chem Biol Interact* 95:141-160(1995).
10. Schwarz D, Kisselev P, Cascorbi I, Schunck WH, Roots I. Differential metabolism of benzo[a]pyrene and benzo[a]pyrene-7,8-dihydrodiol by human CYP1A1 variants. *Carcinogenesis* 22:453-459(2001).
11. Bauer E, Guo Z, Ueng YF, Bell LC, Zeldin D, Guengerich FP. Oxidation of benzo[a]pyrene by recombinant human cytochrome P450 enzymes. *Chem Res Toxicol* 8:136-42(1995).
12. Yang SK, Selkirk JK, Plotkin EV, Gelboin HV. Kinetic analysis of the metabolism of benzo(a)pyrene to phenols, dihydrodiols, and quinones by high-pressure chromatography compared to analysis by aryl hydrocarbon hydroxylase assay, and the effect of enzyme induction. *Cancer Res* 35:3642-3650(1975).
13. Sugihara N, James MO. Binding of 3-hydroxybenzo[a]pyrene to bovine hemoglobin and albumin. *J Biochem Mol Toxicol* 17:239-47(2003).
14. Moorthy B, Miller KP, Jiang W, Williams ES, Kondraganti SR, Ramos KS. Role of cytochrome P4501B1 in benzo[a]pyrene bioactivation to DNA-binding metabolites in mouse vascular smooth muscle cells: evidence from 32P-postlabeling for formation of 3-hydroxybenzo[a]pyrene and benzo[a]pyrene-3,6-

- quinone as major proximate genotoxic intermediates. *J Pharmacol Exp Ther* 305:394-401(2003).
15. Selkirk JK, Croy RG, Roller PP, Gelboin HV. High-pressure liquid chromatographic analysis of benzo( $\alpha$ )pyrene metabolism and covalent binding and the mechanism of action of 7,8-benzoflavone and 1,2-epoxy-3,3,3-trichloropropane. *Cancer Res* 34:3474-3480(1974).
  16. Bouchard M, Viau C. Urinary excretion kinetics of pyrene and benzo(a)pyrene metabolites following intravenous administration of the parent compounds or the metabolites. *Toxicol Appl Pharmacol* 139:301-309(1996).
  17. Lee W, Shin HS, Hong JE, Pyo H, Kim Y. Studies on the analysis of benzo(a)pyrene and its metabolites in biological samples by using high performance liquid chromatography/fluorescence detection and gas chromatography/mass spectrometry. *Bull Korean Chem Soc* 24:559-565(2003).

## **5.7. Appendix**

All equations associated with the calculation of the response factors, percentage recovery, and final concentrations for BaP metabolites are listed in this section. The following equation was used to correlate the concentration of BaP metabolites with the peak area analyzed by HPLC,

$$C_M = \frac{A_M}{A_{IS}} \times \frac{RF_{IS} \times C_{IS}}{RF_M} \quad (A5-1)$$

where  $A_i$  represents the peak area measured by HPLC for substrate  $i$ .  $RF_i$  and  $C_i$  represent the response factor and concentration, respectively, for substrate  $i$ . The subscripts  $M$  and  $IS$  were used to denote BaP metabolites and internal standard (BghiP), respectively. Standard calibration curves were obtained by plotting the peak area ratio of individual metabolites to internal standard ( $A_M/A_{IS}$ ) as a function of the concentrations of individual metabolites ( $C_M$ ). The slope of the standard curve for metabolite  $M$  is equal to the value of  $(RF_M/RF_{IS}/C_{IS})$ .

The percentage recovery of BaP metabolites ( $RCV_M$ ) from solutions containing recombinant human enzymes was then calculated by the following equation,

$$RCV_M = \frac{A_M}{A_{IS}} \times \frac{1}{C_M} \times \frac{RF_{IS} \times C_{IS}}{RF_M} \times RCV_{IS} \quad (A5-2)$$

where  $A_M/A_{IS}$  values were the peak area ratios analyzed by HPLC and  $C_M$  is the known spiked concentration of metabolite  $M$ . ( $RF_M/RF_{IS}/C_{IS}$ ) values were obtained from standard calibration curves. Percentage recovery of internal standard ( $RCV_{IS}$ ) in Equation A5-2 was calculated by

$$RCV_{IS} = \frac{A_{IS}}{RF_{IS} \times C_{IS}} \quad (A5-3)$$

where  $C_{IS}$  is equal to 1.6  $\mu\text{M}$  (pmol/mL).  $A_{IS}$  is the mean of the peak area of BghiP from the entire recovery study.  $RF_{IS}$  is the mean of the values of ( $A_{IS}/C_{IS}$ ) from the entire standard calibration study. Please note that Equation A5-1 is the simplified form of Equation A5-2 used to describe the standard calibration curves. Since no extraction steps were involved for standard curves,  $RCV_M$  and  $RCV_{IS}$  were assumed to be 100% and not shown in Equation A5-1.

The final concentrations of BaP metabolites formed in time course samples were obtained by rewriting Equation A5-2,

$$C_M = \frac{A_M}{A_{IS}} \times \frac{RCV_{IS}}{RCV_M} \times \frac{RF_{IS} \times C_{IS}}{RF_M} \quad (A5-4)$$

where all the values in the right hand side of the equation can be obtained from the HPLC analysis of time course samples, the standard curves, and the recovery studies.

**Table 5.1.** Time program for the multi-step gradient of mobile phase for RP-AmideC16 HPLC column

Time (min)	Composition of mobile phase (%)	
	A*	B*
0	40	60
1	40	60
26	20	80
47	20	80
49	0	100
58	0	100
60	40	60
69	40	60

\* Mobile phase A: 0.3% (v/v) acetic acid in H<sub>2</sub>O (pH 4.1); Mobile phase B: acetonitrile:methanol (50/50).

**Table 5.2.** Time program for the fluorescence detector for measuring BaP and its fluorescent metabolites

Time (min)	Wavelength (nm)		Compounds
	Excitation	Emission	
0.0 - 13.6	278	407	9,10-diol, 7,10/8,9-tetrol, 7,9/8,10-tetrol
13.6 - 18.1	263	388	4,5-diol
18.1 - 23.0	348	402	7,8-diol
23.0 - 69.0	375	441	BaP, 3-OH, 7-OH, 9-OH, BghiP

**Table 5.3.** Limits of detection (LOD) and Limits of quantitation (LOQ) for BaP metabolites

	7,10/8,9-tetrol	7,9/8,10-tetrol	9,10-diol	4,5-diol	7,8-diol	9-OH	7-OH	3-OH
*LOD (nM)	0.078	0.087	0.031	0.13	0.078	0.057	0.55	0.14
*LOQ (nM)	0.26	0.29	0.10	0.44	0.26	0.19	1.8	0.47

\*Based on 20- $\mu$ L injection.

**Table 5.4.** Percentage recovery of BaP metabolites<sup>a</sup>

7,10/8,9-tetrol		7,9/8,10-tetrol		9,10-diol		4,5-diol	
Conc. (nM)	% Recovery						
0.990	87.7±12.2	1.00	88.4±1.4	0.990	93.2±17.2	0.989	109.0±14.8
2.97	92.3±2.4	3.00	90.8±3.3	2.97	96.5±5.3	2.97	108.6±3.3
9.90	93.3±1.5	10.0	89.3±3.4	9.90	96.3±1.4	9.89	104.3±0.8
34.0	90.2±0.6	34.3	90.4±1.8	33.9	96.0±0.4	33.9	102.8±0.8
106	90.1±2.3	107	91.2±2.6	106	93.4±2.3	106	99.0±1.4
170	90.4±1.5	171	92.1±1.5	170	94.3±0.3	170	100.0±0.5
				<sup>b</sup> 357	93.9±2.1	357	102.0±0.9
				<sup>b</sup> 571	93.7±3.2	570	102.7±2.4
7,8-diol		9-OH		7-OH		3-OH	
Conc. (nM)	% Recovery						
0.985	73.7±8.9	0.987	37.7±5.6				
2.96	77.2±5.5	2.96	45.9±4.8				
9.85	80.8±0.2	9.90	69.2±1.9	10.0	55.2±2.2	10.2	15.7±0.6
33.8	73.4±0.3	34.0	74.8±2.2	34.3	55.2±5.1	34.9	11.7±2.4
106	74.6±2.6	106	81.8±2.4	107	69.0±2.5	109	29.6±2.9
169	72.9±1.5	169	85.7±2.5	172	73.0±2.3	174	33.5±4.5
<sup>b</sup> 356	75.4±1.4	354	90.1±2.6	354	80.1±2.5	358	44.7±2.1
<sup>b</sup> 570	74.1±0.3	<sup>b</sup> 567	90.1±2.4	567	85.9±3.3	<sup>b</sup> 573	53.2±3.2

<sup>a</sup>The results are the mean of percentage recoveries ± one standard deviation from four data points (two injections from each duplicated sample).

<sup>b</sup>A 1:4 dilution was required to obtain peak that is on-scale.

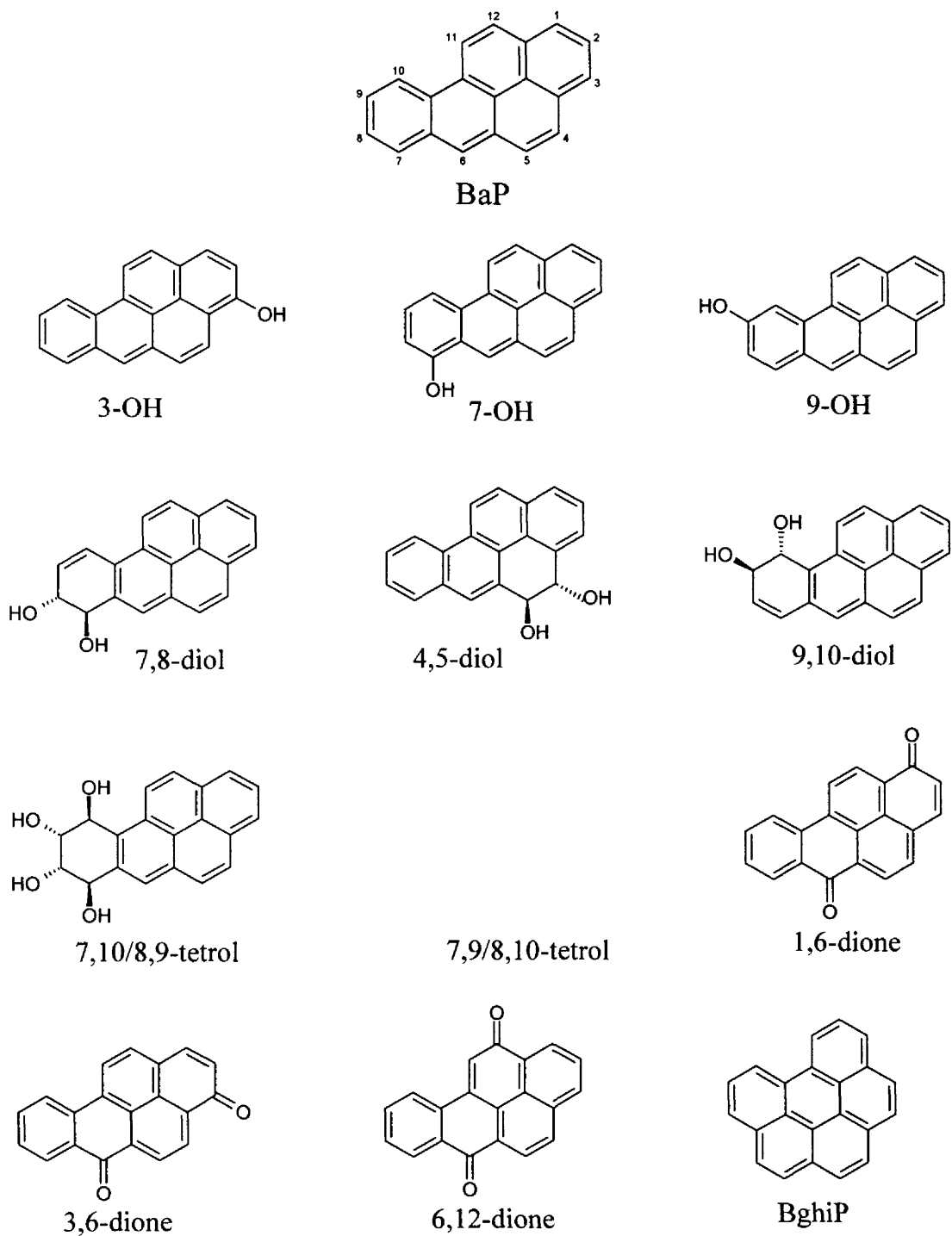


**Figure 5.1.** Chemical structures of BaP, its metabolites, and BghiP (only one structural isomer is shown).

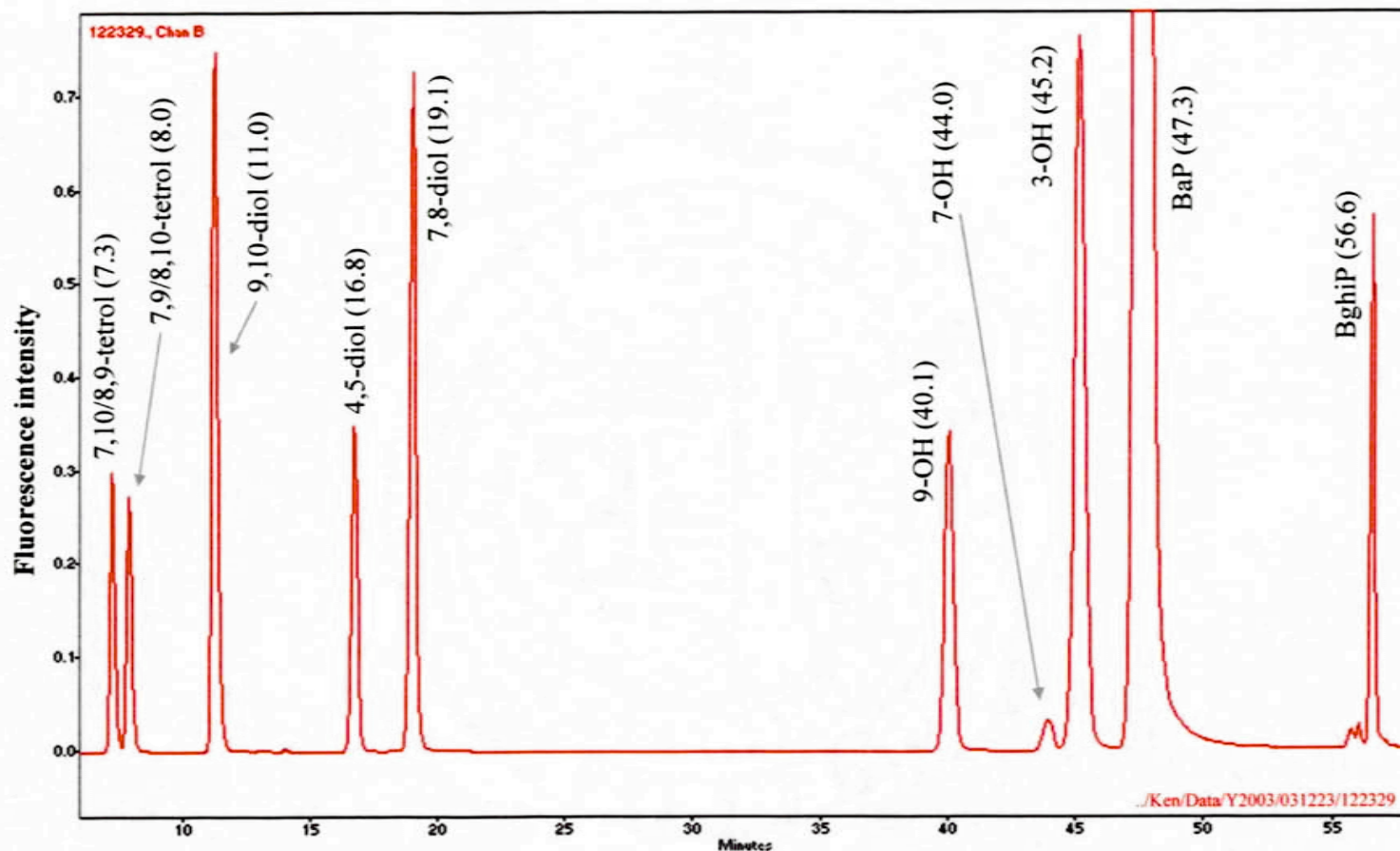


**Figure 5.2.** HPLC profile of the authentic standards of BaP and its fluorescent metabolites. The numbers enclosed in parenthesis represent the retention time of the compounds in minutes. The metabolite peaks represented different fluorescence responses to the same concentration (3.4 pmol) for the eight BaP metabolites. BghiP peak represented the fluorescence response for 32 pmol of the compound. The BaP peak was off-scale and represented 200 pmol of the compound.

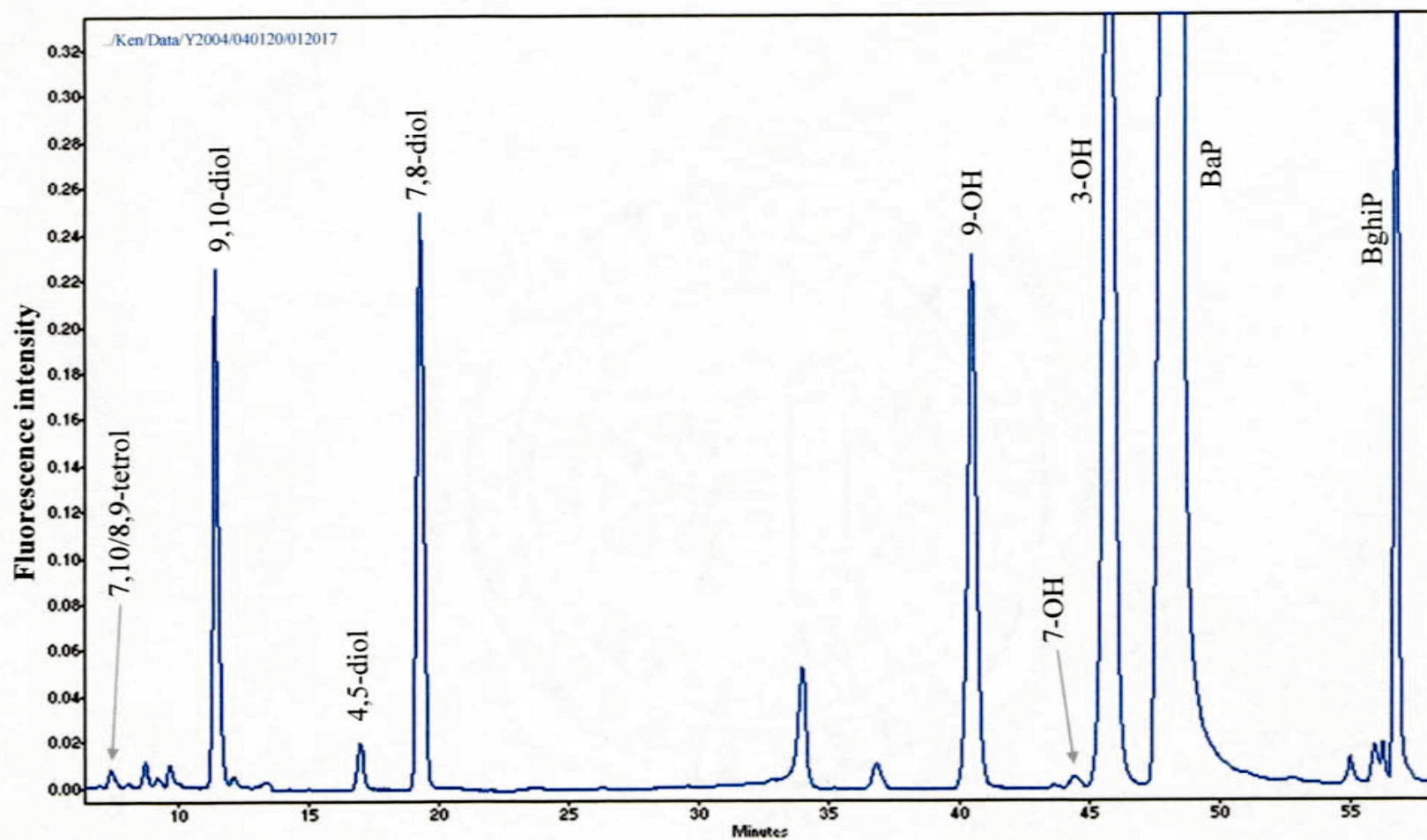


**Figure 5.3.** HPLC profile of BaP metabolism using recombinant human CYP1A1 and mEH. BaP (10  $\mu$ M) was incubated with 9.0 pmol CYP1A1 and 0.05 mg EH protein in one mL solution (pH 7.4) at 37°C for 31 min. The concentration of 3-OH is 4.2 times the concentration of 7-OH.

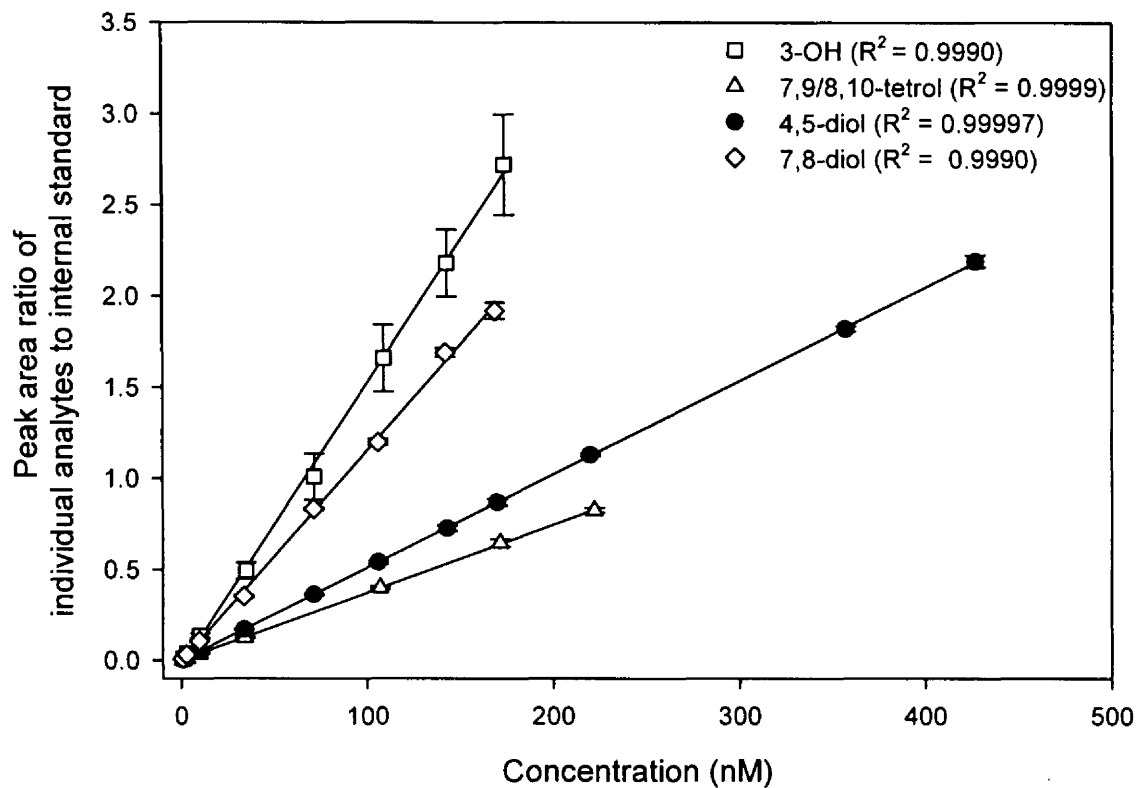


**Figure 5.4.** Standard calibration curves for 3-OH, 4,5-diol, 7,8-diol, and 7,9/8,10-tetrol. Symbols represent experimental data ( $\pm$  standard deviation) and lines represent linear regression results.

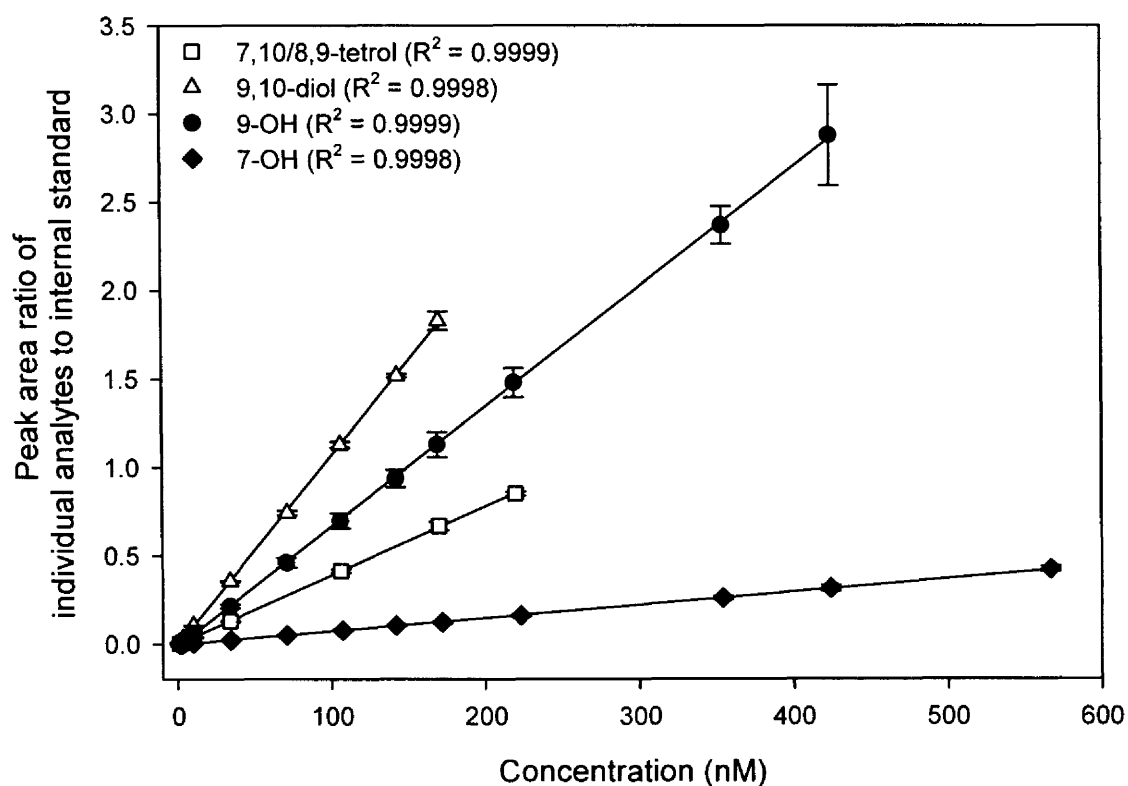


**Figure 5.5.** Standard calibration curves for 7-OH, 9-OH, 9,10-diol, and 7,10/8,9-tetrol. Symbols represent experimental data ( $\pm$  standard deviation) and lines represent linear regression results.

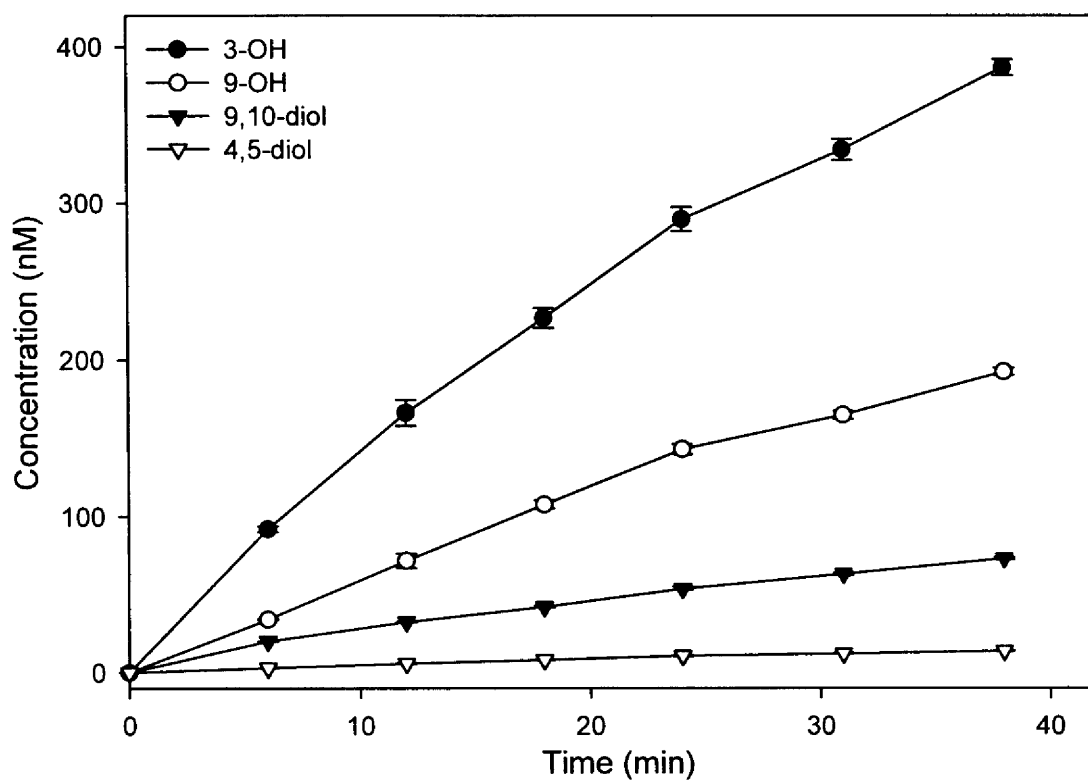


**Figure 5.6.** Time course profiles of 3-OH, 9-OH, 9,10-diol, and 4,5-diol after incubating 10  $\mu$ M BaP with recombinant human CYP1A1 and EH. Symbols represent the mean of the metabolite concentrations calculated by Equation A5-4  $\pm$  one standard deviation from 4 data points (2 injections from each duplicated sample).

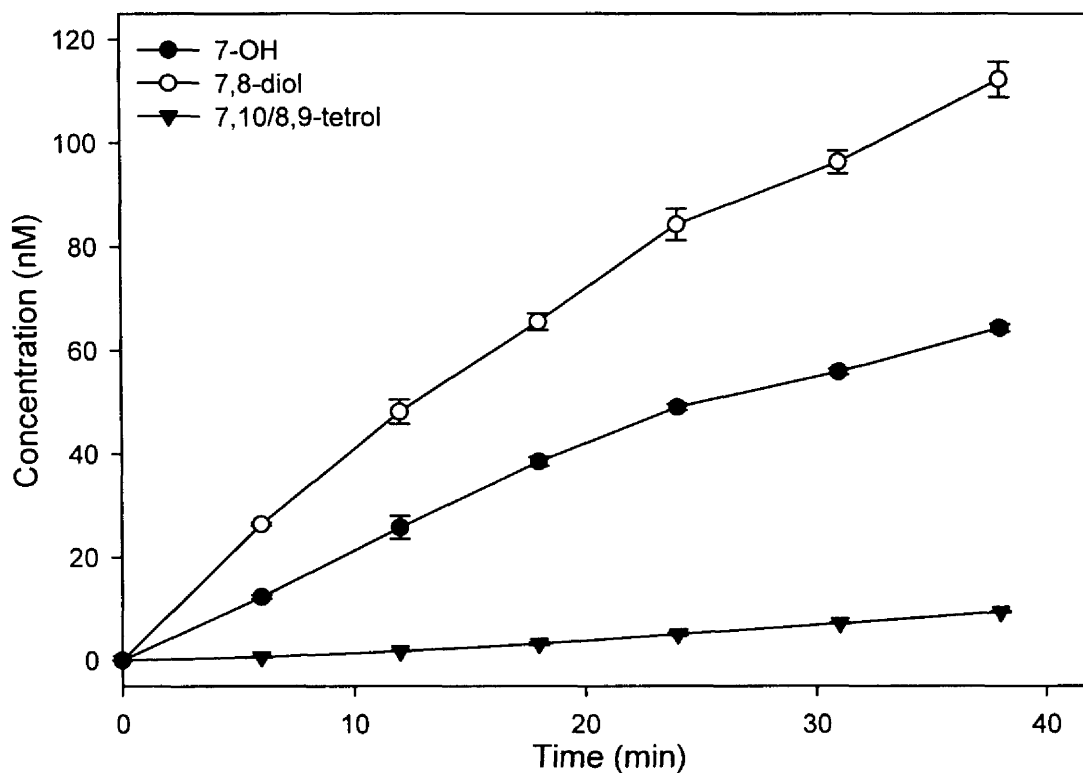


**Figure 5.7.** Time course profiles of 7-OH, 7,8-diol, and 7,10/8,9-tetrol after incubating 10  $\mu\text{M}$  BaP with recombinant human CYP1A1 and EH. Symbols represent the mean of the metabolite concentrations  $\pm$  one standard deviation from 4 data points (2 injections from each duplicated sample).

## Chapter 6

### A Novel, Sensitive Method for Determining Benzo[*a*]pyrene-Diones Using High-Performance Liquid Chromatography with Post-Column Zinc Reduction

#### 6.1. Introduction

The biotransformation of benzo[*a*]pyrene (BaP) was studied in our laboratory using *in vitro* enzymatic experiments as part of our overall plan to develop a Reaction Network (RN) model for the prediction of the mammalian metabolism of BaP. To determine BaP and its metabolites with high detection sensitivities, high-performance liquid chromatography (HPLC) methods were developed and validated. We used HPLC to monitor the formation of 11 BaP metabolites, namely BaP-1,6-dione (1,6-dione), BaP-3,6-dione (3,6-dione), BaP-6,12-dione (6,12-dione), 3-hydroxy-BaP (3-OH), 7-hydroxy-BaP (7-OH), 9-hydroxy-BaP (9-OH), BaP-4,5-dihydrodiol (4,5-diol), BaP-7,8-dihydrodiol (7,8-diol), BaP-9,10-dihydrodiol (9,10-diol), BaP-r-7,t-8,t-9,c-10-tetrahydrotetrol (7,10/8,9-tetrol), and BaP-r-7,t-8,c-9,t-10-tetrahydrotetrol (7,9/8,10-tetrol). Except for the BaP-diones (1,6-, 3,6-, and 6,12-diones), all of these BaP metabolites fluoresce. Thus, fluorescence detection was used to analyze BaP metabolites, as described in Chapter 5. Due to the non-fluorescent nature of BaP-diones, alternative detectors are required to achieve the same detection sensitivities (*I*). Using UV absorbance, the detection sensitivities of BaP-diones using UV absorbance are at least 2

orders of magnitudes lower than those of the other fluorescent BaP metabolites using a fluorescence detector. An interesting characteristic of BaP-diones is that they yield the corresponding BaP-hydroquinones upon chemical reduction. The BaP-hydroquinones are highly fluorescent (2), and thus can be monitored by a fluorescence detector at very low levels. However, BaP-hydroquinones are unstable in the presence of air and readily autoxidize to BaP-diones (3). To develop a simple technique to reduce BaP-diones to their respective hydroquinones, we adapted a method that had been used to analyze vitamin K. To analyze vitamin K compounds by HPLC, methods were developed to reduce vitamins K<sub>1</sub> and K<sub>3</sub> on-line to their fluorescent analogues using a post-column zinc reducer, resulting in enhanced detection sensitivities (4, 5). Here we report the development and validation of a simple HPLC method, utilizing a post-column zinc reducer to reduce BaP-diones to their corresponding fluorescent BaP-hydroquinones. The zinc reducer increased the detection sensitivity by more than two orders of magnitude. This new method is simple, uses readily available equipment, and avoids labor-intensive and time-consuming sample preparation involving reducing agents.

The HPLC methods described in this chapter (for the determination of BaP-diones) and in Chapter 5 (for determining fluorescent BaP metabolites) were used to monitor the formation of 11 BaP metabolites in time-course experiments using human (Chapter 7) and rat (Chapter 8) enzymes. The experimental data obtained from these time-course studies were further utilized to calibrate and validate the RN kinetics model for BaP metabolism (Chapter 7) and the RN/physiologically based pharmacokinetic model for BaP and its metabolites (Chapter 8).

## **6.2. Materials and Methods**

### *6.2.1. Chemicals and Reagents*

BaP, benzo[ghi]perylene (BghiP), acetic acid (99.7%, A.C.S. reagent), and Trizma Pre-set crystal (pH 7.4 at 37°C) were purchased from Sigma-Aldrich (St. Louis, MO). 1,6-Dione, 3,6-dione, 6,12-dione, 3-OH, 7-OH, 9-OH, 4,5-diol, 7,8-diol, 9,10-diol, 7,10/8,9-tetrol, and 7,9/8,10-tetrol were purchased from National Cancer Institute Chemical Carcinogen Reference Standard Repository (Kansas City, MO) and stored at -20°C. HPLC grade methanol, acetone, ethyl acetate, and dimethyl sulfoxide (DMSO) were purchased from Fisher Scientific (Hampton, NH). Zinc powder (-140+325 mesh; 99.9% on metals basis) was purchased from Alfa Aesar (Ward Hill, MA)

### *6.2.2. Enzymes*

Microsomal preparations of recombinant human cytochrome P450 1A1 expressed in *Escherichia coli* (106 pmol CYP1A1/mg protein) were purchased from XenoTech, LLC (Lenexa, KS). Human lymphoblast microsomes containing human microsomal epoxide hydrolase were purchased from BD Gentest (Bedford, MA). NADPH regenerating system, containing glucose-6-phosphate dehydrogenase, NADP<sup>+</sup>, glucose-6-phosphate, and MgCl<sub>2</sub>, was also purchased from BD Gentest.

### *6.2.3. HPLC Instruments*

The HPLC system consisted of a Beckman Coulter System Gold (Fullerton, CA), composed of 126 pumps, 507 autosampler, and 166 UV detector, coupled, in line, to a Jasco (Easton, MD) FP-920 fluorescence detector. BaP-diones were separated on a

Discovery C18 Column (250 × 4.6 mm I.D., 5 µm; Supelco, Bellefonte, PA). A 0.5 µm precolumn filter (Upchurch Scientific, Oak Harbor, WA) and a C18 SecurityGuard cartridge (4.0 × 3.0 mm I.D.; Phenomenex, Torrance, CA) were used to protect the analytical column. An eight-channel Degasys Populaire vacuum degasser (Chrom Tech, Inc., Apple Valley, MN) was used to de-gas the mobile phases.

#### *6.2.4. Chromatographic Conditions*

Twenty µL of sample dissolved in methanol was injected for HPLC analysis. The flow rate was 0.7 mL/min during separation (0-57 min) and increased to 1.0 mL/min at the end of the run to re-equilibrate the column (57-66 min). Mobile Phase A contained water with 0.3% (v/v) acetic acid (pH 4.1). Mobile Phase B was methanol. The time program for the multi-step gradient is described in Table 6.1. BaP-diones were reduced to BaP-hydroquinones by a post-column zinc reducer and monitored using the fluorescence detector at 400 nm for excitation and 500 nm for emission. The wavelengths used for monitoring other BaP metabolites were listed in Table 6.2.

#### *6.2.5. Post-Column Zinc Reducer*

An apparatus was designed to reduce BaP-diones to their corresponding fluorescent BaP-hydroquinones on-line (Figure 6.1). The major component of this apparatus is the post-column zinc reducer that consisted of a 20 × 2 mm I.D. guard column with 0.5 µm frits (Upchurch Scientific) packed with zinc powder (-140+325 mesh equivalent to 44-105 microns). To pack the zinc reducer, the guard column was first manually filled with zinc powder. The packed zinc column was then placed in a

vertical position and conditioned by 1) pumping 100% Mobile Phase B from 0 to 1.5 mL/min in 5 min; 2) switching to 100% Mobile Phase A over 5 min; 3) switching back to 100% Mobile Phase B over 5 min and finally turning off the flow in 2 min. The inlet of the zinc column was then disassembled to visually examine the filling. If any head space was observed, more zinc powder was added to the top of the column. Acetic acid was added to Mobile Phase A in order to facilitate reduction and prevent the BaP-hydroquinones from autoxidation. In order to prevent the coating of the flow cells by a reducer-derived material (as yet unidentified), an additional pump (L-6200A Smart Pump; Hitachi, San Jose, CA) was used to deliver 0.3% (v/v) acetic acid in H<sub>2</sub>O at 0.3 mL/min (Figure 6.1) directly to the detectors via a “T-connector union” between the column and the first detector.

#### 6.2.6. Calibration Procedures

Seven calibration standards, each containing a mixture of 1,6-dione, 3,6-dione, 6,12-dione, BaP, BghiP, 3-OH, 7-OH, 9-OH, 7,8-diol, 4,5-diol, 9,10-diol, 7,10/8,9-tetrol, and 7,9/8,10-tetrol, were prepared in methanol. The concentrations for metabolites ranged from 1.0 to 220 nM, and the concentrations of BaP and BghiP were fixed at 10 μM and 1.6 μM, respectively. Standard calibration curves were obtained by plotting the peak area ratio of individual BaP-hydroquinones to internal standard ( $A_D/A_{IS}$ ) as a function of the concentrations of their corresponding BaP-diones ( $C_D$ ). Standard curves were then used to determine the recovery of BaP-diones from solutions containing recombinant human enzymes. The equations used to calculate the response factors are listed in the appendix.

#### 6.2.7. Limits of Detection, Limits of Quantitation, and Instrument Precision

The limit of detection (LOD) was determined as the concentration of the metabolite corresponding to a peak height that is three times the baseline noise of the fluorescence detector ( $\sigma$ ). A 10:1 ratio of peak height to baseline noise was used to determine the limit of quantitation (LOQ). Instrument precision was measured as the relative standard deviation (RSD) of the peak area ratio of BaP-hydroquinones to internal standard ( $A_D/A_{IS}$ ) from six consecutive injection of a mixture of authentic standards at 170 nM.

#### 6.2.8. Samples for Extraction Recovery Study

One mL of a solution containing CYP1A1 (0.085 mg microsomal protein) and EH (0.05 mg microsomal protein) in 50 mM Tris-HCl buffer (pH 7.4 at 37°C) was spiked with a mixture of 1,6-dione, 3,6-dione, and 6,12-dione in 10  $\mu$ L of DMSO to achieve final concentrations of 10 to 226 nM of BaP-diones. After incubation at 37°C for 50 min, 1.0 mL of acetone containing 1.6 nmol of BghiP as an internal standard was added to mimic the termination of reactions. The extraction procedures were adapted from a previously published method (7). BaP and its metabolites were extracted with ethyl acetate (4.0 mL). The solution containing the reaction mixture, acetone, and ethyl acetate was centrifuged at 3000 rpm (1841 $\times$ g) for 10 min to separate the organic and aqueous layers. The organic solvent extracts were evaporated to dryness using a SPD121P SpeedVac concentrator (Thermo Electron, Woburn, MA) at 35°C. The residues were

dissolved in 1.0 mL methanol and analyzed by HPLC. The equations used to calculate the percentage recovery of BaP-diones are listed in appendix.

#### *6.2.9. Time-Course Studies of BaP Metabolism Using Recombinant Human Enzymes*

Incubation mixtures contained 0.085 mg CYP1A1 protein, 0.05 mg EH protein, 1.3 mM NADP<sup>+</sup>, 3.3 mM glucose-6-phosphate, 0.4 U/mL glucose-6-phosphate dehydrogenase, 3.3 mM magnesium chloride in 50 mM Tris-HCl buffer (pH 7.4 at 37°C), in a final volume of 1.0 mL. After pre-incubation at 37°C for 2 min, reactions were initiated by adding BaP in DMSO to achieve final concentration of 10 µM of BaP and 1% (v/v) DMSO. Reactions were stopped at various time points by adding 1.0 mL acetone containing 1.6 nmol of internal standard (BghiP). The same extraction procedures described in the previous section were used to recover BaP and its metabolites from the reaction mixture.

#### *6.2.10. Other Methods Tested during Method Development*

The methods described in this section, which did not involve the usage of the third pump delivering 0.3% acetic acid to the detectors, were tested but did not provide optimal results or produced problems. Zinc powder with smaller particle size (median 6-9 micron; Alfa Aesar) than the one described above was also used to pack the zinc reducer. However, when the small particles were used, back pressure as high as 3800 PSI was observed, which can potentially damage the analytical column. Various acid concentrations in the mobile phases were tested before reaching the optimized method. With Mobile Phases A (water) and B (methanol) both containing 0.1% (v/v) acetic acid,

no separation of the three BaP-diones was found. Instead, only a large and broad peak was observed, possibly a result of the mixing of the three BaP-diones within the space in the zinc reducer produced by channeling. After the column was disassembled, severe channeling in zinc reducer was visible. When the concentration of acetic acid in water and methanol was reduced to 0.01%, no channeling was observed. However, at this acid concentration, the baseline from the fluorescence and UV detectors became steeper and the offset value on the UV detector increased progressively from run to run. This was a result of contamination of the flow cells by unknown compounds, and confirmed by the observation of a white coating inside the flow cell. The coating in the flow cells could be eliminated by washing the flow cells with 0.3% (v/v) acetic acid in water.

Other modifications of the mobile phases included the use of zinc chloride (10 mM), sodium acetate (5 mM), and acetic acid (4.5 mM) in both water and methanol, as adapted from a previous report (8). However, severe channeling was observed under this condition. On the other hand, high back pressure was observed when the mobile phases contained methanol and HCl in water (pH 4.05).

## **6.3. Results**

### *6.3.1. Chromatogram*

A representative HPLC profile for the authentic standards of BaP-diones and other BaP metabolites is shown in Figure 6.2. Although the focus of this study is to enhance the detection sensitivities BaP-diones, the method can also be used to separate 8 other BaP metabolites. Each peak in the chromatogram was well separated, except for 7-OH and 3-OH. A different method was developed to separate 7-OH and 3-OH, which

was discussed in Chapter 5. A representative HPLC profile for BaP metabolism using recombinant human CYP1A1 is shown in Figure 6.3. The metabolites observed were 1,6-dione, 3,6-dione, 6,12-dione, 9-OH, 7-OH, and 3-OH, while no unknown peaks interfered with the separation of these metabolites. The sharp shifts on baseline observed at 22.5 and 35 min (Figure 6.3) were caused by the change of wavelengths for the fluorescence detector.

### 6.3.2. Standard Calibration Curves and Detection Limits

The slopes and coefficients of determination ( $R^2$ ) for the standard calibration curves, *i.e.* peak area ratio ( $A_D/A_{IS}$ ) versus dione concentration ( $C_D$ ), are shown in Table 6.3. The slope of the standard calibration curve for each BaP-dione varied from sequence to sequence. However, good linear correlation was observed between  $A_D/A_{IS}$  and  $C_D$  within each sequence ( $R^2 \geq 0.9976$ ) at BaP-diones concentrations ranging from 1.0 to 220 nM. The variations in the slopes of standard curves were assumed to be the result of the changes in the catalytic activity of zinc toward the conversion of BaP-diones to BaP-hydroquinones. This assumption was made based on the fact that the peak area of the internal standard stayed constant for every sequence. Like the slopes of standard curves, LOD and LOQ values also varied from sequence to sequence (Table 6.3). Generally, the method provides similar detection sensitivities for 1,6-dione and 6,12-dione with LOD values approximately equal to one half of the value for 3,6-dione.

### 6.3.3. Instrument Precision

Instrument precision was measured as RSD of the peak area ratio ( $A_D/A_{IS}$ ) from six consecutive injections of a mixture of authentic standards at 170 nM. The RSD for 1,6-dione, 3,6-dione, and 6,12-dione were 1.24%, 1.86%, and 0.81%. The differences in the RSD is likely due to the large differences in the peak sizes between 3,6-dione and the other two BaP-diones.

### 6.3.4. Impact of the Post-Column Zinc Reducer

The increases in the detection sensitivity for BaP-diones is shown in Figure 6.4 by comparing the peak area of each BaP-diones measured under the following conditions: a) no zinc reducer, b) with zinc reducer and no acid in the mobile phase, c) with zinc reducer using acidic mobile phase. The peak areas were determined using UV absorbance under the first condition, and the ones for the latter two conditions were measured using fluorescence detection. Even with no acid added to the mobile phase, the use of the zinc reducer resulted in the increases of peak areas of 190-, 50-, and 140-fold for 1,6-dione, 3,6-dione, and 6,12-dione, respectively. With the combination of the zinc reducer and 0.003% acetic acid in Mobile Phase A, the peak areas were 1700, 530, and 760 times the ones measured with no zinc reducer. 0.3% acetic acid in water from the third pump (0.3 mL/min) was only delivered when acid mobile phase was used, and the peak areas shown in Figure 6.4 were adjusted to account for the dilution.

### 6.3.5. Extraction Recovery

The results of extraction recovery studies are shown in Table 6.4. The percentage recovery of BghiP ( $RCV_{IS}$ ) was  $102.6\% \pm 2.8\%$ . The percentage recoveries for 1,6-dione and 3,6-dione increase with increasing spiked concentrations. On the other hand, less than 8% of 6,12-dione was recovered, and the percentage recovery was independent of the concentration of the dione from 10.2 to 227 nM.

### 6.3.6. Application of the Method to a Time-Course Study of BaP Metabolism

To demonstrate an application of the method, the dynamics of BaP metabolism were studied using recombinant human CYP1A1 and EH. The results of the time course profiles of BaP-diones are shown in Figure 6.5. The concentrations for all three BaP-diones shown in Figure 6.5 are not corrected for recovery, because the recovery of 6,12-dione from the reaction mixture may be too low to provide accurate extrapolation. The concentrations of 1,6-dione and 3,6-dione increased with reaction time. On the other hand, the concentration of 6,12-dione did not appear to be a function of reaction time. This might not reflect the trend for the formation of 6,12-dione from BaP due to the low recovery of 6,12-dione.

## **6.4. Discussion**

This study reports the development and validation of a novel HPLC method for qualitative and quantitative analysis of BaP-diones with high detection sensitivity. A post-column zinc reducer was used to convert BaP-diones to their corresponding fluorescent BaP-hydroquinones. Thus, BaP-hydroquinones can be analyzed using

fluorescence detector with detection sensitivities at least two orders of magnitude higher than the ones for non-converted BaP-diones using UV absorbance. With the high detection sensitivities, this method is suitable for studies where limited amounts of BaP-diones are present, such as metabolic studies using recombinant enzymes. In the previous studies involving BaP metabolism using recombinant enzymes, the formation of BaP-diones was either not measured (9) or measured by radioactivity detectors using radiolabeled BaP (7, 10, 11). Another method that can detect BaP-diones in airborne particulate matter with good sensitivity utilized liquid chromatography/mass spectrometry with atmospheric pressure chemical ionization (1).

Acetic acid was used in Mobile Phase A to facilitate reduction and prevent the BaP-hydroquinones from autoxidizing to BaP-diones. However, the acidic mobile phase resulted in problems that were not reported in previous publications using a post-column zinc reducer (4, 5). When low concentration of acetic acid was used in mobile phase, an unknown substance coated the flow cells of the detectors and resulted in the inconsistent reading from the detectors. At high concentration of acetic acid, channeling within the zinc column was observed although the flow cells were not contaminated. An extra pump that delivered a diluted acetic acid solution to the flow cells without passing through the zinc column successfully prevents the contamination of the flow cells without damaging the packing of zinc powder.

While this method was designed to separate three BaP-diones and other fluorescent BaP metabolites, the run time may be shortened if BaP-diones are the only compounds to be analyzed. This may be achieved by using acetonitrile or other solvents stronger than methanol as the organic mobile phase.

Due to the change in the catalytic activity of zinc toward the conversion of BaP-diones to BaP-hydroquinones, sequence-to-sequence variation was observed in the slopes of standard curves. However, good linear correlation was observed between  $A_D/A_{IS}$  and  $C_D$  within each sequence ( $R^2 \geq 0.9976$ ) at BaP-diones concentrations ranging from 1.0 to 220 nM. This sequence-to-sequence variation can be corrected using the peak areas from the authentic standards injected after every four to six runs.

The recoveries of 1,6-dione and 6,12-dione from the enzymatic reaction mixture increased with spiked concentrations, with lower concentrations showing poor recoveries. These results suggest saturable binding of these diones to proteins and/or DNA. This interpretation is supported by the identification of 3,6-dione DNA adducts after incubating 3,6-dione with mouse aortic smooth muscle cells (12) and incubating BaP with monkey kidney COS1 cells co-transfected with CYP1A1 and P450 reductase (13). Reindl and colleagues (14) reported 62% recovery of 3,6-dione (2  $\mu$ M) from rat liver microsomes (0.087 mg protein/mL). Although 62% recovery of 3,6-dione is higher than the results from this study, the only substrate concentration (2  $\mu$ M) used by Reindl et al. (14) was 8.8 times the highest concentration used here with the protein concentrations at a comparable level. Other than possible binding to protein and/or DNA, the poor recovery of 6,12-dione from reaction mixture may be due to dione degradation during the extraction processes.

Results from a preliminary study showed higher recoveries of all three BaP-diones than those shown in Table 6.4. Specifically, the reaction solution was spiked with the mixtures of 10  $\mu$ M BaP and various concentrations of the eleven BaP metabolites described above. The higher recoveries might be partly due to the spontaneous

conversion of BaP to BaP-diones. Low levels of BaP-diones (3 to 5 nM) were observed when 10  $\mu$ M of BaP was incubated with enzymes at concentrations described above (no NADPH). Non-enzymatic oxidation of 3-OH to 3,6-dione (15) might occur during incubation and/or extraction, which can also cause higher recovery of 3,6-dione in the presence of BaP metabolites other than BaP-diones in the spiking solution.

## **6.5. Conclusions**

A novel HPLC method with a post-column zinc reducer was developed and validated for determining BaP-dione with high detection sensitivity. With the combination of a zinc reducer and acidic mobile phase, the detection sensitivities for BaP-diones was enhanced by at least two orders of magnitude. The LODs for all three BaP-diones tested were below 1 nM based on 20- $\mu$ L injections. Wide linear ranges for the standards were also provided by this method. This method is ideal for studies that require the detection of low levels of BaP-diones when radiolabeled BaP or radioactivity detectors are not available. Moreover, the method avoids time-consuming derivatization or reduction required by other methods.

## **6.6. References**

1. Koeber R, Bayona JM, Niessner R. Determination of benzo[a]pyrene diones in air particulate matter with liquid chromatography mass spectrometry. *Environ Sci Technol* 33:1552-1558(1999).
2. Osborne MR, Crosby NT. *Benzopyrenes*. Cambridge:Cambridge University Press, 1987.
3. Lorentzen RJ, Ts'o PO. Benzo[a]yrenedione/benzo[a]pyrenediol oxidation-reduction couples and the generation of reactive reduced molecular oxygen. *Biochemistry* 16:1467-1473(1977).

4. Billedeau SM. Fluorimetric determination of vitamin K<sub>3</sub> (menadione sodium bisulfite) in synthetic animal feed by high-performance liquid chromatography using a post-column zinc reducer. *J Chromatogr A* 472:371-379(1989).
5. Haroon Y, Bacon DS, Sadowski JA. Reduction of quinones with zinc metal in the presence of zinc ions: application of post-column reactor for the fluorometric detection of vitamin K compounds. *Biomed Chromatogr* 2:4-8(1987).
6. ICH. Validation of Analytical Procedures: Methodology. Guideline Q2B. Geneva: The International Conference on Harmonisation of Technical Requirements for Registration of Pharmaceuticals for Human Use, 1996.
7. Shou M, Korzekwa KR, Crespi CL, Gonzalez FJ, Gelboin HV. The role of 12 cDNA-expressed human, rodent, and rabbit cytochromes P450 in the metabolism of benzo[a]pyrene and benzo[a]pyrene trans-7,8-dihydrodiol. *Mol Carcinog* 10:159-168(1994).
8. Koivu-Tikkanen TJ, Ollilainen V, Piironen VI. Determination of phylloquinone and menaquinones in animal products with fluorescence detection after postcolumn reduction with metallic zinc. *J Agric Food Chem* 48:6325-6331(2000).
9. Gautier JC, Urban P, Beaune P, Pompon D. Simulation of human benzo[a]pyrene metabolism deduced from the analysis of individual kinetic steps in recombinant yeast. *Chem Res Toxicol* 9:418-425(1996).
10. Schwarz D, Kisselev P, Cascorbi I, Schunck WH, Roots I. Differential metabolism of benzo[a]pyrene and benzo[a]pyrene-7,8-dihydrodiol by human CYP1A1 variants. *Carcinogenesis* 22:453-459(2001).
11. Kim JH, Stansbury KH, Walker NJ, Trush MA, Strickland PT, Sutter TR. Metabolism of benzo[a]pyrene and benzo[a]pyrene-7,8-diol by human cytochrome P450 1B1. [erratum appears in *Carcinogenesis* 1999 Mar;20(3):515]. *Carcinogenesis* 19:1847-1853(1998).
12. Moorthy B, Miller KP, Jiang W, Williams ES, Kondraganti SR, Ramos KS. Role of cytochrome P4501B1 in benzo[a]pyrene bioactivation to DNA-binding metabolites in mouse vascular smooth muscle cells: evidence from 32P-postlabeling for formation of 3-hydroxybenzo[a]pyrene and benzo[a]pyrene-3,6-quinone as major proximate genotoxic intermediates. *J Pharmacol Exp Ther* 305:394-401(2003).
13. Joseph P, Jaiswal AK. NAD(P)H:quinone oxidoreductase I (DT diaphorase) specifically prevents the formation of benzo[a]pyrene quinone-DNA adducts generated by cytochrome P4501A1 and P450 reductase. *Proc Natl Acad Sci U S A* 91:8413-7(1994).
14. Reindl M, Seidel A, Frank H, Platt KL. Detection of reactive quinones in the metabolism of polycyclic aromatic hydrocarbons by the formation of their glutathione conjugates. *Polycycl Aromat Comp* 10:77-84(1996).
15. Selkirk JK, Croy RG, Roller PP, Gelboin HV. High-pressure liquid chromatographic analysis of benzo(α)pyrene metabolism and covalent binding and the mechanism of action of 7,8-benzoflavone and 1,2-epoxy-3,3,3-trichloropropane. *Cancer Res* 34:3474-3480(1974).

## **6.7. Appendix**

All equations associated with the calculation of the response factors and percentage recovery for BaP-diones are listed in this section. The following equation was used to correlate the concentration of BaP-diones with the peak area analyzed by HPLC,

$$C_D = \frac{A_D}{A_{IS}} \times \frac{RF_{IS} \times C_{IS}}{RF_D} \quad (1)$$

where  $A_i$  represents the peak area measured by HPLC for compound  $i$ .  $RF_i$  and  $C_i$  represent the response factor and concentration, respectively, for compound  $i$ . The subscripts  $D$  and  $IS$  were used to denote BaP-diones and internal standard (BghiP), respectively. Standard calibration curves were obtained by plotting the peak area ratio of individual BaP-hydroquinones to internal standard ( $A_D/A_{IS}$ ) as a function of the concentrations of corresponding BaP-diones ( $C_D$ ). The slope of the standard curve for metabolite  $D$  is equal to the value of ( $RF_D/RF_{IS}/C_{IS}$ ).

The percentage recovery of BaP-diones ( $RCV_D$ ) from solutions containing recombinant human enzymes was then calculated by the following equation,

$$RCV_D = \frac{A_D}{A_{IS}} \times \frac{1}{C_D} \times \frac{RF_{IS} \times C_{IS}}{RF_D} \times RCV_{IS} \quad (2)$$

where  $A_D/A_{IS}$  values were the peak area ratios analyzed by HPLC and  $C_D$  is the known spiked concentration of BaP-dione  $D$ . ( $RF_D/RF_{IS}/C_{IS}$ ) values were obtained from standard calibration curves. Percentage recovery of internal standard ( $RCV_{IS}$ ) in Equation 2 was calculated by

$$RCV_{IS} = \frac{A_{IS}}{RF_{IS} \times C_{IS}} \quad (3)$$

where  $C_{IS}$  is equal to 1.6  $\mu\text{M}$  (pmol/mL).  $A_{IS}$  is the mean of the peak area of BghiP from the entire recovery study.  $RF_{IS}$  is the mean of the values of  $(A_{IS}/C_{IS})$  from the entire standard calibration study. Equation 1 is the simplified form of Equation 2, where  $RCV_{IS}$  and  $RCV_{IS}$  were assumed to be 100%.

**Table 6.1.** Time program for the mobile phase gradient for analyzing BaP-diones

Time (min)	Composition of mobile phase (%)	
	A*	B*
0	40	60
1	40	60
26	20	80
37	20	80
39	4	96
56	4	96
57	40	60
66	40	60

\*Mobile Phase A: H<sub>2</sub>O with 0.003% (v/v) acetic acid; Mobile Phase B: methanol

**Table 6.2.** Time program for the fluorescence detector for measuring BaP-diones and other BaP metabolites

Time (min)	Wavelength (nm)		Compounds
	Excitation	Emission	
0.0 – 14.0	278	407	9,10-diol, 7,10/8,9-tetrol, 7,9/8,10-tetrol
14.0 – 22.5	263	388	4,5-diol
22.5 – 25.5	348	402	7,8-diol
25.5 – 35.0	400	500	1,6-dione, 3,6-dione, 6,12-dione
35.0 - 66.0	375	441	BaP, 3-OH, 7-OH, 9-OH, BghiP

**Table 6.3.** Standard calibration curves and detection limits of BaP-diones

	Sequence #	Standard curve ( $A_D/A_{IS}$ vs. $C_D$ )		LOD (nM)	LOQ (nM)
		Slope	$R^2$		
<b>1,6-dione</b>	Seq. 1	$6.16 \times 10^{-3}$	0.9981	0.18	0.61
	Seq. 2	$6.58 \times 10^{-3}$	0.9994	0.19	0.62
	Seq. 3	$8.16 \times 10^{-3}$	0.9988	0.12	0.39
	Seq. 4	$4.29 \times 10^{-3}$	0.9991	0.41	1.35
<b>3,6-dione</b>	Seq. 1	$2.82 \times 10^{-3}$	0.9978	0.40	1.32
	Seq. 2	$3.16 \times 10^{-3}$	0.9994	0.36	1.19
	Seq. 3	$3.91 \times 10^{-3}$	0.9986	0.21	0.69
	Seq. 4	$1.74 \times 10^{-3}$	0.9981	0.90	2.99
<b>6,12-dione</b>	Seq. 1	$5.73 \times 10^{-3}$	0.9983	0.17	0.55
	Seq. 2	$5.79 \times 10^{-3}$	0.9994	0.20	0.67
	Seq. 3	$7.71 \times 10^{-3}$	0.9985	0.11	0.37
	Seq. 4	$5.07 \times 10^{-3}$	0.9976	0.33	1.09

**Table 6.4.** Percentage recovery of BaP-diones

Concentration (nM)	% Recovery*		
	<b>1,6-dione</b>	<b>3,6-dione</b>	<b>6,12-dione</b>
10.2	14.4% ± 1.6%	19.7% ± 2.2%	7.5% ± 1.8%
34.0	19.3% ± 1.7%	24.6% ± 4.6%	7.2% ± 1.2%
113	26.6% ± 4.6%	32.8% ± 4.4%	6.6% ± 2.7%
227	33.1% ± 1.6%	40.5% ± 3.0%	7.9% ± 2.6%

\*Results are the mean of % recovery ± standard deviation from four data points (two injections from each duplicated sample).

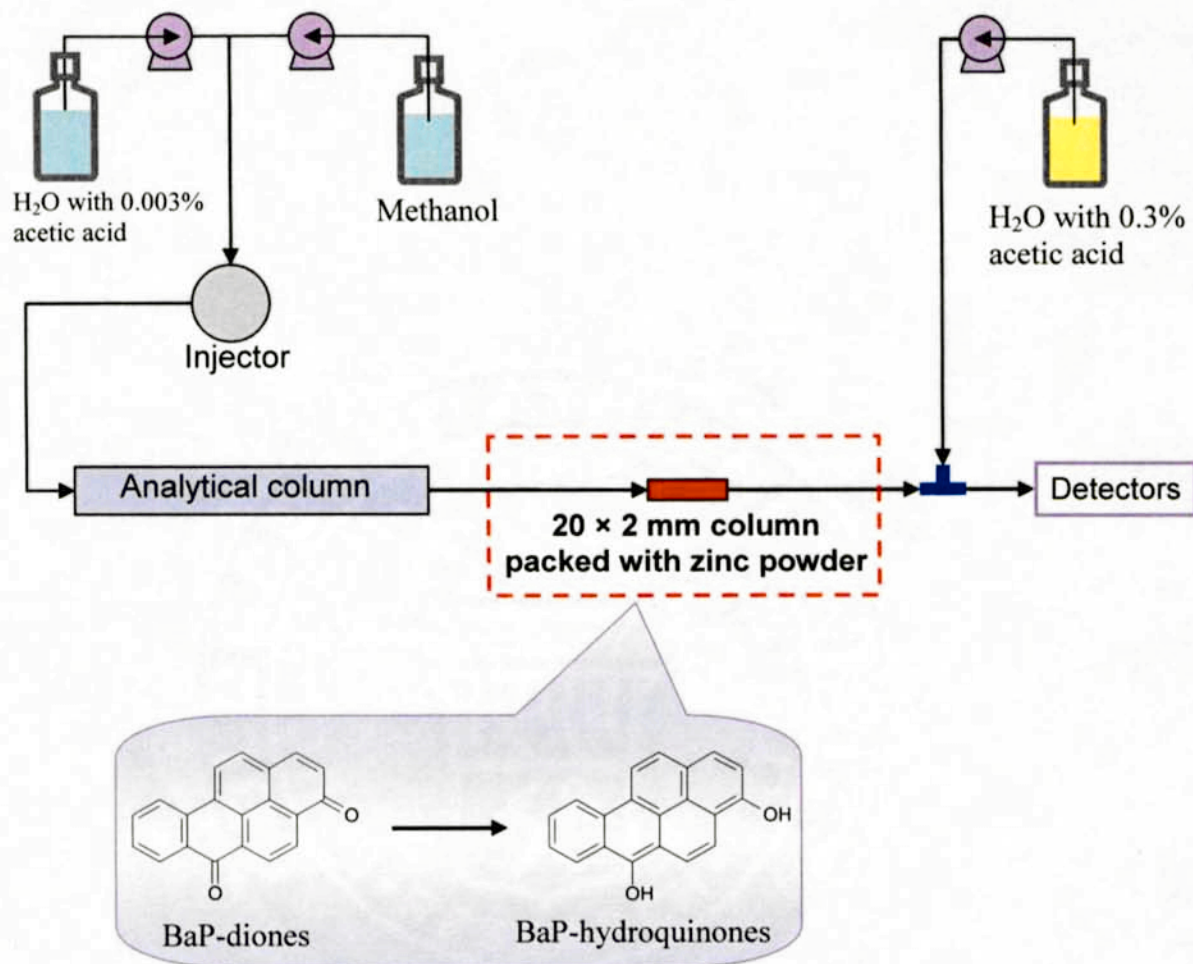


**Figure 6.1.** Apparatus for reducing BaP-diones on-line to their correspond fluorescent BaP-hydroquinones

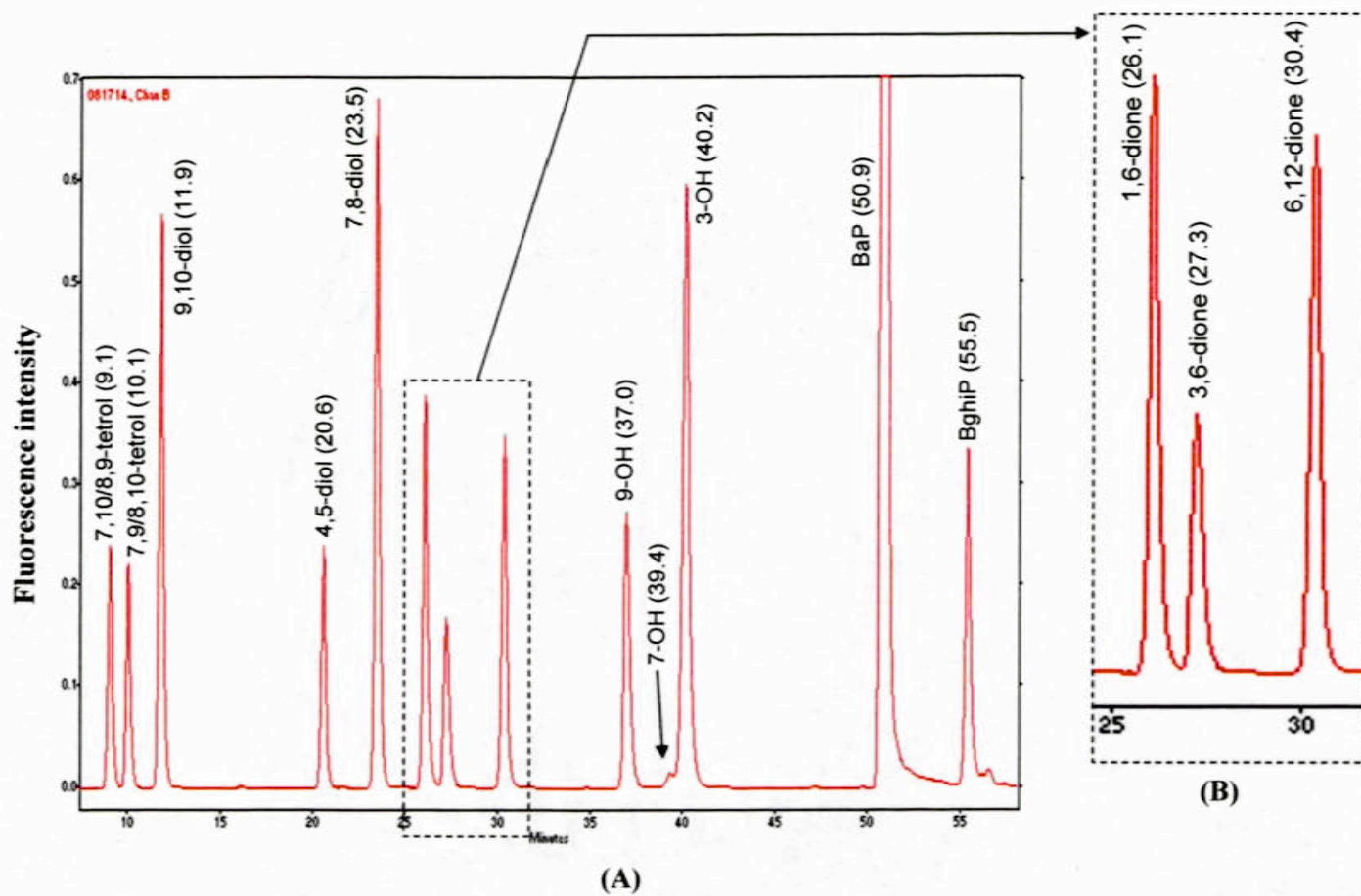


**Figure 6.2.** HPLC profile of the authentic standards of BaP and its metabolites (A). The peaks shown in panel (B) represent BaP-diols, which were reduced from their corresponding BaP-diones by a post-column zinc reducer. The numbers enclosed in parenthesis represent the retention time of the compounds in minutes. The metabolite peaks and BghiP peak represented 3.4 pmol and 32 pmol of the compounds, respectively. The BaP peak was off-scale and represented 200 pmol of the compound.

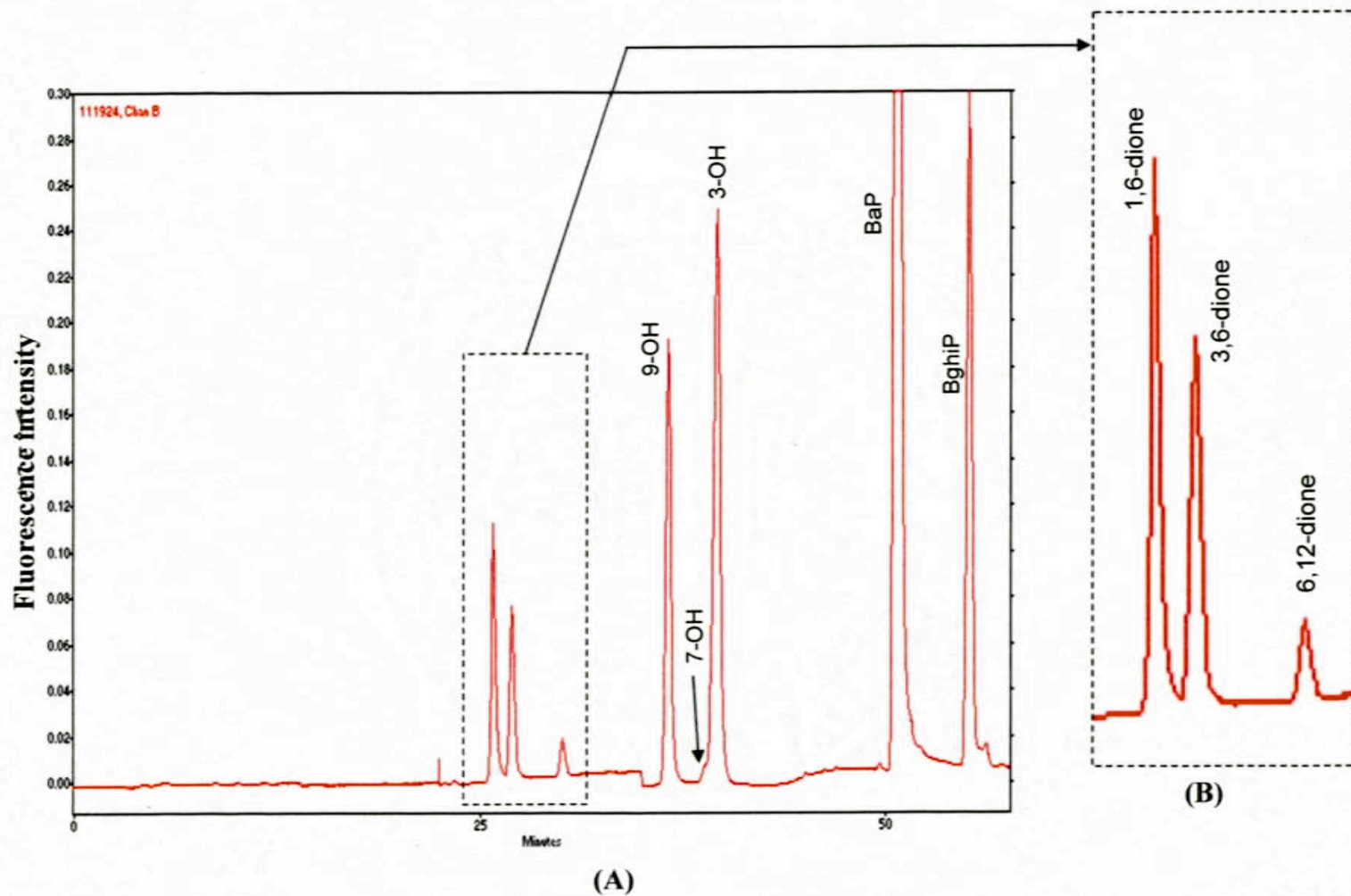


**Figure 6.3.** HPLC profile of BaP metabolism using recombinant human CYP1A1. BaP (10  $\mu$ M) was incubated with 9.0 pmol CYP1A1 in 1.0 mL solution (pH 7.4) at 37  $^{\circ}$ C for 24 min.

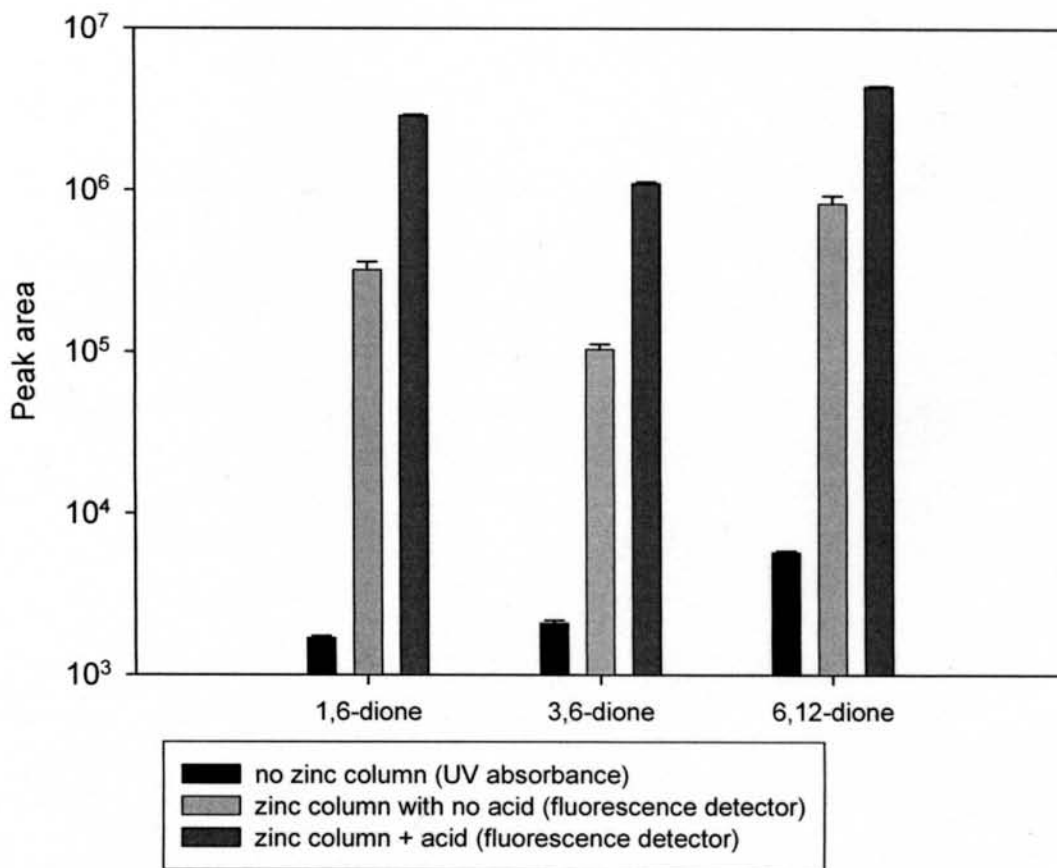


**Figure 6.4.** Comparison of the peak area of BaP-diones measured in the presence and absence of a zinc post column reducer. Results shown are the mean  $\pm$  one standard deviation from six measurements, except for the zinc column with no acid samples (for which were from three measurements).

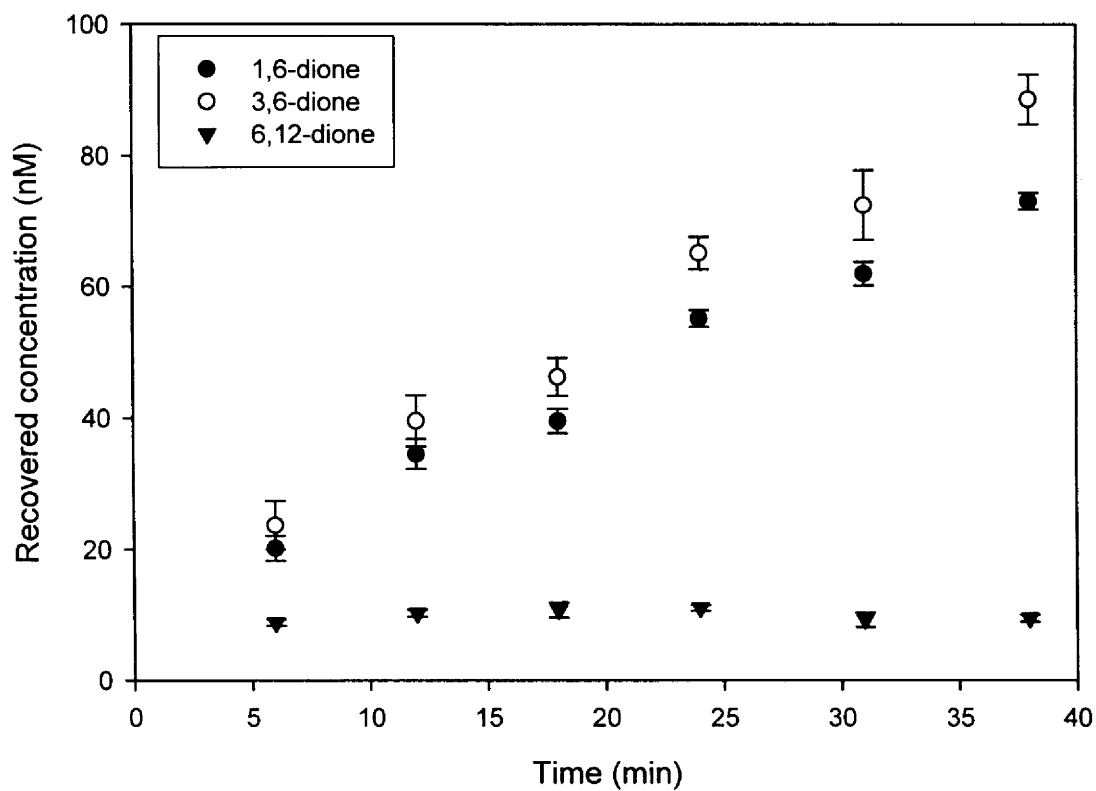


**Figure 6.5.** Time course profiles of BaP-diones after incubating BaP (10  $\mu$ M) with recombinant human CYP1A1 (9.0 nM) and EH (0.05 mg protein/mL) at 37  $^{\circ}$ C. Results are the the mean of the recovered concentrations  $\pm$  one standard deviation from 4 data points (2 injections from each duplicated sample).

## Chapter 7

### A Reaction Network Kinetics Model of Benzo[*a*]pyrene Metabolism Catalyzed by Recombinant Human Enzymes

#### 7.1. Introduction

In Chapter 4, a Reaction Network (RN) pathway model was developed to predict the possible reactions for the mammalian metabolism of benzo[*a*]pyrene (BaP) by encoding the chemical structures and reaction rules using atomic connectivity (1-5). The RN pathway model provided valuable predictions of the possible metabolic pathways of BaP in mammals. In addition to this knowledge of pathways, it is crucial to estimate the associated reaction rates in order to determine whether a specific metabolite is present at a level that causes adverse effects in cells or tissues. In this chapter, we report the development of a RN kinetics model to predict the time course of mammalian metabolism of BaP. Due to the lack of enzyme kinetics data that are suitable for the calibration and validation of the RN kinetics model for BaP, the time course of BaP metabolism was studied in our laboratory using recombinant human cytochrome P450 1A1 (CYP1A1) and microsomal epoxide hydrolase (EH). The high performance liquid chromatography (HPLC) methods described in Chapters 5 and 6 were used to determine the concentrations of BaP and 11 of its metabolites in these time-course studies. The 11 metabolites (Figure 7.1) analyzed here are 3-hydroxy-BaP (3-OH), 7-hydroxy-BaP (7-OH), 9-hydroxy-BaP (9-OH), BaP-*trans*-4,5-dihydrodiol(±) (4,5-diol), BaP-*trans*-7,8-

dihydrodiol( $\pm$ ) (7,8-diol), BaP-*trans*-9,10-dihydrodiol( $\pm$ ) (9,10-diol), BaP-7,8,9,10-tetrol-7,8,9,10-tetrahydro-(7 $\alpha$ ,8 $\beta$ ,9 $\beta$ ,10 $\alpha$ )-( $\pm$ ) (7,10/8,9-tetrol), and BaP-7,8,9,10-tetrol-7,8,9,10-tetrahydro-(7 $\alpha$ ,8 $\beta$ ,9 $\alpha$ ,10 $\beta$ )-( $\pm$ ) (7,9/8,10-tetrol), BaP-1,6-dione (1,6-dione), BaP-3,6-dione (3,6-dione), and BaP-6,12-dione (6,12-dione). These metabolites were selected based on the previous reports of metabolism of BaP (6-8). The formation of these 11 metabolites was predicted by the RN kinetics model for BaP using the following reaction rules: i) epoxidation of BaP and BaP-dihydrodiol catalyzed by CYP1A1; ii) hydrolysis of arene oxides catalyzed by EH; iii) abiotic isomerization of arene oxides to phenols (NIH Shift); iv) one-electron oxidation of BaP catalyzed by CYP1A1; v) auto-oxidation of BaP-diols to BaP-diones. The time course profiles of BaP metabolism using recombinant human enzymes were nicely predicted by the RN kinetics model.

## **7.2. Materials and Methods**

### *7.2.1. Chemicals and Reagents*

BaP, benzo[ghi]perylene (BghiP), acetic acid (99.7%, A.C.S. reagent), and Trizma Pre-set crystal (pH 7.7 at 25°C) were purchased from Sigma-Aldrich (St. Louis, MO). 3-OH, 7-OH, 9-OH, 4,5-diol, 7,8-diol, 9,10-diol, 1,6-dione, 3,6-dione, 6,12-dione, 7,10/8,9-tetrol (listed as BaP-r-7,t-8,t-9,c-10-tetrahydrotetrol), and 7,9/8,10-tetrol (listed as BaP-r-7,t-8,c-9,t-10-tetrahydrotetrol) were purchased from the National Cancer Institute Chemical Carcinogen Reference Standard Repository (Kansas City, MO) and stored at -20°C. HPLC grade methanol, acetonitrile, acetone, ethyl acetate, and dimethyl sulfoxide (DMSO) were purchased from Fisher Scientific (Hampton, NH).

### 7.2.2. *Enzymes and Cofactors*

Microsomal preparations of recombinant human cytochrome P450 1A1 expressed in *Escherichia coli* (Bactosomes CYP1A1; 106 pmol/mg protein) were purchased from XenoTech, LLC (Lenexa, KS). Human lymphoblast microsomes containing human microsomal epoxide hydrolase (styrene oxide hydrolase activity of 25 nmol/min/mg protein) were purchased from BD Gentest (Bedford, MA). NADPH regenerating system, containing glucose-6-phosphate dehydrogenase, NADP<sup>+</sup>, glucose-6-phosphate, and MgCl<sub>2</sub>, was also purchased from BD Gentest.

### 7.2.3. *HPLC Analysis of BaP and its Fluorescent Metabolites*

The HPLC system consisted of a Beckman Coulter System Gold (Fullerton, CA), composed of Model 126 pumps, Model 507 autosampler, and Model 166 UV detector, coupled, in line, to a Jasco (Easton, MD) FP-920 fluorescence detector. BaP and its metabolites were separated on a Discovery RP-AmideC16 column (250 × 4.6 mm I.D., 5 μm; Supelco, Bellefonte, PA). A 0.5-μm precolumn filter (Upchurch Scientific, Oak Harbor, WA) and a Discovery RP-AmideC16 Superguard cartridge (5 μm; Supelco) were used to protect the analytical column. An eight-channel Degasys Populaire vacuum degasser (Chrom Tech, Inc., Apple Valley, MN) was used to de-gas the mobile phases.

Twenty μL solution of sample dissolved in methanol was injected for HPLC analysis. The flow rate was 0.7 mL/min during separation (0-59 min) and increased to 1.0 mL/min to re-equilibrate the column (60-69 min). Mobile phase A consisted of 0.3% (v/v) acetic acid in water (pH 4.1), and mobile phase B was a 50:50 blend of acetonitrile and methanol. The time program for the multi-step gradient is described in Table 7.1.

BaP in the column effluent was monitored by UV absorbance at 280 nm. The metabolites listed in the introduction section, except for BaP-diones, were monitored by the fluorescence detector, in which a time program was set to adjust wavelength for individual compounds (Table 7.2).

#### 7.2.4. HPLC Analysis for BaP-Diones

Due to the non-fluorescent nature of BaP-diones, the limits of quantitation of BaP-diones are at least 2 orders of magnitudes higher than other fluorescent BaP metabolites. A novel HPLC method with a post-column zinc reducer was developed to increase the detection sensitivities for BaP-diones for two orders of magnitude by reducing BaP-diones to their corresponding fluorescent BaP-hydroquinones on-line (Chapter 6). Briefly, the HPLC system described in the previous section was equipped with a Discovery C18 HPLC column (250 × 4.6 mm I.D., 5 μm; Supelco) and a 20 × 2 mm I.D. guard column (Upchurch Scientific, Oak Harbor, WA) packed with zinc powder (-140+325 mesh; Alfa Aesar, Ward Hill, MA). In order to prevent the coating of an unknown compound onto the flow cells, an additional pump (L-6200A Smart Pump; Hitachi, San Jose, CA) was used to deliver 0.3% (v/v) acetic acid in H<sub>2</sub>O at 0.3 mL/min (Figure 6.1) directly to the detectors. The flow rate was 0.7 mL/min during separation (0-57 min) and increased to 1.0 mL/min to re-equilibrate the column (57-66 min). Mobile phase A contained water with 0.3% (v/v) acetic acid (pH 4.1). Mobile phase B was methanol. The time program for the multi-step gradient is described in Table 7.3. BaP-diones were reduced to BaP-hydroquinones by post-column zinc reducer and monitored by the fluorescence detector at 400 nm for excitation and 500 nm for emission.

#### *7.2.5. Time-Course Studies of BaP Metabolism Using Recombinant Human Enzymes*

Incubation mixtures contained 9.0 pmol CYP1A1, 1.3 mM NADP<sup>+</sup>, 3.3 mM glucose-6-phosphate, 0.4 U/mL glucose-6-phosphate dehydrogenase, and 3.3 mM magnesium chloride in 50 mM Tris-HCl buffer (pH 7.4 at 37 °C), in a final volume of 1.0 mL. EH in the form of microsomal protein from human lymphoblasts was added to the reaction mixtures where indicated at a final concentration of 50 µg/mL. After pre-incubation at 37 °C for 2 min, reactions were initiated by adding BaP in DMSO to achieve a final concentration of 10 µM of BaP and 1.0% (v/v) DMSO. Reactions were stopped at various time points by adding 1.0 mL acetone containing 1.6 nmol of BghiP as an internal standard. The extraction procedures were adapted from a previously published method (9). BaP and its metabolites were extracted with ethyl acetate (4.0 mL) and centrifuged at 3000 rpm for 10 min. The organic solvent extracts were evaporated to dryness using a SPD121P SpeedVac concentrator (Thermo Electron, Woburn, MA) at 35 °C. The residues were dissolved in 1.0 mL methanol and analyzed by HPLC.

#### *7.2.6. Extraction Recovery Study*

To simulate the reaction and extraction procedures, the reaction mixture without NADPH was spiked with known concentrations of the authentic standards of BaP and its metabolites and incubated for 50 min at 37 °C as described in Chapters 5 and 6. The same extraction procedures described in the previous section were used to recover BaP and its metabolites from the reaction mixture. The metabolite concentrations in solution

were related to the metabolite concentration bound to proteins (sorbate concentration) using the Langmuir isotherm (10):

$$q = \frac{q_{\max} K_L C}{1 + K_L C} \quad (7-1)$$

where  $q$  is the sorbate concentration (pmol metabolite/mg protein) at equilibrium with  $C$ , the concentration of metabolites in reaction solution (pmol metabolite/mL solution).  $K_L$  is the Langmuir constant and  $q_{\max}$  is the maximum sorbate concentration.  $K_L$  and  $q_{\max}$  values were calculated using nonlinear regression functions provided by SigmaPlot 2000 (SPSS Inc., Chicago, IL)

#### *7.2.7. Qualitative Prediction of the BaP Metabolic Reactions Using a Reaction Network Pathway Model*

A Reaction Network pathway model of BaP metabolic pathways was constructed using the methods described in Chapter 4. Briefly, the chemical structures of reactants were encoded in matrix format to represent atomic connectivity within the molecules. The changes in atomic connectivity as a result of a chemical reaction were also accounted for using a matrix. The uniqueness of all species, including reactants and products, were determined by the comparison of the model-generated unique string codes of the species. The RN pathway modeling software containing all of these elements was written in C language for solution on a standard 900 MHz personal computer.

#### *7.2.8. Rate Equations for BaP Metabolic Pathways*

The experimental data from the time course studies were used to estimate the kinetic parameters of BaP metabolic reactions. The enzymatic reaction rates were

assumed to follow the Michaelis-Menten mechanism with competitive inhibition. When substrate  $S_i$  is converted to product  $P_j$  catalyzed by enzyme E via the formation of enzyme-substrate complex ( $ES_i$ ), the reaction rate  $r_{ij}$  is expressed as,

$$r_{ij} = \frac{d[P_j]}{dt} = \frac{k_{ij} \cdot [E]_t \cdot \frac{[S_i]}{K_i}}{1 + \sum_l \frac{[S_l]}{K_l}} \quad (7-2)$$

where  $[E]_t$  is the total concentration of enzyme and  $k_{ij}$  is the rate constant of the breakdown of  $ES_i$  to form product  $P_j$  (11).  $K_i$  is the dissociation constant of  $ES_i$  complex ( $[E][S_i]/[ES_i]$ ). Note that the stoichiometric coefficients for all substrates in BaP metabolic reactions are equal to one and not shown in Equation 7-2. The denominator of Equation 7-2 accounts for all substrates  $l$  that bind to enzyme E and reflects the competitive inhibitions from alternative substrates. Competitive inhibitions are expected to exist in both CYP1A1 and epoxide hydrolase catalyzed reactions. For example, BaP-4,5-, 7,8-, and 9,10-oxides compete with each other for epoxide hydrolase. Furthermore, dihydrodiols can compete with BaP for CYP1A1. While accounting for all products ( $P_1, P_2, \dots, P_j$ ) derived from substrate  $S_i$ , the rate of change in the concentration of  $S_i$  is

$$\frac{d[S_i]}{dt} = - \frac{\sum_j (k_{ij}) \cdot [E]_t \cdot \frac{[S_i]}{K_i}}{1 + \sum_l \frac{[S_l]}{K_l}} \quad (7-3)$$

On the other hand, spontaneous reactions, e.g. NIH shift reactions, were treated as first-order reactions.

## **7.3. Results and Discussion**

### *7.3.1. Chromatogram*

A representative HPLC profile composed of the authentic standards of BaP and its fluorescent metabolites is shown in Figure 7.2. Each peak in the chromatogram was well separated. The separation shown in Figure 7.2 was achieved with a new RP-AmideC16 column, and the retention times of all chemicals varies as a function of the column age. The chromatogram shown in Figure 7.3 represents the reaction product mixture after incubation of BaP with CYP1A1 and EH for 31 min. Clearly, this method provides good separation of 7-OH and 3-OH, even when the concentration of 3-OH is greater than that of 7-OH (4.2:1 in Figure 7.3), thus overcoming an important limitations of other HPLC methods. Several peaks shown in Figure 7.3 did not correspond to any of the authentic standards of BaP metabolites used in the present method. These unknown peaks will be discussed in the following section.

### *7.3.2. Metabolic Profiles of BaP Using Recombinant Human Enzymes*

When BaP was incubated with Bactosomes CYP1A1 and NADPH regenerating system, the major metabolites detected were 3-OH, 7-OH, 9-OH, 1,6-dione, 3,6-dione, and 6,12-dione. With the addition of EH, 7,8-diol, 9,10-diol, 4,5-diol, and 7,10/8,9-tetrol were also detected besides the phenols and quinones listed above. These results suggest that the rearrangement of BaP-oxides to phenols, *i.e.* NIH shift (12, 13), appears to predominate over the hydrolysis of BaP-oxides in the absence of EH. This finding is consistent with previous studies with human CYP1A1 cDNA expressed in AHH-1TK+/-

human B lymphoblastoid cell line (9), and with reconstituted rat cytochrome P-448 (P-450 1A) systems (14).

On the other hand, Kim et al (15) and Schwarz et al (16) detected considerable amounts of 7,8-diol and 9,10-diol after incubating BaP with a microsomal preparation from insect cells expressing human CYP1A1, even in the absence of EH. In this laboratory, BaP-dihydrodiols were also detected, in the absence of EH, in preliminary studies using human CYP1A1 SUPERSOMES™ from BD Gentest (Woburn, MA). The CYP1A1 activities of SUPERSOMES™ originate from microsomes prepared from insect cells (BTI-TN-5B1-4) that were infected by Baculovirus expressing human CYP1A1 cDNA. The presence of BaP-dihydrodiols in the studies using microsomal preparation from insect cells suggests the existence of endogenous EH activities from these cells. In fact, *Trichoplusia ni* (cabbage looper), from which BTI-TN-5B1-4 cell line was derived, contains membrane bound epoxide hydrolase activities (17).

There were four minor peaks eluting between 7,10/8,9-tetrol and 9,10-diol. Because these unknown peaks were not observed in the absence of EH (data not shown), they might represent the further metabolites of BaP-dihydrodiols, or some BaP-dihydrodiols not identified in the present method. Another two unknown peaks eluting at 34.0 and 36.9 minutes showed considerable peak sizes with fluorescence detection (Figure 7.3). However, the UV absorbance (280 nm) of these two unknown compounds did not show peaks above the limit of detection, which suggests that these two compounds were not major metabolites of BaP. These two compounds could be the hydroxyl-BaPs not identified in this method, since they were detected in the presence and absence of EH.

### 7.3.3. Extraction Recovery

The results of extraction recoveries for the BaP fluorescent metabolites are shown in Table 7.4. One mL of reaction mixture containing 0.34 mg CYP1A1 protein and 0.34 mg EH protein was spiked with a mixture of BaP and its metabolites at various concentrations. The recoveries of 3-OH, 7-OH, and 9-OH from the reaction mixture increased with increasing spiked concentrations, which suggests saturable bindings of these hydroxyl-BaPs to proteins. The relationship between the sorbate and recovered concentrations of these hydroxyl-BaPs was described using the Langmuir isotherm (Figure 7.4). The sorbate concentration  $q$  (pmol metabolite/mg protein) were calculated using the equation

$$q = \frac{C_{spiked} - C}{M_{protein}} \quad (7-4)$$

where  $C_{spiked}$  is the spiked metabolite concentration and  $C$  is the metabolite concentration recovered from the reaction solution.  $M_{protein}$  is the mass of protein used in the recovery study (0.34 mg CYP1A1 protein and 0.34 mg EH protein), with the assumption that the metabolites have the same binding affinities toward CYP1A1 and EH. However, it was further discovered that factors other than protein binding might also contribute to the loss of the metabolites during the extraction processes. This was suggested by the observation that the recoveries of the hydroxyl-BaPs from Tris-HCl buffer without enzymes, although higher than the ones from reaction mixture with enzymes, were still lower than 100%. This might be due to the binding of hydroxyl-BaPs to the polypropylene tubes in which the reaction took place, and/or the portion of these metabolites staying in the aqueous phase. To account for these factors, Equation 7-4 was modified as

$$q = \frac{C_{spiked} - C}{M_{protein} + X} \quad (7-5)$$

where X is the “virtual mass” like polypropylene tubes that the metabolites can bind to expressed in the unit equivalent to mg protein. The values of X were obtained by fitting Equation 7-1 to predict the sorbate concentration from the recoveries of the metabolites from Tris-HCl buffer.

On the other hand, the recovery of 7,10/8,9-tetrol, 7,9/8,10-tetrol, 4,5-diol, 7,8-diol, and 9,10-diol from the reaction mixtures did not vary with the spiked concentrations, which suggest non-saturable binding ( $K_L C \ll 1$  in Equation 7-1) or no binding (*e.g.* 4,5-diol). One hundred percent recovery was used for 4,5-diol in this study. The recoveries of other metabolites with non-saturable binding were described using Equations 7-1 ( $K_L C \ll 1$ ) and 7-5. The parameters for Equations 7-1 and 7-5 are listed in Table 7.5.

The results of the recoveries of BaP-diones from reaction mixtures are shown in Table 7.6. One mL of reaction mixture containing 0.085 mg CYP1A1 protein and 0.05 mg EH protein was spiked with a mixture of 1,6-dione, 3,6-dione, and 6,12-dione at various concentrations. The percentage recoveries for 1,6-dione and 3,6-dione shown in Table 7.6 were used directly to correlate the recovered concentrations with the final concentrations without the adjustment for protein concentrations. This is because the protein concentrations used in the time course study containing CYP1A1 and EH were the same as the ones used in recovery study. Furthermore, the recoveries of BaP-diones from 0.085 mg CYP1A1 protein without EH (another condition used for the time course study) showed no difference from the results with the addition of 0.05 mg EH protein (data not shown). On the other hand, less than 8% of 6,12-dione was recovered and the

percentage recovery was not a function of spiked concentrations in the range of 10.2 to 227 nM. The low recoveries of 6,12-dione might be due to severe degradation during extraction and/or protein binding during incubation. Since the recovery of 6,12-dione might be too low to provide accurate extrapolation, the time course profile of the metabolic formation of 6,12-dione was not included in the model.

#### *7.3.4. Relationship between Enzyme Concentrations and Metabolite Formation*

Ten  $\mu\text{M}$  BaP was incubated with various concentration of Bactosomes CYP1A1 for 30 min to examine the dependency of the metabolite formation on enzyme concentrations. The consumption of BaP and the formation of 3-OH, 7-OH, and 9-OH all increased linearly with the enzyme concentrations from 3.6 to 9.0 nM CYP1A1 (Figure 7.5). The decline in the slopes between 9.0 and 18.0 nM might be caused by the reduced enzyme activity due to the aggregation of proteins at high concentrations. In fact, the Bactosomes CYP1A1 activity was only linear with enzyme concentrations up to 2.5 nM using 7-ethoxycoumarin as the substrate according the product information sheet. Nine nM of CYP1A1 was used in the time course studies to ensure the linearity of metabolite formation versus enzyme concentrations.

The relationship between the metabolite formation and EH concentrations were also studied (Figure 7.6). Ten  $\mu\text{M}$  BaP was incubated with various concentrations of EH for 18 min, while CYP1A1 concentration was fixed at 9.0 nM. When the EH concentration increased from 0.05 to 0.2 mg protein/mL, the concentration of 9-OH decreased, which was accompanied by an increase in the level of 9,10-diol. These results suggest that the hydrolysis of 9,10-oxide to 9,10-diol becomes dominant when EH

concentration increases, assuming the formation of 9,10-oxide from BaP is not affected by EH concentrations. Hence, the formation of 9-OH from the rearrangement of 9,10-oxide diminished. This finding is consistent with the data published by Gautier et al (18). On the other hand, the formation of 7-OH decreased when EH concentrations increased, but the concentrations of 7,8-diol did not increase significantly as 9,10-diol did.

Assuming the 7,8-oxide formation remains unaffected by the changes in EH concentration, the decrease in 7-OH formation should be accompanied by either the increase in 7,8-diol or the accumulation of 7,8-oxide. The latter case is less likely to occur especially when EH concentration increases. The constant level of 7,8-diol might reflect the fact that the formation of 7,8-diol indeed increased but the compound was then converted to other metabolites not identified in the present method. The consumption of BaP was not affected by EH concentration in the range of 0.05 to 0.5 mg protein. It is noteworthy that the formation of 7,8-diol and 9,10-diol did not show the same trend at the highest EH concentration (0.5 mg protein/mL) as at other EH concentrations. To be exact, the concentrations of these metabolites formed at 0.5 mg EH protein/mL are all slightly smaller than those at 0.2 mg EH protein/mL. Since 0.5 mg EH protein/mL is outside of the range of concentrations used in the recovery study, the amount of metabolites bound to EH protein might not be accurately extrapolated using the recovery data studied at lower protein concentrations. The concentration of 0.05 mg EH protein/mL was used in the time-course studies because adequate amounts of BaP-dihydrodiols were detected using EH at this level.

### 7.3.5. Predictions of BaP Metabolic Reactions by the Reaction Network Pathway Model

As discussed in Chapter 4, the RN pathway model for BaP metabolic reactions predicts that 246 reactions can occur, resulting in 150 products when BaP is incubated with CYP and EH. Some of these products may never be observed because either the reaction rates are too low for their formation or the subsequent reactions for the products have very high reaction rates. Based on the metabolic profiles of BaP observed in the time course studies conducted in this laboratory, the rate constants for the reactions leading to the formation of non-detectable metabolites were set to zero. A truncated reaction network containing only the reactions with non-zero rate constants is shown in Figure 7.7. While the 11 metabolites analyzed here were selected based on literature reports of BaP metabolism (6-8), this selection of metabolites was also limited by the availability of authentic standards and analytical methods. For example, the only identifiable major metabolite of 7,8-diol was 7,10/8,9-tetrol. Hence, 7,10/8,9-tetrol and 7,8-diol-9,10-oxide, which is formed via the epoxidation of 7,8-diol and then hydrolyzed to 7,10/8,9-tetrol, were included as the further metabolites of 7,8-diol (Figure 7.7). On the other hand, several unknown peaks were detected after 9,10-diol was incubated with CYP1A1 and neither of the BaP-7,8,9,10-tetrol stereoisomers analyzed in this method appeared to be the major metabolites of 9,10-diol. It was reported that BaP-9,10-diol-7,8-epoxide and BaP-7,8,9,10-tetrols were the major metabolites of 9,10-diol in hamster embryo cells (19) and in hamster lung (20), but not in rat liver metabolizing systems (21). Although the metabolism of 9,10-diol was not extensively studied using human enzyme systems, it is likely that the 9,10-diol undergoes epoxidation to form BaP-9,10-diol-7,8-

epoxide in the presence of CYP enzymes. Therefore, this reaction was included in the current version of the model.

The rearrangement of 4,5-oxide to 4-OH was included in the model (Figure 7.7), although there was no direct evidence of 4-OH being a metabolite of BaP from this study and others (22). 4,5-Diol was only detected in this study when BaP was incubated with EH and CYP1A1, but not detected in the absence of EH. If the rearrangement of 4,5-oxide does not occur, 4,5-diol is expected to be detected in this study even in the absence of EH. This is because 4,5-oxide is unstable and likely to undergo hydrolysis in the presence of acid and water in the mobile phase used for HPLC analysis. Furthermore, it was reported that 4,5-oxide was converted into 4-OH after incubating with polyriboguanlyc acid (23). Therefore, it is likely that 4,5-oxide was rearranged to 4-OH, which eluted as an unknown peak during the HPLC analysis.

### *7.3.6. Reaction Network Kinetics Model Parameters*

The differential equations corresponding to the reactions shown in Figure 7.7 were generated by RN kinetics modeling software and are listed in appendix. Model parameters (Table 7.7) were determined using literature data (24-26) and the experimental data generated from time course studies using 10  $\mu$ M BaP (Figures 7.8 and 7.9). The deactivation of CYP1A1 by BaP-oxides was considered in the RN kinetics model based on the results of time course studies. To be exact, the rates of formation for all metabolites declined as reaction time increased, which was not expected when BaP concentration was still higher than 85% of the initial value (Figures 7.8 and 7.9). Furthermore, the amount of metabolites formed was increased in the presence of EH. A

possible explanation of this finding is that the absence of EH enhances the accumulation of BaP-oxides, which undergo hydrolysis in the presence of EH. Because the reactive BaP-oxides might bind to and inactivate enzymes in the reaction solution, CYP1A1 activity can be reduced in the absence of EH due to the accumulation of BaP-oxides. The equation used to describe the deactivation of CYP1A1 by BaP-oxides is

$$\frac{d[1A1]}{dt} = -\sum_i k_i \times [\text{oxide}_i] \times [1A1] \quad (7-6)$$

where [1A1] is the concentration of CYP1A1. [oxide<sub>*i*</sub>] and *k<sub>i</sub>* are the concentration of oxide *i* and the rate constant for its binding to CYP1A1.

The value for the dissociation constant between BaP and CYP1A1 (6.6 μM) was adopted from published data (24). The same value was used for 7,8-diol and 9,10-diol. The dissociation constants between arene oxides and EH are difficult to measure because BaP-oxides are very unstable in the presence of air. Therefore, the value of dissociation constants between EH and all three BaP-oxides in model was assumed to be equal to the *K<sub>m</sub>* value of 7,8-oxide (1.7 μM) measured using purified rat EH (25). The concentration of EH (42.9 nM equivalent to 0.05 mg protein/mL) was calculated by comparing its styrene oxide hydrolase activity with the activity measured using epoxide hydrolase purified from human liver (26).

Since BaP-oxides are unstable, the rate constants for the conversion of BaP to BaP-oxides (*k<sub>23ox</sub>*, *k<sub>45ox</sub>*, *k<sub>78ox</sub>*, *k<sub>910ox</sub>*) were estimated based on the formation of the further metabolites of BaP-oxides, *i.e.* hydroxyl-BaPs and BaP-diols. The rate constants for the rearrangement and hydrolysis of BaP-oxides were estimated using the amount of hydroxyl-BaPs and BaP-diols formed. The value of *k<sub>3nih</sub>* (rearrangement of 2,3-oxide to

3-OH) was set to be very high ( $1000 \text{ min}^{-1}$ ) based on the previous finding that no BaP-2,3-dihydrodiol has been detected even in the presence of EH (7, 14, 27).

### 7.3.7. Reaction Network Kinetics Model Simulations

The RN kinetics model stimulations for the metabolic profiles of BaP metabolism using CYP1A1 only and the combination of CYP1A1 and EH are shown in Figures 7.8 and 7.9, respectively. BaP and nine of its metabolites were included in the model simulations. When BaP was incubated with CYP1A1 only, the formation of hydroxyl-BaPs and BaP-diones increased with reaction time. Hydroxy-BaPs were formed via the epoxidation of BaP catalyzed by CYP1A1, followed by the rearrangement of BaP-oxides, *i.e.* NIH shift (12). BaP-diones were the auto-oxidation product of 6-OH, which was formed by one-electron oxidation of BaP catalyzed by CYP1A1 (28-30). No BaP-dihydrodiols or BaP-tetrols were detected when incubating BaP with CYP1A1 only, which was simulated by the model when the value of EH concentration was set to zero (Figure 7.8). With the addition of EH, the formations of 7,8-diol, 9,10-diol, 4,5-diol, and 7,10/8,9-tetrol were also observed and their concentrations increased with reaction time (Figure 7.9). BaP-dihydrodiols were formed via the hydrolysis of BaP-oxides catalyzed by EH, and 7,10/8,9-tetrol was the further metabolite of 7,8-diol catalyzed by CYP1A1. As a result of the competition between the hydrolysis and NIH shift reactions of BaP-oxides, the concentrations of 7-OH and 9-OH formed in the presence of EH were lower than the ones formed in the absence of EH.

Without considering the deactivation of CYP1A1, it was not possible to use the same set of model parameters to simulate the results from CYP1A1-catalyzed reactions

and CYP1A1/EH-catalyzed reactions. The hypothesis that CYP1A1 activity was reduced due to the accumulation of BaP-oxides in the absence of EH was supported by the model simulations. Furthermore, with the consideration of the deactivation of CYP1A1, the model was able to simulate the decreases in the formation rates of BaP metabolites with the increasing reaction time. The deactivation of enzyme by reactive metabolites was previously reported by Lilly et al. (31). CYP2E1 activity toward 1,2-dichloroethylene (DCE) was inhibited by the reactive metabolites of DCE *in vivo* and *in vitro* (31).

There were two metabolites, 6,12-dione and 7,9/8,10-tetrol, analyzed in this study but not included in the model predictions. 6,12-dione was not included in the model because it was only detected at low levels and the concentrations did not increase with reaction time. This was caused by the low recovery of 6,12-dione from the reaction mixture. 7,9/8,10-tetrol was detected at very low level (< 0.02% of BaP concentration) and the peak was interfered by unknown peaks. Therefore, 7,9/8,10-tetrol was not included in the model prediction.

After the parameters were defined, the model was validated using the metabolic profile of BaP studied at lower concentration (Figure 7.10). The consumption of BaP and the formation of nine metabolites were nicely predicted by the model, which suggests the model can be used to extrapolate the metabolic profiles from high to low substrate concentrations.

The model stimulations showed higher BaP concentrations than those of experimental data after 24 min of reaction (Figures 7.8 and 7.9). The underestimation of BaP consumptions might be caused by the conversion of BaP to unknown metabolites that were not measured in this study. Another possible explanation is the experimental

errors associated with adding a small volume of BaP stock solutions to the reaction mixtures. BaP was introduced to 1.0 mL reaction mixture by adding 10  $\mu$ L stock solution in DMSO using 25  $\mu$ L Hamilton syringe. The model did not provide as good fits for 1,6-dione and 3,6-dione as for other metabolites. The experimental data of these diones might be less reliable because of their relatively low recoveries from the reaction mixtures (Table 7.6). Non-enzymatic oxidation of 3-OH to 3,6-dione was previously reported (32). Kinetics of this reaction should be further investigated using time course studies and included in an updated model. This is because the model simulations on the pathways associated with the formations of both 3-OH and 3,6-dione might be affected by this oxidation reaction.

Overall, the present work represents the first time course study that BaP and as many as 11 of its metabolites were determined after BaP was incubated with recombinant human enzymes. Gautier *et al.* (18) studied BaP metabolism using human CYP1A1 and EH expressed in yeast cells. Only 3-OH, 9-OH, 7,8-diol, 4,5-diol, and 7,10/8,9-tetrol were included in their time course study (18). In several other studies of BaP metabolism were reported using recombinant human enzymes expressed in insect cells (9, 15, 16). Time course profiles of BaP metabolism were not reported in any of these studies. Furthermore, HPLC methods reported in these studies did not completely resolve 3-OH from 7-OH (9, 15, 16).

The RN kinetics model of BaP is the first model to predict the formation of as many as 19 metabolites, and the consumption of BaP. The model predictions for the time course of BaP and 9 of these 19 metabolites were validated using experimental data. Some metabolites (*e.g.* BaP-oxides) were not measurable by experiments because they

have very short half-life and rapidly underwent other reactions. These metabolites are often reactive and harmful to tissues or cells. A major advantage of applying RN kinetics model to study toxicology is that the kinetics model can be used to predict the reactive intermediates that are not measurable by experiments. The Gautier *et al.* (18) also reported a kinetics model for the formation of BaP metabolites, but the consumption of BaP was not included. Furthermore, their model stimulations were only validated using the experimental data of five metabolites included in their time course study (18).

#### *7.3.8. Initial Development of the Quantitative Structure/Reactivity Correlations for the Reaction Rates of BaP Metabolism*

The model parameters estimated here can serve as a starting point for the construction of Quantitative Structure/Reactivity Correlations (QSRCs) for biochemical reactions. QSRCs are semi-empirical methods that correlate the reaction rates with measurable structural properties (33, 34). The construction of QSRCs for the epoxidation of BaP is shown here as an example, although the attempt was not successful. The enzymatic epoxidation of double bonds catalyzed by cytochrome P450 is likely to start with the formation of a charge-transfer complex between the ferryl oxygen on P450 and  $\pi$  bond on the substrate (35). Therefore, the rate constants of the enzymatic epoxidation at distinct positions of BaP are expected to correlate with bond order of the reaction site. The bond orders for all possible sites for the epoxidation of BaP were calculated by Dewar and Trinajstic (36) and are listed in Table 7.8. Although the 4-5 bond has the highest bond order in BaP, the formation of 4,5-oxide is slower than other epoxidation reactions tested in this study. This suggests that the rate of epoxidation might not be

predicted by the value of bond order. Furthermore, the high reaction rate of the epoxidation of BaP to 2,3-oxide can not be correlated to the relatively low bond order of 2-3 bond in BaP. The formations of 1,2-oxide, 11,12-oxide, and their further metabolites were not commonly observed (22), although the bond orders for 1-2 and 11-12 bonds are higher than the one for 2-3 bond.

Another property that might be correlated with the rate of epoxidation of BaP is the resonance energy, a measure of the extra stability of the actual molecular entity compared to the contributing structure of lowest potential energy (37), of the epoxide product. Note that the resonance energies used here were only an approximate estimation based on the numbers of rings retaining their aromaticities after the epoxidation reaction (Table 7.8). For example, 2,3-oxide maintain the aromaticity equivalent to anthracene, which has the resonance energy of 83.5 kcal/mol (37). The naphthalene-type of resonance for 8,9-oxide has the lowest resonance energy, *i.e.* the least extent of stability, among the epoxides listed in Table 7.8. In fact, the formation of 8,9-oxide has not been reported. However, the resonance energies for the other BaP-oxides listed in Table 7.8 can not be correlated with the rate constants estimated from the model. For example, the relatively fast reaction of the epoxidation on 2-3 bond of BaP can not be explained by the relatively low resonance energy of 2,3-oxide, compared with other BaP-oxides. Therefore, the construction of the QSRCs for the epoxidation of BaP may require the calculation of other structural properties related to the chemical structure or the structure of the enzyme active sites.

## **7.4. Conclusions**

BaP metabolism was studied using recombinant human enzymes with the determination of BaP and eleven of its metabolites at various time points. The metabolites observed when incubating BaP with CYP1A1 were formed via the epoxidation of BaP, the rearrangements of BaP-oxides to hydroxy-BaP, and one-electron oxidation of BaP. With the addition of EH, BaP-oxides underwent hydrolysis reaction and resulted in the decrease in hydroxyl-BaP formations. CYP1A1 activity was reduced in the absence of EH, probably due to the accumulation of BaP-oxides that can deactivate CYP1A1.

The time course profiles of BaP and its metabolites were nicely predicted by the RN kinetics model of BaP with the rate equations generated automatically by the modeling program. The RN kinetics model was validated using the experimental data of BaP and nine its metabolites detected. A major advantage of applying RN kinetics model to study toxicology is that the kinetics model can be used to predict the reactive intermediates that are not measurable by experiments.

## **7.5. References**

1. Liao KH, Dobrev ID, Dennison JE, Jr., Andersen ME, Reisfeld B, Reardon KF, Campaign JA, Wei W, Klein MT, Quann RJ, Yang RS. Application of biologically based computer modeling to simple or complex mixtures. *Environ Health Perspect* 110 Suppl 6:957-63(2002).
2. Klein MT, Hou G, Quann RJ, Wei W, Liao KH, Yang RS, Campaign JA, Mazurek MA, Broadbelt LJ. BioMOL: a computer-assisted biological modeling tool for complex chemical mixtures and biological processes at the molecular level. *Environ Health Perspect* 110 Suppl 6:1025-9(2002).
3. Broadbelt LJ, Stark SM, Klein MT. Computer generated pyrolysis modeling: on-the-fly generation of species, reactions, and rates. *Ind Eng Chem Res* 33:790-799(1994).

4. Broadbelt LJ, Stark SM, Klein MT. Computer-generated reaction networks: on-the-fly calculation of species properties using computational quantum chemistry. *Chem Eng Sci* 49:4991-5010(1994).
5. Broadbelt LJ, Stark SM, Klein MT. Computer generated reaction modelling: decomposition and encoding algorithms for determining species uniqueness. *Comput Chem Eng* 20:113-129(1996).
6. Harvey RG. Polycyclic Aromatic Hydrocarbons: Chemistry and Carcinogenicity. Cambridge:Cambridge University Press, 1991.
7. Levin W, Wood A, Chang R, Ryan D, Thomas P, Yagi H, Thakker D, Vyas K, Boyd C, Chu SY, Conney A, Jerina D. Oxidative metabolism of polycyclic aromatic hydrocarbons to ultimate carcinogens. *Drug Metab Rev* 13:555-580(1982).
8. Miller KP, Ramos KS. Impact of cellular metabolism on the biological effects of benzo[a]pyrene and related hydrocarbons. *Drug Metab Rev* 33:1-35(2001).
9. Shou M, Korzekwa KR, Crespi CL, Gonzalez FJ, Gelboin HV. The role of 12 cDNA-expressed human, rodent, and rabbit cytochromes P450 in the metabolism of benzo[a]pyrene and benzo[a]pyrene trans-7,8-dihydrodiol. *Mol Carcinog* 10:159-168(1994).
10. Blanch HW, Clark DS. Biochemical Engineering. New York:Marcel Dekker, 1996.
11. Segel IH. Enzyme Kinetics: Behavior and Analysis of Rapid Equilibrium and Steady-State Enzyme Systems. New York:Wiley, 1993.
12. Jerina DM, Daly JW. Arene oxides: a new aspect of drug metabolism. *Science* 185:573-582(1974).
13. Guroff G, Daly JW, Jerina DM, Renson J, Witkop B, Udenfrie.S. Hydroxylation-induced migration: the NIH shift. *Science* 157:1524-1530(1967).
14. Holder G, Yagi H, Dansette P, Jerina DM, Levin W, Lu AY, Conney AH. Effects of inducers and epoxide hydase on the metabolism of benzo(a)pyrene by liver microsomes and a reconstituted system: analysis by high pressure liquid chromatography. *Proc Natl Acad Sci U S A* 71:4356-4360(1974).
15. Kim JH, Stansbury KH, Walker NJ, Trush MA, Strickland PT, Sutter TR. Metabolism of benzo[a]pyrene and benzo[a]pyrene-7,8-diol by human cytochrome P450 1B1. [erratum appears in *Carcinogenesis* 1999 Mar;20(3):515]. *Carcinogenesis* 19:1847-1853(1998).
16. Schwarz D, Kisselev P, Cascorbi I, Schunck WH, Roots I. Differential metabolism of benzo[a]pyrene and benzo[a]pyrene-7,8-dihydrodiol by human CYP1A1 variants. *Carcinogenesis* 22:453-459(2001).
17. Roe RM, Kallapur V, Linderman RJ, Viviani F, Harris SV, Walker EA, Thompson DM. Mechanism of action and cloning of epoxide hydrolase from the cabbage looper, *Trichoplusia ni*. *Arch Insect Biochem Physiol* 32:527-535(1996).
18. Gautier JC, Urban P, Beaune P, Pompon D. Simulation of human benzo[a]pyrene metabolism deduced from the analysis of individual kinetic steps in recombinant yeast. *Chem Res Toxicol* 9:418-425(1996).
19. MacLeod MC, Kootstra A, Mansfield BK, Slaga TJ, Selkirk JK. Specificity in interaction of benzo[a]pyrene with nuclear macromolecules: implication of

- derivatives of two dihydrodiols in protein binding. *Proc Natl Acad Sci U S A* 77:6396-400(1980).
20. Cohen GM, Moore BP. The metabolism of benzo(a)pyrene, 7,8-dihydro-7,8-dihydroxybenzo(a)pyrene and 9,10-dihydro-9,10-dihydroxybenzo(a)pyrene leads to (a)pyrene by short-term organ cultures of hamster lung. *Biochem Pharmacol* 26:1481-7(1977).
  21. Booth J, Sims P. Different pathways involved in the metabolism of the 7,8- and 9,10-dihydrodiols of benzo(a)pyrene. *Biochem Pharmacol* 25:979-80(1976).
  22. Osborne MR, Crosby NT. *Benzopyrenes*. Cambridge:Cambridge University Press, 1987.
  23. Murray AW, Grover PL, Sims P. The conversion of benzo[a]pyrene 4,5-oxide into 4-hydroxybenzo[a]pyrene in the presence of polyriboguanilic acid. *Chem Biol Interact* 13:57-66(1976).
  24. Cvrk T, Strobel HW. Role of THR501 residue in substrate binding and catalytic activity of cytochrome P4501A1. *Arch Biochem Biophys* 389:31-40(2001).
  25. Levin W, Buening MK, Wood AW, Chang RL, Kedzierski B, Thakker DR, Boyd DR, Gadaginamath GS, Armstrong RN, Yagi H, Karle JM, Slaga TJ, Jerina DM, Conney AH. An enantiomeric interaction in the metabolism and tumorigenicity of (+)- and (-)-benzo[a]pyrene 7,8-oxide. *J Biol Chem* 255:9067-9074(1980).
  26. Lu AY, Thomas PE, Ryan D, Jerina DM, Levin W. Purification of human liver microsomal epoxide hydrase. Differences in the properties of the human and rat enzymes. *J Biol Chem* 254:5878-5881(1979).
  27. Yang SK, Roller PP, Fu PP, Harvey RG, Gelboin HV. Evidence for a 2,3-epoxide as an intermediate in the microsomal metabolism of benzo[a]pyrene to 3-hydroxybenzo[a]pyrene. *Biochem Biophys Res Commun* 77:1176-82(1977).
  28. Lesko S, Caspary W, Lorentzen R, Ts'o POP. Enzymic formation of 6-oxobenzo[a]pyrene radical in rat liver homogenates from carcinogenic benzo[a]pyrene. *Biochemistry* 14:3978-3984(1975).
  29. Lorentzen RJ, Caspary WJ, Lesko SA, Ts'o POP. The autoxidation of 6-hydroxybenzo[a]pyrene and 6-oxobenzo[a]pyrene radical, reactive metabolites of benzo[a]pyrene. *Biochemistry* 14:3970-3977(1975).
  30. Cavalieri EL, Rogan EG, Cremonesi P, Devanesan PD. Radical cations as precursors in the metabolic formation of quinones from benzo[a]pyrene and 6-fluorobenzo[a]pyrene. Fluoro substitution as a probe for one-electron oxidation in aromatic substrates. *Biochem Pharmacol* 37:2173-2182(1988).
  31. Lilly PD, Thornton-Manning JR, Gargas ML, Clewell HJ, Andersen ME. Kinetic characterization of CYP2E1 inhibition in vivo and in vitro by the chloroethylenes. *Arch Toxicol* 72:609-21(1998).
  32. Selkirk JK, Croy RG, Roller PP, Gelboin HV. High-pressure liquid chromatographic analysis of benzo(α)pyrene metabolism and covalent binding and the mechanism of action of 7,8-benzoflavone and 1,2-epoxy-3,3,3-trichloropropane. *Cancer Res* 34:3474-3480(1974).
  33. Neurock M, Klein MT. Linear free energy relationships in kinetic analyses: Applications of quantum chemistry. *Polycyclic Aromatic Compounds* 3:231-246(1993).

34. Korre SC, Neurock M, Klein MT, Quann RJ. Hydrogenation of polynuclear aromatic hydrocarbons. II. Quantitative structure/reactivity correlations. *Chem Eng Sci* 49:4191-4210(1994).
35. Josephy PD. Cytochrome P-450. In: *Molecular Toxicology* (Josephy PD, ed). New York:Oxford University Press, 1997;209-252.
36. Dewar MJS, Trinajst.N. Quantum chemical data. 1. Scf molecular orbitals for benzenoid hydrocarbons. *Collect Czech Chem Commun* 35:3136-89(1970).
37. Wheland GW. *Resonance in Organic Chemistry*. New York:Wiley, 1955.
38. Streitwieser A. *Molecular Orbital Theory for Organic Chemists*. New York:Wiley, 1961.

## 7.6. Appendix

All equations listed here, except for the ones associated with the deactivation of CYP1A1, were generated by the Reaction Network model of BaP for solution using Advanced Continuous Simulation Language (ACSL; AEGIS Technologies, Huntsville, AL). The equations associated with the deactivation of CYP1A1 by BaP-oxides were added manually and expressed in italic print. Lines starting with exclamation marks are comments and not executed by the program. Variables starting with upper case C represent concentrations. Rates for enzyme-catalyzed reactions are represented using Michaelis-Menten kinetics (Equation 7-2).

### !-----Part 1: Rate expressions for each reaction-----!

```

! CCC(H)C(H)CC(H)C(H)C(H)CC(H)C(H)CC(H)C(H)C(H)C(H)C(H)C:C: + (OO) ->
! CCC(H)C(H)CC(H)C(H)OC(H)CC(H)C(H)CC(H)C(H)C(H)C(H)C(H)C:C: + (O)
! BaP + O2 -> k(Epoxidation) BaP_23_oxide + O
  rxn1= k23ox * Ccyp / KcypBaP / KcypTotal * CBaP

! CCC(H)C(H)CC(H)C(H)C(H)CC(H)C(H)CC(H)C(H)C(H)C(H)C(H)C:C: + (OO) ->
! CCC(H)C(H)CC(H)C(H)C(H)CC(H)OC(H)CC(H)CC(H)C(H)C(H)C(H)C(H)C:C: + (O)
! BaP + O2 -> k(Epoxidation) BaP_45_oxide + O
  rxn2= k45ox * Ccyp / KcypBaP / KcypTotal * CBaP

! CCC(H)C(H)CC(H)C(H)C(H)CC(H)C(H)CC(H)C(H)C(H)C(H)C(H)C:C: + (OO) ->
! CCC(H)C(H)CC(H)C(H)C(H)C(H)CC(H)C(H)CC(H)OC(H)C(H)C(H)C(H)C:C: + (O)
! BaP + O2 -> k(Epoxidation) BaP_78_oxide + O
  rxn3= k78ox * Ccyp / KcypBaP / KcypTotal * CBaP

! CCC(H)C(H)CC(H)C(H)C(H)CC(H)C(H)CC(H)C(H)C(H)C(H)C(H)C:C: + (OO) ->
! CCC(H)C(H)CC(H)C(H)C(H)C(H)CC(H)C(H)CC(H)C(H)C(H)C(H)OC(H)C:C: + (O)
! BaP + O2 -> k(Epoxidation) BaP_910_oxide + O
  rxn4= k910ox * Ccyp / KcypBaP / KcypTotal * CBaP

```



! CCC(H)C(H)CC(H)C(H)C(O(H))CC(H)C(H)CC(O(H))CC(H)C(H)C(H)C(H)C:C: -> (H2) +  
 !CCC(H)C(H)CC(H)C(H)C(O)CC(H)C(H)CC(O)CC(H)C(H)C(H)C(H)C:C:  
 ! BaP\_36HQ -> k(AutoOxidation) H2 + BaP\_36dione  
 rxn19= k36auto \* CBaP\_36HQ

! CCC(H)C(H)C(H)C(H)C(O(H))CC(H)C(H)CC(H)C(H)C(O(H))C(H)C:C: -> (H2) +  
 !CCC(H)C(H)C(H)C(H)C(O)CC(H)C(H)CC(H)C(H)C(O)C(H)C:C:  
 ! BaP\_612HQ -> k(AutoOxidation) H2 + BaP\_612dione  
 rxn20= k612auto \* CBaP\_612HQ

! CCC(H)C(H)CC(H)C(H)C(O(H))CC(H)C(H)CC(H)C(O(H))C(H)OC(H)C:C: + O(H2) ->  
 !CCC(H)C(H)CC(H)C(H)C(O)CC(H)C(H)CC(H)C(O(H))C(H)OC(H)C:C:  
 ! BaP\_78diol\_910oxide + H2O -> k(Hydroxidation) BaP\_78910\_tetrol  
 rxn21= k78910auto \* CBaP\_78diol\_910oxide

! Denominator for CYP reactions  
 KcypTotal = 1 + (CBaP / KcypBaP) + (CBaP\_78\_diol / KcypBaP\_78\_diol) + (CBaP\_910\_diol / KcypBaP\_910\_diol)

! Denominator for EH reactions  
 KehTotal = 1 + (CBaP\_45\_oxide / KehBaP\_45\_oxide) + (CBaP\_78\_oxide / KehBaP\_78\_oxide) ...  
 + (CBaP\_910\_oxide / KehBaP\_910\_oxide)

! -----Part 2: Rate expressions for each chemical-----

! ODE for BaP  
 RCBaP = - rxn1 - rxn2 - rxn3 - rxn4 - rxn5  
 CBaP = INTEG(RCBaP, C0BaP)

! ODE for BaP\_23\_oxide  
 RCBaP\_23\_oxide = + rxn1 - rxn6  
 CBaP\_23\_oxide = INTEG(RCBaP\_23\_oxide, 0.0)

! ODE for BaP\_45\_oxide  
 RCBaP\_45\_oxide = - rxn7 - rxn8 + rxn2 - k45add\*C45ox\*C1A1  
 CBaP\_45\_oxide = INTEG(RCBaP\_45\_oxide, 0.0)

! ODE for BaP\_78\_oxide  
 RCBaP\_78\_oxide = - rxn9 + rxn3 - rxn10 - k78add\*C78ox\*C1A1  
 CBaP\_78\_oxide = INTEG(RCBaP\_78\_oxide, 0.0)

! ODE for BaP\_910\_oxide  
 RCBaP\_910\_oxide = + rxn4 - rxn11 - rxn12 - k910add\*C910ox\*C1A1  
 CBaP\_910\_oxide = INTEG(RCBaP\_910\_oxide, 0.0)

! ODE for 6\_OH\_BaP  
 RC6\_OH\_BaP = - rxn13 - rxn14 - rxn15 + rxn5  
 C6\_OH\_BaP = INTEG(RC6\_OH\_BaP, 0.0)

! ODE for 3\_OH\_BaP  
 RC3\_OH\_BaP = + rxn6  
 C3\_OH\_BaP = INTEG(RC3\_OH\_BaP, 0.0)

! ODE for BaP\_45\_diol  
 RCBaP\_45\_diol = + rxn7  
 CBaP\_45\_diol = INTEG(RCBaP\_45\_diol, 0.0)

! ODE for 4\_OH\_BaP  
 RC4\_OH\_BaP = + rxn8  
 C4\_OH\_BaP = INTEG(RC4\_OH\_BaP, 0.0)

! ODE for BaP\_78\_diol  
 RCBaP\_78\_diol = + rxn9 - rxn16  
 CBaP\_78\_diol = INTEG(RCBaP\_78\_diol, 0.0)

```

! ODE for 7_OH_BaP
RC7_OH_BaP = + rxn10
C7_OH_BaP = INTEG(RC7_OH_BaP, 0.0)

! ODE for BaP_910_diol
RCBaP_910_diol = - rxn17 + rxn11
CBaP_910_diol = INTEG(RCBaP_910_diol, 0.0)

! ODE for 9_OH_BaP
RC9_OH_BaP = + rxn12
C9_OH_BaP = INTEG(RC9_OH_BaP, 0.0)

! ODE for BaP_36HQ
RCBaP_36HQ = + rxn13 - rxn19
CBaP_36HQ = INTEG(RCBaP_36HQ, 0.0)

! ODE for BaP_16HQ
RCBaP_16HQ = + rxn14 - rxn18
CBaP_16HQ = INTEG(RCBaP_16HQ, 0.0)

! ODE for BaP_612HQ
RCBaP_612HQ = + rxn15 - rxn20
CBaP_612HQ = INTEG(RCBaP_612HQ, 0.0)

! ODE for BaP_78diol_910oxide
RCBaP_78diol_910oxide = - rxn21 + rxn16
CBaP_78diol_910oxide = INTEG(RCBaP_78diol_910oxide, 0.0)

! ODE for BaP_910diol_78oxide
RCBaP_910diol_78oxide = + rxn17
CBaP_910diol_78oxide = INTEG(RCBaP_910diol_78oxide, 0.0)

! ODE for BaP_16dione
RCBaP_16dione = + rxn18
CBaP_16dione = INTEG(RCBaP_16dione, 0.0)

! ODE for BaP_36dione
RCBaP_36dione = + rxn19
CBaP_36dione = INTEG(RCBaP_36dione, 0.0)

! ODE for BaP_612dione
RCBaP_612dione = + rxn20
CBaP_612dione = INTEG(RCBaP_612dione, 0.0)

! ODE for BaP_78910_tetrol
RCBaP_78910_tetrol = + rxn21
CBaP_78910_tetrol = INTEG(RCBaP_78910_tetrol, 0.0)

!C1A1 = CONCENTRATION of 1A1 (nM) - DEACTIVATION OF ENZYME IS CONSIDERED
RC1A1 = - k78add*C78ox*C1A1 - k910add*C910ox*C1A1 - k45add*C45ox*C1A1
C1A1 = INTEG(RC1A1,C1A10)

```

**Table 7.1.** Time program for the multi-step gradient of mobile phase for RP-AmideC16 HPLC column

Time (min)	Composition of mobile phase (%)	
	A*	B*
0	40	60
1	40	60
26	20	80
47	20	80
49	0	100
58	0	100
60	40	60
69	40	60

\* Mobile phase A: 0.3% (v/v) acetic acid in water (pH 4.1); Mobile phase B, acetonitrile:methanol (50/50).

**Table 7.2.** Time program for the fluorescence detector for measuring BaP and its fluorescent metabolites

Time (min)	Wavelength (nm)		Compounds
	Excitation	Emission	
0.0 - 13.6	278	407	9,10-diol, 7,10/8,9-tetrol, 7,9/8,10-tetrol
13.6 - 18.1	263	388	4,5-diol
18.1 - 23.0	348	402	7,8-diol
23.0 - 69.0	375	441	BaP, 3-OH, 7-OH, 9-OH, BghiP

**Table 7.3.** Time program for the mobile phase gradient for analyzing BaP-diones

Time (min)	Composition of mobile phase (%)	
	A*	B*
0	40	60
1	40	60
26	20	80
37	20	80
39	4	96
56	4	96
57	40	60
66	40	60

\* Mobile phase A: H<sub>2</sub>O with 0.003% (v/v) acetic acid (pH 4.1); Mobile phase B: methanol

**Table 7.4.** Percentage recovery of fluorescent BaP metabolites<sup>a</sup>

7,10/8,9-tetrol		7,9/8,10-tetrol		9,10-diol		4,5-diol	
Conc. (nM)	% Recovery						
0.990	87.7±12.2	1.00	88.4±1.4	0.990	93.2±17.2	0.989	109.0±14.8
2.97	92.3±2.4	3.00	90.8±3.3	2.97	96.5±5.3	2.97	108.6±3.3
9.90	93.3±1.5	10.0	89.3±3.4	9.90	96.3±1.4	9.89	104.3±0.8
34.0	90.2±0.6	34.3	90.4±1.8	33.9	96.0±0.4	33.9	102.8±0.8
106	90.1±2.3	107	91.2±2.6	106	93.4±2.3	106	99.0±1.4
170	90.4±1.5	171	92.1±1.5	170	94.3±0.3	170	100.0±0.5
				<sup>b</sup> 357	93.9±2.1	357	102.0±0.9
				<sup>b</sup> 571	93.7±3.2	570	102.7±2.4
7,8-diol		9-OH		7-OH		3-OH	
Conc. (nM)	% Recovery						
0.985	73.7±8.9	0.987	37.7±5.6				
2.96	77.2±5.5	2.96	45.9±4.8				
9.85	80.8±0.2	9.90	69.2±1.9	10.0	55.2±2.2	10.2	15.7±0.6
33.8	73.4±0.3	34.0	74.8±2.2	34.3	55.2±5.1	34.9	11.7±2.4
106	74.6±2.6	106	81.8±2.4	107	69.0±2.5	109	29.6±2.9
169	72.9±1.5	169	85.7±2.5	172	73.0±2.3	174	33.5±4.5
<sup>b</sup> 356	75.4±1.4	354	90.1±2.6	354	80.1±2.5	358	44.7±2.1
<sup>b</sup> 570	74.1±0.3	<sup>b</sup> 567	90.1±2.4	567	85.9±3.3	<sup>b</sup> 573	53.2±3.2

<sup>a</sup>Metabolites were recovered from the reaction mixture containing 0.34 mg/mL CYP1A1 and 0.34 mg/mL EH. Results are the mean of % recovery ± standard deviation from four data points (two injections from each duplicated sample).

<sup>b</sup>A 4-fold dilution was required to obtain peak that is on-scale.

**Table 7.5.** Parameters used for Langmuir isotherms to describe the sorbate and recovered concentrations of BaP metabolites (Equations 7-1 and 7-5)

	$K_L$ (mL/pmol)	$q_{max} \times K_L$ (mL/mg protein)	X (mg protein)
9-OH	$7.353 \times 10^{-3}$	0.3126	0.4824
7-OH	$6.670 \times 10^{-3}$	0.4482	0.8878
3-OH	$7.612 \times 10^{-3}$	3.548	0.1317
7,8-diol	$K_L C \ll 1$	0.2580	0.6603
9,10-diol	$K_L C \ll 1$	0.08124	0.1492
7,10/8,9-tetrol	$K_L C \ll 1$	0.05573	1.267
7,9/8,10-tetrol	$K_L C \ll 1$	0.06233	0.6966

**Table 7.6.** Percentage recovery of BaP-diones

Concentration (nM)	% Recovery*		
	1,6-dione	3,6-dione	6,12-dione
10.2	14.4% ± 1.6%	19.7% ± 2.2%	7.5% ± 1.8%
34.0	19.3% ± 1.7%	24.6% ± 4.6%	7.2% ± 1.2%
113	26.6% ± 4.6%	32.8% ± 4.4%	6.6% ± 2.7%
227	33.1% ± 1.6%	40.5% ± 3.0%	7.9% ± 2.6%

\*BaP-diones were recovered from the reaction mixture containing 0.085 mg/mL CYP1A1 and 0.05 mg/mL EH. Results are the mean ± one standard deviation from four data points (two injections from each duplicated sample).

**Table 7.7.** Model parameters for the Reaction Network model of BaP

Model Parameter	Symbol	Value
<i>Rate constants for CYP1A1-catalyzed reactions (nM product / min / nM CYP1A1)</i>		
BaP->2,3-oxide	k23ox	1.8
BaP->7,8-oxide	k78ox	1.3
BaP->9,10-oxide	k910ox	2.0
BaP->4,5-oxide	k45ox	0.2
BaP->6-OH	k6ox	4.5
7,8-diol->7,8-diol-9,10-oxide	k78910ox	12.9
9,10-diol->9,10-diol-7,8-oxide	k91078ox	0.5
<i>Rate constants for EH-catalyzed reactions (nM product / min / nM EH)</i>		
7,8-oxide->7,8-diol	k78hydro	147
9,10-oxide->9,10-diol	k910hydro	47.6
4,5-oxide->4,5-diol	k45hydro	43.6
<i>Dissociation constants between substrates and enzymes (nM)</i>		
BaP and CYP1A1	KcypBaP	6600
7,8-diol and CYP1A1	Kcyp78diol	6600
9,10-diol and CYP1A1	Kcyp910diol	6600
7,8-oxide and EH	Keh78ox	1700
9,10-oxide and EH	Keh910ox	1700
4,5-oxide and EH	Keh45ox	1700
<i>Rate constants for spontaneous reactions (min<sup>-1</sup>)</i>		
2,3-oxide->3-OH	k3nih	1000
7,8-oxide->7-OH	k7nih	1.8
9,10-oxide->9-OH	k9nih	2.9
4,5-oxide->4-OH	k4nih	1.0
7,8-diol-9,10-oxide->7,10/8,9-tetrol	k71089auto	100
6-OH-BaP->BaP-1,6-diol	k16ox	30.3
6-OH-BaP->BaP-3,6-diol	k36ox	32
6-OH-BaP->BaP-6,12-diol	k612ox	2
1,6-HQ->1,6-dione	k16auto	100
3,6-HQ->3,6-dione	k36auto	100
6,12-HQ->6,12-dione	k612auto	100
<i>Rate constants for the formation of oxide-CYP1A1 adduct (1 / nM / min)</i>		
7,8-oxide and CYP1A1	k78add	0.001
9,10-oxide and CYP1A1	k910add	0.009
4,5-oxide and CYP1A1	k45add	0.015

**Table 7.8.** Probable structural properties associated with the QSRCs for the epoxidation of BaP

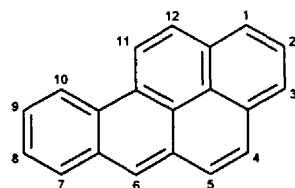
Reactions	Rate constants (nM product/ min/ nM CYP1A1)	<sup>a</sup> Bond order at the reaction site of BaP	<sup>b</sup> Resonance energy for epoxide products (kcal/mol)
BaP → 2,3-oxide	1.8 (k23ox)	0.617	83.5 (anthracene) <sup>c</sup>
BaP → 4,5-oxide	0.2 (k45ox)	0.904	116.5 (chrysene) <sup>c</sup>
BaP → 7,8-oxide	1.3 (k78ox)	0.792	108.9 (pyrene) <sup>d</sup>
BaP → 9,10-oxide	2.0 (k910ox)	0.789	108.9 (pyrene) <sup>d</sup>
BaP → 1,2-oxide	-	0.718	91.3 (phenanthrene) <sup>c</sup>
BaP → 11,12-oxide	-	0.853	111.6 (benz[a]anthracene) <sup>c</sup>
BaP → 8,9-oxide	-	0.523	61.0 (naphthalene) <sup>c</sup>

<sup>a</sup>From Dewar and Trinajstić (36)

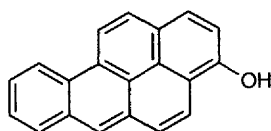
<sup>b</sup>Approximate estimation based on the numbers of rings retaining their aromaticities after the epoxidation reaction.

<sup>c</sup>From Wheland (37).

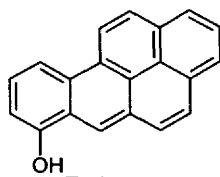
<sup>d</sup>From Streitwieser (38).



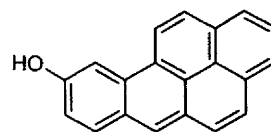
BaP



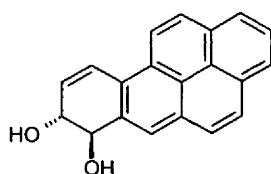
3-OH



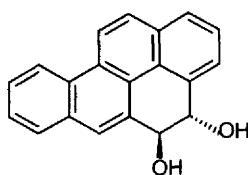
7-OH



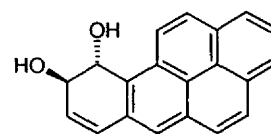
9-OH



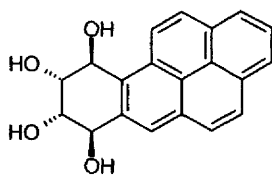
7,8-diol



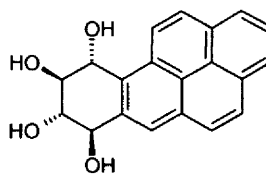
4,5-diol



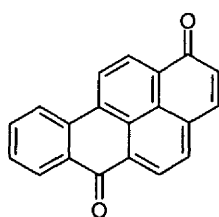
9,10-diol



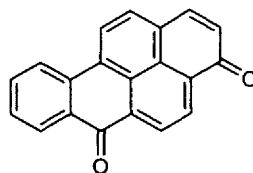
7,10/8,9-tetrol



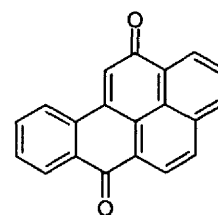
7,9/8,10-tetrol



1,6-dione



3,6-dione



6,12-dione

**Figure 7.1.** Chemical structures of BaP and its metabolites (only one structural isomer is shown).

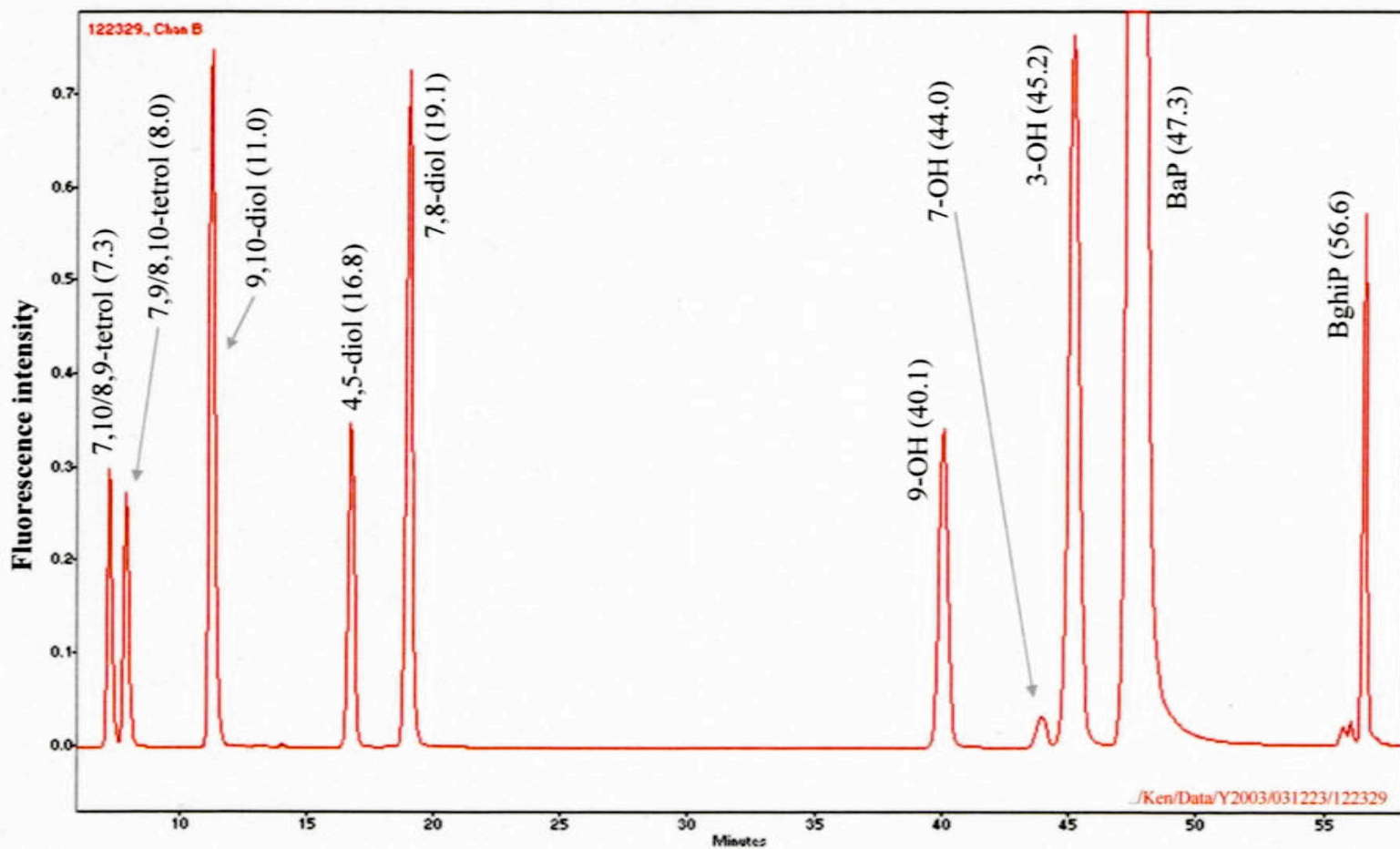


**Figure 7.2.** HPLC profile of the authentic standards of BaP and its fluorescent metabolites. The numbers enclosed in parenthesis represent the retention times of the compounds in minutes. The metabolite peaks and BghiP peak represented 3.4 pmol and 32 pmol of the compounds, respectively. The BaP peak was off-scale and represented 200 pmol of the compound.

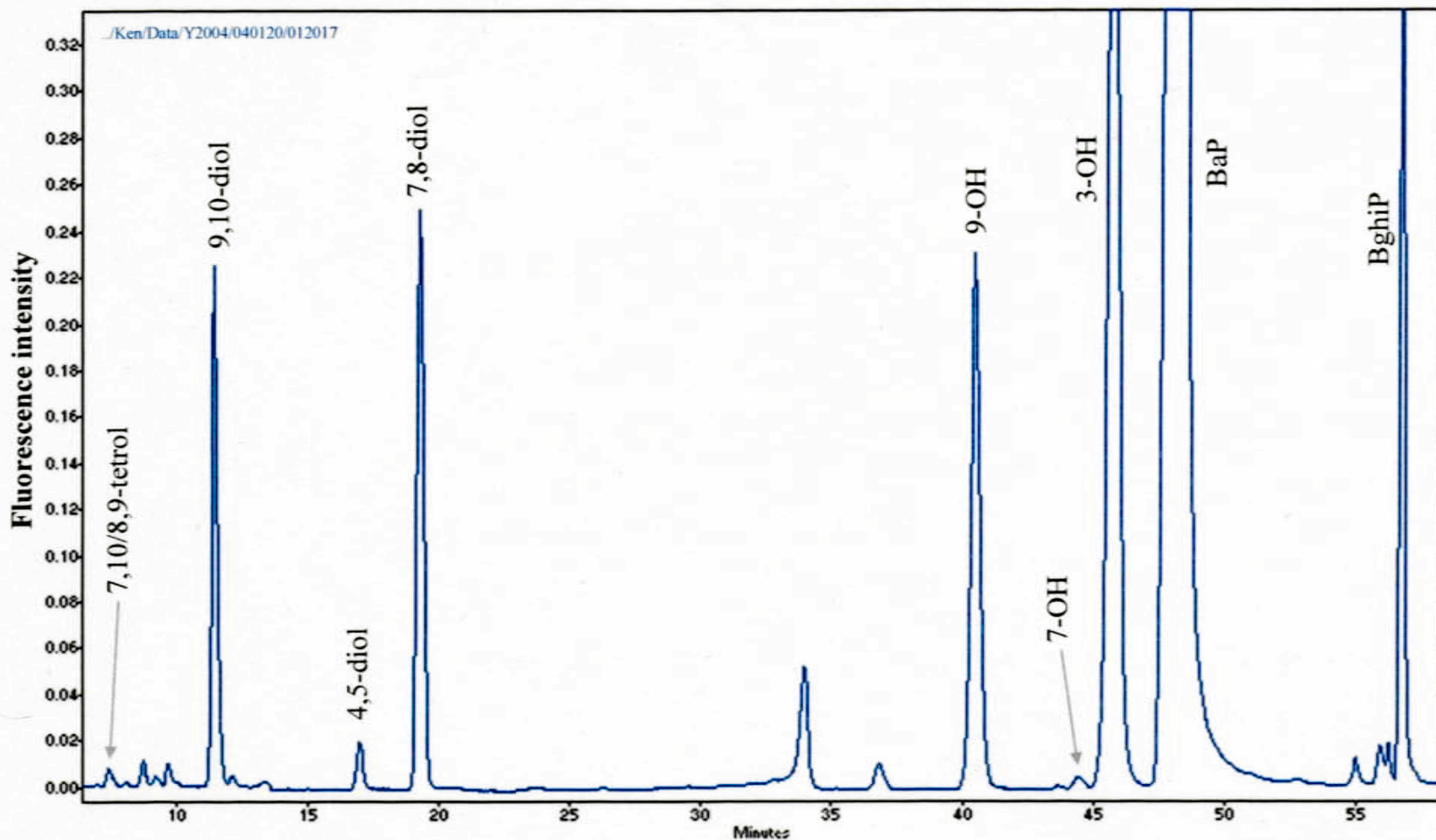


**Figure 7.3.** HPLC profile of BaP metabolism using recombinant human CYP1A1 and EH. BaP was incubated with 9.0 pmol CYP1A1 and 0.05 mg EH protein in one mL solution (pH 7.4) at 37°C for 31 min. The concentration of 3-OH is 4.2 times the concentration of 7-OH.

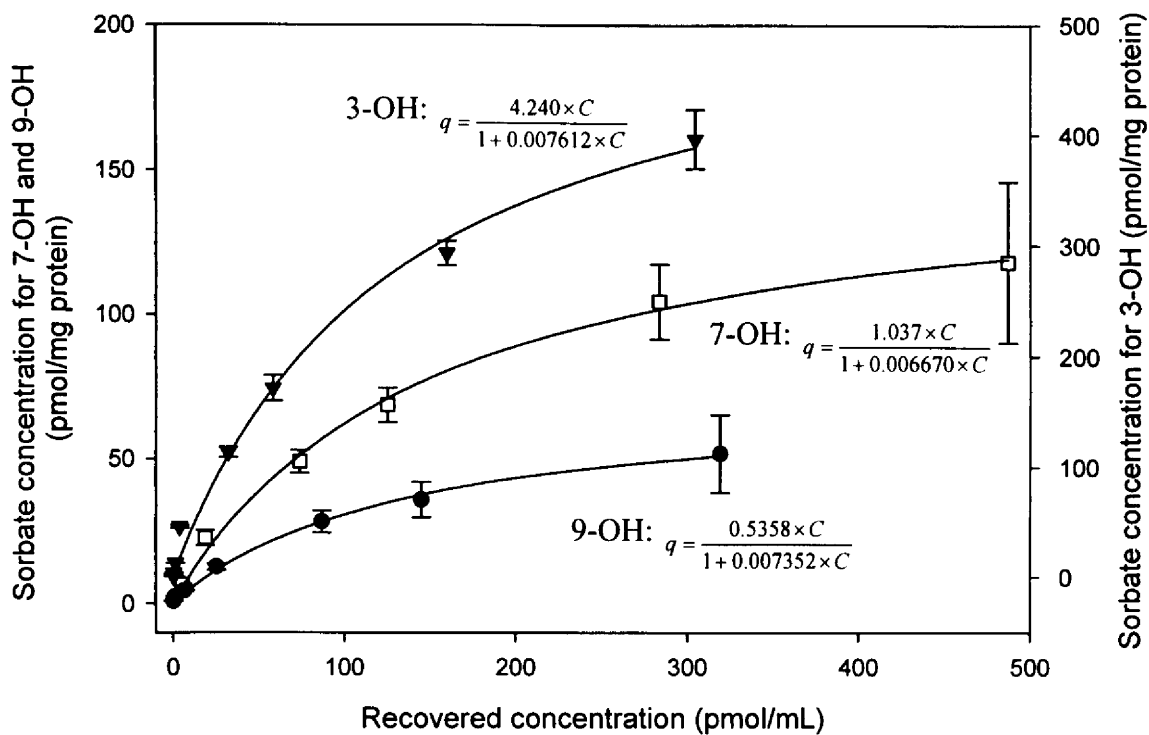


**Figure 7.4.** Langmuir isotherms of the recoveries of hydroxyl-BaPs from the reaction mixture. Symbols are the mean  $\pm$  one standard deviation from four determinations. Solid lines are the Langmuir isotherm with the equations listed in the figure.

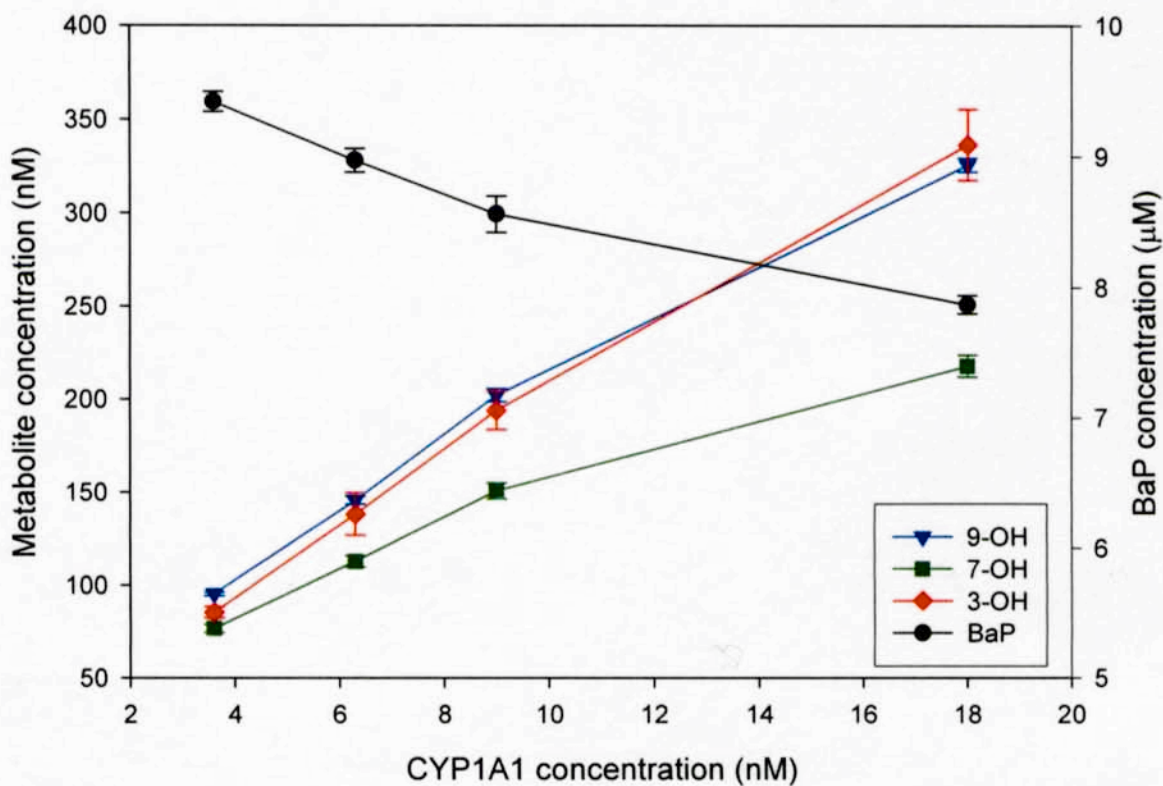


**Figure 7.5.** The relationship between metabolite formation and CYP1A1 concentrations. Ten  $\mu\text{M}$  of BaP was incubated with various concentration CYP1A1 for 30 min at  $37^\circ\text{C}$ . The metabolite concentrations are represented by the left y-axis, while BaP concentrations are represented by the right y-axis.

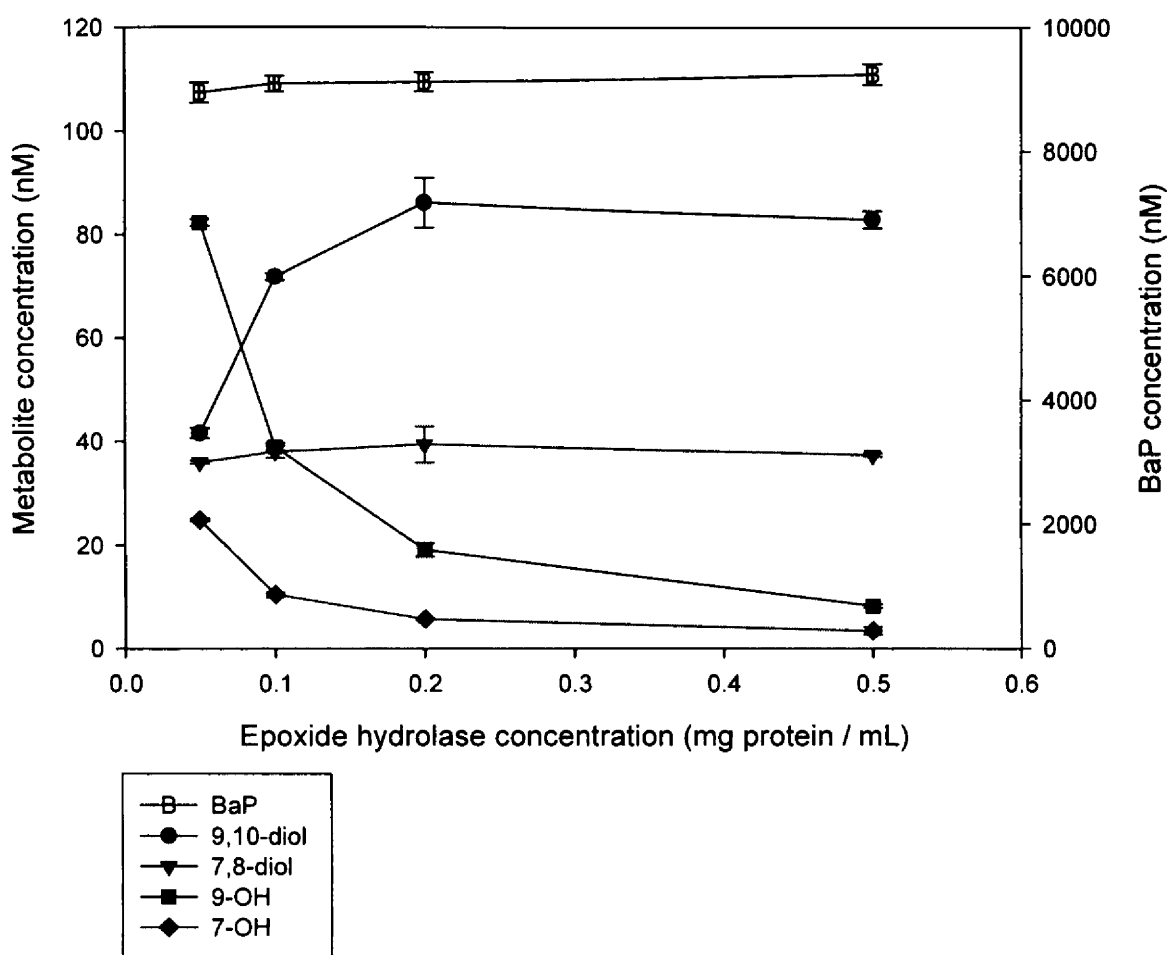


**Figure 7.6.** The relationship between metabolite formation and epoxide hydrolase concentrations. Ten  $\mu\text{M}$  of BaP was incubated with various concentration of epoxide hydrolase for 18 min at 37 °C, while the CYP1A1 concentration was fixed at 9.0 nM. The metabolite concentrations are represented by the left y-axis, while BaP concentrations are represented by the right y-axis.

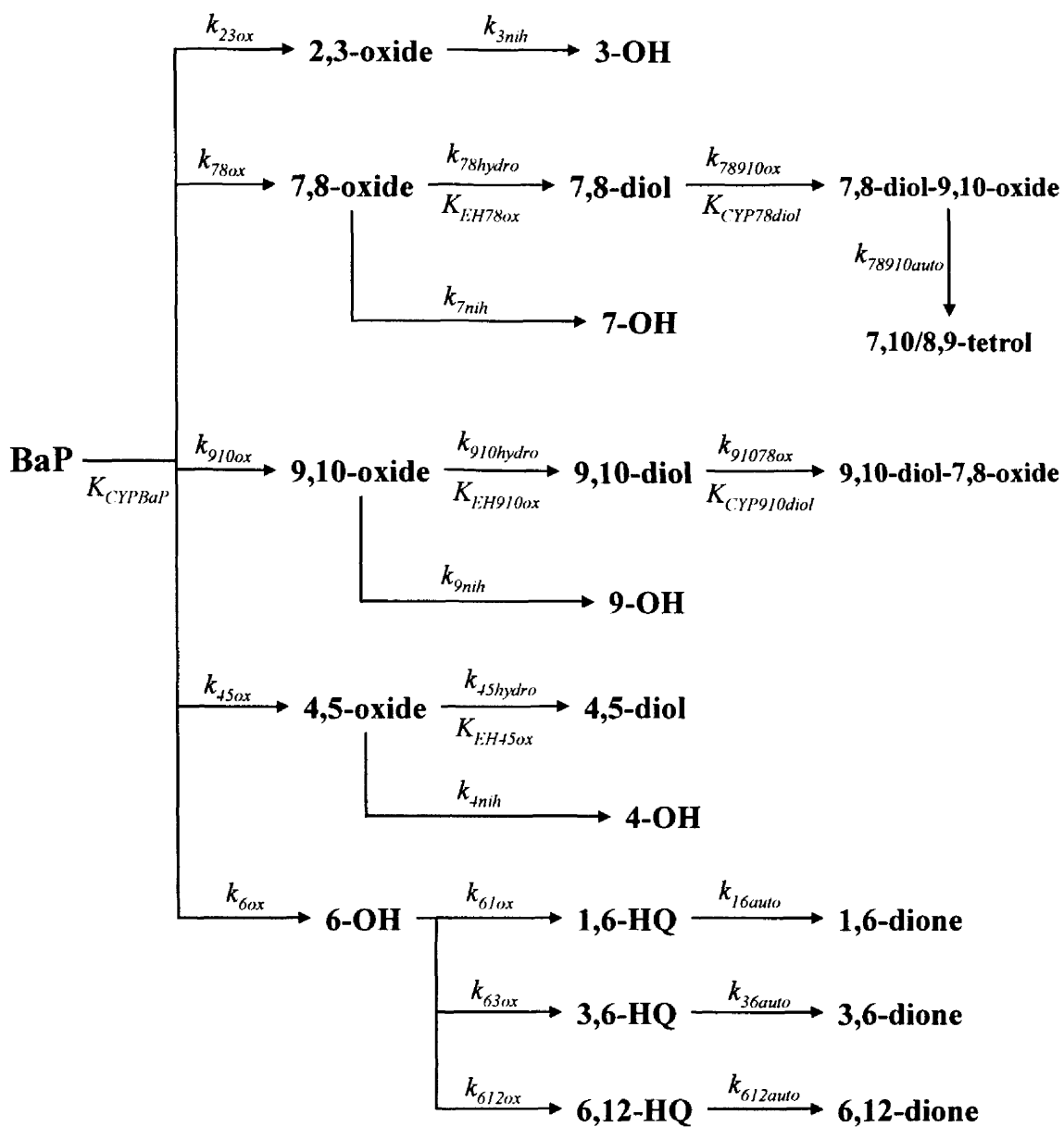


**Figure 7.7.** Truncated metabolic pathways of BaP predicted by the Reaction Network pathway model. Oxide represents BaP-dihydroepoxide and HQ represents BaP-hydroquinones.

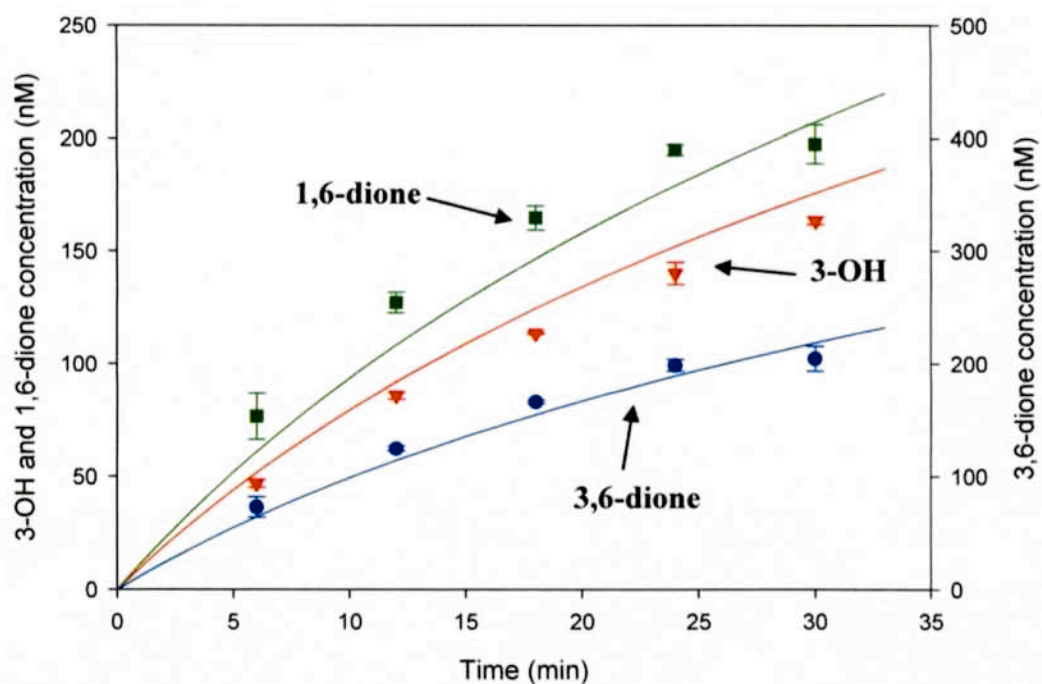
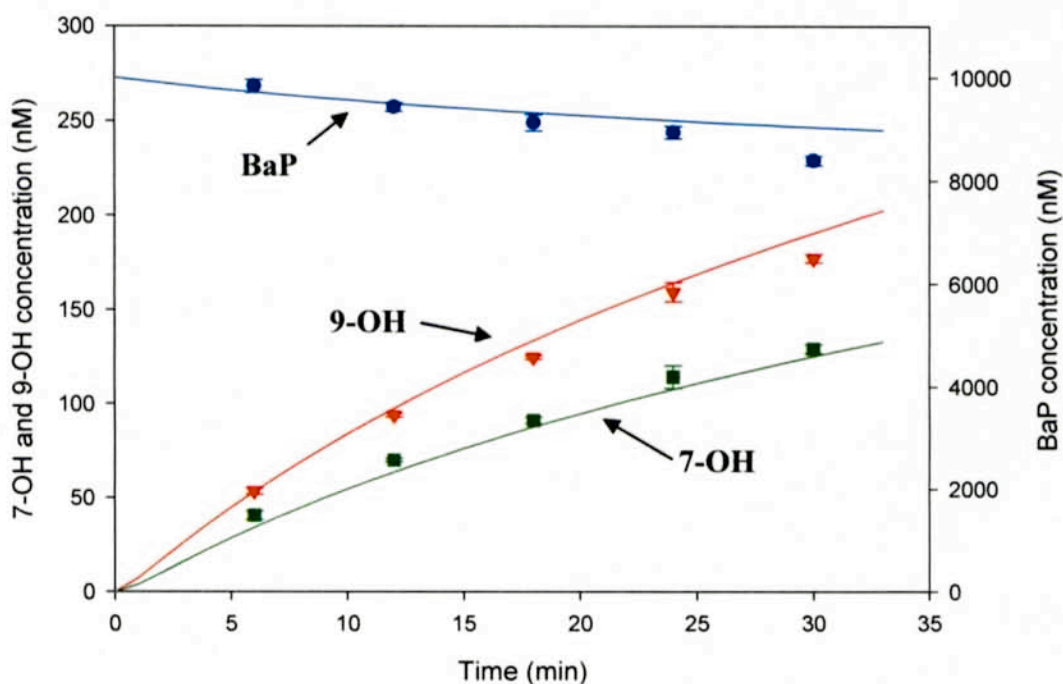


**Figure 7.8.** RN kinetics model simulation of the time course profiles of BaP metabolism using CYP1A1. Ten  $\mu\text{M}$  BaP was incubated with 9.0 nM CYP1A1 and NADPH regenerating system at 37 °C. Solid lines represent model simulations and symbols represent experimental data  $\pm$  standard deviation from four determinations.

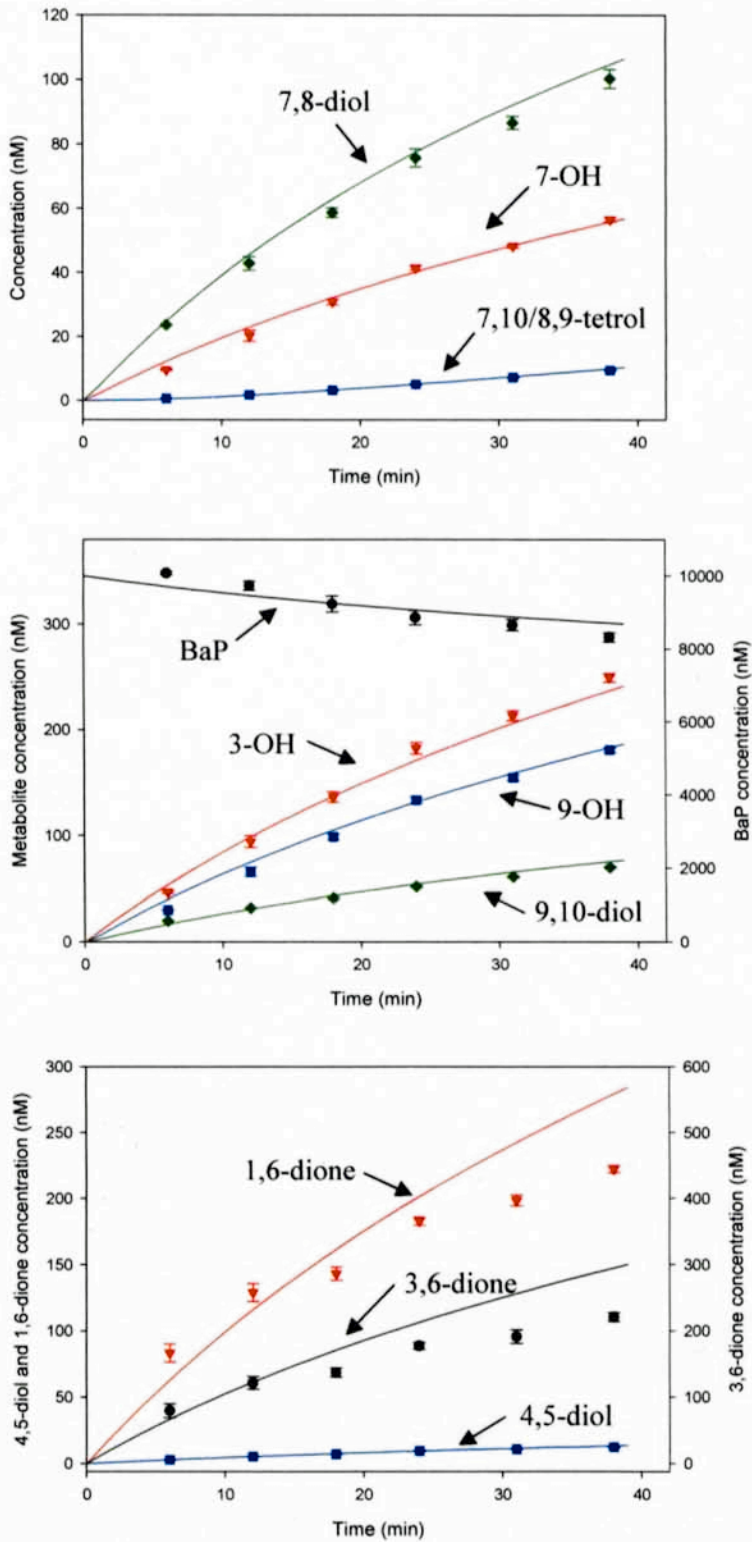


**Figure 7.9.** RN kinetics model simulation of the time course profiles of BaP metabolism (high concentration) using CYP1A1 and EH. Ten  $\mu\text{M}$  BaP was incubated with 9.0 nM CYP1A1, 43 nM EH, and NADPH regenerating system at 37 °C. Solid lines represent model simulations and symbols represent experimental data  $\pm$  standard deviation from four determinations.

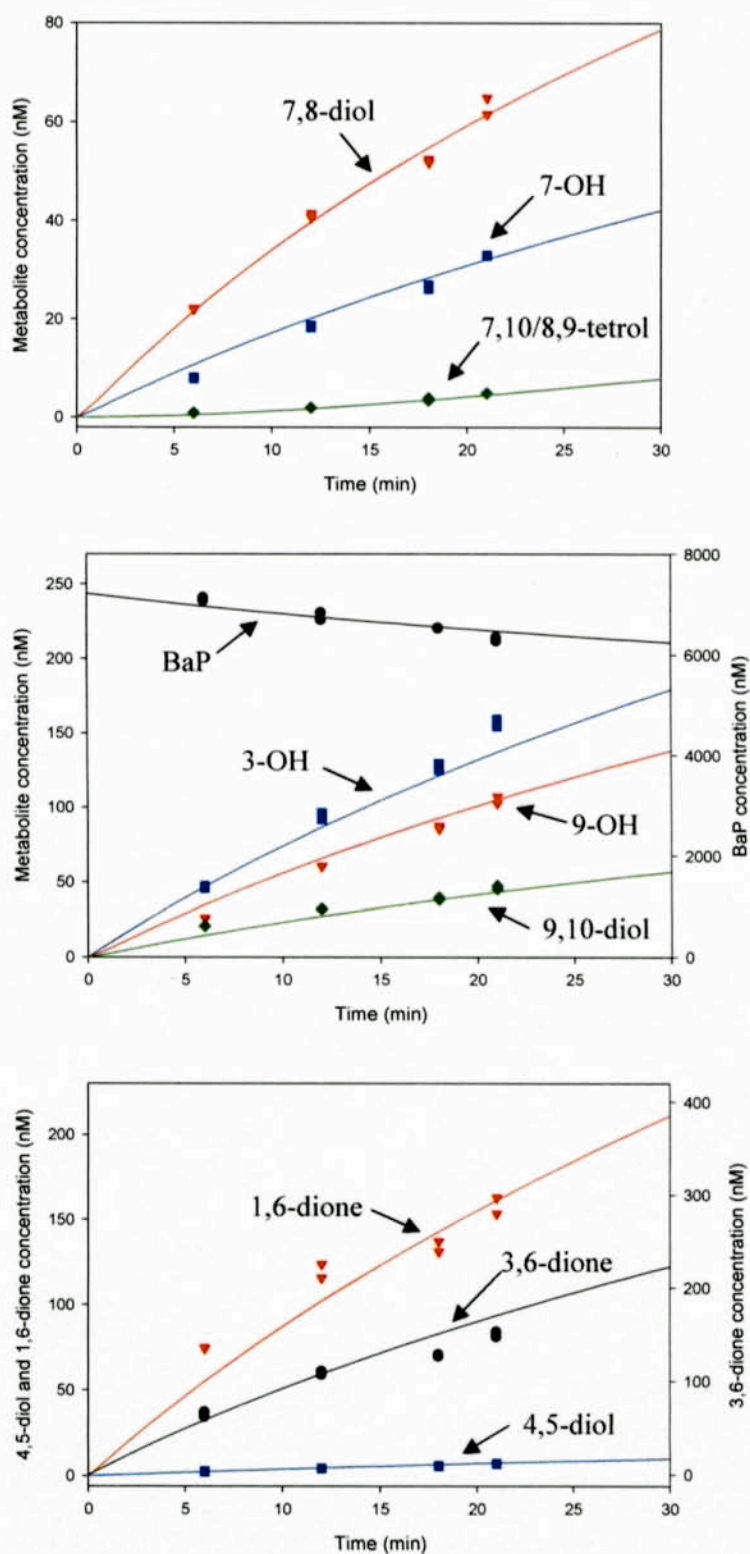


**Figure 7.10.** RN kinetics model predictions of the time course profiles of BaP metabolism (low concentration) using CYP1A1 and EH. BaP (7.2  $\mu\text{M}$ ) was incubated with 9.0 nM CYP1A1, 43 nM EH, and NADPH regenerating system at 37  $^{\circ}\text{C}$ . Solid lines represent model simulations and symbols represent experimental data.

## Chapter 8

### Development and Validation of a Hybrid Reaction Network-Physiologically Based Pharmacokinetic Model of Benzo[*a*]pyrene and Its Metabolites

#### **8.1. Introduction**

A physiologically based pharmacokinetic (PBPK) model describes the processes of absorption, distribution, metabolism, and excretion of chemicals in the body based on physiological characteristics and biochemical kinetics. A major advantage of using a PBPK model over a classical data-based pharmacokinetic model is that due to its biological and mechanistic basis, a PBPK model is suitable for extrapolation of the kinetics of chemicals from animals to humans, from one exposure route to another, and from high dose to low dose (*1*). A PBPK model coupled with a Reaction Network (RN) model, which predicts the detailed metabolic fate of chemicals, can serve as a powerful tool to describe the distribution, interaction, and disposition of parent compounds and their metabolites. Thus, RN/PBPK modeling has the potential of providing a computer simulation platform for the modeling of biological processes from the whole organism down to the molecular interaction level. The RN/PBPK modeling approach will be most useful for chemicals that involve complex metabolic pathways and/or exert their toxicities via biotransformation.

Here we present a hybrid RN/PBPK model for benzo[*a*]pyrene (BaP) in which the possible metabolic reactions were predicted by a RN pathway model (Chapter 4) and the rates of formation of BaP metabolites were predicted by a RN kinetics model. The parameters for the RN kinetics model were estimated using a time-course study of BaP metabolism, similar to the studies described in the Chapter 7, catalyzed by rat liver microsomes. Although recombinant human enzymes were used in the those prior studies, rat enzymes were used here because the pharmacokinetics of BaP have been studied in rats (2-4), but not in human. In addition to rat liver microsomes, recombinant rat cytochrome P450 1A1 (CYP1A1) was used here to compare its catalytic activity toward BaP with the activity for rat liver microsomes, which contain many isozymes of cytochrome P450 (CYP) including CYP1A1. The catalytic activity of rat CYP1A1 was also compared with the activity of human CYP1A1 as determined in Chapter 7. The formation of BaP metabolites in the above time-course studies was monitored using analytical methods described in Chapters 5 and 6.

## **8.2. Methods**

### *8.2.1. Model Structure*

The proposed RN/PBPK model of BaP and its metabolites is shown in Figure 8.1. The basic PBPK model structure is similar to previous published models of styrene (5) and methylene chloride (6, 7). The lung and liver compartments are linked to the Reaction Network model due to their abilities to metabolize BaP. The PBPK model predicts the amount of BaP circulated to these metabolic organs, while the RN kinetics

model calculates the amounts of metabolites formed as well as unmetabolized BaP, which can be distributed to other tissues.

The rate of change of BaP and its metabolites in each compartment shown in Figure 8.1 was described as

$$V_i \frac{dC_{ij}}{dt} = Q_i (CA_j - CV_{ij}) - Metab_{ij} - Elim_{ij} \quad (8-1)$$

where  $V_i$  represent the volume of tissue group  $i$ .  $Q_i$  is the blood flow rate to tissue group  $i$ .  $CA_j$  is the concentration of chemical  $j$  in arterial blood.  $C_{ij}$  and  $CV_{ij}$  are the concentrations of chemical  $j$  in tissue group  $i$  and in the effluent venous blood from tissue group  $i$ , respectively.  $Metab_{ij}$  is the rate of metabolism for chemical  $j$  in tissue group  $i$ .  $Metab_{ij}$  was predicted by RN models in the liver and lung compartments and was set to zero in other tissue groups.  $Elim_{ij}$  represent the rates of biliary excretion from liver ( $KBE_j \cdot VL \cdot CVL_j$ ) and is equal to zero for other tissue groups (Figure 8.1).

It was assumed that chemicals were homogeneously distributed in the tissues.  $CV_{ij}$  is in equilibrium with  $C_{ij}$  with their relationship defined as

$$CV_{ij} = \frac{C_{ij}}{P_{ij}} \quad (8-2)$$

where  $P_{ij}$  is the tissue-blood partition coefficient of chemical  $j$ .

### 8.2.2. Parameters for the PBPK Model

The pharmacokinetic data published by Weyand and Bevan (2) was utilized to calibrate the RN/PBPK model for BaP and its metabolites. In this pharmacokinetic study, male Sprague-Dawley rats were exposed to [ $^3\text{H}$ ]BaP by intratracheal instillation and  $^3\text{H}$  radioactivity was measured for lungs, liver, intestines, intestinal contents, carcass,

kidney, stomach, testes, spleen, heart, urine, and blood at various time points (2). More importantly, the metabolites of BaP were analyzed for tissues isolated from lung and liver and for intestinal contents at various time points (2), which were used to calibrate the RN/PBPK model. Tissues from lung and liver were analyzed because both of them are the sites for BaP metabolism. Intestinal contents were analyzed since most of BaP metabolites are excreted via this route.

Physiological parameters such as tissue volume and blood flow were taken from the literature (8-10). Tissue:blood partition coefficients of BaP and its metabolites were estimated by fitting Weyand and Bevan data (2). Elimination of BaP via metabolism and the formation of metabolites were accounted for using the RN kinetics model and the approach is discussed in the next section.

### *8.2.3. Parameters for the Reaction Network Kinetics Model*

Time course profiles of BaP metabolism were studied using experiments and analytical methods similar to the ones described in the previous chapters. The only modification of the metabolic experiments was the use of rat enzymes instead of human enzymes. Recombinant rat CYP1A1 SUPERSOMES<sup>TM</sup> (769 pmol CYP1A1/mg protein; 7-Ethoxyresorufin-O-deethylase activity: 33 nmol/min/mg protein) was purchased from BD Gentest (Woburn, MA). The CYP1A1 activities of SUPERSOMES<sup>TM</sup> originate from microsomes prepared from insect cells (BTI-TN-5B1-4) which were infected by Baculovirus expressing rat CYP1A1 cDNA. Liver microsomes (450 pmol total CYP/mg protein; 7-Ethoxyresorufin-O-deethylase activity: 0.2 nmol/min/mg protein) from male Sprague-Dawley rats (BD Gentest) were also used to study BaP metabolism. Incubations

contained cytochrome P450 enzymes (8.8 pmol rat CYP1A1 or 0.19 mg rat liver microsomal protein), 1.3 mM NADP<sup>+</sup>, 3.3 mM glucose-6-phosphate, 0.4 U/mL glucose-6-phosphate dehydrogenase, and 3.3 mM magnesium chloride in 50 mM Tris-HCl buffer (pH 7.4 at 37 °C), in a final volume of 1.0 mL. Reaction mixtures were preincubated at 37 °C for 2 min. Reactions were initiated by adding BaP in DMSO to achieve a final reaction mixture concentration of 10 µM of BaP and 1% (v/v) DMSO. Termination of the reactions was achieved at various time points by adding 1 mL acetone containing 1.6 nmol of internal standard (BghiP). The same extraction procedures described in Chapter 7 were used to recover BaP and its metabolites from the reaction mixture. The concentration of BaP and its metabolites were analyzed by high performance liquid chromatography (HPLC) using the methods discussed in Chapters 5 and 6. The concentrations of BaP and its metabolites recovered from the reaction mixtures were directly used for modeling without the correction according to extraction recovery. The recovered concentrations were used here because the pharmacokinetic data reported by Weyand and Bevan (2) were from the concentrations of BaP and its metabolites directly measured from the ethyl acetate extracts of organ homogenates. The metabolites analyzed here were the same as the ones discussed in the previous chapters, *i.e.* 3-hydroxy-BaP (3-OH), 7-hydroxy-BaP (7-OH), 9-hydroxy-BaP (9-OH), BaP-*trans*-4,5-dihydrodiol(±) (4,5-diol), BaP-*trans*-7,8-dihydrodiol(±) (7,8-diol), BaP-*trans*-9,10-dihydrodiol(±) (9,10-diol), BaP-7,8,9,10-tetrol-7,8,9,10-tetrahydro-(7 $\alpha$ ,8 $\beta$ ,9 $\beta$ ,10 $\alpha$ )-(±) (7,10/8,9-tetrol), and BaP-7,8,9,10-tetrol-7,8,9,10-tetrahydro-(7 $\alpha$ ,8 $\beta$ ,9 $\alpha$ ,10 $\beta$ )-(±) (7,9/8,10-tetrol), BaP-1,6-dione (1,6-dione), BaP-3,6-dione (3,6-dione), and BaP-6,12-dione (6,12-dione).

### **8.3. Results and Discussion**

#### *8.3.1. BaP Metabolism Catalyzed by Recombinant Rat Enzymes*

The metabolites detected after incubating BaP with 8.8 nM rat CYP1A1 were 3-OH, 7-OH, 9-OH, 1,6-dione, 3,6-dione, 6,12-dione, 4,5-diol, 7,8-diol, and 9,10-diol. The detection of the BaP-dihydrodiols was unexpected in the absence of epoxide hydrolase (EH), since they are the metabolites of BaP-oxides via hydrolysis catalyzed by EH. The formation of BaP-hydrodiols observed here might be a result of the endogenous EH activities from the insect cells (BTI-TN-5B1-4) where SUPERSOMES<sup>TM</sup> rat CYP1A1 was expressed. BTI-TN-5B1-4 cell line was derived from *Trichoplusia ni*, which contains membrane bound EH activities (11). Recombinant rat EH was not used in this study because it was not commercially available at the time the experiments were conducted.

The time course profiles of BaP metabolism using rat CYP1A1 are shown in Figure 8.2. The concentrations of all metabolites detected increased continuously with reaction time except for that of 6,12-dione. The detected concentrations of 6,12-dione were low and independent of reaction time, which might be a result of the low recovery of 6,12-dione from the reaction mixtures as discussed in Chapter 7. The model simulations described in Figure 8.2 were based on the equations shown in the appendix of Chapter 7. Dissociation constants between metabolites and enzymes were assumed to be equal to the ones used for human enzymes in Chapter 7. Other modeling parameters were estimated by fitting the time course profiles of BaP metabolites using rat CYP1A1. While the endogenous EH concentration in BTI-TN-5B1-4 cells was not measured, EH

concentrations used in the model was set to be one-tenth of the value (4.29 nM) used in Chapter 7.

The activities of rat and human enzymes toward BaP were compared using the rates of metabolite formation per unit of enzyme used (Table 8.1). Compared with recombinant human CYP1A1, recombinant rat CYP1A1 had lower activities toward the formation of hydroxyl-BaPs and higher activities toward the formation of BaP-diones.

### 8.3.2. BaP Metabolism Catalyzed by Rat Liver Microsomes

The time course profiles of BaP metabolism using rat liver microsomes are shown in Figure 8.3. The concentrations of 3-OH, 7-OH, 9-OH, 1,6-dione, 3,6-dione, 4,5-diol, 7,8-diol, and 9,10-diol increased with reaction time. Several unknown peaks in the HPLC chromatograms did not correspond to any of the 11 metabolites analyzed. These unknown compounds might be produced by enzymes other than CYP and EH that are present in rat liver microsomes. The model simulations shown in Figure 8.3 were based on the equations similar to the ones shown in the appendix of Chapter 7. Deactivation of CYP was not considered here because most of the reactive BaP-oxides formed, which might cause deactivation, were likely to undergo glutathione conjugation in addition to hydrolysis and NIH shift. Conjugations of hydroxyl-BaPs, *e.g.* glucuronidation, were considered in the model using pseudo first-order rate equations. The RN kinetics model parameters are shown in Table 8.2. The concentration of total CYP (87 nM) was calculated using data provided from product information sheets. The concentration of EH in microsomes (653 nM) were estimated using published data that rat liver microsomes contained 165  $\mu\text{g}$  EH/mg protein (12) and the molecular weight of rat EH

was 49000 (13). The dissociation constants between enzymes and substrates were set to be equal to the values used for human enzymes in Chapter 7. BaP concentrations simulated by the RN kinetics model were originally higher than the experiment data (*i.e.*, the consumption rate was lower than predicted). The underestimated BaP consumption might be a result of the unknown metabolites that were not analyzed in this study, or caused by not considering extraction recoveries of BaP metabolites from the reaction mixtures. These unknown metabolites might be formed via reactions catalyzed the enzymes other than CYP and EH in rat liver microsomes. To overcome this problem, an extra oxidation reaction of BaP catalyzed by CYP was used to account for the formation unknown metabolites. The rate constant of this reaction,  $k_{un}$ , was estimated by fitting the time course change of BaP concentrations.

The metabolite formation using recombinant rat CYP1A1 was also compared with the result using rat liver microsomes (Table 8.1). For every mole of CYP used, rat CYP1A1 resulted in the formation of more moles of hydroxyl-BaPs and BaP-diones than did rat liver microsomes, which containing a mixture of several CYP isozymes. When compared on the basis of rates (nM metabolites formed per min), rates of metabolite formation using rat liver microsomes were higher than the rates using rat CYP1A1. Although the total CYP content is higher in rat microsomes (87 nM) than in rat CYP1A1 (8.8 nM), the CYP1A1 activity in microsomes was only one-tenth of the activity in recombinant rat CYP1A1 using 7-ethoxyresorufin as the substrate. These results suggest that CYP isozymes other than CYP1A1 can also catalyze the metabolism of BaP, although CYP1A1 has higher a specific activity for BaP than other isozymes (14, 15).

### 8.3.3. PBPK Model parameters and Model Simulations

Physiological parameters used in the RN/PBPK model of BaP and its metabolites were taken from literature (8-10) and are listed in Table 8.3. BaP metabolism in liver and lung was described by the RN kinetics model using the parameters estimated using rat liver microsomes (Table 8.2). The concentration of total CYP in liver was estimated by fitting the time course of BaP in venous blood (Figure 8.4) from Weyand and Bevan (2). The estimated value was 12 nmol CYP/g liver. It was previously reported that rat liver slices contained 0.136 nmol CYP/mg protein (16). This value is equivalent to 27.2 nmol CYP/g liver based on the estimated liver protein content of 200 mg protein /g liver (16). The value of CYP concentration used in the model was thus a reasonable estimate, considering that CYP enzymes are not evenly distributed in the liver and that the CYP concentration measured from liver slices might not represent the whole liver. The CYP concentration in lung was set to 0.039% of the one in liver, based on  $V_{max}$  values of BaP for whole organs reported by Wiersma and Roth (17). The ratio of EH to CYP concentrations estimated in the rat liver microsomes study (EH=653 nM; CYP=87 nM) was used to calculate EH concentrations in liver and lung based on their corresponding CYP concentrations.

Tissue-blood partition coefficients for BaP and its metabolites have not previously been measured. Therefore, the values for tissue-blood partition coefficients and biliary excretion rate constants for BaP (Table 8.4) were estimated by fitting the model to experimental data reported by Weyand and Bevan (2). The model simulation of the time course of BaP in venous blood (Figure 8.4) was most sensitive to the CYP concentration and the fat-blood partition coefficient for BaP. Fat was expected to be one of the major

repository for BaP since BaP is very lipophilic with log octanol-water partition coefficient equal to 5.98 (18). BaP was rapidly eliminated from lung and blood due to metabolism after administration. This was followed by a log linear phase in which the removal of BaP from blood was limited by the slow release of BaP from fat tissue. Liver-blood and lung-blood partition coefficients for BaP were estimated by fitting BaP concentrations in liver and lung (Figure 8.4), respectively. The simulations of BaP concentrations in intestinal contents were achieved by adjusting the biliary excretion rate constant ( $KBE_{BaP}$ ) of BaP (Figure 8.4).

The tissue-blood partition coefficients for BaP metabolites (Table 8.4) were estimated by fitting the time course of metabolites in liver, lung, and intestinal contents (Figures 8.5 to 8.7) measured by Weyand and Bevan (2). Biliary excretion rate constants for the metabolites were estimated by fitting BaP concentrations intestinal contents (Figure 8.6). Metabolite concentrations in liver and intestinal increased rapidly in the first hour, accompanied by the fast decline in BaP concentration. BaP was converted to metabolites that are more hydrophilic than BaP and can be eliminated through fecal excretions. The concentrations of all metabolites found in the intestinal contents were at least ten times those found in the liver six hours after BaP was administrated. On the other hand, only small levels of BaP were detected in the intestinal contents. The concentrations of 9-OH were underestimated by the model in both liver and intestinal contents unless the rate constant for the rearrangement (NIH Shift) of 9,10-oxide to 9-OH ( $k_{9nih}$ ) was increased to four times the value shown in Table 8.3. This indicates that the EH concentrations in liver and lung might be overestimated, since that would lead to the predominance of hydrolysis over rearrangement for 9,10-oxide. The model simulation

did not match well with measured metabolite concentrations in lung (Figure 8.7) at the first time point (5 min). This might indicate that the CYP concentration in lung was underestimated. Another reason for the mismatch stems from the fact that BaP was dissolved in triethylene glycol and injected to the bronchial bifurcation through the tracheal cannula in the study reported by Weyand and Bevan (2). The amount of BaP that was absorbed and available for metabolism might not be accurately estimated by the model at the early time points. As a result, the metabolite concentrations simulated by the RN/PBPK model did not match well with the experiment results initially. However, subsequent data points were well fit by the model.

#### 8.3.4. Model Validation

There are very few pharmacokinetic studies available for the validation of the RN/PBPK model for BaP, and studies involving BaP metabolites are even more limited. Data sets reported by Wiersma and Roth (4) and Schlede *et al.* (3) were used to validate the RN/PBPK model prediction of BaP, while the RN/PBPK model predictions of the metabolites were not validated at current time.

After the model parameters were estimated, the RN/PBPK model was validated using data reported by Wiersma and Roth (4). In that study, male Sprague-Dawley rats were injected with 117 nmol/kg body weight (29.5 µg/kg) of BaP intraarterially. BaP concentrations in arterial blood were analyzed at various time points. Using the same set of model parameters determined above, the time course of BaP in arterial blood was nicely predicted by the RN/PBPK model (Figure 8.8). Since this experiment was performed using a different route of administration and the dose is 29.5 times higher than

that used by Weyand and Bevan (2), the quality of the RN/PBPK model prediction demonstrates its ability to extrapolate from one dosing route to another and from low dose to high dose.

The model was further validated using data reported by Schlede *et al.* (3). In this study, ten µg (55.6 µg/kg) of BaP was administered to female Sprague-Dawley rats intravenously. BaP concentrations in blood, liver, fat, and brain were analyzed at various time points up to 6 h. BaP concentrations in blood predicted by the RN/PBPK model were generally in agreement with the experimental data (Figure 8.9). The model overestimated the BaP concentrations in the liver (Figure 8.9). The overestimation of BaP concentration might be caused by the sex difference in the metabolic capacities. The two studies described above were performed in male rats, while female rats were used by Schlede *et al.* (3). Furthermore, the younger rats (175-185 g) used by Schlede *et al.* (3) might have had larger relative liver weights compared with older rats (9). The underestimated liver size would be expected to cause the overestimation of BaP concentrations in liver (pmol/kg liver). The model predicted that BaP concentrations in fat would decrease after the first hour, while the data from Schlede *et al.* (3) showed a constant level of BaP during the same period of time (Figure 8.9). One explanation for this difference is that the diffusion of BaP from fat tissue to its effluent venous blood might be slow with respect to blood flow rate. To account for this, the fat compartment could be treated as diffusion-limited.

BaP metabolism in the lung and liver was accounted for using the RN kinetics model for BaP, in which the kinetics parameters were estimated using *in vitro* experiments with rat liver microsomes. The extrapolation of kinetics parameters from *in*

*vitro* to *in vivo* conditions was based on the assumptions that all metabolisms were catalyzed by membrane-bound enzymes and the preparation of microsomes did not change the properties of these enzymes. The RN/PBPK model for BaP fitted the experimental data well without any adjustments according the extrapolation from *in vitro* to *in vivo* conditions. However, in a previously reported PBPK model (19) for butadiene and butadiene monoxide (BMO), it was found that EH affinity to BMO measured *in vitro* (BMO was directly added to the incubation) was lower than the affinity observed *in vivo* (BMO was formed via the epoxidation of butadiene catalyzed by CYP). The difference in enzyme affinities for *in vitro* and *in vivo* conditions was assumed to be caused by the difference in the distances for BMO to diffuse to EH for these two conditions (19).

One difficulty in developing this RN/PBPK model is that tissue-blood partition coefficients of BaP and its metabolites have not been measured previously, which would be a problem for any PBPK model that includes metabolites. The values of partition coefficient estimated here need to be validated by incubating minced tissues with BaP and its metabolites in buffer solution. Semi-empirical methods for the estimation of the partition coefficients for non-volatile chemicals have also been reported (20). Poulin and Theil (20) recently described the correlation between tissue-blood partition coefficient and the combination of log vegetable oil: water partition coefficients and unbound fractions of chemicals in plasma. These approaches can be incorporated into the updated RN/PBPK model.

A fully validated RN/PBPK model can not only predict the biotransformation of xenobiotics, but also simulate the distribution and elimination of the metabolites outside of the metabolism organs. Some metabolites might cause adverse effects to tissues other

than the sites of the metabolism. The formation of metabolites that are potentially harmful to tissues can be predicted under different exposure scenarios and doses, and extrapolated from animals to humans.

#### **8.4. References**

1. Krishnan K, Andersen ME. Physiologically based pharmacokinetic modeling in toxicology. In: Principles and Methods of Toxicology (Hayes AW, ed). New York:Raven Press, 1994.
2. Weyand EH, Bevan DR. Benzo(a)pyrene disposition and metabolism in rats following intratracheal instillation. *Cancer Res* 46:5655-5661(1986).
3. Schlede E, Kuntzman R, Haber S, Conney AH. Effect of enzyme induction on the metabolism and tissue distribution of benzo( $\alpha$ )pyrene. *Cancer Res* 30:2893-2897(1970).
4. Wiersma DA, Roth RA. Total body clearance of circulating benzo(a)pyrene in conscious rats: effect of pretreatment with 3-methylcholanthrene and the role of liver and lung. *J Pharmacol Exp Ther* 226:661-667(1983).
5. Ramsey JC, Andersen ME. A physiologically based description of the inhalation pharmacokinetics of styrene in rats and humans. *Toxicol Appl Pharmacol* 73:159-175(1984).
6. Andersen ME, Clewell HJ, III, Gargas ML, Smith FA, Reitz RH. Physiologically based pharmacokinetics and the risk assessment process for methylene chloride. *Toxicol Appl Pharmacol* 87:185-205(1987).
7. Clewell III HJ. The use of physiologically based pharmacokinetic modeling in risk assessment: A case study with methylene chloride. In: *Low-Dose Extrapolation of Cancer Risks : Issues and Perspectives* (Olin S, Farland C, Park C, Rhomberg L, Scheuplein R, Starr T, Wilson J, eds). Washington, D.C.:ILSI Press, 1995.
8. Brown RP, Delp MD, Lindstedt SL, Rhomberg LR, Beliles RP. Physiological parameter values for physiologically based pharmacokinetic models. *Toxicol Ind Health* 13:407-484(1997).
9. Schoeffner DJ, Warren DA, Muralidara S, Bruckner JV, Simmons JE. Organ weights and fat volume in rats as a function of strain and age. *J Toxicol Environ Health A* 56:449-62(1999).
10. Delp MD, Manning RO, Bruckner JV, Armstrong RB. Distribution of cardiac output during diurnal changes of activity in rats. *Am J Physiol* 261:H1487-93(1991).
11. Roe RM, Kallapur V, Linderman RJ, Viviani F, Harris SV, Walker EA, Thompson DM. Mechanism of action and cloning of epoxide hydrolase from the cabbage looper, *Trichoplusia ni*. *Arch Insect Biochem Physiol* 32:527-535(1996).

12. de Waziers I, Cugnenc PH, Yang CS, Leroux JP, Beaune PH. Cytochrome P 450 isoenzymes, epoxide hydrolase and glutathione transferases in rat and human hepatic and extrahepatic tissues. *J Pharmacol Exp Ther* 253:387-394(1990).
13. Bentley P, Oesch F, Tsugita A. Properties and amino acid composition of pure epoxide hydratase. *FEBS Letters* 59:296-299(1975).
14. Gautier JC, Lecoœur S, Cosme J, Perret A, Urban P, Beaune P, Pompon D. Contribution of human cytochrome P450 to benzo[a]pyrene and benzo[a]pyrene-7,8-dihydrodiol metabolism, as predicted from heterologous expression in yeast. *Pharmacogenetics* 6:489-499(1996).
15. Kim JH, Stansbury KH, Walker NJ, Trush MA, Strickland PT, Sutter TR. Metabolism of benzo[a]pyrene and benzo[a]pyrene-7,8-diol by human cytochrome P450 1B1. [erratum appears in *Carcinogenesis* 1999 Mar;20(3):515]. *Carcinogenesis* 19:1847-1853(1998).
16. Price RJ, Ball SE, Renwick AB, Barton PT, Beamand JA, Lake BG. Use of precision-cut rat liver slices for studies of xenobiotic metabolism and toxicity: comparison of the Krumdieck and Brendel tissue slicers. *Xenobiotica* 28:361-71(1998).
17. Wiersma DA, Roth RA. The prediction of benzo[a]pyrene clearance by rat liver and lung from enzyme kinetic data. *Molecular Pharmacology* 24:300-308(1983).
18. Miller MM, Wasik SP, Huang GL, Shiu WY, Mackay D. Relationships between octanol water partition-coefficient and aqueous solubility. *Environ Sci Technol* 19:522-529(1985).
19. Johanson G, Filser JG. A physiologically based pharmacokinetic model for butadiene and its metabolite butadiene monoxide in rat and mouse and its significance for risk extrapolation. *Arch Toxicol* 67:151-63(1993).
20. Poulin P, Theil FP. A priori prediction of tissue:plasma partition coefficients of drugs to facilitate the use of physiologically-based pharmacokinetic models in drug discovery. *J Pharm Sci* 89:16-35(2000).

**Table 8.1.** Formation of BaP metabolites catalyzed by human and rat enzymes<sup>a</sup>

Enzymes	Formation Rate of BaP metabolites <sup>b</sup>							
	3-OH	7-OH	7,8-diol	9-OH	9,10-diol	4,5-diol	1,6-dione	3,6-dione
Human CYP1A1 <sup>c</sup>	0.516 (4.64)	0.490 (4.41)	-	0.784 (7.06)	-	-	0.314 (2.82)	0.379 (3.41)
Rat CYP1A1 <sup>d</sup>	0.428 (3.77)	0.149 (1.32)	0.025 (0.219)	0.326 (2.87)	0.029 (0.255)	0.249 (2.20)	0.499 (4.402)	0.441 (3.89)
Rat liver microsomes <sup>e</sup>	0.307 (26.80)	0.022 (1.91)	0.035 (3.03)	0.169 (14.75)	0.080 (6.95)	0.034 (3.00)	0.100 (8.71)	0.180 (15.74)

<sup>a</sup>BaP (10  $\mu$ M) was incubated at 37°C in 50 mM Tris-HCl buffer (pH 7.4) for 12 min with enzymes.

<sup>b</sup>The results are expressed in the unit of (pmol metabolites formed)/(min)/(pmol CYP). The numbers enclosed in the parentheses are the rate in nM metabolites formed per min. All results were calculated based on the concentrations recovered from the reaction mixture without correction according to extraction recovery data.

<sup>c</sup>9.0 nM human CYP1A1 (0.085 mg protein/mL)

<sup>d</sup>8.8 nM rat CYP1A1 (0.011 mg protein/mL)

<sup>e</sup>87 nM rat total CYP (0.194 mg protein/mL)

**Table 8.2.** Model parameters for the Reaction Network kinetic model of BaP metabolism using rat liver microsomes

Model Parameter	Symbol	Value
<i>Rate constants for CYP1A1-catalyzed reactions (nM product / min / nM CYP1A1)</i>		
BaP->2,3-oxide	k23ox	0.7
BaP->7,8-oxide	k78ox	0.13
BaP->9,10-oxide	k910ox	0.55
BaP->4,5-oxide	k45ox	0.063
BaP->6-OH	k6ox	0.52
BaP->unknown metabolites	kun	1.6
<i>Rate constants for mEH-catalyzed reactions (nM product / min / nM mEH)</i>		
7,8-oxide->7,8-diol	k78hydro	1.4
9,10-oxide->9,10-diol	k910hydro	0.8
4,5-oxide->4,5-diol	k45hydro	2.3
<i>Dissociation constants between substrates and enzymes (nM)</i>		
BaP and CYP1A1	KcypBaP	6600
7,8-diol and CYP1A1	Kcyp78diol	6600
9,10-diol and CYP1A1	Kcyp910diol	6600
7,8-oxide and mEH	Keh78ox	1700
9,10-oxide and mEH	Keh910ox	1700
4,5-oxide and mEH	Keh45ox	1700
<i>Rate constants for spontaneous reactions (min<sup>-1</sup>)</i>		
2,3-oxide->3-OH	k3nih	1000
7,8-oxide->7-OH	k7nih	0.3
9,10-oxide->9-OH	k9nih	0.5
6-OH-BaP->BaP-1,6-diol	k16ox	37
6-OH-BaP->BaP-3,6-diol	k36ox	72
6-OH-BaP->BaP-6,12-diol	k612ox	5
1,6-HQ->1,6-dione	k16auto	100
3,6-HQ->3,6-dione	k36auto	100
6,12-HQ->6,12-dione	k612auto	100
<i>Rate constants for the conjugation reactions of hydroxyl-BaPs (min<sup>-1</sup>)</i>		
3-OH	k3conj	0.045
7-OH	k7conj	0.019
9-OH	k9conj	0.013

**Table 8.3.** Physiological parameters for PBPK model of BaP

Model Parameter	Symbol	Value
Body weight (kg)	BW	0.250
Cardiac output (L/h/kg <sup>0.75</sup> )	QCC	15.6 <sup>a</sup>
<i>Blood flow (fraction of cardiac output)</i>		
Liver	QLC	0.024 <sup>b</sup>
GI tract	QGC	0.14 <sup>b</sup>
Fat	QFC	0.07 <sup>b</sup>
Slowly perfused tissues	QSC	0.24
Rapidly perfused tissues	QRC	0.515
<i>Tissue volumn<sup>d</sup> (fraction of body weight)</i>		
Liver	VLC	0.0386 <sup>c</sup>
Fat	VFC	0.0648 <sup>c</sup>
Lung	VLUC	0.0043 <sup>c</sup>
Slowly perfused tissues	VSC	0.75
Rapidly perfused tissues	VRC	0.05

<sup>a</sup>Taken from Delp *et al.*, 1991 (10).

<sup>b</sup>Taken from Brown *et al.*, 1997 (8).

<sup>c</sup>Taken from Schoeffner *et al.*, 1999 (9).

<sup>d</sup>Assuming the specific gravity of all tissues are equal to 1.

**Table 8.4.** Tissue-blood partition coefficients and biliary excretion rate constants for BaP and its metabolites used in RN/PBPK model<sup>a</sup>

	BaP	3-OH	7,8-diol	9-OH	9,10-diol	4,5-diol	1,6-dione	3,6-dione
Liver (PL <sub>j</sub> )	66	0.5	2.7	20	1.9	14	4.2	2.4
Fat (PF <sub>j</sub> )	25	70	70	40	100	30	50	60
Lung (PL <sub>j</sub> )	175	8.0	42	200	15	100	40	40
Richly and Slowly perfused (PR <sub>j</sub> and PS <sub>j</sub> )	0.7	1.0	1.0	1.0	1.0	1.0	1.0	1.0
Biliary excret. (KBE <sub>j</sub> ) <sup>b</sup>	1.1	0.84	6.6	20	2.0	30	5.5	3.0

<sup>a</sup>All parameters shown in this table were estimated by fitting the model to experimental data reported by Weyand and Bevan (2).

<sup>b</sup>1/h.

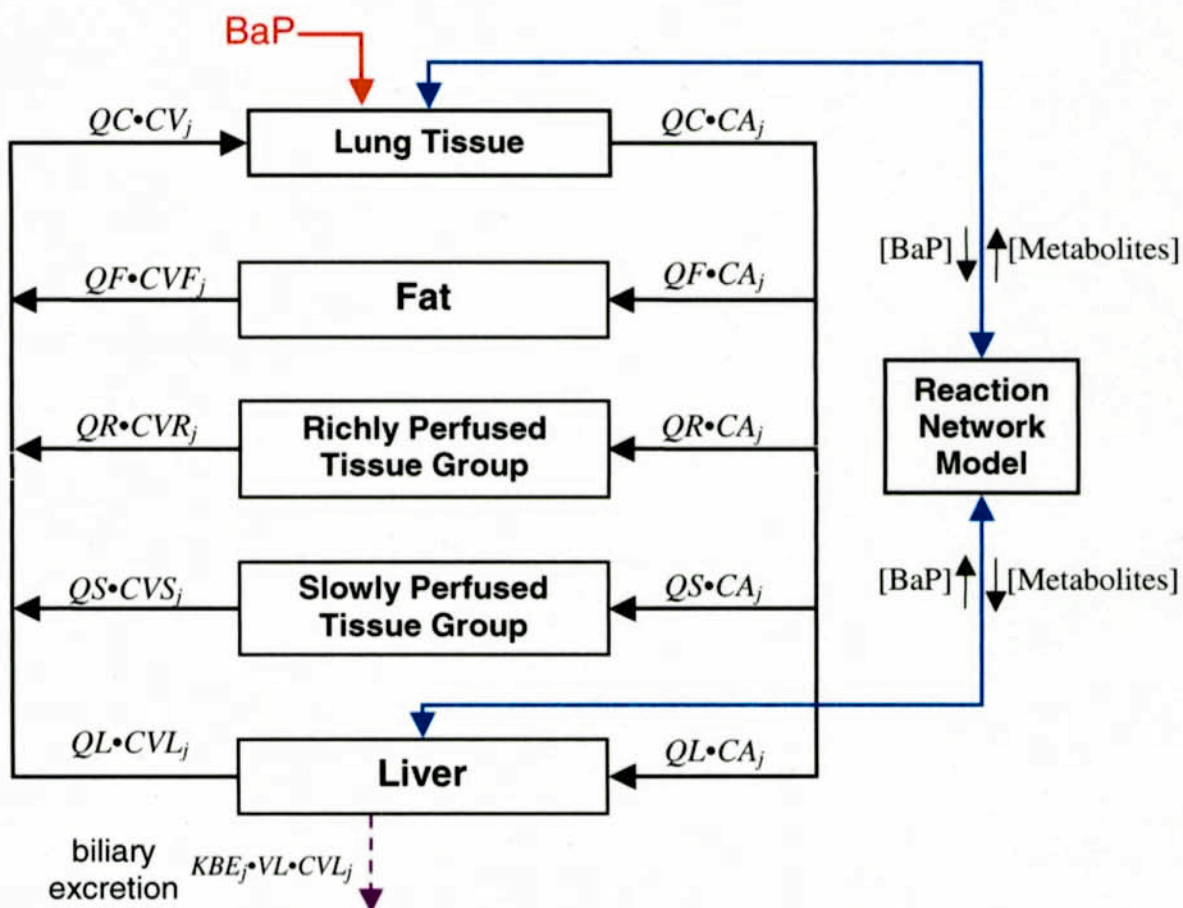


**Figure 8.1.** RN/PBPK model structure for of BaP and its metabolites. Symbols starting with Q and C represent blood flow rate and concentrations, respectively, used for Equation 8-1.

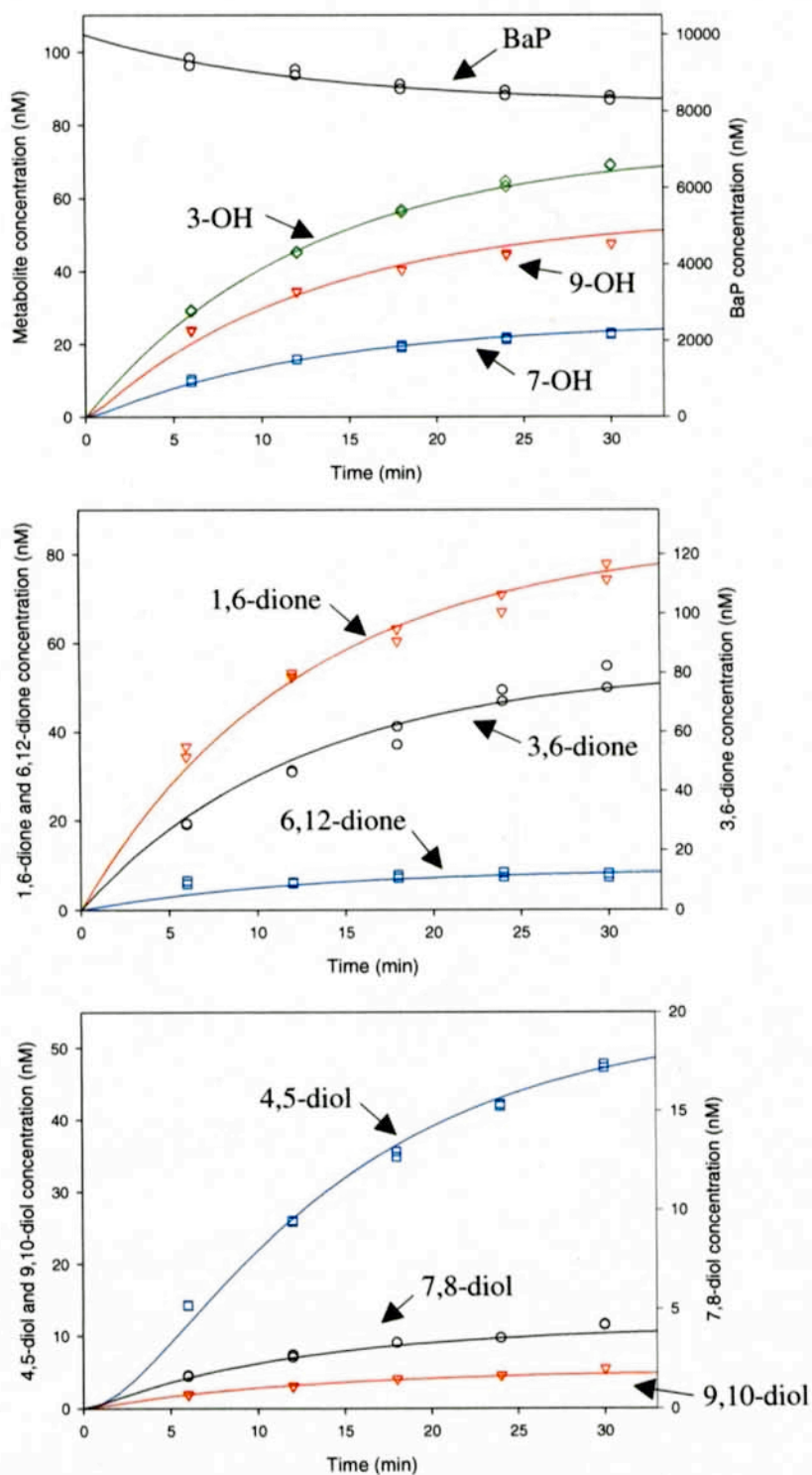


**Figure 8.2.** RN kinetics model simulation of the time course profiles of BaP metabolism using recombinant rat CYP1A1. Ten  $\mu\text{M}$  BaP was incubated with 8.8 nM CYP1A1 and NADPH regenerating system at 37 °C. Solid lines represent model simulations and symbols represent experimental data.

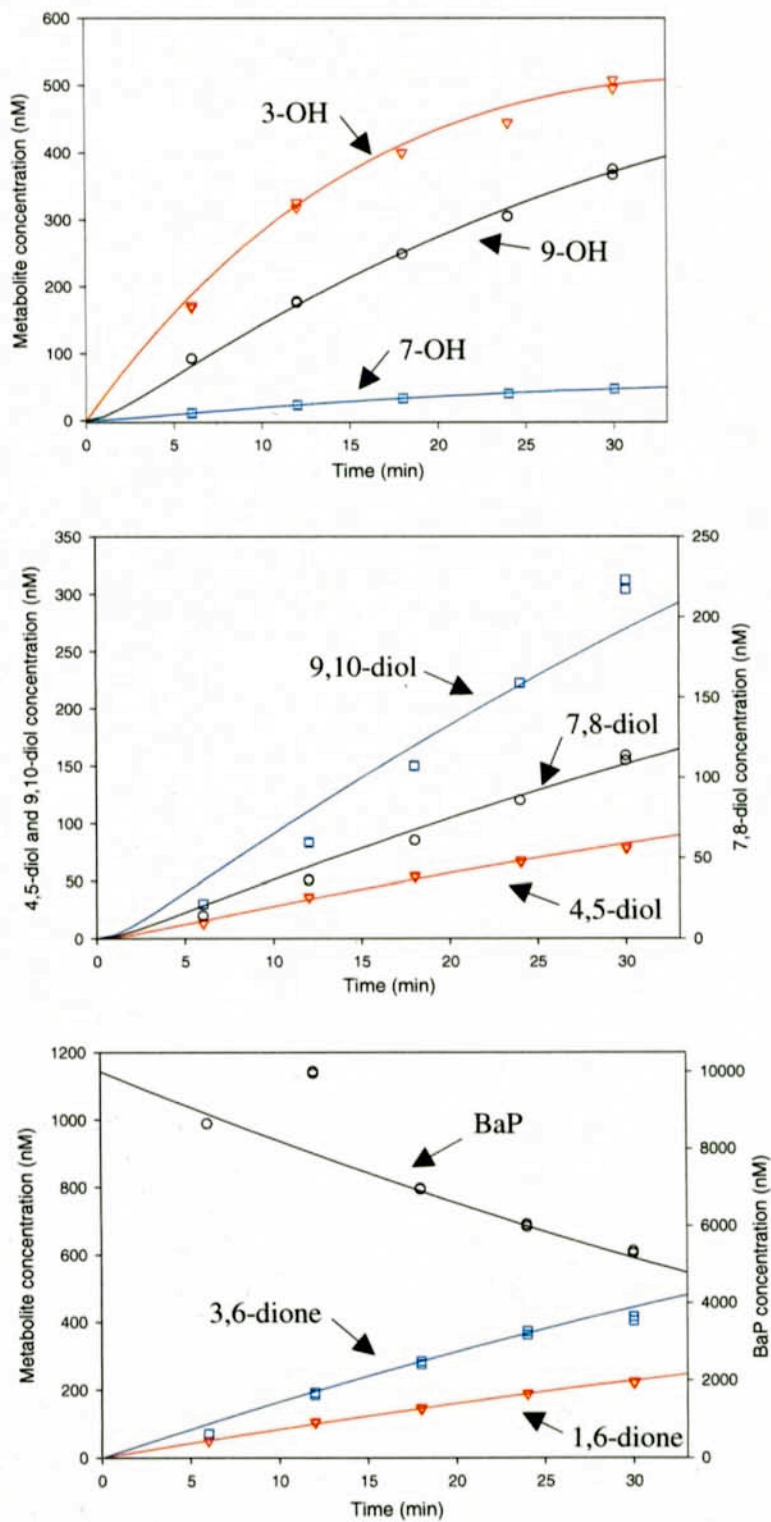


**Figure 8.3.** RN kinetics model simulation of the time course profiles of BaP metabolism using rat liver microsomes. Ten  $\mu\text{M}$  BaP was incubated with 0.194 mg protein/mL and NADPH regenerating system at 37 °C. Solid lines represent model simulations and symbols represent experimental data.

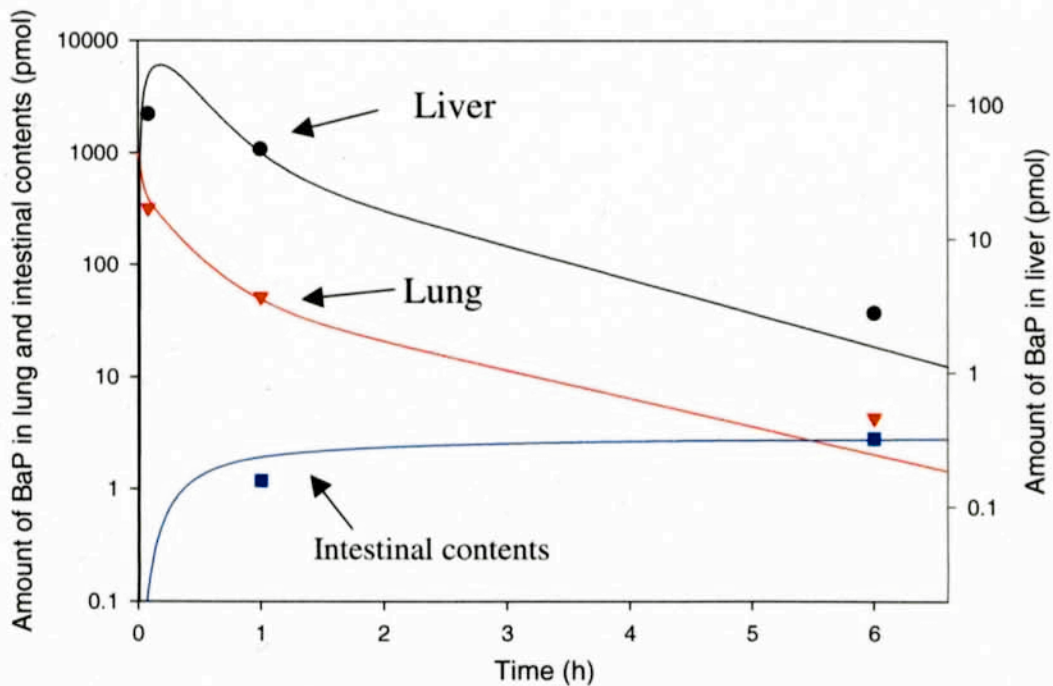
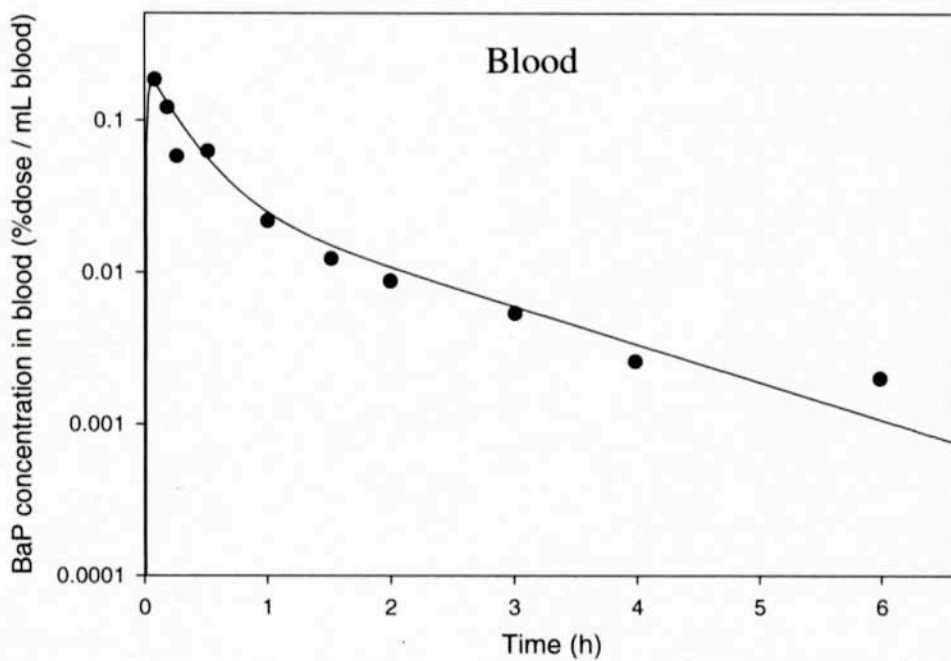


**Figure 8.4.** BaP concentrations in the venous blood, liver, lung, and intestinal contents of rats after exposure to BaP intratracheally at 1  $\mu\text{g}/\text{kg}$  body weight. Symbols represent experimental data from Weyand and Bevan (2). Solid lines represent RN/PBPK model simulations.

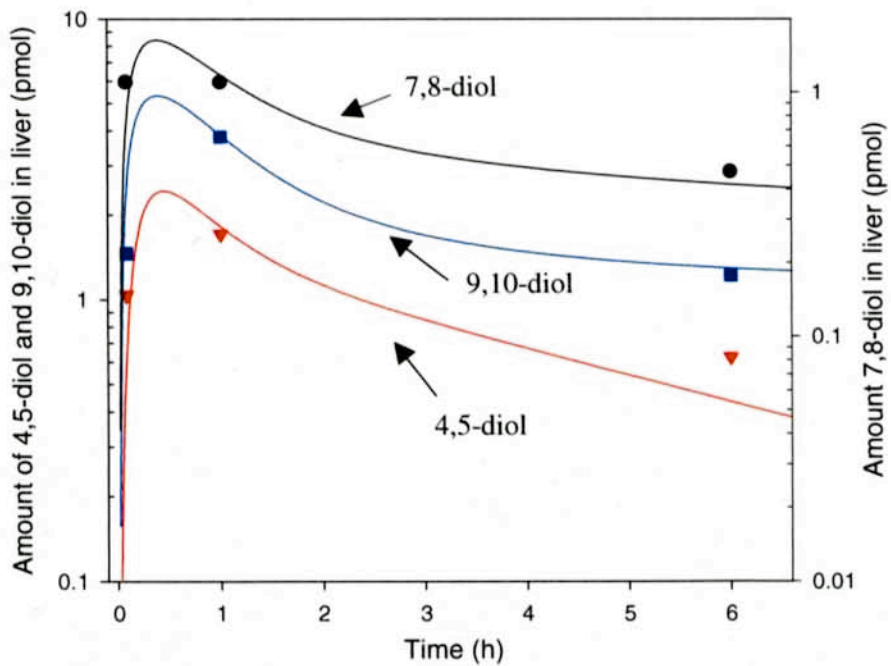
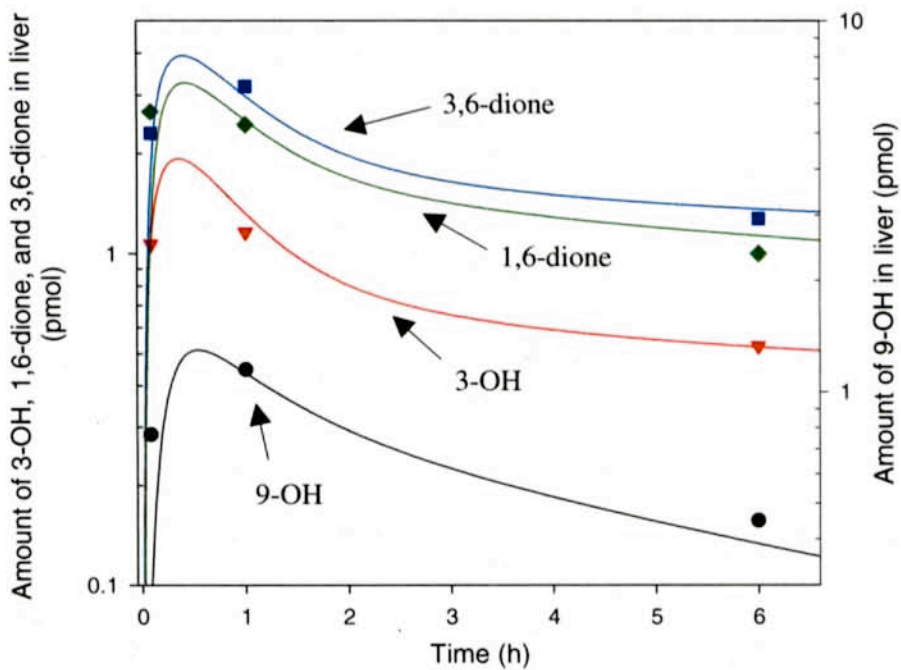


**Figure 8.5.** Amounts of BaP metabolites in liver of rats after exposure to BaP intratracheally at 1  $\mu\text{g}/\text{kg}$  body weight. Symbols represent experimental data from Weyand and Bevan (2). Solid lines represent RN/PBPK model simulations.

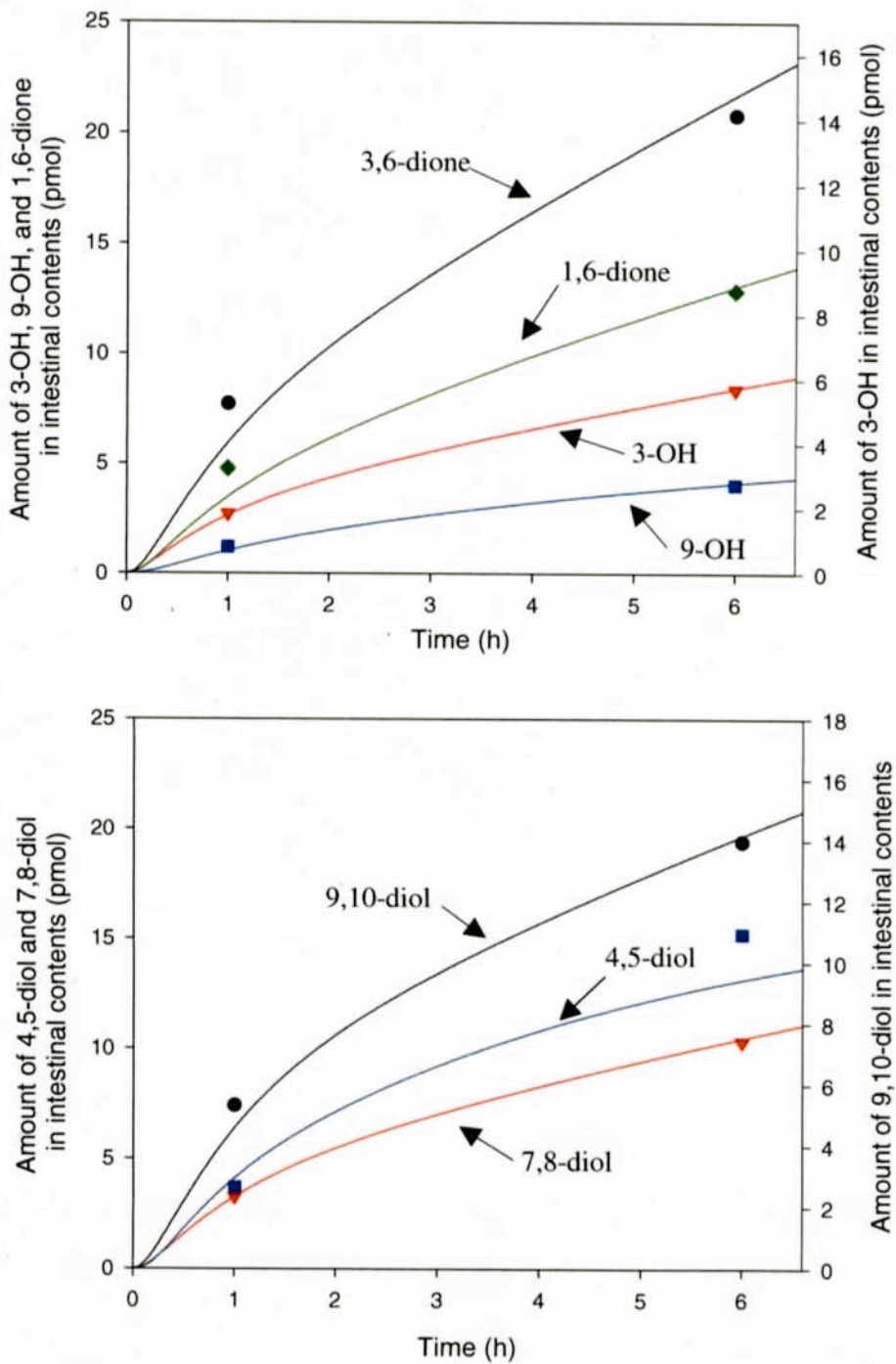


**Figure 8.6.** Amounts of BaP metabolites in intestinal contents of rats after exposure to BaP intratracheally at 1  $\mu\text{g}/\text{kg}$  body weight. Symbols represent experimental data from Weyand and Bevan (2). Solid lines represent RN/PBPK model simulations.

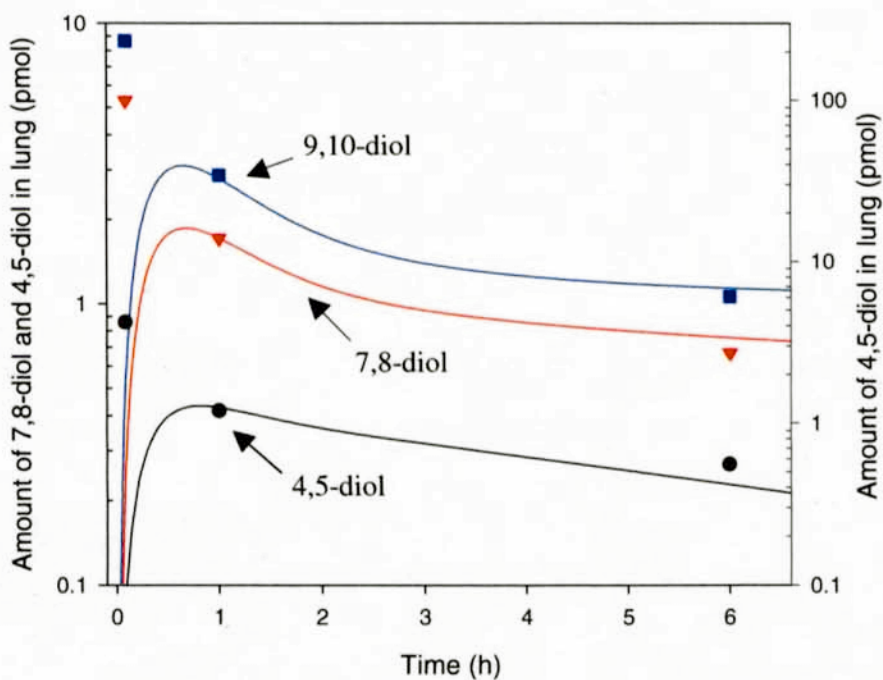
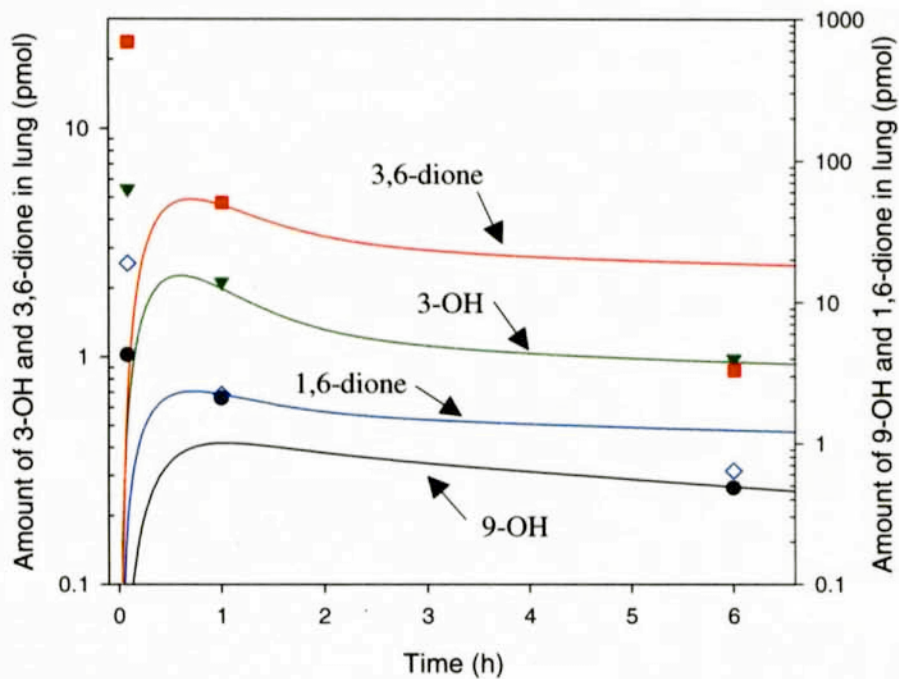


**Figure 8.7.** Amounts of BaP metabolites in lung of rats after exposure to BaP intratracheally at 1  $\mu\text{g}/\text{kg}$  body weight. Symbols represent experimental data from Weyand and Bevan (2). Solid lines represent RN/PBPK model simulations.

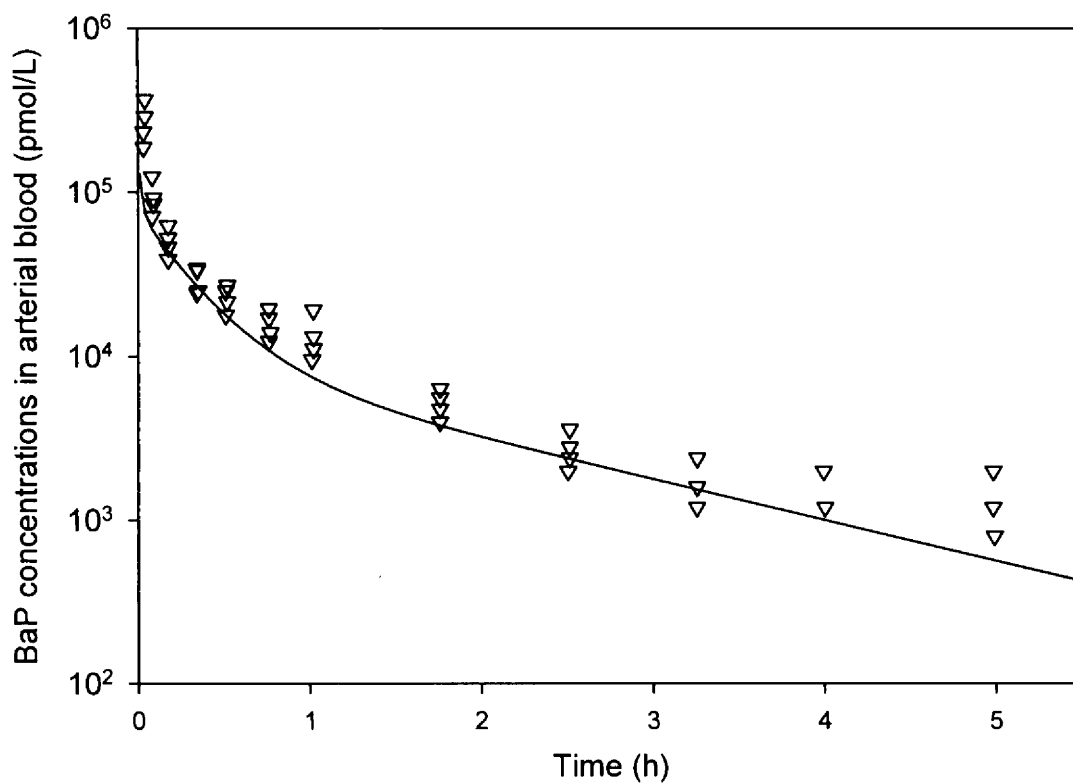


**Figure 8.8.** BaP concentrations in the arterial blood of rats after exposure to BaP intraarterially at 117 nmol/kg body weight. Symbols represent experimental data from Wiersma and Roth (4). Solid lines the model predictions using RN/PBPK model of BaP.

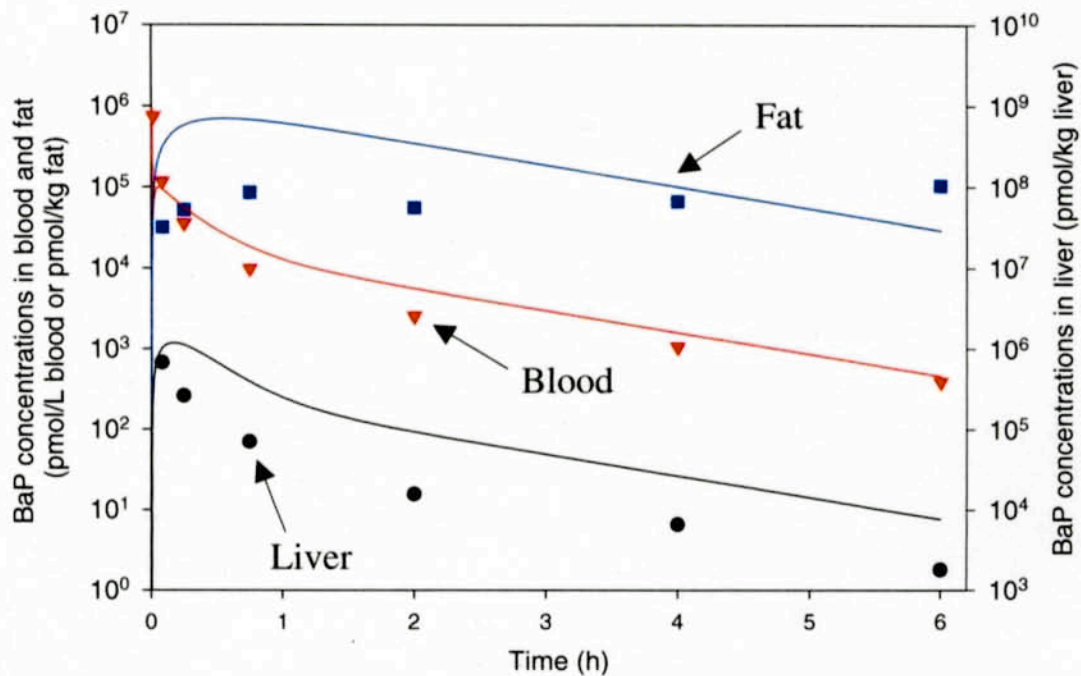


**Figure 8.9.** BaP concentrations in venous blood, liver, and fat of rats after exposure to 10  $\mu\text{g}$  of BaP intravenously. Symbols represent experimental data from Schlede *et al.* (3). Solid lines are the model predictions using RN/PBPK model of BaP.

## Chapter 9

### Conclusions and Future Perspectives

#### **9.1. Conclusions**

Progress toward our ultimate goal of predicting the biotransformation reactions and kinetics for chemical and chemical mixtures in mammalian systems was initiated by the development of the Reaction Network (RN) pathway and kinetics models for benzo[*a*]pyrene (BaP) metabolism. The RN pathway model predicted the possible reactions encountered by BaP in the presence of mammalian cytochrome P450 (CYP) and epoxide hydrolase (EH). The RN pathway model predictions were achieved by using matrices to represent the chemical structures of reactants and the structural changes caused by chemical reactions at the level of atomic connectivity. The RN pathway model for BaP can be readily applied to predict the biotransformation of many other polycyclic aromatic hydrocarbons (PAHs), which undergo the same types of reactions catalyzed by CYP and EH due to their structural similarity. When the RN pathway modeling approach is applied to chemicals other than PAHs, it is necessary to account for the biotransformation reactions pertinent to these chemicals, and will be discussed in the next section. Since a RN pathway model predicts all the possible metabolites associated with the biotransformation of the chemical of interest, the model predictions may include toxic metabolites that have never been studied before. These potential toxic metabolites

predicted by the RN pathway model could contribute to the future discovery of unknown modes of action for many toxic chemicals, although the presence of these metabolites needs to be confirmed using proper analytical methods.

The RN kinetics model for BaP metabolism was calibrated and validated using experimental data. Although the calibration of the current model appears to require a large set of experimental data, a longterm goal is to establish Quantitative Structure/Reactivity Correlations (QSRCs) to predict the rates of biotransformation reactions using structural properties pertinent to the chemicals and/or the enzymes, based on validated RN kinetics models like the one developed here for BaP. QSRCs for the RN kinetics models in petroleum refinery processes were developed based on a large kinetics database (1-3) and proven to be able to predict reaction rates with minimal numbers of experiments. The development of QSRCs for the RN kinetics model for the biotransformation of BaP, and other chemicals, require additional kinetics data obtained from the enzymatic experiments similar to those presented in Chapter 7. Furthermore, QSRCs for biotransformation reactions may rely on the knowledge of the three-dimensional structure of the enzyme active sites, which is not currently available for human CYP enzymes.

The hybrid Reaction Network/physiologically based pharmacokinetics (RN/PBPK) model for BaP and its metabolites were calibrated using *in vitro* experimental data generated in this laboratory and the pharmacokinetics data of BaP in rats reported by Weyand and Bevan (4). The RN/PBPK model for BaP was validated using two different data sets from the literature (5, 6), while the model for the metabolites was not validated due to the lack of data for BaP metabolites. The partition coefficients

for BaP and its metabolites used in the RN/PBPK model were estimated by fitting the experimental data. The values of these partition coefficients need to be validated using *in vitro* experiments in which BaP and its metabolites are incubated with minced tissues in buffer solution and their concentrations in tissues and buffer solution are analyzed. A fully validated RN/PBPK model can be used to predict the distribution and disposition of BaP and its metabolic reaction network in whole animals. For some very reactive metabolites that are not likely to be distributed to other tissues, the RN/PBPK model can predict the concentration of these metabolites within the site of metabolism based on the whole body exposure concentrations. Some metabolites can be transported out of the site of metabolism and cause adverse effect in other tissues. RN/PBPK models can also be used to predict the concentrations of these metabolites in different tissue compartments.

## **9.2. Future Perspectives**

The development of RN pathway and kinetics models for BaP metabolism represents the first step of applying the RN modeling approach to predict the biotransformation of a variety of chemicals. In order to apply RN pathway modeling to chemicals other than PAHs, it is necessary to account for the possible enzymes responsible for the biotransformation of the chemicals of interest, as well as the possible types of biotransformation reactions relevant to these enzymes and chemicals. One approach is to first develop a RN pathway model for the prototypical compounds for a group of chemicals with similar structure and metabolized by the same enzymes. After the RN pathway model of the prototypical compounds is validated, it can be applied to predict the biotransformation reactions for other analogous chemicals. For example,

3,3',4,4',5-pentachlorobiphenyl (PCB 126) can be used as the prototypical compound to develop the RN pathway model for coplanar polychlorinated biphenyls (PCBs), which are likely to undergo biotransformation reactions catalyzed by CYP 1A isozymes (7). On the other hand, CYP 2B isozymes are principally responsible for the biotransformation of non-planar PCBs (7) and 2,2',4,4',5,5'-hexachlorobiphenyl (PCB 153) can be used as the representative compound for this type of PCBs.

The RN kinetics model for BaP was calibrated based on enzymatic experiments using recombinant human cytochrome P450 1A1 (CYP1A1) and EH. CYP1A1 was used in the enzymatic experiments because it is the major isozyme responsible for the oxidative metabolism of BaP (8). Other CYP isozymes, *e.g.* 1A2, 1B1, 2C8, 2C9, 2C18, 2C19, and 3A4, can also contribute to the metabolism of BaP, although to a lesser extent than CYP1A1 (9, 10). Therefore, these CYP isozymes need to be used in the future enzymatic experiments to investigate the contribution of different isozymes to BaP metabolism.

To further calibrate and validate the RN kinetics model of BaP, it is necessary to identify the unknown metabolites of BaP detected in the current study. For example, BaP-9,10-dihydrodiol (9,10-diol) was metabolized to form unidentified metabolites in this study, which might cause the underestimation of the formation of 9,10-diol and BaP-9,10-oxide (hydrolyzed to from 9,10-diol). Furthermore, in the current kinetics model, the values for the dissociation constants of substrate-enzyme complexes were adapted from literature data. In order to accurately estimate the dissociation constants under the experimental conditions used in this study, a wider range of BaP concentrations need to be used in the future enzymatic experiments.

When applying this RN modeling approach to study the metabolism of chemical mixtures, the RN pathway model predictions can be achieved by simply combining the bond-electron and reaction matrices for the individual chemicals in the mixture. For RN kinetics modeling, it is necessary to consider the induction and inhibition of enzymes associated with exposure to chemical mixtures. For example, when an animal is exposed a mixture of PAHs containing BaP, the amount of BaP metabolized will be different from the amount metabolized while animal is exposed to BaP alone. This is because PAHs can induce CYP1A1 synthesis (11). The enzyme induction can be accounted for in the RN kinetics model by adjusting the total enzyme concentrations. On the other hand, different PAHs in the mixture can also compete for the active sites of CYP1A1. To consider enzyme inhibition by different substrates in the RN kinetics model for PAH mixtures, the CYP1A1 activities toward the metabolism of different PAHs need to be investigated using enzymatic experiments containing a mixture of the PAHs of interest.

Another way in which the RN/PBPK model of BaP should be refined is the addition of conjugation reactions. The amount of BaP metabolites that undergo conjugation can only be accurately accounted for when the relevant reaction rules are included in the model and proper analytical methods are used to determine the conjugation products. Precision-cut liver and lung slices (12, 13) can also be used in the future *in vitro* experiments for BaP metabolism to verify whether rat liver microsomes used in this study properly represented the enzymatic activities in the metabolism organs.

We have taken the first step to integrate reaction network modeling with PBPK modeling. As presented above, to fully utilize this technology, particularly the potential computer-assisted modeling, many “training sets” of chemical metabolic reaction

networks will have to be studied and incorporated into the database of RN pathway and kinetics models to formulate a robust predictive tool for complex metabolic reaction networks including those of chemical mixtures. It will be a long and winding road; however, the reward of developing such a tool will be the benefit of resolving a difficult and puzzling problem in toxicology – the toxicology of chemical mixtures.

### **9.3. References**

1. Neurock M, Klein MT. Linear free energy relationships in kinetic analyses: Applications of quantum chemistry. *Polycycl Aromat Comp* 3:231-246(1993).
2. Neurock M, Klein MT. When you can't measure - model. *Chemtech* 23:26-32(1993).
3. Korre SC, Neurock M, Klein MT, Quann RJ. Hydrogenation of polynuclear aromatic hydrocarbons. II. Quantitative structure/reactivity correlations. *Chem Eng Sci* 49:4191-4210(1994).
4. Weyand EH, Bevan DR. Benzo(a)pyrene disposition and metabolism in rats following intratracheal instillation. *Cancer Res* 46:5655-5661(1986).
5. Wiersma DA, Roth RA. Total body clearance of circulating benzo(a)pyrene in conscious rats: effect of pretreatment with 3-methylcholanthrene and the role of liver and lung. *J Pharmacol Exp Ther* 226:661-667(1983).
6. Schlede E, Kuntzman R, Haber S, Conney AH. Effect of enzyme induction on the metabolism and tissue distribution of benzo( $\alpha$ )pyrene. *Cancer Res* 30:2893-2897(1970).
7. Hu K, Bunce NJ. Metabolism of polychlorinated dibenzo-p-dioxins and related dioxin-like compounds. *J Toxicol Environ Health B Crit Rev* 2:183-210(1999).
8. Kawajiri K, Hayashi SI. The CYP1 family. In: *Cytochromes P450: Metabolic and Toxicological Aspects* (Ioannides C, ed). Boca Raton: CRC Press, 1996;77-97.
9. Gautier JC, Lecoeur S, Cosme J, Perret A, Urban P, Beaune P, Pompon D. Contribution of human cytochrome P450 to benzo[a]pyrene and benzo[a]pyrene-7,8-dihydrodiol metabolism, as predicted from heterologous expression in yeast. *Pharmacogenetics* 6:489-499(1996).
10. Kim JH, Stansbury KH, Walker NJ, Trush MA, Strickland PT, Sutter TR. Metabolism of benzo[a]pyrene and benzo[a]pyrene-7,8-diol by human cytochrome P450 1B1. [erratum appears in *Carcinogenesis* 1999 Mar;20(3):515]. *Carcinogenesis* 19:1847-1853(1998).
11. Roos PH, Tschirbs S, Welge P, Hack A, Theegarten D, Mogilevski G, Wilhelm M. Induction of cytochrome P450 1A1 in multiple organs of minipigs after oral exposure to soils contaminated with polycyclic aromatic hydrocarbons (PAH). *Arch Toxicol* 76:326-34(2002).

12. Lake BG, Meredith C, Scott MP, Renwick AB, Price RJ. Use of cultured precision-cut rat lung slices to study the in vitro induction of pulmonary cytochrome P450 forms. *Xenobiotica* 33:691-702(2003).
13. Price RJ, Ball SE, Renwick AB, Barton PT, Beaman JA, Lake BG. Use of precision-cut rat liver slices for studies of xenobiotic metabolism and toxicity: comparison of the Krumdieck and Brendel tissue slicers. *Xenobiotica* 28:361-71(1998).